KfK 4171
August 1988

CORA Scoping Test B

Test Results Report

S. Hagen, W. Hering, K. Vogel
Hauptabteilung Ingenieurtechnik
Hauptabteilung Versuchstechnik
Projektgruppe LWR-Sicherheit

Kernforschungszentrum Karlsruhe

KERNFORSCHUNGSZENTRUM KARLSRUHE
HAUPTABTEILUNG INGENIEURTECHNIK
HAUPTABTEILUNG VERSUCHSTECHNIK
PROJEKTGRUPPE LWR-SICHERHEIT

KfK 4171

CORA Scoping Test B
Test Results Report

S. Hagen, W. Hering, K. Vogel

Kernforschungszentrum Karlsruhe GmbH, Karlsruhe

Kernforschungszentrum Karlsruhe GmbH
Postfach 3640, 7500 Karlsruhe 1

ISSN 0303-4003

Summary

The out-of-pile experiments of the CORA-program are planned to investigate the damage processes in LWR fuel elements under Severe Fuel Damage conditions. The CORA-facility was built at the Hauptabteilung Ingenieurtechnik (HIT) to perform these tests. Experiment CORA-B with Al_2O_3-pellets should test the high temperature behaviour of the facility without the danger of radioactive contamination. But the high temperature behavior of Al_2O_3-pellts in zircaloy tubing is also of interest for the understanding of the damage initiation in burnable poison rods for PWR's. There the Al_2O_3 pellets inside the zircaloy (Zry) cladding are the matrix for B_4C (1.4 wt.%), which is used as burnable absorber material.

In test CORA-B as a result of a power input of up to 80 KW a maximum temperature of about 1800°C was reached. Significant melting of the Al_2O_3/Zry-rods started at about 1500°C due to the interaction between Zry and Al_2O_3. The formation of a metallic (Zr, Al) alloy plays an important role in this interaction process. At the end of the test nearly the whole bundle was liquefied. The melt refroze at the lower end of the bundle forming a large lump, which was blocking the bundle cross section. The melt formation in an Al_2O_3/Zry bundle is much stronger than in a UO_2/Zry bundle for the same temperature history.

Vorversuch CORA-B; Ergebnisbericht

Kurzfassung

Die out-of-pile Experimente des CORA-Programms sollen die Schadensprozesse an LWR-Brennelementen unter den Bedingungen schwerer Kernschäden untersuchen. Für diese Versuche wurde die CORA-Anlage von der Hauptabteilung Ingenieurtechnik (HIT) aufgebaut. Der Versuch CORA-B mit Al_2O_3-Pellets sollte das Hochtemperaturverhalten der Anlage unter Vermeidung von radioaktiver Kontamination überprüfen. Das Hochtemperaturverhalten von Al_2O_3-Pellets in Zircaloy (Zry)-Hüllmaterial ist aber auch von großem Interesse für das Verständnis der Schadensphänomene von abbrennbaren Absorbergiftstäben in Druckwasserreaktoren. Bei ihnen dient das Al_2O_3 in den Zry-Hüllrohren als Matrix für 1,4 Gew.% B_4C.

Im Test CORA-B wurde eine elektrische Leistung zwischen 6 und 80 KW eingespeist. Damit wurde eine Maximaltemperatur von ca. 1800°C erreicht. Deutliches Schmelzen setzte ab 1500°C ein. Der Auflösungsprozess ist eine Folge der Wechselwirkung zwischen Zry und Al_2O_3 und ist wesentlich mit der Bildung einer Zr, Al-Legierung verbunden. Am Testende war nahezu das gesamte Bündel geschmolzen. Die Schmelze erstarrte im unteren Bündelbereich unter Ausbildung eines großen Klumpens, der das untere Bündelende blockierte. Die Schmelzbildung im Al_2O_3-Bündel ist deutlich ausgeprägter als im UO_2/Zry-Bündel.

Contents

1. Introduction

The TMI-2 accident has demonstrated that a severe fuel damage transient will not necessarily escalate to an uncontrolled core melt down accident, if the design basis accident limits are exceeded, as was assumed in earlier risk studies. Therefore, comprehensive research programs have been initiated in various countries to investigate the relevant fuel rod bundle damage mechanisms acting with increasing temperature on an uncovered core and to develop computer codes for estimating the damage in the core, when the design limit temperature is exceeded, but the transient can be stopped before core meltdown.

In the Federal Republic of Germany at the Kernforschungszentrum Karlsruhe (KfK) the Severe Fuel Damage (SFD) Program /1/ was initially coordinated by the Project Nuclear Safety (PNS) now LWR Safety Project Group (PRS). As part of this program, out-of-pile experiments (the CORA-Program/2/) are being conducted at the Hauptabteilung Ingenieurtechnik (HIT). These experiments are designed to give information on the integral behaviour of the fuel rod bundle damage processes, which are investigated in detail and under well defined conditions in the seperate effect tests /3-6/ of our SFD-Program. Especially the influence of the absorber rod and structural materials of the bundle will be investigated. The out-of-pile experiments will also be used for the assesment of the SFD computer codes. In addition these experiments directly complement the in-pile tests conducted within the international SFD-research community.

For the realization of these experiments we can use two facilities.The existing NIELS-facility was used for pretests, on the temperature escalation due to the exothermal zircaloy/steam reaction /7-16/ and the influence of the absorber rod materials /17, 18, 19/. The CORA-facility was built especially for the Severe Fuel Damage tests. The tests to be run in this facility can be seen from the test matrix given in table 1.

In this report test CORA-B is discussed. CORA-B is the first of two tests in which the UO_2 of the bundle is replaced by Al_2O_3. Two goals are realized by these experiments: 1. The facility could be tested at higher temperatures without the danger of any radioactive contamination and 2. The interaction behavior between Al_2O_3-pellets and zircaloy cladding is of interest for the burnable poison rods in PWR reactors. There, the Al_2O_3 pellets inside the

Zry-cladding are the matrix material for B_4C (1.4 wt.%), which is used as absorber material.

2. Short Description of the CORA-Facility

2.1 The Facility

The CORA facility is described in KfK-report 3677. Here are given only the information which are necessary for the understanding of this test. Fig. 1 shows the scheme of the CORA facility. Fig. 2 is a scaled axial section of the components within the containment. The central part of the facility is the fuel rod bundle. The bundle is enclosed in a Zry-shroud. A high temperature radiation shield surrounds the bundle, leaving an annular space. The bundle is connected to the power supply system at the upper and lower end.

Below the bundle is the quench unit with a water filled quench cylinder, which can be raised around the bundle with a hydraulically controlled speed. The cylinder is guided by three rods, which also connect the electric power to the bundle lower end.

In this test the quench cylinder stayed at a constant elevation. At the beginning of the test the water level was 221 mm below the "zero elevation" of the bundle. The "zero elevation corresponds to the lower end of the pellets in the heated rods.

The bundle upper end is fixed in the bundle head funnel. The bundle head funnel consists mainly of an insulating plate, which provides the pressure seal of the rods. The plate is connected by a funnel shaped tube to the surge condensor. The surge condensor is double-walled, leaving access to the bundle end fittings above the bundle head funnel.

Normally the steam is produced in the steam generator, superheated and guided to the lower end of the bundle, entering at "zero elevation". The steam not consumed is condensed in the condensor and the hydrogen produced is given to the off-gas system. In this test the steam production unit was not connected to the facility.

2.2 Rod and Bundle Design

Two types of fuel rod simulators can be used: electrically heated rods and unheated solid rods.The arrangement of the rods for test CORA-B is shown in Fig. 14. We have used 25 rods: 16 heated and 9 unheated rods. Fig. 9a shows the heated rod. The heated fuel rod simulator is sheathed with standard PWR zircaloy cladding tube. The central part of the internal rod consists of 6 mm tungsten rod surrounded by annular pellets. In the future tests these annular pellets are made of UO_2. In tests CORA-B and CORA-C we have used Al_2O_3 annular pellets. The tungsten heater has a length of 1000 mm. The tungsten heater is screwed into Mo-electrodes of 250 mm length which fit directly into the zircaloy cladding. The molybdenum electrodes are connected to copper electrodes and both are insulated from the zircaloy cladding by a flame-sprayed ZrO_2 layer. The zircaloy cladding is sealed to the copper electrodes by swage-lock fittings. To the upper and lower copper electrodes flexible copper power cables are connected. The fuel rod simulator is screwed into the bundle flange from the top, producing a hermetic seal. The bundle flange thus gives the fix point for the axial thermal movement of the rod.

The unheated rod is shown in Fig. 9a. Normally solid UO_2 pellets are foreseen inside the zircaloy cladding. In test CORA-B and CORA-C annular Al_2O_3 pellets were used.

Three spacers are used in the test bundle to maintain the radial position of the rods. We have used the original PWR spacers, made of zircaloy. These spacers are positioned at the following elevations: (upper edge): -55 mm, +565mm, +1175mm. The length of the spacers comes to about 50 mm.

The bundle head funnel (Fig. 7) is water-cooled by a double walled chamber. To make the cooling more effective the space around the rods inside this chamber is filled with water. Also the lower ends of the heated fuel rod simulators are standing in the water of the quench cylinder. The water level before the test is at -228 mm elevation. The unheated simulators extend only to -200 mm. They have no contact to the water of the quench cylinder.

2.3 Power Supply

24 of the 45 fuel rod simulators can be heated. In CORA-B 16 rods out of 25 are heated. The rods can be separately connected to one of three available power systems, each of which can supply a different voltage. By grouping the rods in various ways, we can influence the power distribution of the bundle. The number of rods can be different in the groups. In CORA-B we have 6 and 6 and 4 rods in the 3 groups (Fig. 15). In this test the power input should be the same for all rods. Since the voltages and currents of the individual rods are measured, we know the power input for each rod.

The power input is controlled by a computer. The time dependent power history is programmed before the test. During the test the programmed power can be overridden and manually controlled. We can reduce or increase the power of each of the three groups in steps or completely. The electric heating is done by direct current which was necessary to avoid eddy currents in the containment.

2.4 High temperature shield

To keep the heat losses as low as possible, the center bundle is surrounded by a high temperature shield (HTS) during the test. The vertical and the horizontal cross sections of the high temperature shield are given in Figures 3 and 4. The high temperature shield consists mainly of ceramic fiber plates. The two inner rows of plates are ZrO_2, and the two outer ones are Al_2O_3. The fiber ceramics are excellent insulators and have a low density which results in a low heat capacity. The thermal shock behaviour of the fiber ceramics is also excellent.

The mechanical strength of the high temperature shield is provided by the outer walls of stainless steel. The fiber ceramic plates are attached to the stainless steel cover by ceramic nails. The inner ZrO_2 layer is 38 mm thick, and the outer Al_2O_3 layer 76 mm thick. The distance from the inner insulation surface to the center of the bundle is 152 mm.

The high temperature shield is located within the pressure tube. In the pressure tube a large number of flanges allow access to the bundle. Through these holes and their extension in the temperature shield, the bundle can be

inspected during the test. Temperature measurements can also be made by two-color pyrometers using these holes as viewing ports.

At the lower end of the heated part of the bundle, steam is introduced through flange H22. The insulated ceramic tube, which provides the connection to the bundle shroud, can be withdrawn at the end of the test to allow the passing of the quench cylinder.

An important design feature of the CORA facility is the ability to lower the high-temperature shield into the quench unit without disturbing the bundle (Fig. 11 and 12).

2.5 Instrumentation

The voltages to the 3 groups of heated fuel rods and the current of each fuel rod is measured, so that we are able to determine the power and the resistance of each fuel rod. The pressure of the system is controlled and measured.

In the data aquisition system we have 68 places for thermocouple measurements. Fig. 36 show the thermocouples used in the bundle and Fig. 53/54 those used in the high temperature shield. The position of the three two color pyrometers are given in Fig. 50.

3. Low temperature tests

To test the facility in the temperature region below 1000°C and to get information of the temperature reaction of the facility to the power input under different conditions we have done some initial tests at low power input. The results of three tests are reported in the following section.

To study the contribution of the convection cooling by argon we have done two tests with the same power input as given in Fig. 72 with test 1 in vacuum of about 10^{-3} bar and test 2 in stagnant argon at a overpressure of 1,2 bar. (The irregularities of the power curve are not real, but are only distortions of the measurement, which could be fixed after this first test.)

The power given in Fig. 72 and Fig. 83 is that of one group with 6 rods. We have used the same power for all rods. The bundle has 16 heated rods, consequently the total power is 16/6 = 2.66 times of the power given.

At 550 mm elevation the measurements in 3 unheated rods, (Fig. 69, 70 and 71) show the clearly higher temperature in vacuum, due to smaller convection heat losses in vacuum compared to argon.

Fig. 73 to 75 compare the temperatures at increasing elevation from 550 mm to 1390 mm elevation. The increase of the temperature in argon compared to that in vacuum is due to the heat transport by argon in connection with the natural circulation.

Fig. 79 and Fig. 80 compare the temperatures in vacuum and argon for two positions inside the high temperature shield insulation. During heating a higher temperature is reached with argon, but after heating the temperature in vacuum is about twice as high as that in argon.

Fig. 81 and Fi. 82 gives the constant power input and the temperatures of a third test. Even after 4000 sec the temperature equilibrium is not completely reached.

4. Test conduct of main test

The first objective of CORA-B was to test the behaviour of the facility at high temperatures. Therefore it was planned to heat the bundle with about 0.5 K/sec to about 2000°C in stagnant argon at a overpressure of 1,2 bar. The steam superheater was not connected to the facility.

The power input to reach a temperature increase of about 0,5 K/sec for the unheated fuel rod is given in Fig. 17. The power was increased from about 5,5 to 84 kW. The time integral of the power input is given in Fig. 16.

The major part of the power was consumed by the radial heat losses. In test CORA-C the same bundle and shroud arrangement was insulated with 19 mm ZrO_2 fiber insulation over a length from 40 to 1040 mm elevation. Additional the annuli between the high temperature shield insulation and the shroud on the inside and pressure wall on the outside were closed by a layer of about 40 mm fiber insulation to impede natural circulation around

the HTS insulation. With these changes only 30 KW were necessary to reach nearly the same max. temperature /20/.

The power supply of the CORA facility consists of 3 independs units, which allow to have 3 groups of heated rods with different power input per rod by applying different voltages to these groups. The voltages of these power units and the currents of each rod are measurred separately. In test CORA-B all rods were heated with the same power. The rods were grouped in 6,6 and 4 rods. The distribution into this groups is given in Fig. 15.

Fig. 18 gives the power inputs to the three rod groups. The irregularity in the power input for group 3 was caused by a manual change of the voltage input in this group, due to mis-interpretation of the irragularities in the measured currents. Fig. 19 gives a time spreaded presentation of the last third of the group powers. The voltage inputs to the 3 groups are given in Figures 20 and 21. The maximum voltage used amounts to about 11,5 V.

The currents of the three groups and the total current through the bundle are given in Fig. 22. A maximum total current of about 7500 Ampere was used to heat the bundel. This corresponds to about 470 Ampere per rod. The course of current with time has a minimum at about 1000 s though the voltage is increasing continously. This is caused by the strong resistance increase of the tungsten heater.

Figures 23 to 31 show the currents of the single rods always compared for the rods within the respective group. Up to 3500 sec we have a uniform course for all rods. After this time we get strong fluctuations . We assume that these fluctuations are due to melting, which changes the resistance for the single rods by relocation of melt from heated and unheated rods. The resulting resistances for the 3 groupes and the single rods are given in Fig. 32 to 35.

5. Temperature measurements

In test CORA-B only a limited number of temperature measurement position were used. The locations for the thermocouples within the bundle are given in Fig. 36. The positions of the 3 two color pyrometers used are shown in Fig. 50. The locations of the thermocouples within the high temperature shield insulation are given in Figures 53 and 54.

Within the heated region of the bundle (region of tungsten heaters) four thermocouples (Fig. 37, 38, 39, 41) were used. They were located inside the annular pellet of the unheated rods at 1000 mm (1TC) and 550 mm (3TC) elevation. Used were tungsten-rhenium thermocouples with 1 mm tantalum sheath. These 4 thermocouples show a similar behaviour of the temperature in the region from 550 mm to 1000 mm elevation in the first 3500 sec. A linear increase of the temperature with 0,5 K/sec up to about 1550°C for the thermocouple at 1000 mm and one at 550 mm and to about 1350°C for the two other thermocouples at 550 mm could be observed.

After 3500 sec the thermocouple at 1000°C survives and is increasing up to 1800°C together with the electric power input. The thermocouples at 550 mm elevation fail after about 3500 sec. The measurement of current for the single rods show strong increase at the same time. We assume that at 3500 sec strong re-arrangement of molten material takes place, which causes also the failure of the thermocouples at 550 mm elevation. As the posttest appearance shows, the bundle is molten in the region from about 20 mm to 1000 mm elevation. The thermocouple at 1000 mm had the chance to survive.

As is discussed in /21/ the early melting of the bundle is due to the interaction of the Zry-cladding with the Al_2O_3 of the pellet. Al_2O_3 is thermodynamical instable in contact to Zry. The Zry takes oxyen from Al_2O_3, so that a liquid metallic ZrAl-alloy is formed. This process leads to the liquefaction of the metallic cladding at about 1350°C and can continue to the complete liquefaction of the Al_2O_3 pellets at about 1550°C. The starting of the melt formation could be clearly seen in test CORA-C /20/ by videoscope.

Fig. 42 to 45 show the behaviour of the thermocouples in a time spreaded presentation. One can recognize, that after cooldown, due to completion of the electric power input, a new junction is formed in the thermocouple.

The temperature of rod 29 was also measured at 500 mm elevation by the two color pyrometer in flange H30 (Fig. 50 and 14). The comparison with the thermocouple measurement is given in Fig. 52. There is a reasonable agreement in the region of overlap. The two other two color pyrometers were looking on the corner rods 43 at 500 mm (H29) and 20 at 900 mm (H40) elevation.They show a much lower temperature. The post-test investigation

shows, that the corner rods were clearly the coldest components of the bundle, but the deformed appearance of the shroud after the test makes the two color pyrometer measurement something suspicious for the last period of the test.

At 1200 mm and 1350 mm elevation the maximum temperature in the unheated rod is decreasing to 1150°C and 750°C (Fig. 40 and 46). At 1224 mm the gas temperature was measured outside the bundle as shown in Fig. 36 to a maximum value of about 1200°C (Fig. 47). For this measurements tungsten-rhenium thermocouples were used, which were covered in a 6 mm ZrO_2 ceramic tube.The temperature of the shroud at the lower end in contact with the steam distribution tube reached values of over 1350°C. (The measurement went of scale at the end of the test.): Fig. 49. The temperature of the water in the quench cylinder was measured at -300 m elevation.

5.1 Temperature measurement in the high temperature shield insulation

The temperature measurement in the high temperature shield insulation was performed with 26 thermocouples. With the exception of the two innermost thermocouples which are PtRh-sheathed these thermocouples are K-type (Ni CrNi)-thermocouples with Inconel sheath. The thermocouple in the insulation survive the test and must not be replaced as the thermocouples in the bundle. The locations of the thermocouples in the high temperature shield insulation is given in Fig. 53 and 54.

The change of the time dependent temperature measurement after 38 mm of ZrO_2 fiber insulation (at radius = 192 mm) with the axial elevation is given in Fig. 55 and 56. The measurements are done on two diametral positions at 345° and 165°. The insulation of the high temperature shield extends from -150 to +1300 mm elevation. The maximum temperatures vary from -50 mm to + 1150 mm from 175°C to 440°C. One clearly can see a displacement of the temperature to the upper part of the bundle. In agreement with the measurement in the bundle one can recognize, that there is only a small change in the region from 530°C to 950°C. The same tendency is found for both azimuthal directions.

The comparison for the temperatures in the two azimuthal directions at different axial elevations is given in Fig. 57. At all elevations one can recognize a higher temperature for the direction of 165°C. We explain this azimutal asymmetry in the temperature by the difference in the natural circulation, which can develop in a stronger way at 165° due the larger opening at the lower end of the high temperature shield at this orientation.

The difference in the temperature at 550 mm elevation for the different directions are shown in Fig. 59. At the maximum temperature the difference amounts for good 50°C.

Fig. 58 shows the same tendency in the axial dependency of the temperature on the outer surface of the insulation. Here the maximum temperature increases from 125 °C to over 400°C between 350 mm to 1150 mm elevation.

The comparison of radial change of the temperature for different axial positions is given in Fig. 60 to 65. As already discussed in connection with the comparison of the temperatures for the radius 192 mm for the two opposite direction 165° and 345° also the radial comparison shows that there must be a remarkable natural circulation around the HTS insulation. The argon is heated up in the annulus between shroud and insulation by the heat losses through the shroud and is then cooled in the gap between high temperature shield insulation and pressure wall by the heat losses to the pressure wall.

At 1550 mm elevation (Fig. 60) the temperature on the outer surface of the insulation at 293 mm is higher than the temperature in the middle of the insulation at the same elevation. The higher temperature on the outer surfaces is explained by the moving hot gas of the natural circulation.

At 950 mm elevation the temperature on the outside for the radius 293 mm is higher than the temperature in the middle for radius 255 mm (Fig. 61). The higher temperature on the outside is explained by natural circulation. The same tendency is seen for the elevation 550 mm (Fig. 63, 64) and elevation 150 mm (Fig. 65).

Fig. 64 shows the strong radial decrease of the temperature at the elevation of 550 mm. The maximum temperature decreases from 750°C after 19 mm of ZrO_2 fiber insulation to below 100°C inside the Al_2O_3/SiO_2 insulation at 255 mm radius and a temperature on the outer surface of about 120°C. The

temperature is only slowly penetrating into the insulation. Figures 66 and 67 show that the temperatures during the test at 255 mm radius always stay below 100°C.

6. Videoscope registration

In test CORA-B we have tested a videoscope system which should give the possibility to observe the bundle during the test. The videoscope is shown in Fig. 85. The water and argon cooled system is introduced through the flange hole and a hole in the HTS insulation to give access to the bundle (Fig. 3). In test CORA-B the flange position 435 (120°, 590 mm elevation) was used. The numbers given in Fig. 3 for the elevation refer to the lower end of the facility (CORA-Kote [mm]). In this system the before used zero-point correspondends to 5112 mm.

The videoscope in flange H35 is looking on the corner of the bundle. The numbers and positions of the rods seen are given in Fig. 84. The pictures show the five heated rods with numbers 18, 20, 3, 8 and 14. The hole in the shroud is moving upward due to the thermal groth of the shroud. From 39 to 80 minutes we have an upward movement of about 2 cm. The hole in the shroud has a too high elevation.

The first melt droplets can be recognized at 60 minutes. This is in agreement with the thermocouple and current measurements which indicate the beginning of melting at about 3500 sec.

7. Aerosol behaviour

The inner surface of the facility was covered by an grey layer. This can be seen for instance on Fig. 85. The inner part of the videoscope is inside the facility. The front end of the insulation cylinder is sticking inside the high temperature shield during the test. This area is protected against gas movement. The grey middle region is positioned in the gap between high temperature shield insulation and outer pressure wall which is closed by the flange shown on the picture. This grey deposition is caused by aerosols. The aerosol deposits can also be recognized on the thermocouple lead-through in

Fig. 86 and on the ceramic disc on the inside of the high temperature insulation of Fig. 87.

8. Posttest appearance of the bundle

The posttest appearance of the bundle is described in Fig. 88 to Fig. 115. Fig. 88 shows the bundle inside the shroud from 4 directions after lowering down of the high-temperature shield. Shroud and bundle are in the state they reached at the end of the test. The construction of the CORA-facility avoids any mechanical handling of the bundle and shroud before they are inspected.

The pictures show that the shroud is undestroyed, but that a deformation of the shroud has taken place, that resulted in an opening along the contact lines. The shroud severely embrittled. A part of the shroud which fell down after dismantling of the bundle was fragmented into many pieces.

Fig. 89 to 91 give close up photographs of the bundle through the opening of the shroud. One can recognize, that for the inner rods cladding on pellets are gone. At the lower and upper end outside cladding and also part of the pellets have survived. The corner rods have survived the most.

The appearance of the bundle after removing of the shroud is shown in Fig. 92 to Fig. 104. Fig. 92 gives an overview and comparison of photographs taken in 4 different directions. The picture in 307,5° is looking on the corner of the bundle and shows from left to right the heated rods 20, 28, 36, 43, 38, 32 and 26. The picture in 232,5° gives the heated rods 43, 38, 32, 26, 18, 10 and 3. The picture in 157,5 degree is looking on one side of the bundle and shows the fuel rods 26, 18, 10 and 3. The picture in 82,5 is looking on the last side and shows the heated rods 3, 8, 17 and 20.

Fig. 93 to 96 show the same pictures in enlarged presentations with one direction on one page. Even more details can be seen in Figures 97 to 104 were in higher magnification the pictures of one direction are given on two pages.

It is remembered that the elevations in this report are referred to the "zero-point" at the lower end of tungsten heaters. This corresponds to the lower end of pellets in the heated rods. In the heated rods the pellets are found up

to 1000 mm. Above this elevation the Zry-cladding is filled with the molybdenum-electrode. The pellets in the unheated rods extend from -200 mm to +1300 mm elevation.

The pictures show that the bundle is nearly completely molten away below 1000 mm elevation.

In the region between 1000 and 900 mm remnants of the fuel rod simulators are glued together by refrozen melt. Below about 900 mm only the tungsten heaters with small amounts of refrozen melt can be found. In the region from 550 mm to 350 mm elevation some of the outer fuel rod simulators have kept partly oxidized cladding on the outside. Below 350 mm elevation nearly all outer fuel rods have kept there outer cladding and are glued together to their neighbours, so that a nearly closed wall is formed. The cross sections, discussed in the next paragraph, will show that inside this wall the bundle is molten down to about 0 mm elevation. The lower end of this containment is filled with melt. On top of the refrozen melt a layer of about 60 mm is found. It is assumed that the rubble has fallen down during cooldown of the bundle. Larger pieces of former cladding are shown in Fig. 105a and 105b.

In Fig. 92 to 104 the lower end of the bundle below 35 mm is covered by the stainless steel steam distribution tube. To show the refrozen melt in the lower region of the bundle the steam distribution tube was removed and the refrozen melt was photographed from 4 directions. The results are given in Fig. 106 to 109.

One can recognize, that a large amount of melt is refrozen inside the bundle flowing through and around the lower spacer. All pictures show that there are two types of melt: a white porous melt and a dark melt of glazy appearance. As discussed in reference 21 the white refrozen melt has an eutectic structure formed of Al_2O_3 and ZrO_2. The melt has formed by interaction between Al_2O_3 and Zry. The black melt is refrozen Zry or Zr-Al alloy.

Part of the melt is not refrozen within the bundle, but has fallen into the water of the quench cylinder, which was cooling the lower end of the bundle. The refrozen material is shown in Fig. 110 to 112. Again here we find the two types of refrozen melt, with Al_2O_3/ZrO_2 eutectic in clear abundance.

Fig. 113 to 115 give photographs of the rubble found below the bundle. The size of the pieces can be recognized by comparison to the ruler. The smooth round surfaces of the pieces in Fig. 114 and 115 give hints that they are refrozen when falling into the water. The composition and structure of this particles is discussed in detail in reference 21.

9. Cross sections of the bundle

After removal of the shroud the bundle was contained with a lucite box (Fig. 13a). The box was sealed to the steam distribution tube at the lower end of the bundle. The steam distribution tube itself was sealed by refreezing paraffin floating on the water level of the quench cylinder brought into the right elevation. The paraffin layer was then strengthened by an additional layer of epoxy before the whole bundle was slowly floated with epoxy through the steam entrance tube.

An overview of the sections cut into the bundle with a diamond saw are given in Fig. 116. From the post test pictures we have seen that the bundle is molten away below about 1000 mm elevation, a crucible like wall had formed between about 350 mm and zero and a large amount of melt is refrozen below. The majority of sections is therefore performed in the upper and lower end of the bundle.

In bundle B three Zry-spacers were positioned at 1175 mm, 565 mm and -35 mm. Given is the elevation of the upper edge of the 40 mm long spacer. The middle spacer is molten away together with the bundle. The upper and lower spacer has survived and can be seen in the cross section.

The cross sections through the upper spacer can be seen in Fig. 117. The pieces cut from the bundle were photographed from the top and bottom side. The pictures are marked by "upper" and "lower". One has to remember that these pictures are side reversed. The numeration for the rods for each type are given below the pictures.

The cross sections show 16 heated and 9 unheated rods. Above 1000 mm elevation in the heated fuel rod the tungsten heater with surrounding anular pellet has changed to the molybdenum solid rod. Consequently the 16 white circular areas are the sections of these molybdenum rods surrounded by the annular section of the zircaloy cladding. The nine unheated rods between give the double annular section resulting from the Al_2O_3 annular

pellet and the Zry-cladding. If we are looking on the unheated rods, one can recognize that even at the highest elevation the cladding has started to melt at some points. The zircaloy molten away was always in contact to the Al_2O_3 pellet.

Fig. 118 gives cross sections from the area were the bundle is molten away. Only the tungsten heaters are left, with the exception of the corner rods, which must have had a much lower temperature.

Fig. 119 shows cross section from the lower third of the bundle, where the "crucible" had formed. Due to the radial heat losses, the radial temperature gradient was melting and that between the outer simulators the melt was refreezing forming a closed crucible.

The eight outer heated fuel rod simualtors 8, 14, 10, 18, 28, 36, 32, 38 and the eight outer unheated fuel rod simulators 9, 15, 21, 29, 37, 31, 25, 17 are thus forming the structure of the "crucible". The radial gradient is large enough that in some cases only the outer part of the simulator has survived. At 269 mm and 251 mm elevation on the right side a double structure of the oxide layer can be seen . It is assumed that the inner layer is belonging to the cladding of fuel rods 28 and 36. Then melt has run along the rods closing also the gaps between the rods. The surface of this melt again is oxidized. Of interest is also the porous structure of the refrozen melt. Again at these elevations one can recognize the much lower temperature of the corner rods.

The cross sections in Fig. 120 show that below 75 mm the "crucible" is filled with rubble. In the region between the heated rods 22, 30 and the unheated rod 29 already at 93 mm this rubble can be recognized. From unheated rod 29 only the outside half is left. The structure of the rubble can be seen in more detail in the vertical cross sections between 1 and 73 mm elevation given in Fig. 161 and following.

Fig. 121 shows that at 1 mm the space between the fuel rod simulators is completely filled with melt. The vertical cross sections mentioned above show that the complete blockage already starts at about 20 mm elevation.

At 1 mm elevation the central unheated rod 23 and the 4 neighbouring heated rods 16, 22, 24, 30 are molten away (with exception of the tungsten heater). The pellet of the unheated center rod can be seen again at -53 mm (Fig. 122). But there is melting of the cladding down to -73 mm. In Fig. 122

the cross section of the heated fuel rods show the solid molybdenum rod and the two cross sections of -16 mm and -18 mm show the transition region from tungsten heater to molybdenum electrods, where the tungsten rod is screewed into the molybdenum rod.

In Fig. 121 the cross sections from 1 mm to -16mm show in the central area a bright appearance of the melt. As is discussed in reference /21/ this central region is filled with refrozen metallic melt, while the outer region is ceramic with eutectic structure due to the interaction between Zry and Al_2O_3.

The comparison of the cross sections at the different elevations show a complete blockage above the spacer, but within the spacer a large fraction of the cross section is voided. The cross sections given are lying in the lower half of the spacer (-35 to -75). In the two upper cross sections at -53 and -55 mm the spacer is destroyed by the melt in the area around rods 9, 16, 17. At -73 mm the Al_2O_3 pellets have survived completely, but the Zry-cladding has changed significantly.

To demonstrate the damage behaviour in more detail the sections of single fuel rod simulators are photographed and shown in larger magnification. Fig. 123 to Fig. 134 give close up photographs of heated fuel rods and Fig. 135 to Fig. 159 representations of unheated fuel rods.

Fig. 123 gives cross sections of heated rods at 901 mm elevation. At this elevation all the simulators with exception of the corner rods are molten away. The full diameter of the tungsten rod is left. The cross section of corner rod 43 shows the flexibility of the oxide layer at the high temperatures of the test. The thickness of the oxide layer varies between 0.7 and 0.4 mm. The bright porous area of the Al_2O_3 pellets shows the first signs of being liquified. In Fig. 124 the refrozen melt between tungsten rods 18 and 26 (see also Fig. 118) in its oxide darker part shows the typical porous structure. On the brighter metallic part one can recognize the beginning of an even oxide layer.

In Fig. 125 the development of the interaction between cladding and pellet can be seen. On rod 43 one can recognize the local interaction on the pellet and on rod 36 more than half of the pellet section has changed into the porous structure of the refrozen melt. In Figure 126 the same types of interaction can be seen at an elevation 18 mm lower. The distortion of the correspondent fuel rods show very similar shapes. In both elevations for rod

36 one can recognize the rest of the unheated rod 37 glued to rod 36. For both rods the thickness of the oxide layer and the structure of the dissolved pellet have the same appearance.

About 150 mm lower the same rods are shown at four elevations between 109 and 75 mm. There is much less interaction in this region. The Al_2O_3 pellets have nearly the original size. The oxidation of the cladding amounts only to the half of that at 251 mm. If one also at these elevation compares the heated rods with the rest parts of the unheated rods on the same picture one again finds a similar behaviour.

In Fig. 131 to Fig. 134 the behaviour of the heated fuel rods is shown in the region of the refrozen melt. In Fig. 131 at 0 mm elevation a clear separation can be seen between the cladding and the refrozen melt. The strongest attack one can find on rod 18. More melting of the cladding can be recognized for the unheated rods. At -16 mm (Fig. 132) for rod 26 the limit between melt and cladding has disappeared. Also at this elevation there is more melting in the cladding of the unheated rods.

Fig. 133 and Fig. 134 at elevation -55 mm and -71 mm show cross sections at the height of the lower spacer. Metallic melt in contact with the cladding or the spacer seems to melt the cladding or the spacer. The boundaries disappear.

Oxidic melt in contact with cladding or spacer oxidizes the zircaloy, so that a black layer is formed along the former boundary. For the walls of the spacer this can give a double layer on both sides. For rod 43 of elevation -71 mm (Fig. 134) the remaining Zry appears to have been melted away. In the same picture in the left upper corner the cladding of unheated rod has formed a similar double oxide layer between melt on the outside and Al_2O_3 pellet on the inside.

Fig. 135 to Fig. 138 show cross section of remnants from unheated rods at 269 mm and 251 mm elevation. These pictures demonstrate the process of the disintegration of the pellet. We can always find the following steps: change of the colour of the pellet from white to black and then the formation of a very porous structure. In Fig. 139 to Fig. 147 the aquivalent cross sections are given for the elevation 109, 93 and 91 mm. Also here the same behaviour is found.

Fig. 148 to 159 show the cross sections of the unheated rods in the region of refrozen melt for the cross sections at 0, -16, -55 and -71 mm. At 0 mm elevation the central unheated rod is disappeared completely. The rods 15, 9, 17, 25 in one corner of the bundle have lost nearly the cladding by interaction with the melt. Rods 21, 29, 37, 31 grouped on the opposite corner have kept their boundaries by forming an oxide layer against the adjacent refrozen melt.

At -16 mm elevation the unheated show nearly the same behaviour with a slight increse in the tendency to form an oxide layer at the surface of the cladding.

At -55 mm elevation also the center unheated rod 23 has survived. For rods 21, 15, 9, 17 from the cladding only a relatively thin strong deformed layer is left. There is only minor attack on the cladding. In the neighbourhood of rod 29 or 37 one can clearly see the oxide layer formation by the melt in contact with the Zry of the spacer.

In Fig. 157 on the cross section at -71 mm elevation one can clearly see the difference between in the influence of metallic and oxidic melt on the cladding. Rod 25 is surrounded by metallic melt. Here the cladding is dissolved by the surrounding melt. Rod 37 is surrounded by oxidic melt. The outer layer of the cladding is oxidized, but the cladding has kept its shape. On the inner surface of the cladding one can recognize the uptake of oxygen in contact to the Al_2O_3 pellet. Quite a different behviour is seen in the contact area between Al_2O_3 pellet and former cladding for the cross sections of Figures 158 and 159. Here strong melting of the zircaloy can be recognized.

Fig. 160 shows the oxidation behavior of heated rod 43 at elevations between 109 mm and 75 mm. In parallel to the oxidation by steam on the outside surface, there is a remarkable oxygen uptake on the inner surface.

The bundle between 73 mm and 1 mm elevations was seperated by vertical cuts as shown in Fig. 162. The resulting vertical surfaces are shown in Figures 161 to 163. The cross sections confirm, that the inner heated and unheated rods are molten away. Only the tungsten heaters are left. Oxidic melt has formed a crucible by gluing together the outer heated and unheated rods by refrozen melt. The bottom of the crucible extends at an elevation of about 20 mm. Below a cover of oxidic melt a central globul of metallic melt is

found. As discussed in detail in /21/, the refrozen oxidic melt is an Al_2O_3/ZrO_2 eutectic and the metallic melt an Al/Zr eutectic alloy. The enlarged presentations of the cross sections in Figures 164 to 168 clearly show the typical porosity of the refrozen oxidic melt. In Fig. 166 at the lower range of the cross sections the central metallic globule can be recognized.

The crucible is filled with rubble. This loose lying rubble consists mainly of cladding remnants and refrozen melt dropplets. The fact that the rubble is not glued together, points out that it must have fallen down from the higher region of the bundle during the cool down phase.

In Figures 169 to 178 enlarged representations of contact region between pellets and melt for different elevations of the vertical cross sections are given. The dissolution of Al_2O_3 pellet by the melt can be clearly recognized. Details of this process are discussed in more detail in /21/.

10. Conclusions

- Test CORA-B could demonstrate the successful operation of the CORA-test facility and deliver information of the behavior of Zry/Al_2O_3/B_4C burnable poison rods.
- Great quantities of ceramic and metallic melts were formed.
- The formation of liquid phases due to the Al_2O_3/Zr interaction started at 1350°C and increased strongly at 1500°C.
- The relocated and solidified melts formed large blockages in the lower region of the bundle. A remarkable porosity of the ceramic melt could be observed.
- The crust of the re-solidified material acts as a catcher for the fragments of the embrittled bundle components.
- Conclusion for burnable poison rods in the fuel element: Since strong chemical interaction between Al_2O_3 and Zry take place, the resulting melt can liquify the Zry much below the melting temperature of Zry (1760°C). Also the UO_2 is attached by the melt.

11. Acknowledgements

The performance and evaluation of the test was only possible with the contribution of many people. The assembly of the test rods and preparation of other bundle components were performed by Messrs. E. Mackert and H. Krause. The bundle was assembled by Messrs. O. Heil, H. Giesmann and Pf. Pfann. Messrs. H. Malauschek and K.P. Wallenfels are acknowledged for the preparation and installation for special test instrumentations and their operation during the test. We thank Messrs. A. Grünhagen and R. Heine for their contribution to the data evaluation.The authors would like to thank Messrs. H. Benz, W. Rötzel and H.J. Röhling for the preparation and performance of the test. We are grateful to Mr. L. Anselment for the sectioning of the bundle and the preparation for the metallographic samples.

The authors would particularly like to thank Dr. P. Hofmann, G. Schanz and L. Sepold for the many discussions in connection with the preparation and performance of this test. We thank Dr. H. Rininsland and Dr. H. Kapulla for the support of the investigations. Finally we thank Mrs. U. Ivanitsch for the careful typing of the manuscript. The work is sponsered by "Projektgruppe LWR-Sicherheit" (PRS). We thank Dr. B. Kuczera for his support.

12. Literature

1. A. FIEGE, Severe Fuel Damage Investigations of KfK/PNS, KfK 3431B, 1983

2. S. HAGEN, et.al.; CORA-Program. KfK 3677 (1986)

3. P. HOFMANN, D.K. KERWIN-PECK; UO_2/Zry Chemical Interactions under Isothermal and Transient Temperature Conditions. J. of Nucl. Mat. 124 (1984) 80-105

4. P. HOFMANN, et.al.; Temperaturtransiente UO_2/Zircaloy-Reaktionsexperimente unter oxidierenden Bedingungen, PNS-Jahresbericht 1984, KfK 3550 (1985) p. 4200/76

5. P. HOFMANN, et.al.; Chemische Auflösung von festem UO_2-Brennstoff durch geschmolzenes Zircaloy-Hüllmaterial, PNS-Jahresbericht 1985, KfK 4000 (1986), p. 4200-56-59

6. S. LEISTIKOW, G. SCHANZ, H.v. Borg, A.E. Aly; Comprehensive Presentation of Extented Zircaloy-4 Steam Oxidation Results (600-1600°C), OECD-NEA-CSNI/IAEA Specialists Meeting on Water Reactor Fuel Safety, Riso National Laboratory (Denmark), 16-20 May, 1983, 188-199, RISØ

7. S. HAGEN; Out-of-pile Experiments on the High Temperature Behaviour of Zry-4 Clad Fuel Rods. KfK 3567 (1983).

8. S. HAGEN, H. MALAUSCHEK, K.P. WALLENFELS. S.O. PECK; Temperature Escalation in PWR Fuel Rod Simulators due to the Zircaloy/Steam Reaction: Tests ESSI 1-3, Test Results Report, KfK 3507 (1983).

9. S. HAGEN, H. MALAUSCHEK, K.P. WALLENFELS, S.O. PECK; Temperature Escalation in PWR Fuel Rod Simulators due to the Zircaloy/Steam Reaction: Tests ESSI 4-11, Test Results Report, KfK 3557 (1985)

10. S. HAGEN, S.O. PECK; Temperature Escalation of Zircaloy-Clad Fuel Rods and Bundles under Severe Fuel Damage Conditions. KfK 3656 (1983).

11. S. HAGEN, S.O.PECK; Out-of-pile Bundle Temperature Escalation under Severe Fuel Damage Conditions. KfK 3568 (1983)

12. S. HAGEN, H. MALAUSCHEK, K.P. WALLENFELS, S.O. PECK; Temperature Escalation in PWR Fuel Rod Simualtors due to the Zircaloy/Steam Reaction: Bundle Test ESBU 1, Test Results Report, KfK 3508 (1983)

13. S. HAGEN, H. MALAUSCHEK, K.P. WALLENFELS, B.J. BUESCHER; Temperature Escalation in PWR Fuel Rod Simulators due to the Zircaloy/Steam Reaction: Bundle Test ESBU 2A, Test Results Report; KfK 3509 (1984)

14. S. HAGEN, et. al.; Post Test Investigation for Single Rod Tests ESSI 1-11, KfK 3768 (1987)

15. S. HAGEN, et.al.; Post Test Investigations for Bundle Test ESBU-1, KfK 3769 (1986)

16. S. HAGEN, et. al.; Post Test Investigations for Bundle Test ESBU 2A, KfK 3789 (1986)

17. S.HAGEN, Damage Behaviour of (AgInCd)Absorber in PWR Fuel Rod Simulator Bundles under Severe Fuel Damage Conditions, Test Results Report, KfK 4102, to be published

18. S. HAGEN, P. HOFMANN; Behaviour of B_4C-Absorber Rods under SFD Conditions, KfK 4103, to be published

19. S. HAGEN, P. HOFMANN; Physical and Chemical Behavior of LWR Fuel Elements up to very High Temperatures, KfK 4104, Juni 1987

20. S. HAGEN, W. HERING, K. VOGEL; CORA-Scoping Test C, Test Results Report, KfK 4312, to be published

21. S. HAGEN, L. SEPOLD, P. HOFMANN, G. SCHANZ; Interaction between Zry-cladding and AL_2O_3-pellet, Post Test Investigation of Tests CORA-B and CORA-C, KfK 4313, to be published

List of Figures

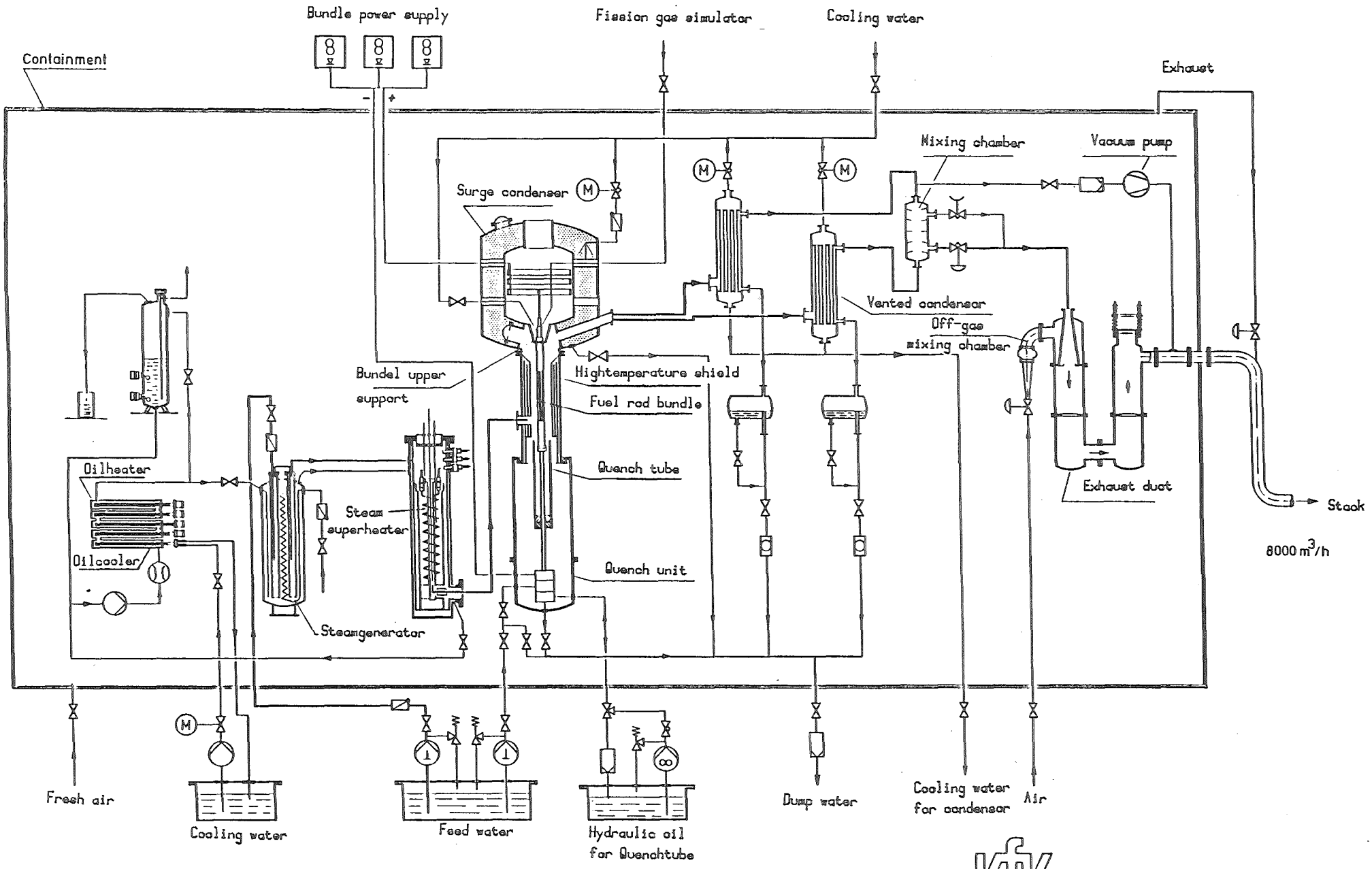

Fig. 1 : Scheme of the CORA Test Facility

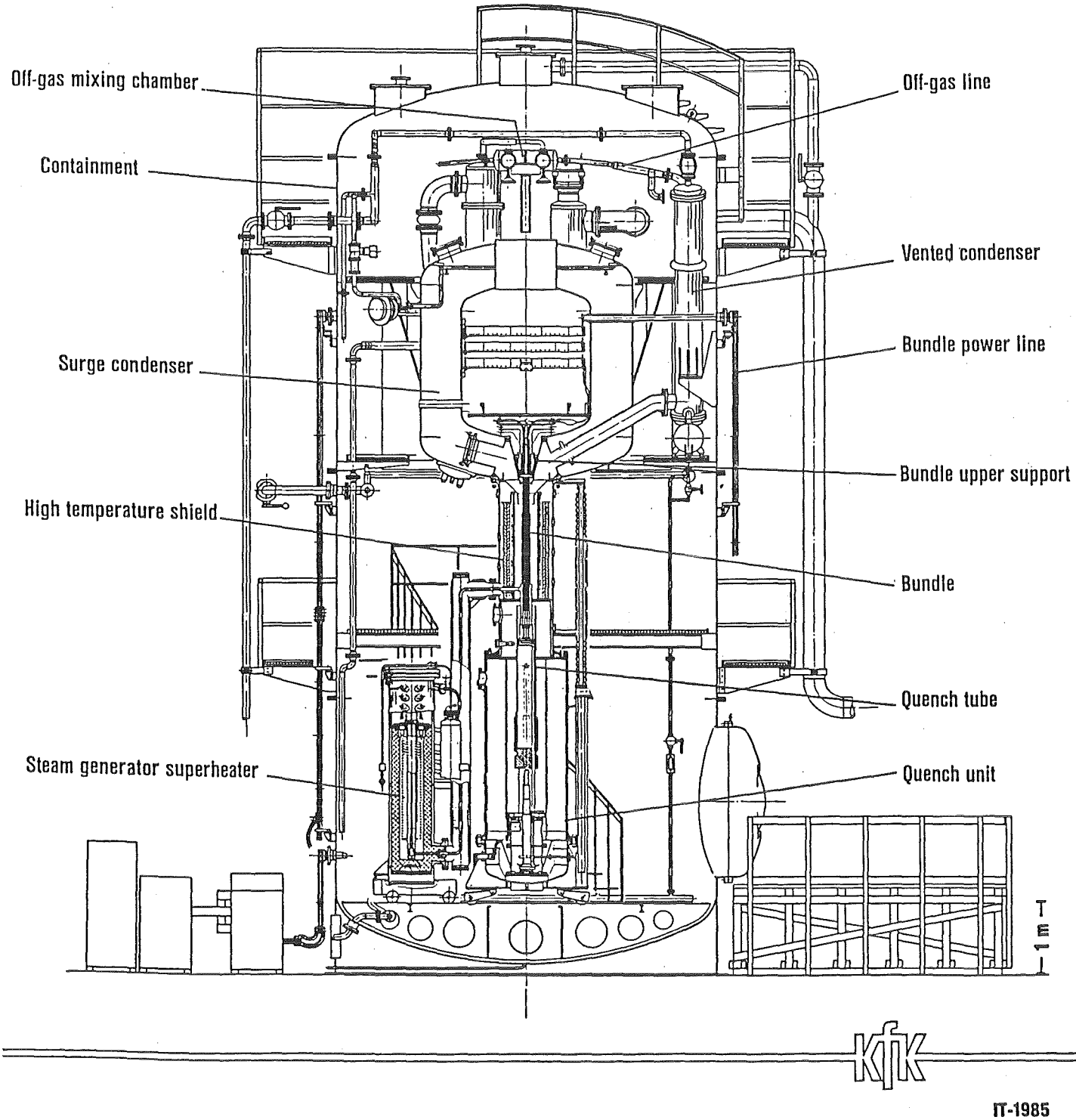

Fig. 2 : SFD-Test Facility CORA

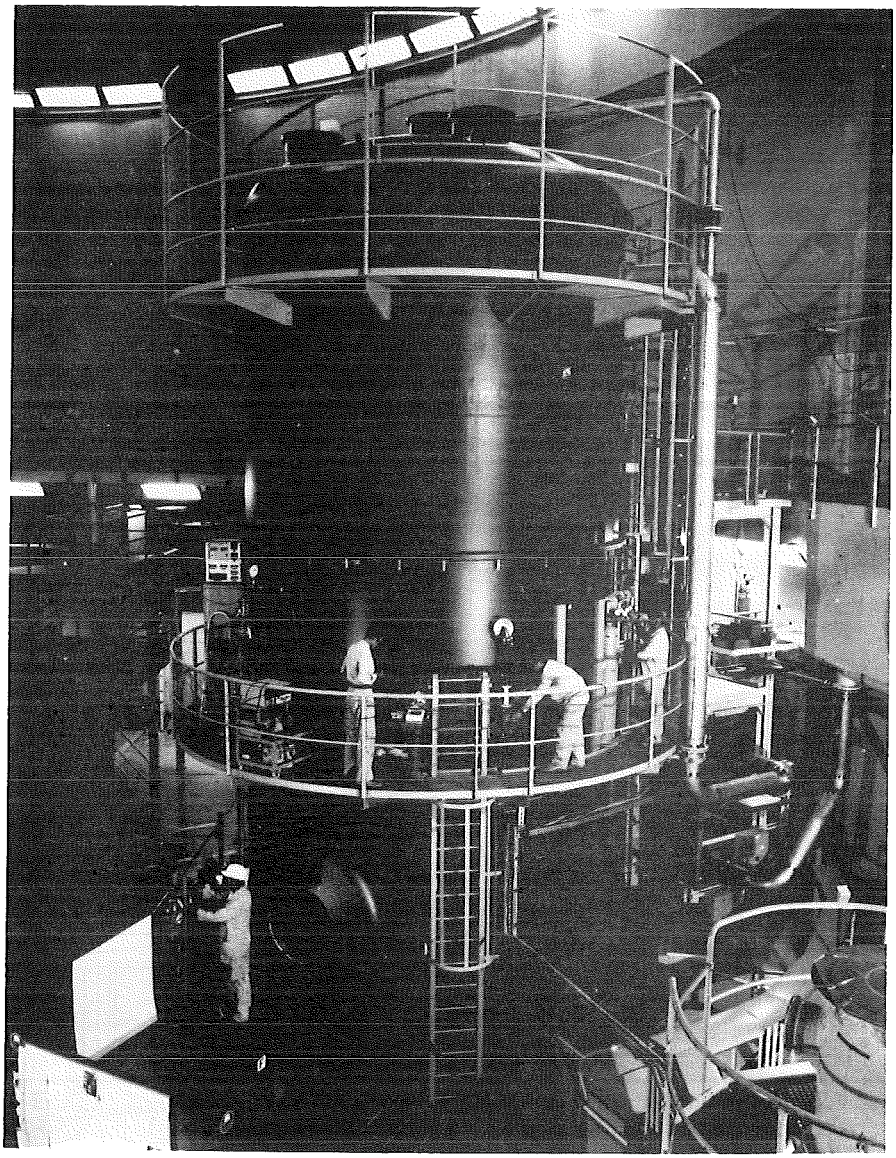

Fig. 2a : Photograph of the CORA Test Facility

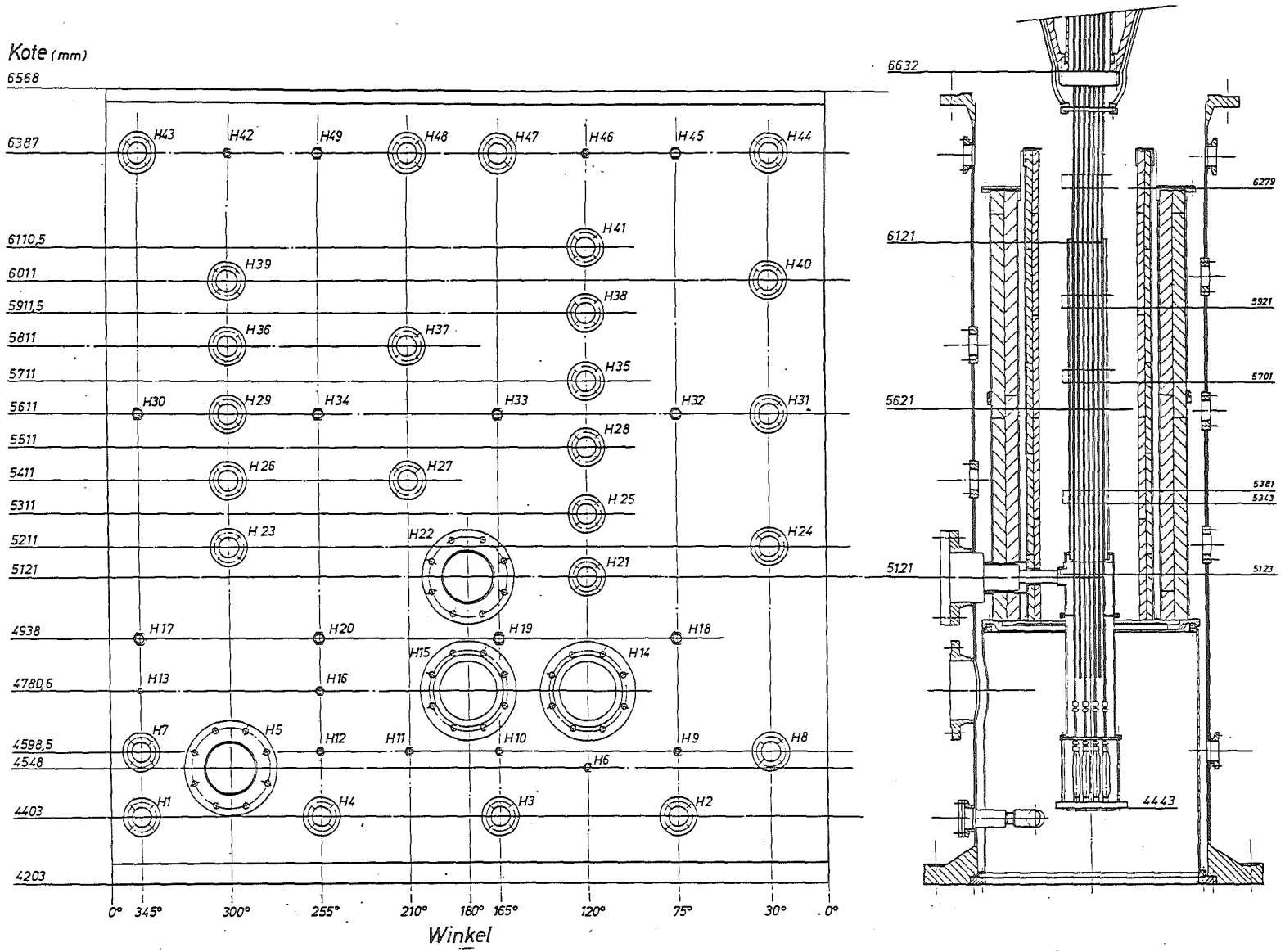

Fig. 3: Vertical cross section of bundle in high temperature shield and position of flanges in the outer wall

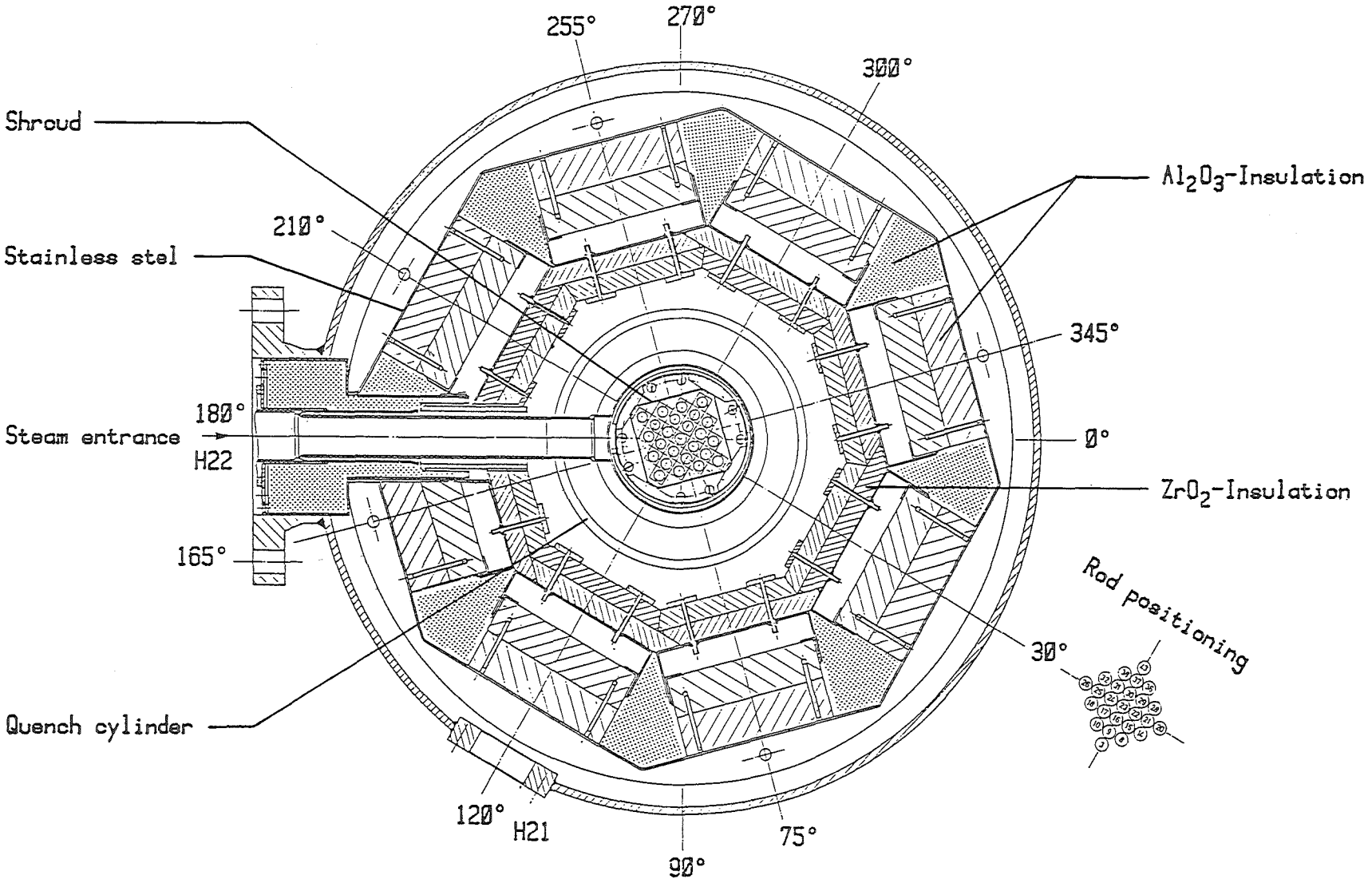

Fig. 4: Cross section of high-temperature-shield

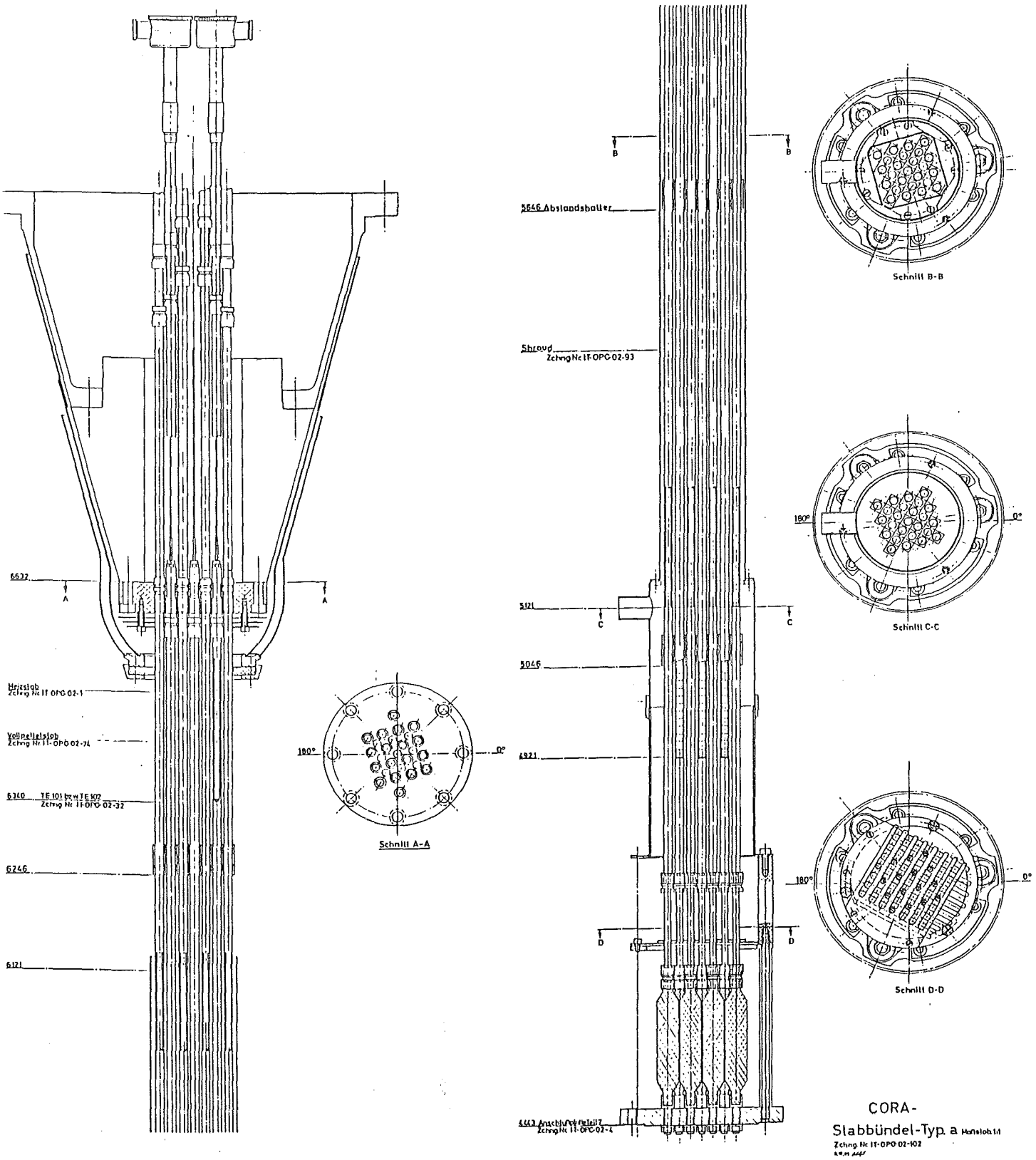

Fig. 5:
CORA bundle B vertical and horizontal cross sections

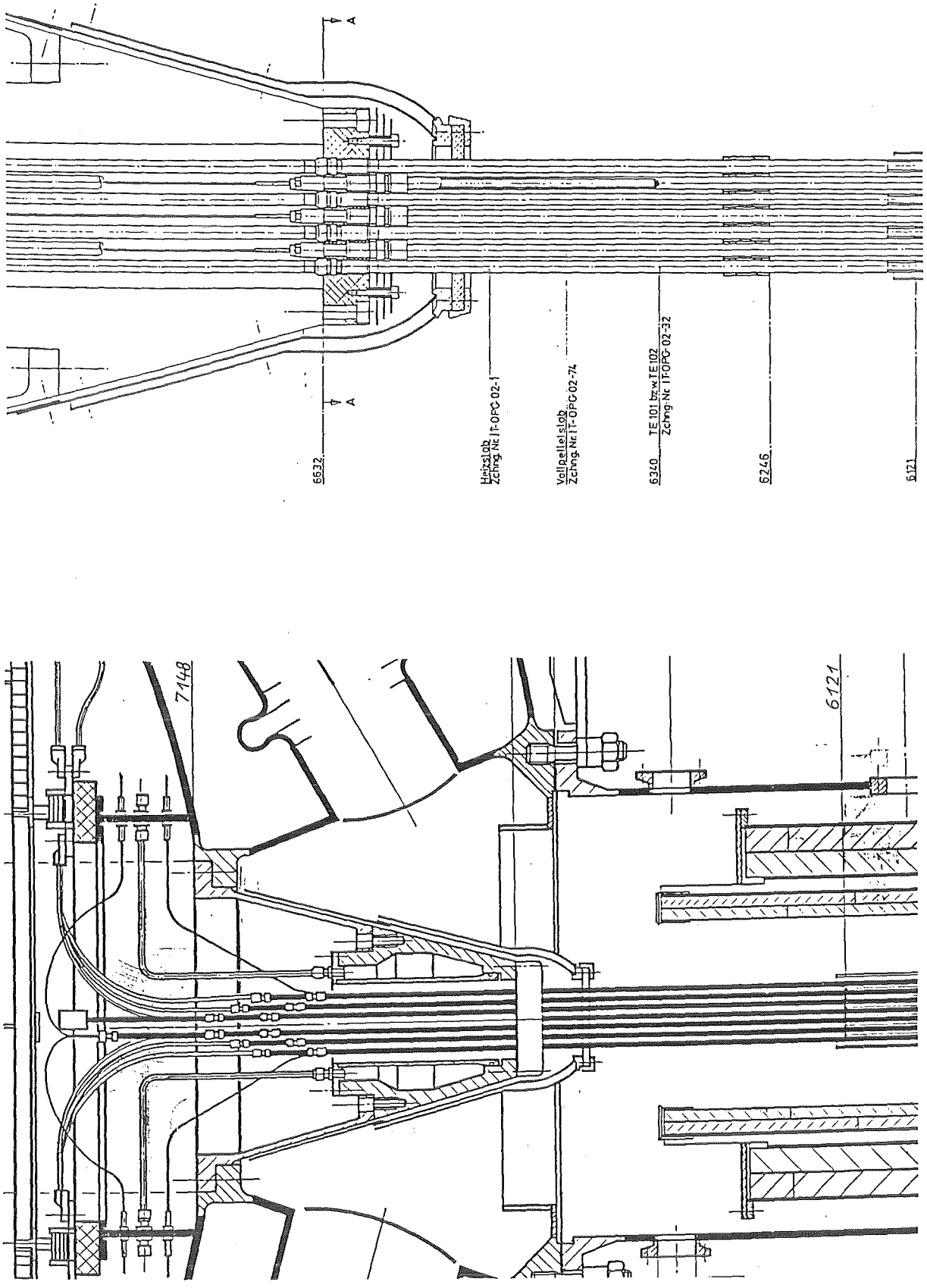

Fig. 7: Upper end of CORA bundle B

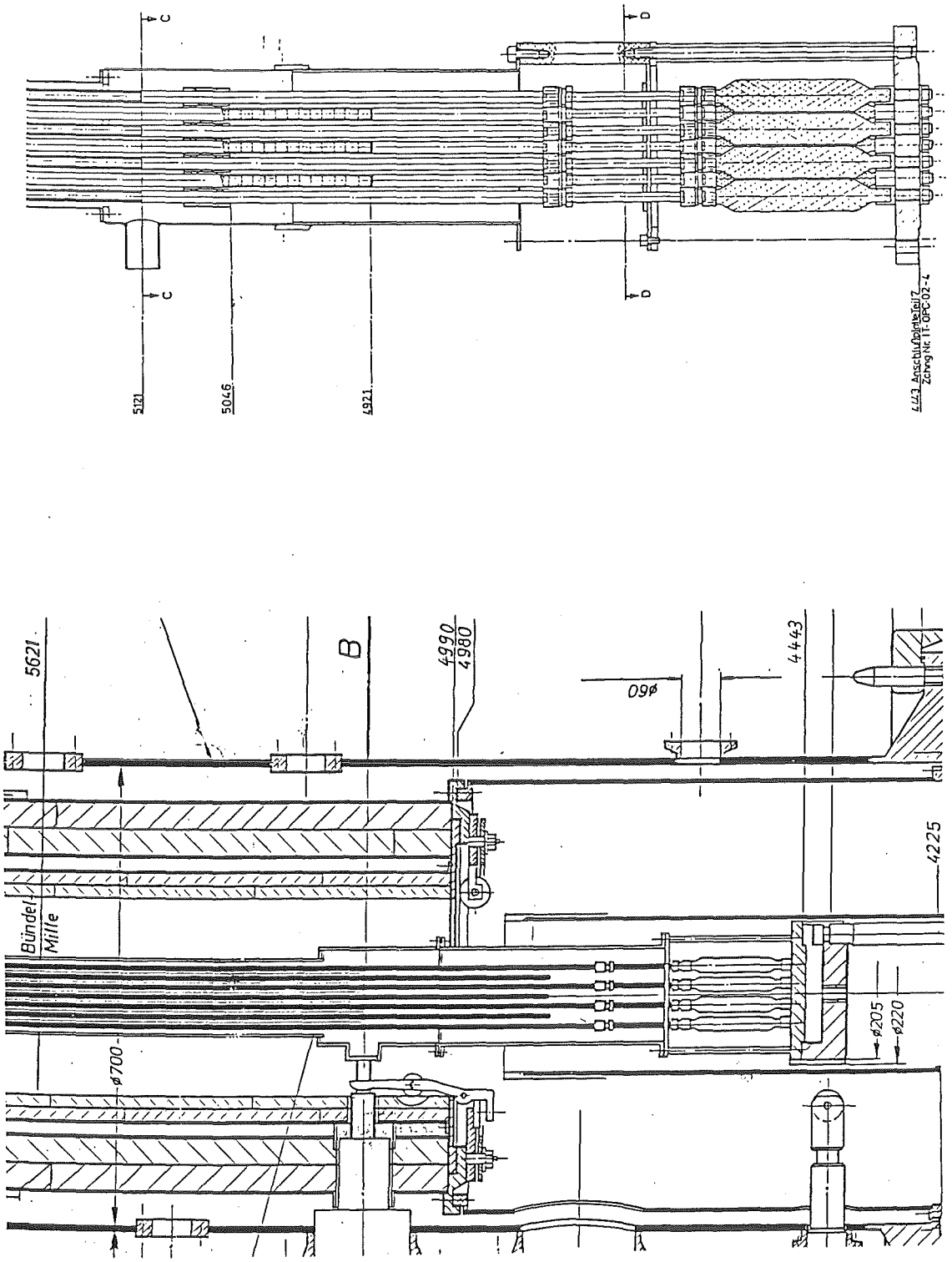

Fig. 8: Lower end of CORA bundle B

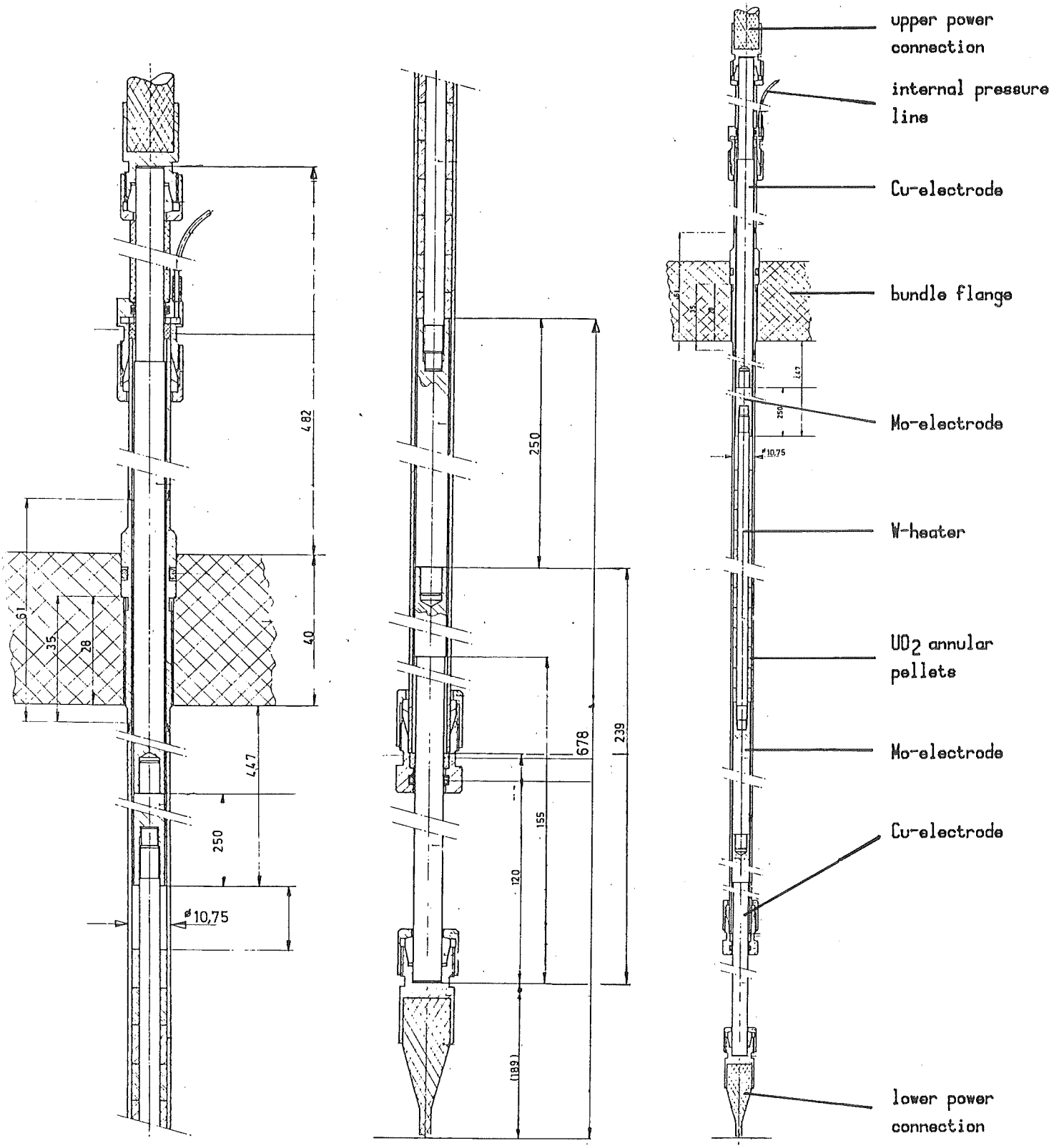

Fig. 9 : Heated fuel rod.

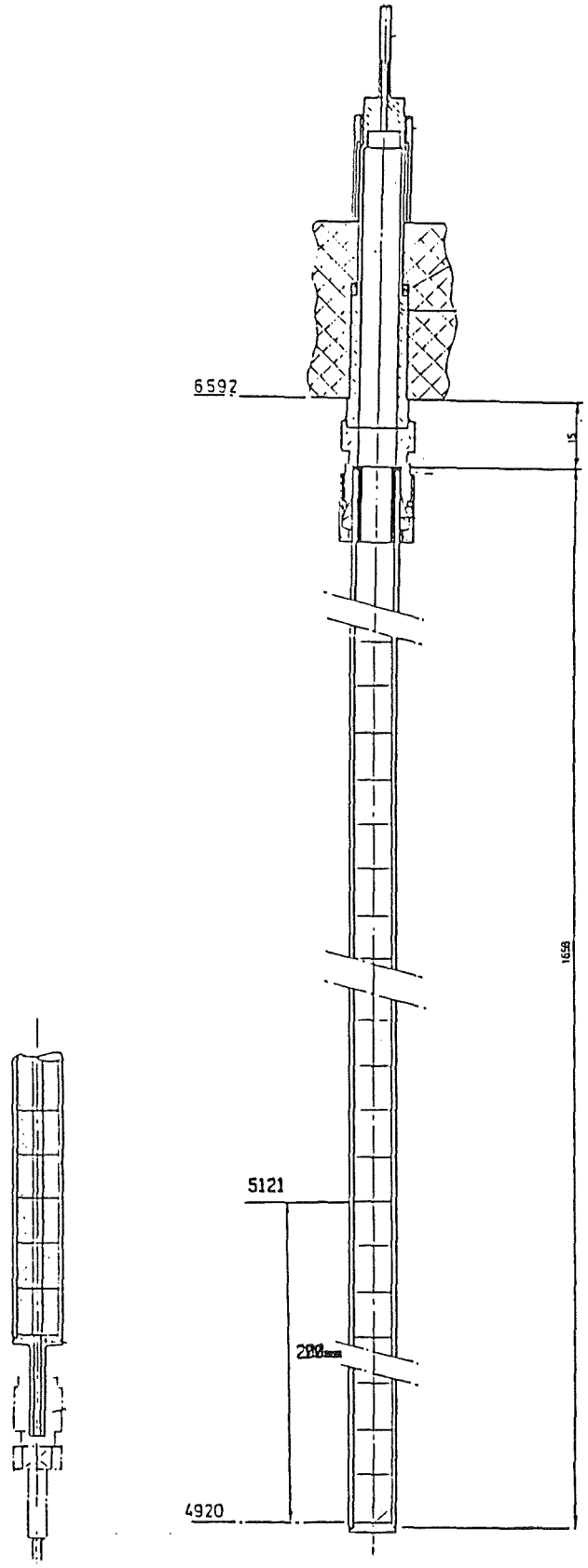

Fig. 9 a: Unheated fuel rod simulator

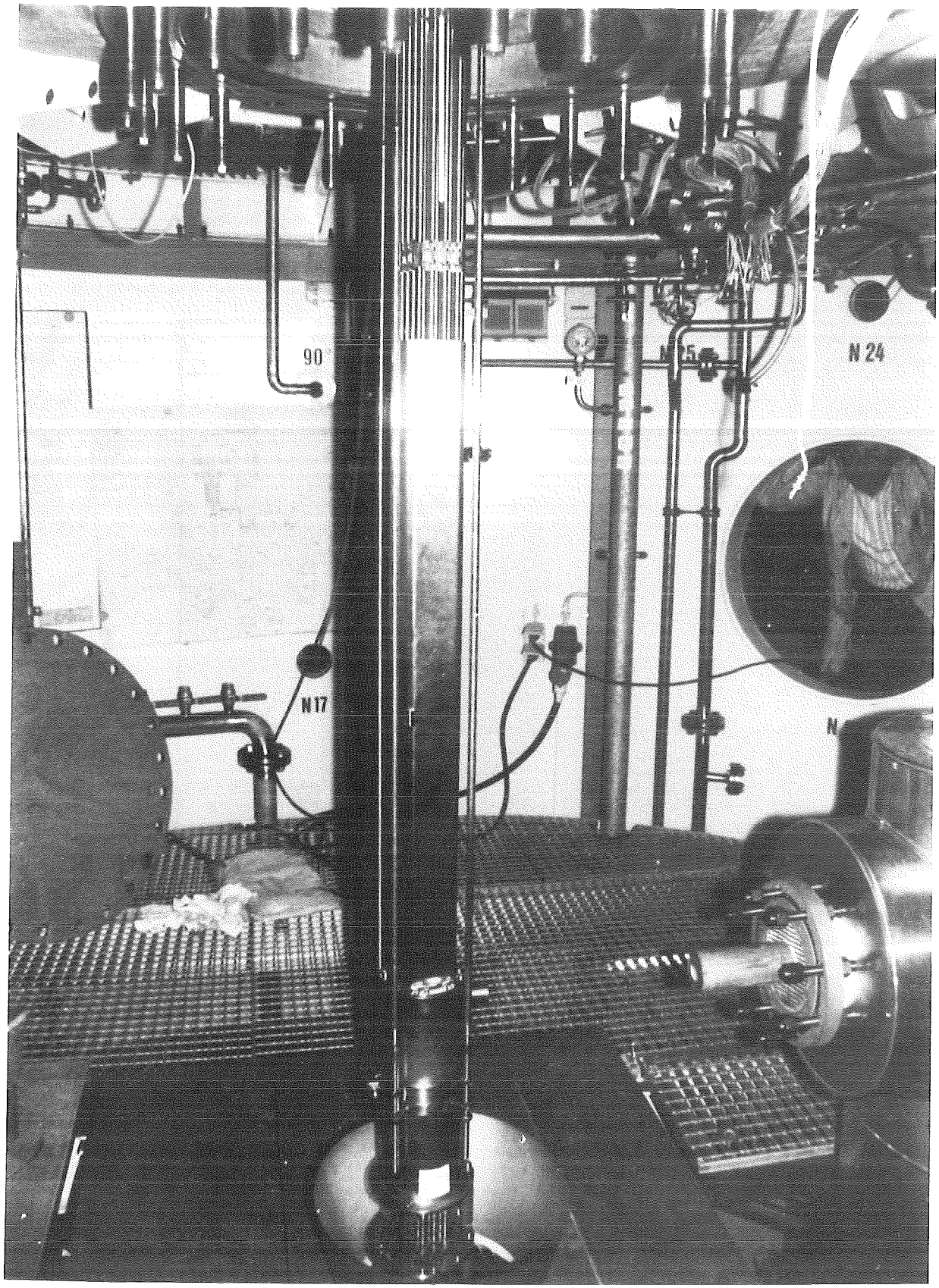

Fig. 10:
CORA bundle B with high temperature shield removed

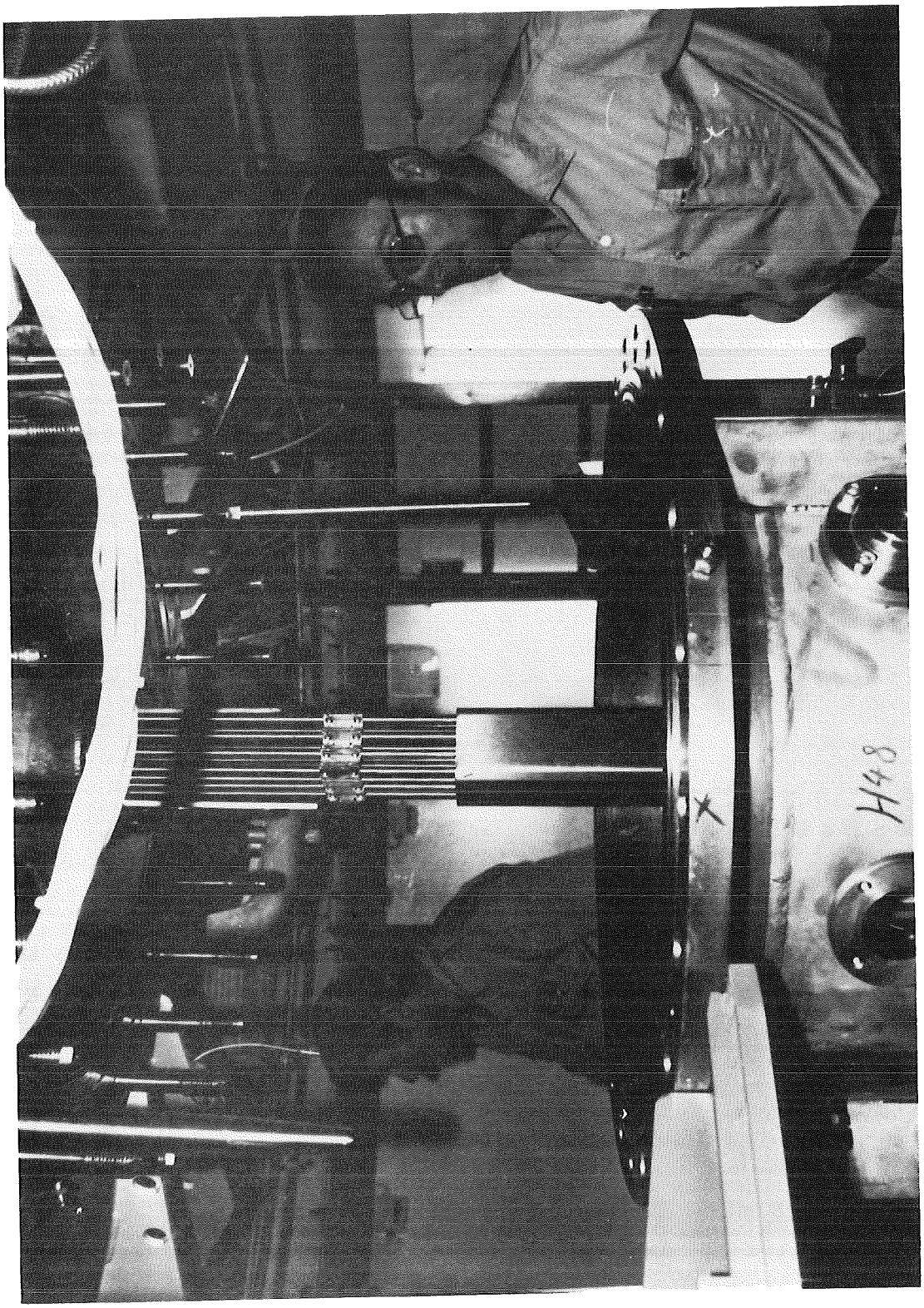

Fig. 11: PARTIALLY LOWERED HIGH TEMPERATURE SHIELD

Fig. 12: BUNDLE INSIDE HIGH TEMPERATURE SHIELD

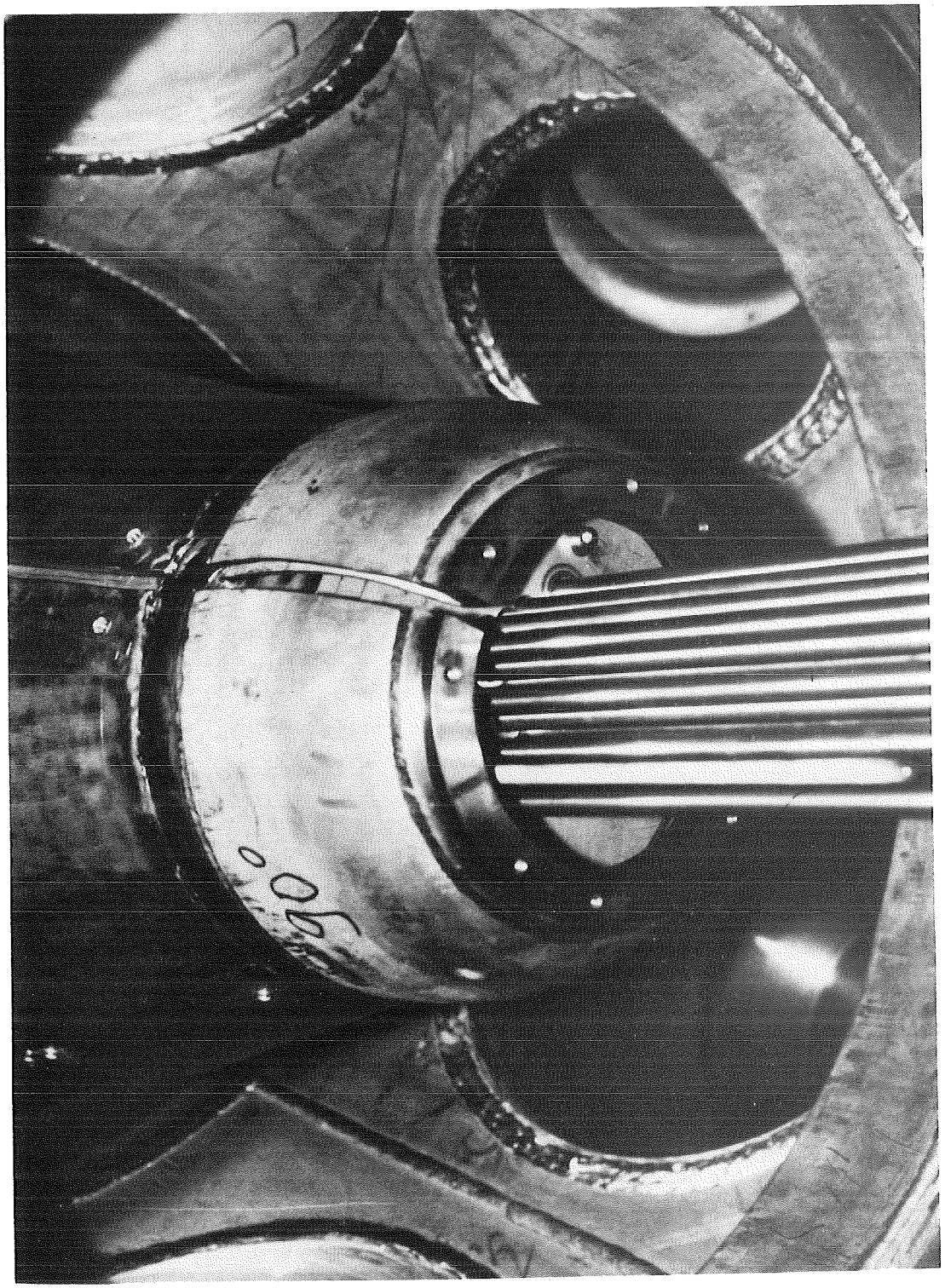

Fig. 13: BUNDLE UPPER END WITH RADIATION SHIELDS FOR HEAD PLATE

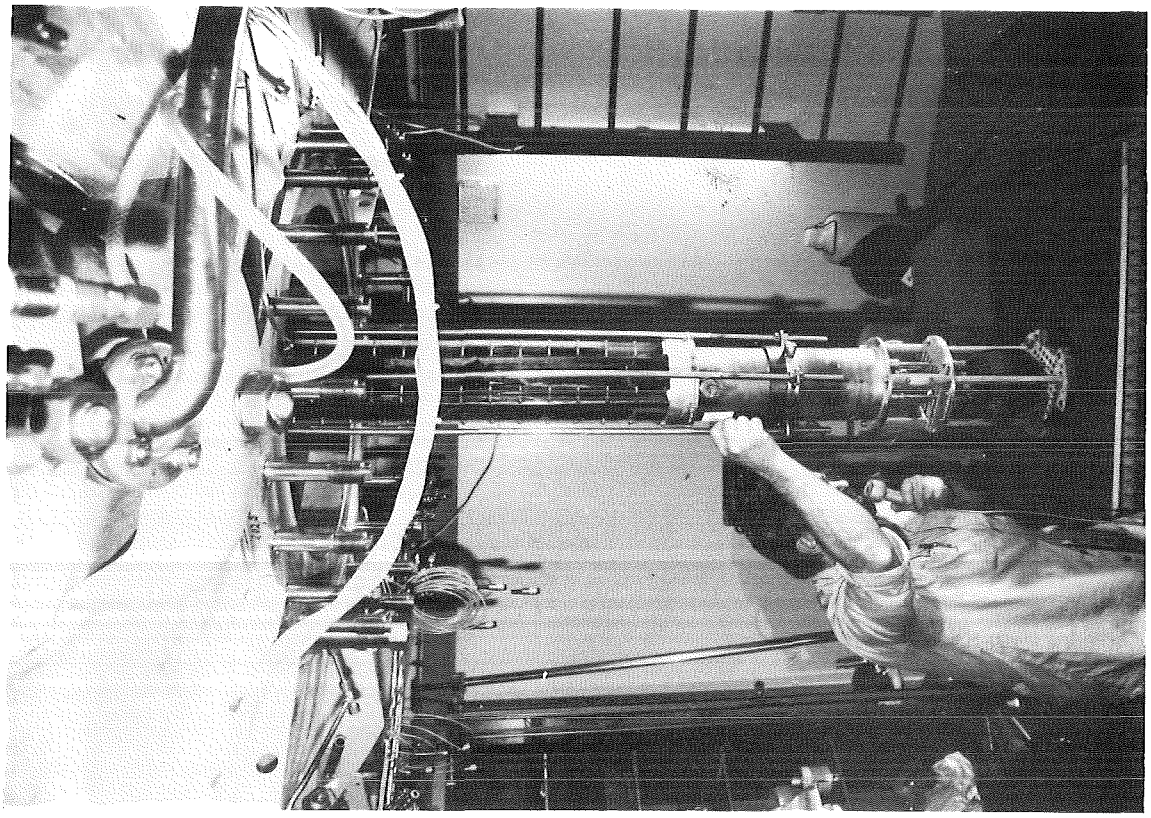

Fig. 13b: Removal of bundle out of facility.

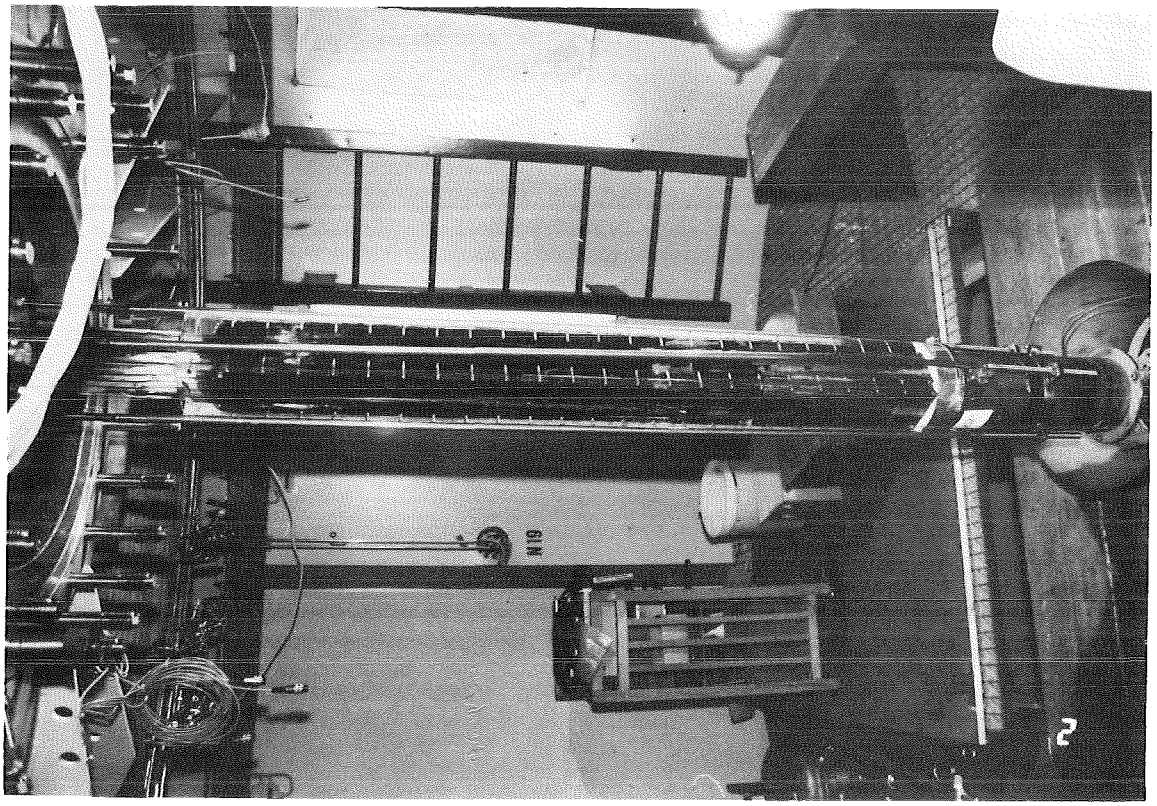

Fig. 13a: CORA bundle B put into epoxy

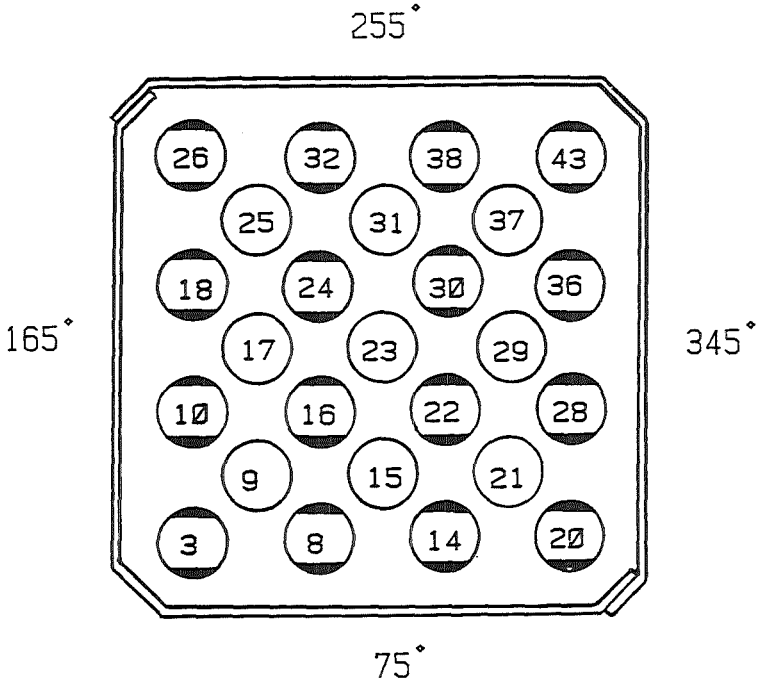

Fig. 14:
Heated (⬭) and unheated rods (○) of CORA bundle B

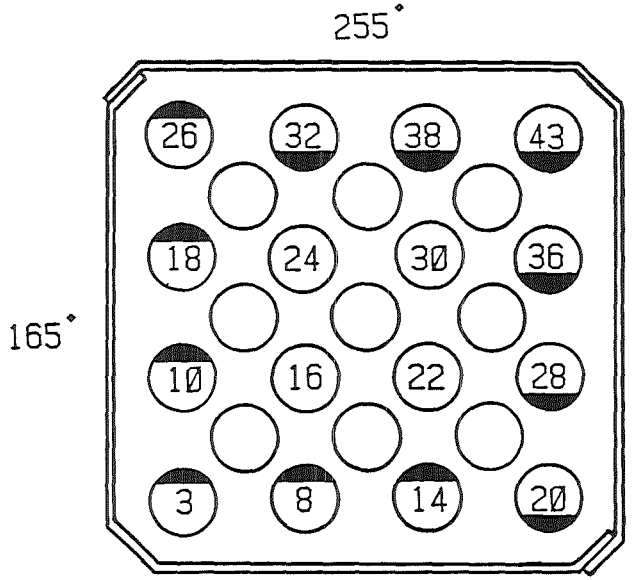

Fig. 15:

GROUP 1 (32, 38, 43, 36, 28, 20)

GROUP 2 (26, 18, 10, 3, 8, 14)

GROUP 3 (24, 30, 16, 22)

Distribution of rods to groups for heated fuel rod simulators (CORA bundle B)

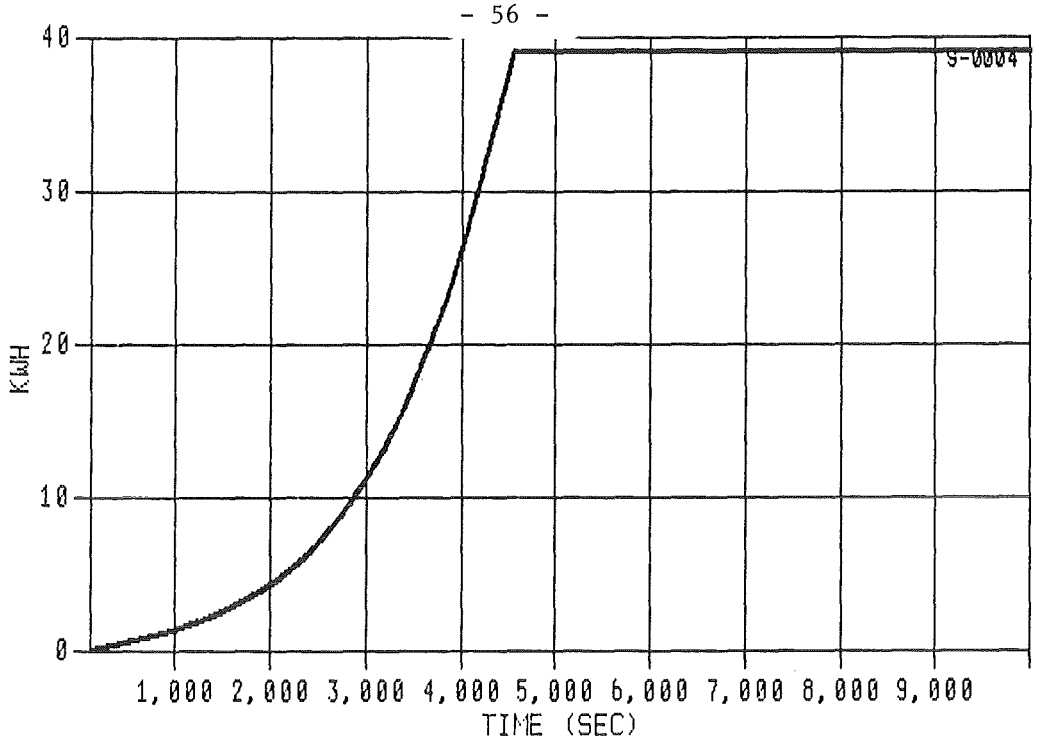

Fig. 16:
Energy input to the CORA bundle B

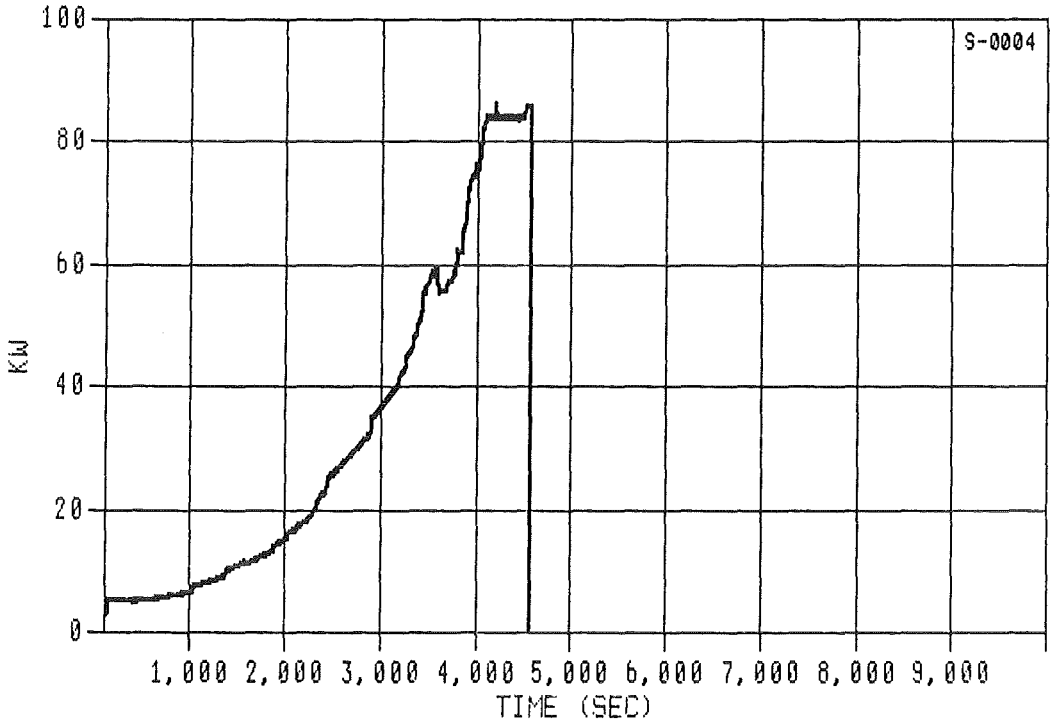

Fig. 17:
Total power input for high temperature test CORA bundle B

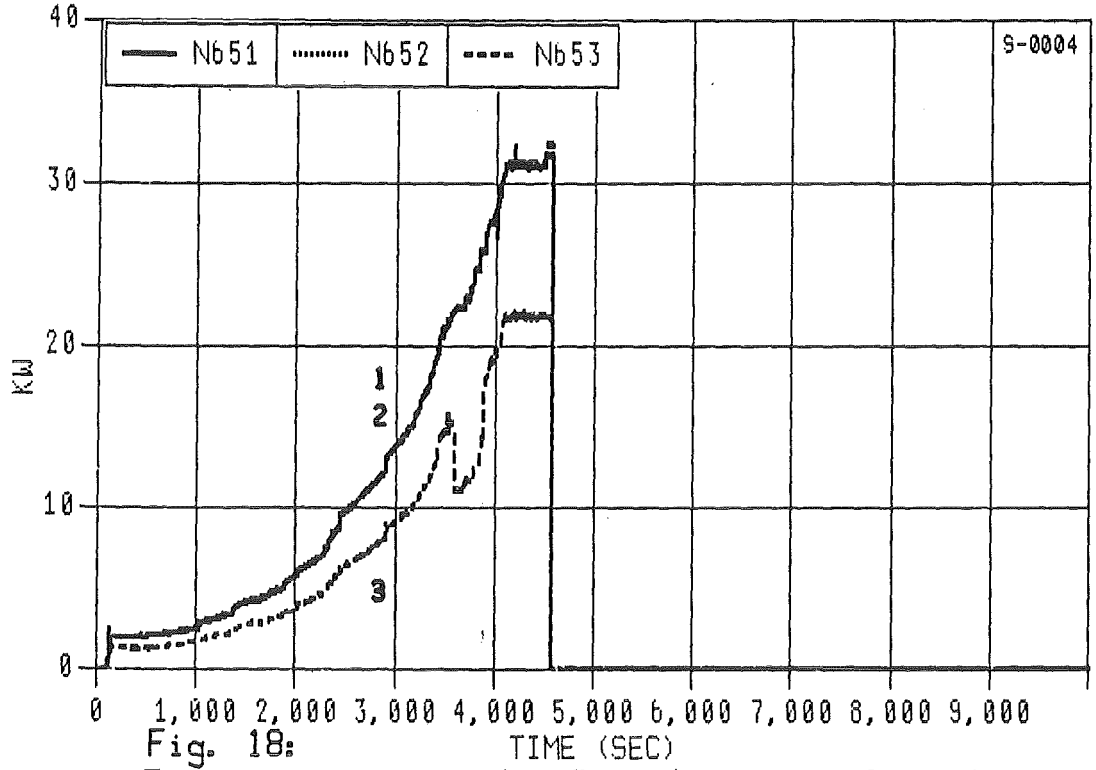

Fig. 18: Power input to the 3 rod groups for the high temperature test CORA bundle B

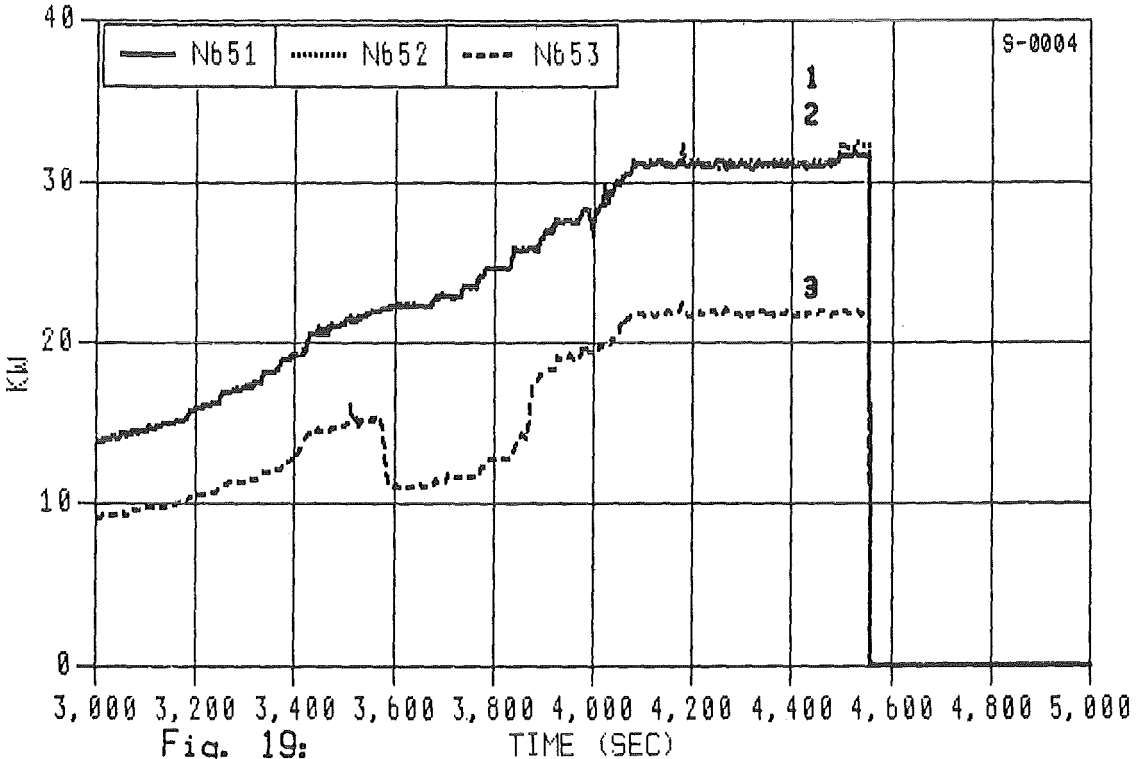

Fig. 19: Power input to the 3 rod groups for the high temperature test CORA bundle B

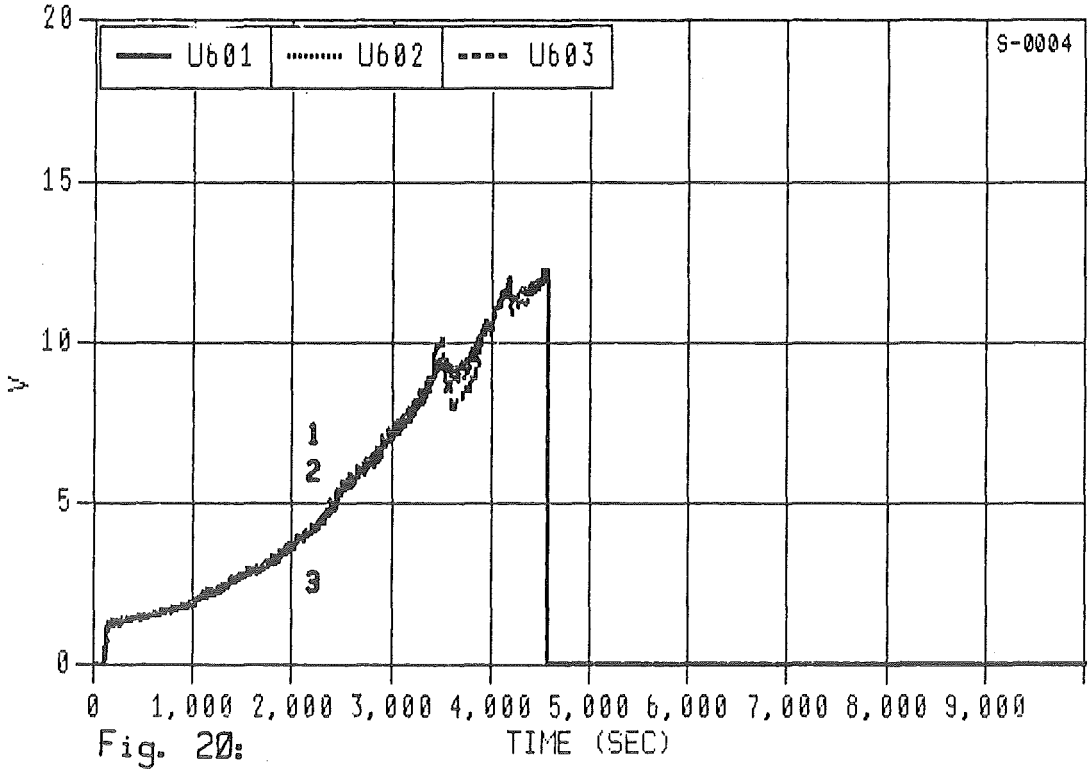

Fig. 20: Voltage input to the 3 rod groups for the high temperature test CORA bundle B

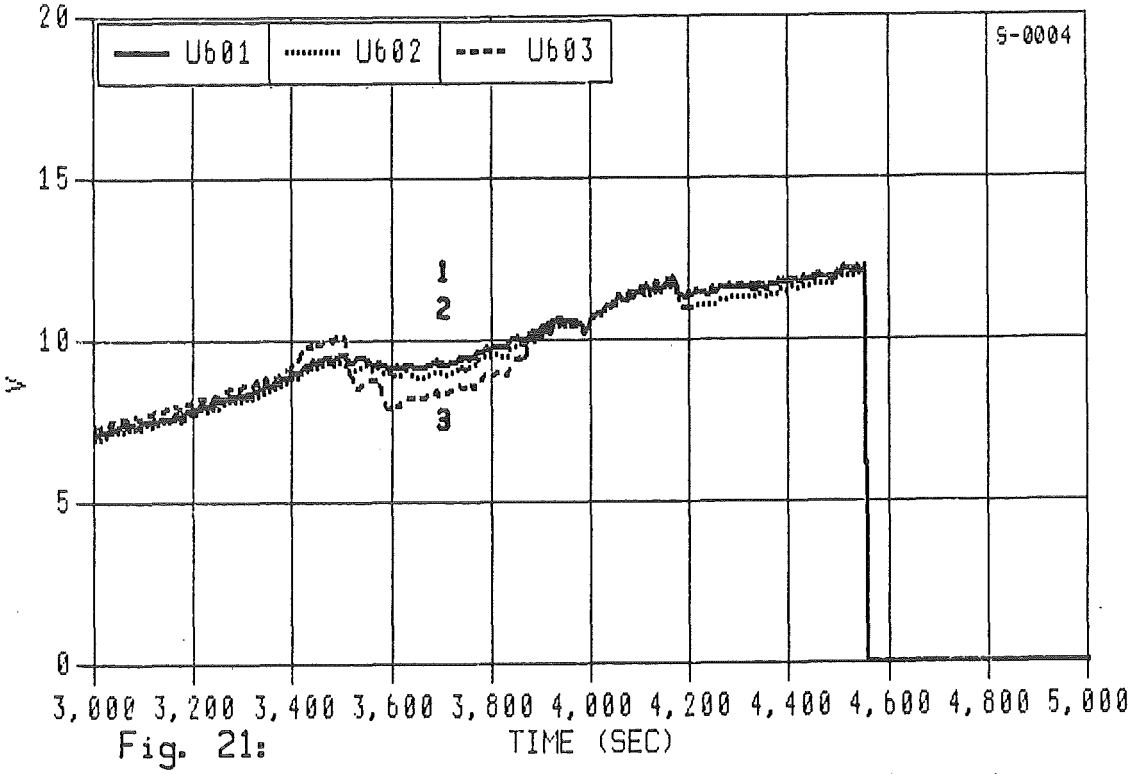

Fig. 21: Voltage input to the 3 rod groups for the high temperature test CORA bundle B

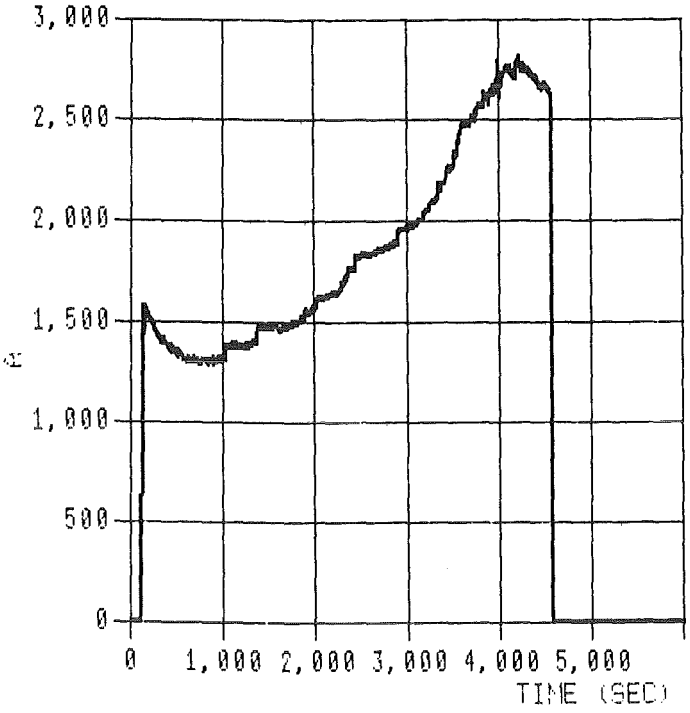

group 1

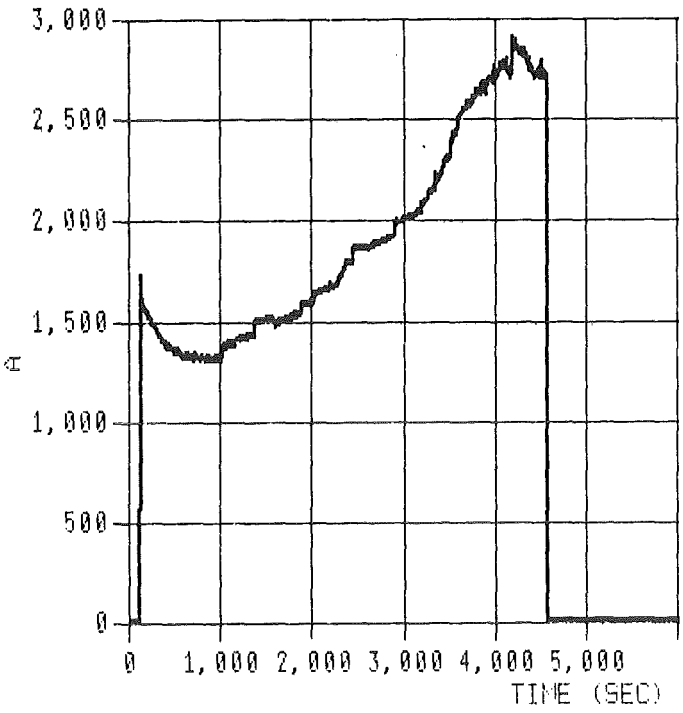

group 2

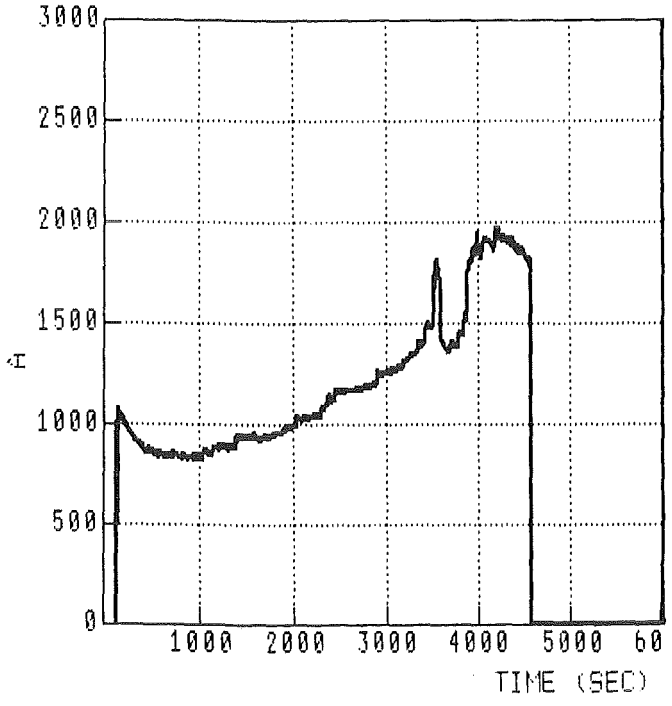

group 3

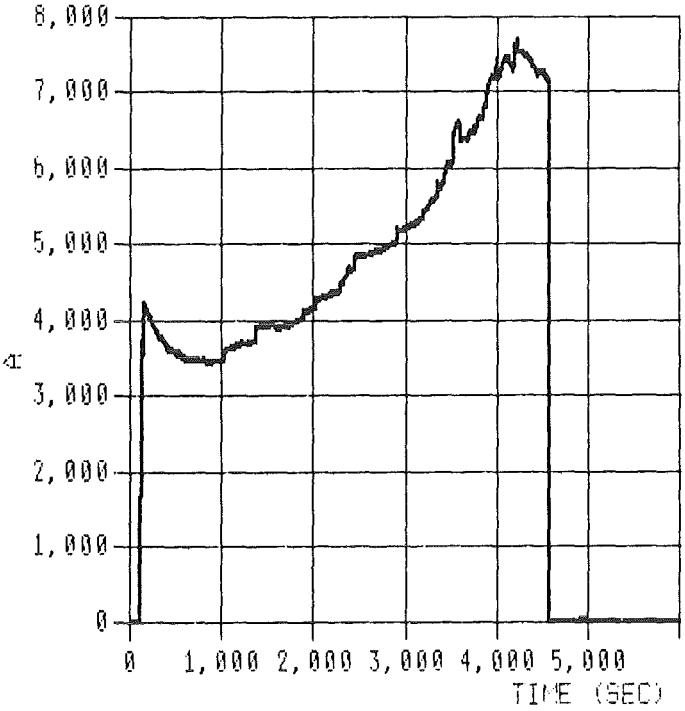

total

Fig. 22:
Currents of groups and total current
CORA bundle B

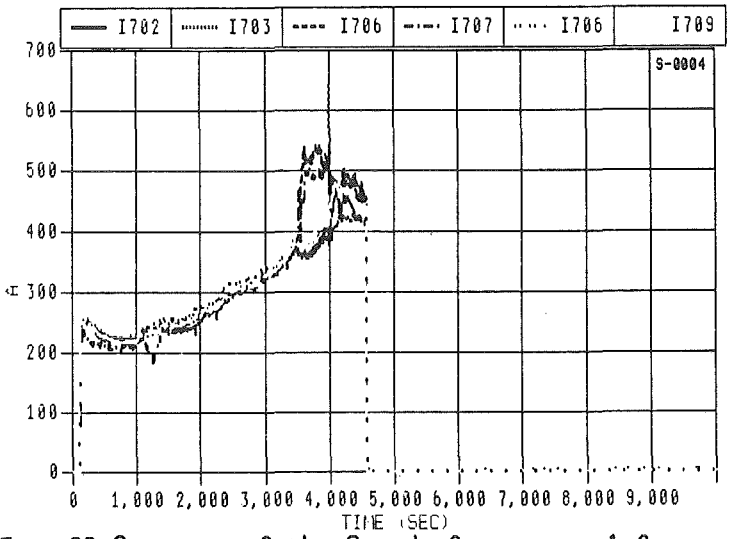

Fig. 23: Currents of the 6 rods from group 1 for high temperature test CORA bundle B

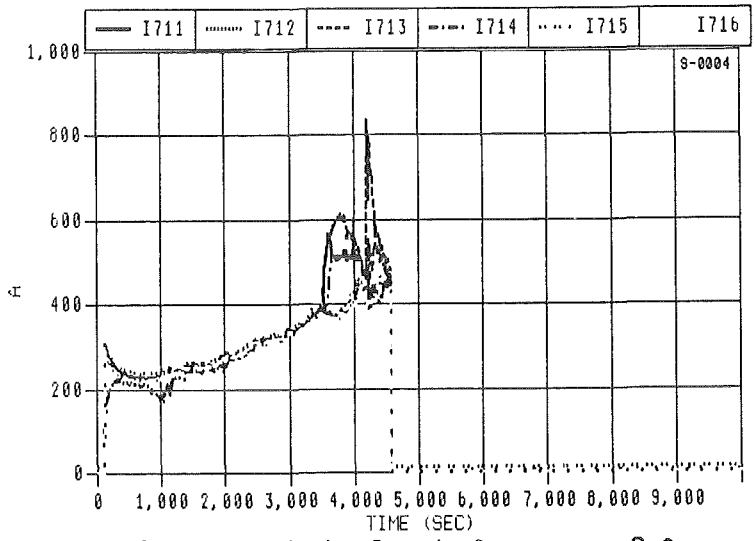

Fig. 24: Currents of the 6 rods from group 2 for high temperature test CORA bundle B

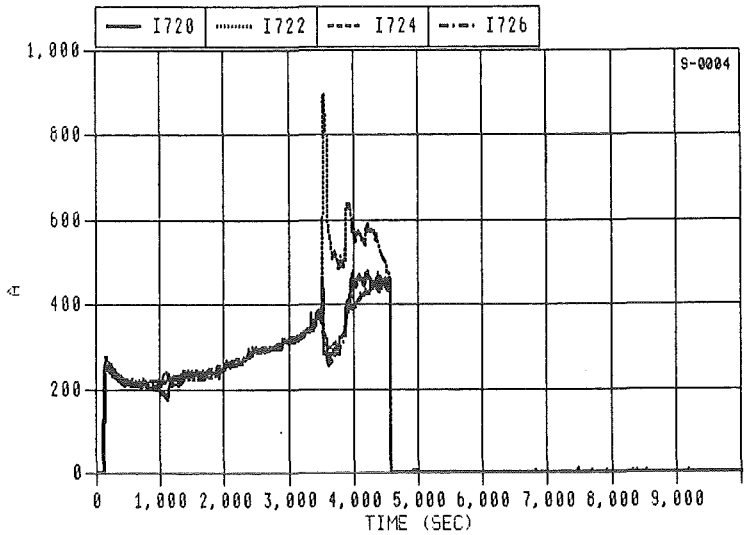

Fig. 25: Currents of the 4 rods from group 3 for high temperature test CORA bundle B

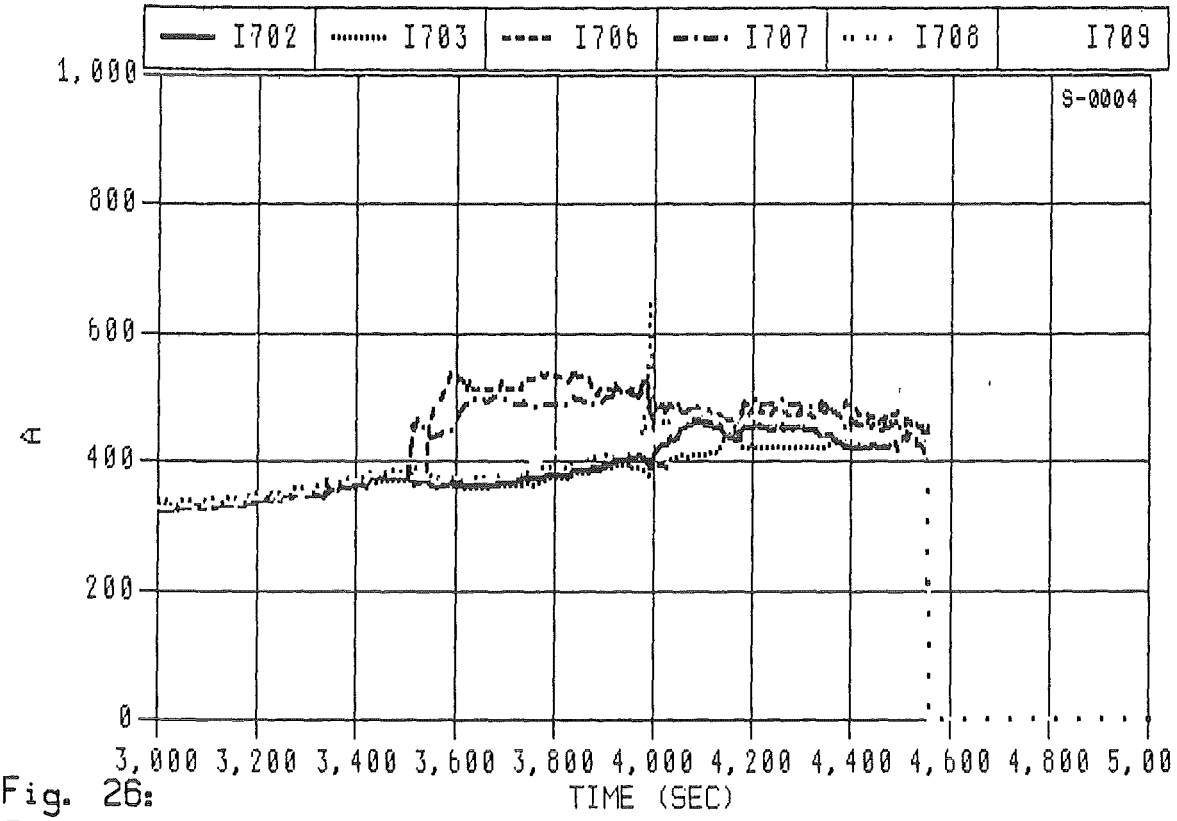

Fig. 26:
Fluctuation of Currents through the 6 rods from group 1 due to melt formation for high temperature test CORA bundle B

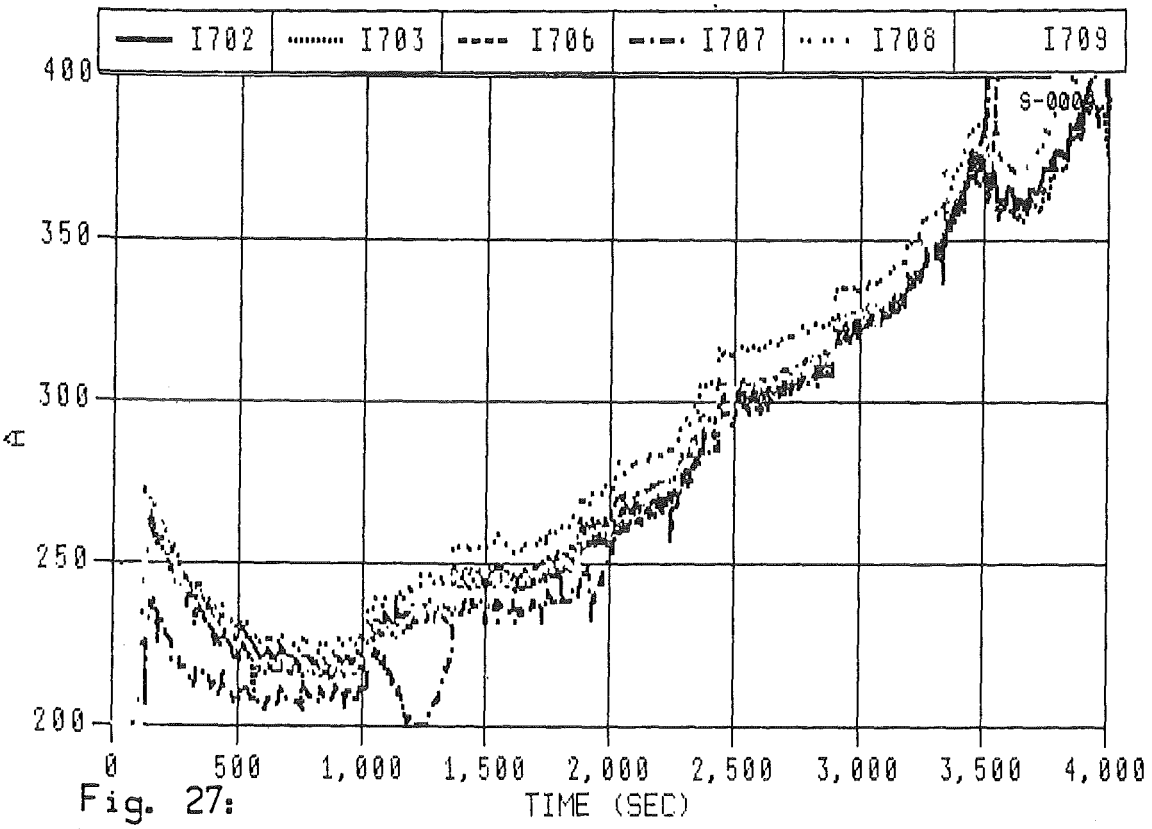

Fig. 27:
Deviation of Currents for rods of same group 1 for high temperature test CORA bundle B

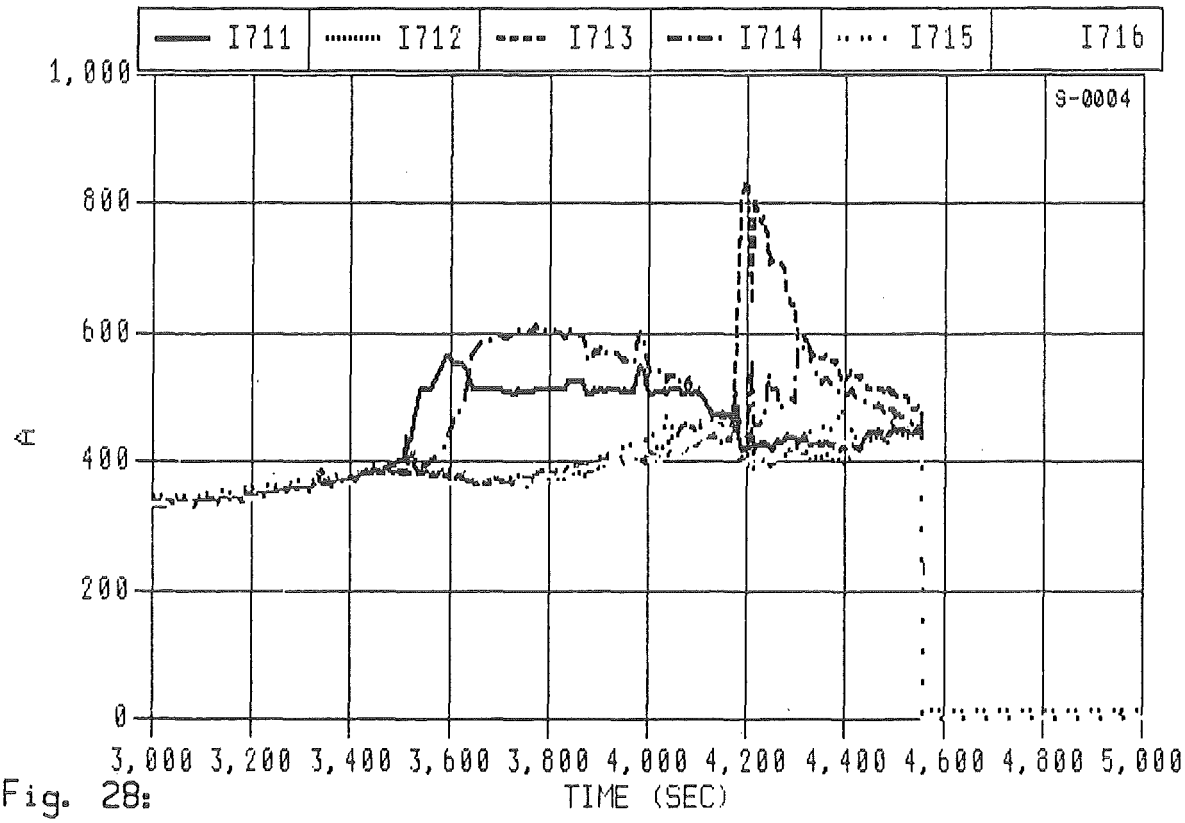

Fig. 28: Fluctuation of Currents through the 6 rods from group 2 due to melt formation for high temperature test CORA bundle B

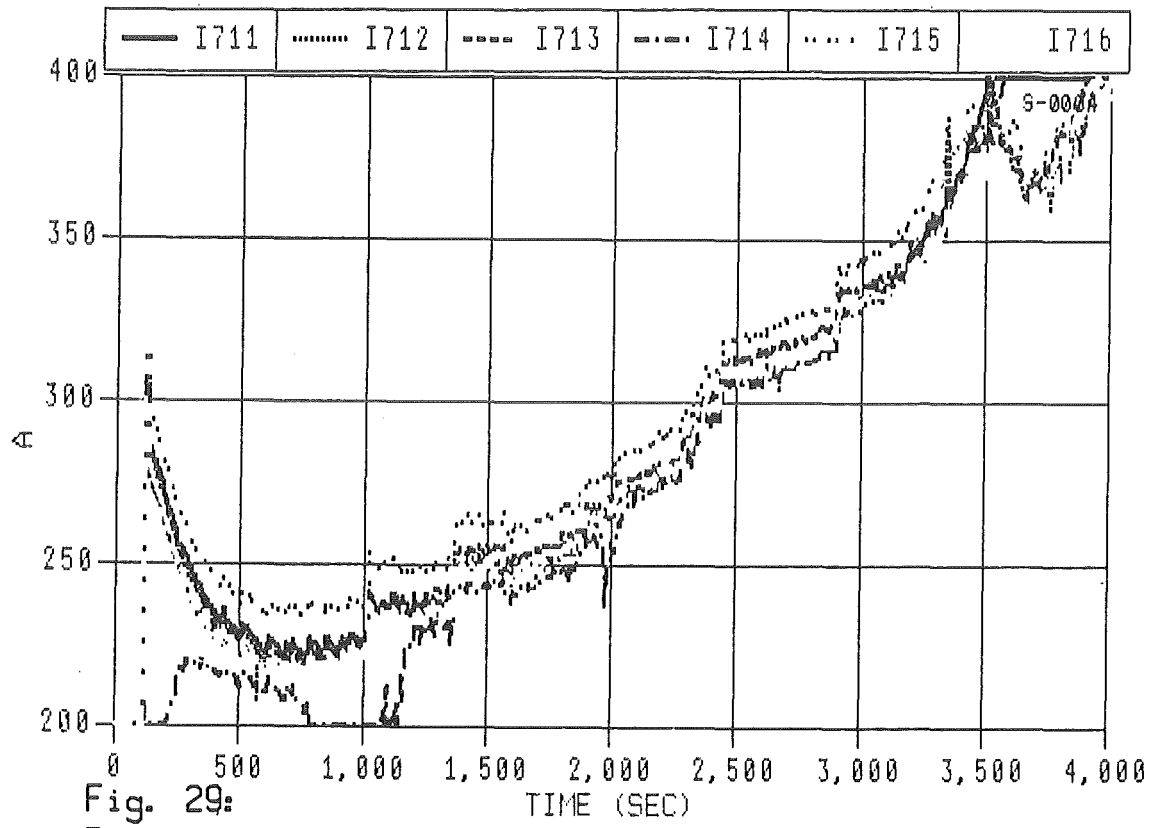

Fig. 29: Deviation of Currents for rods of same group 2 for high temperature test CORA bundle B

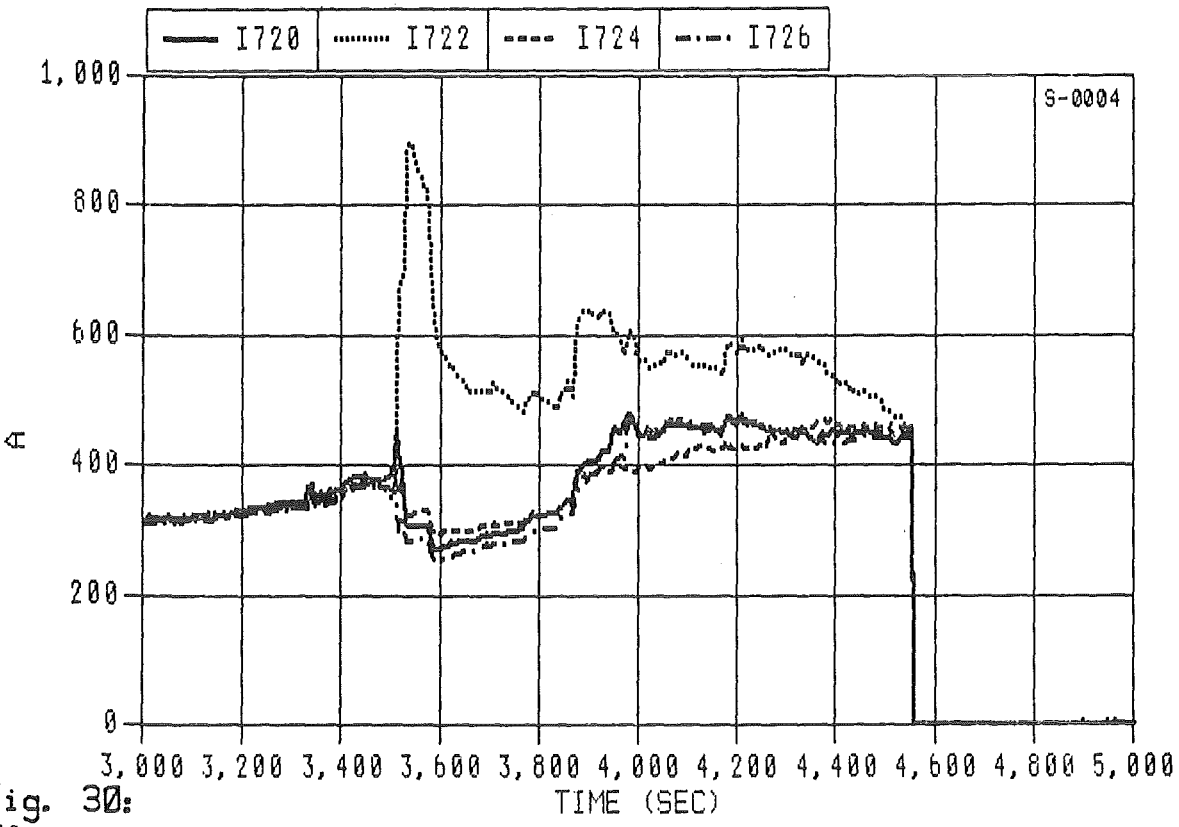

Fig. 30:
Fluctuation of Currents through the 4 rods from group 3 due to melt formation for high temperature test CORA bundle B

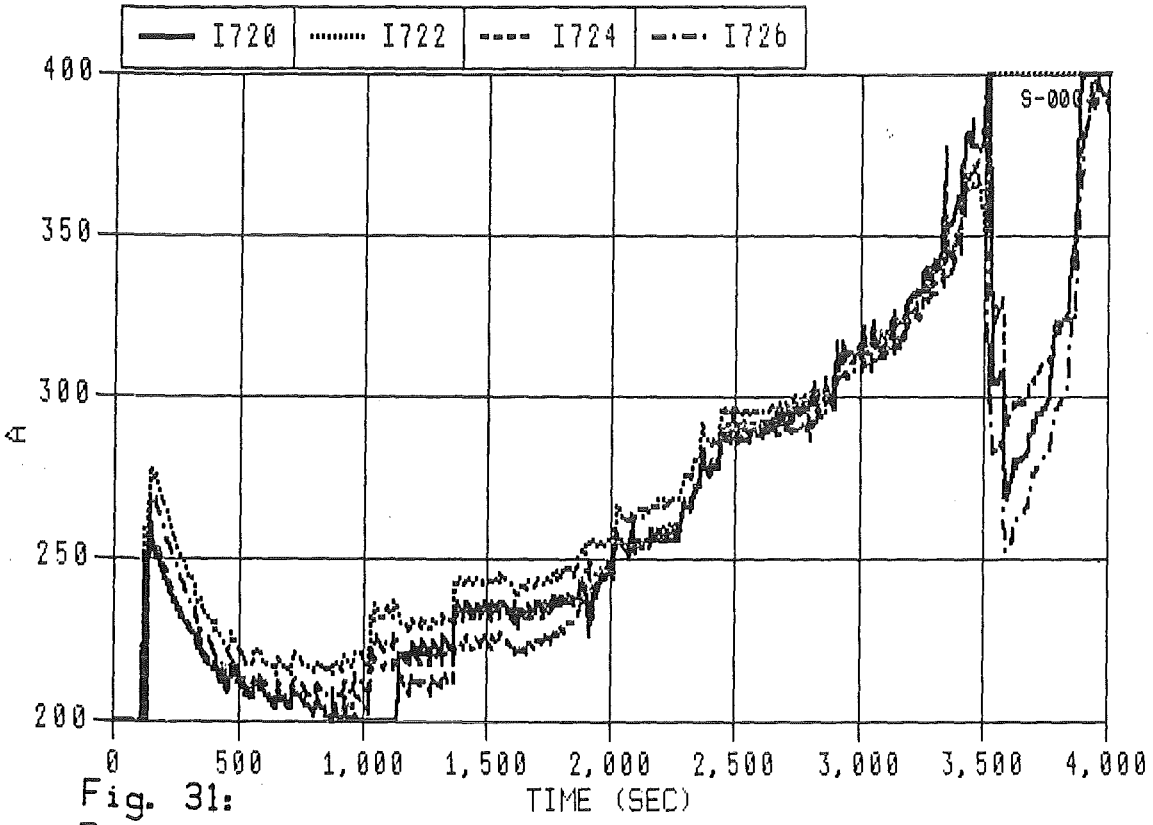

Fig. 31:
Deviation of Currents for rods of same group 3 for high temperature test CORA bundle B

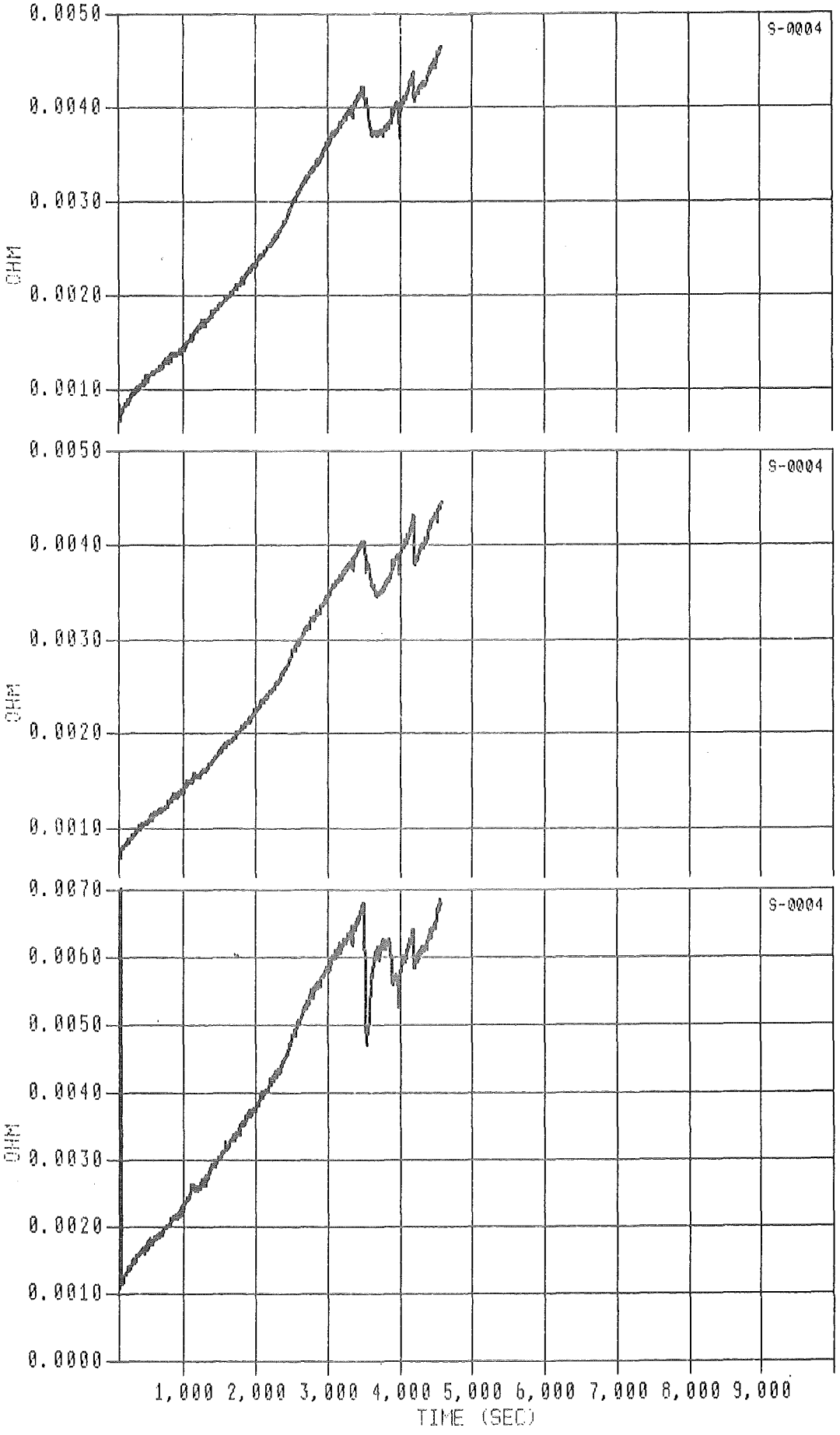

Fig. 32:
Total resistance of rods group 1, 2 and 3
CORA bundle B

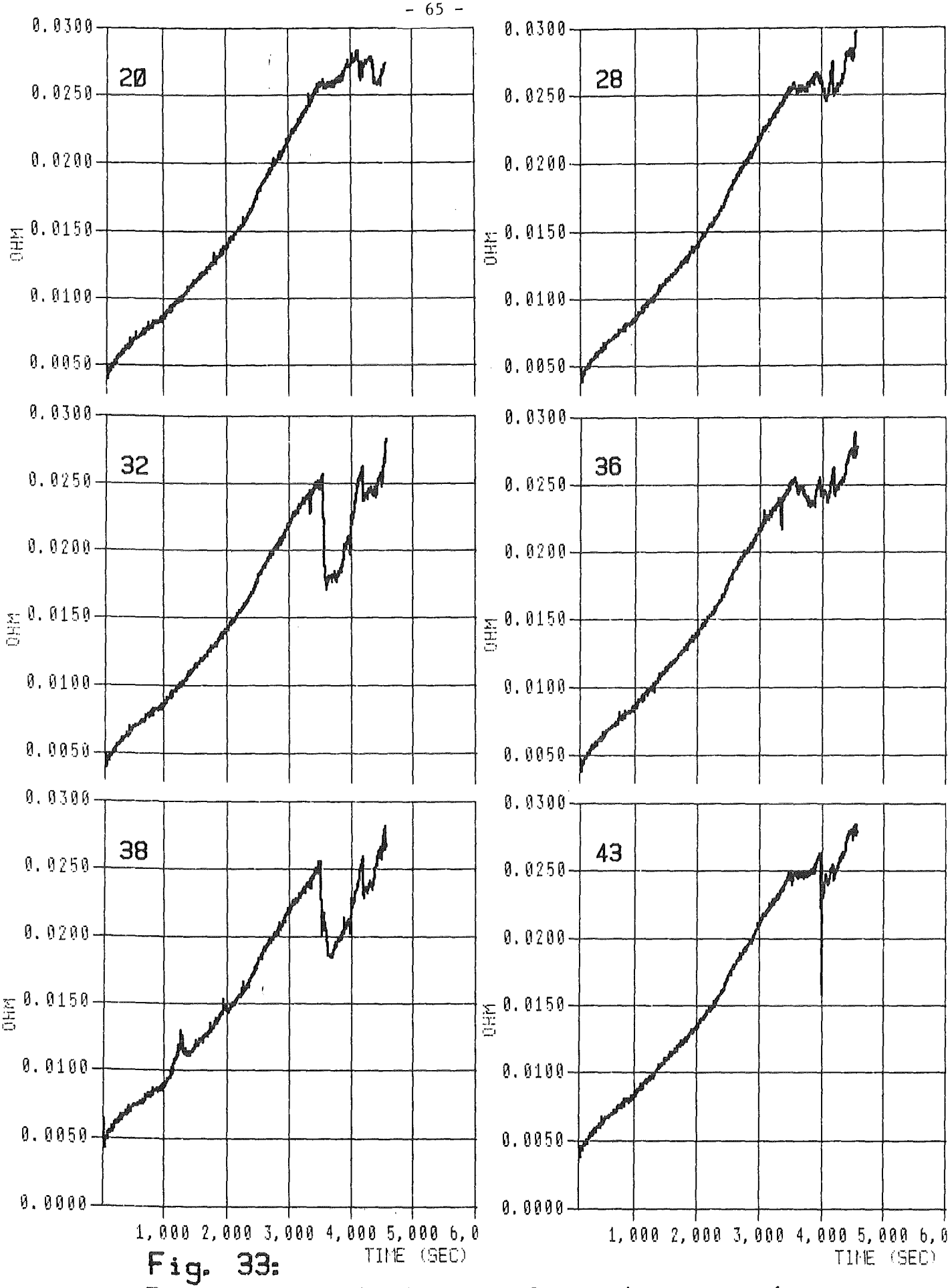

Fig. 33:
Resistance of the single rods group 1
CORA bundle B

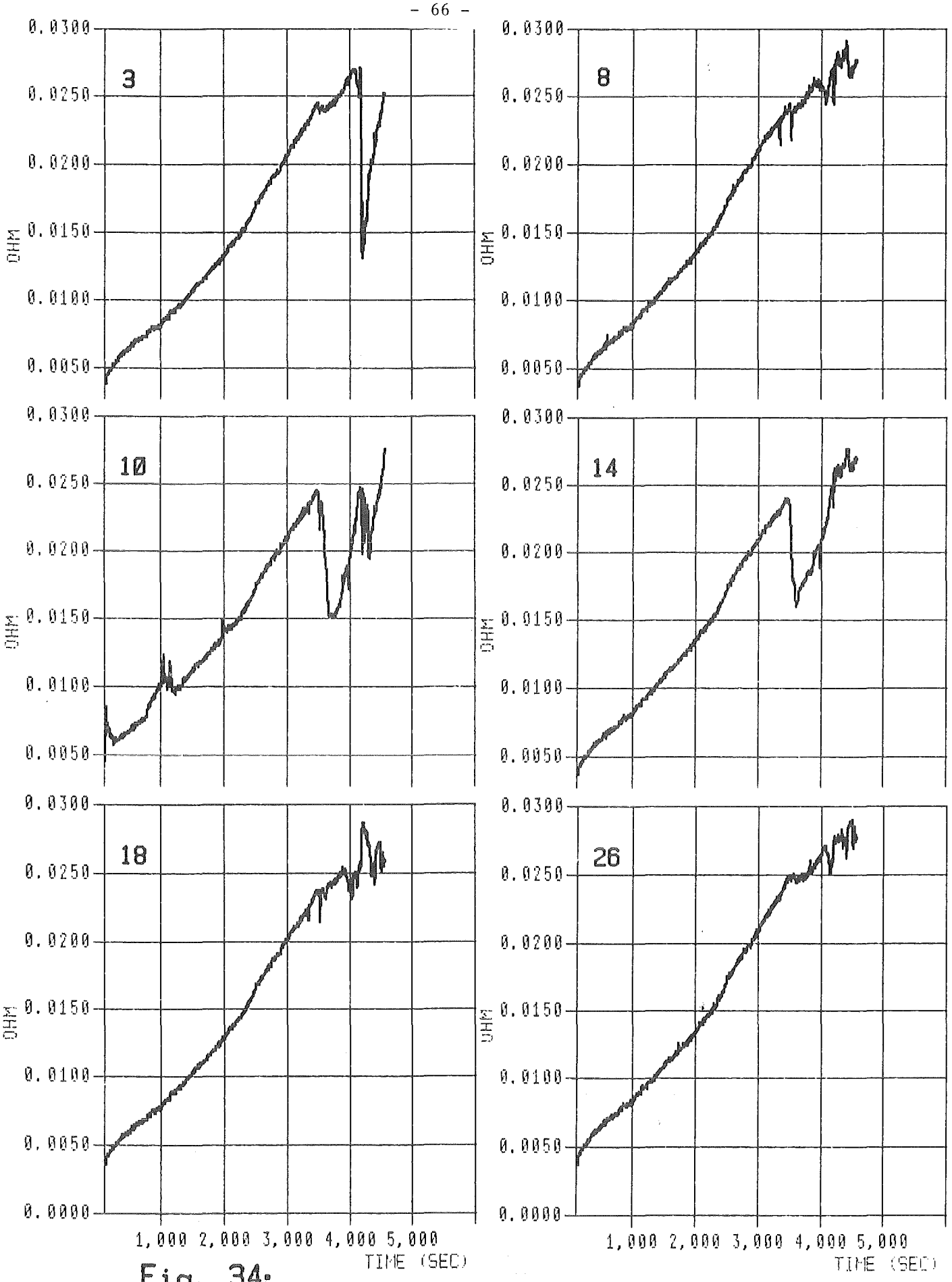

Fig. 34:
Resistance of the single rods group 2
CORA bundle B

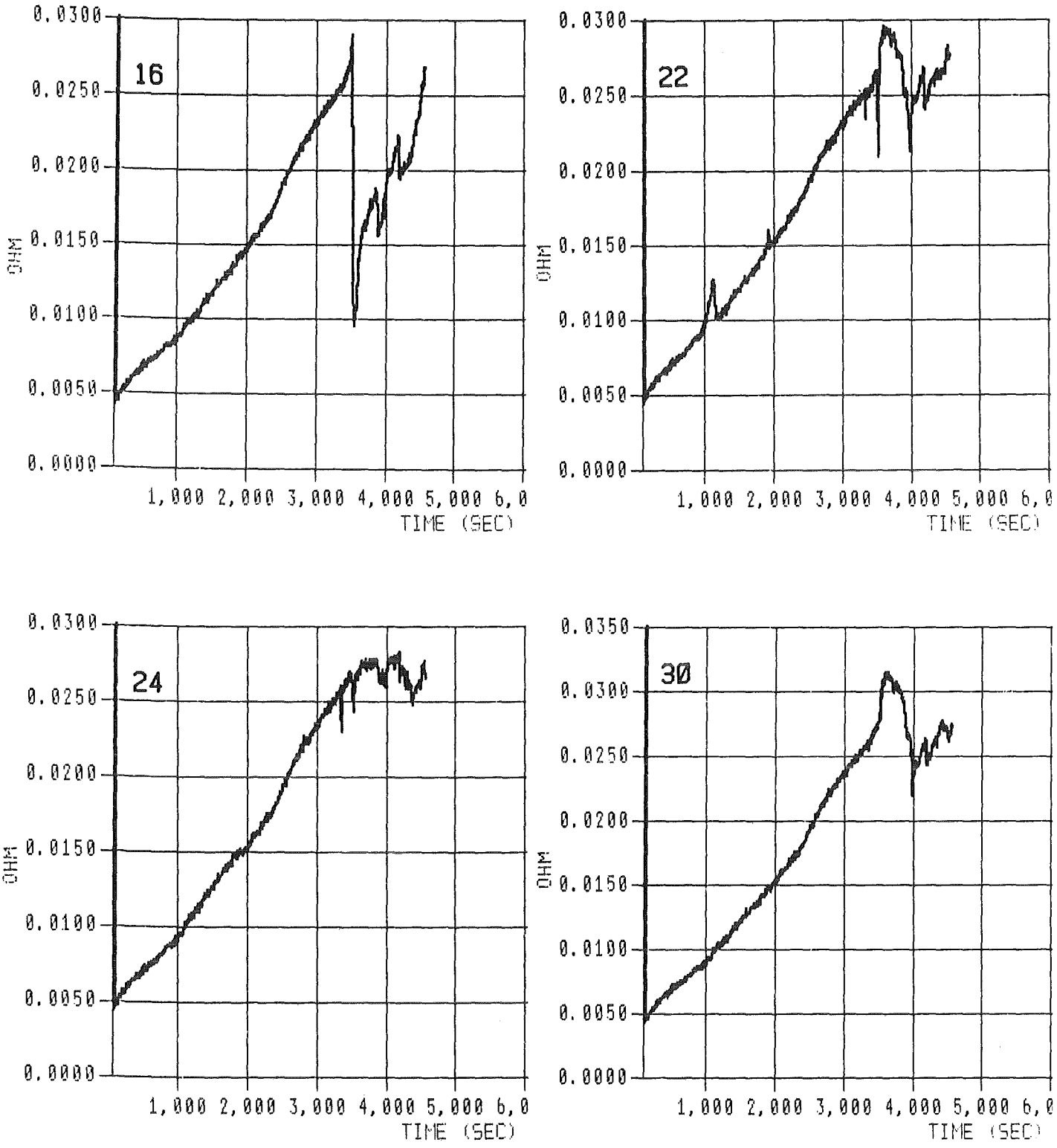

Fig. 35:
Resistance of the single rods group 3
CORA bundle B

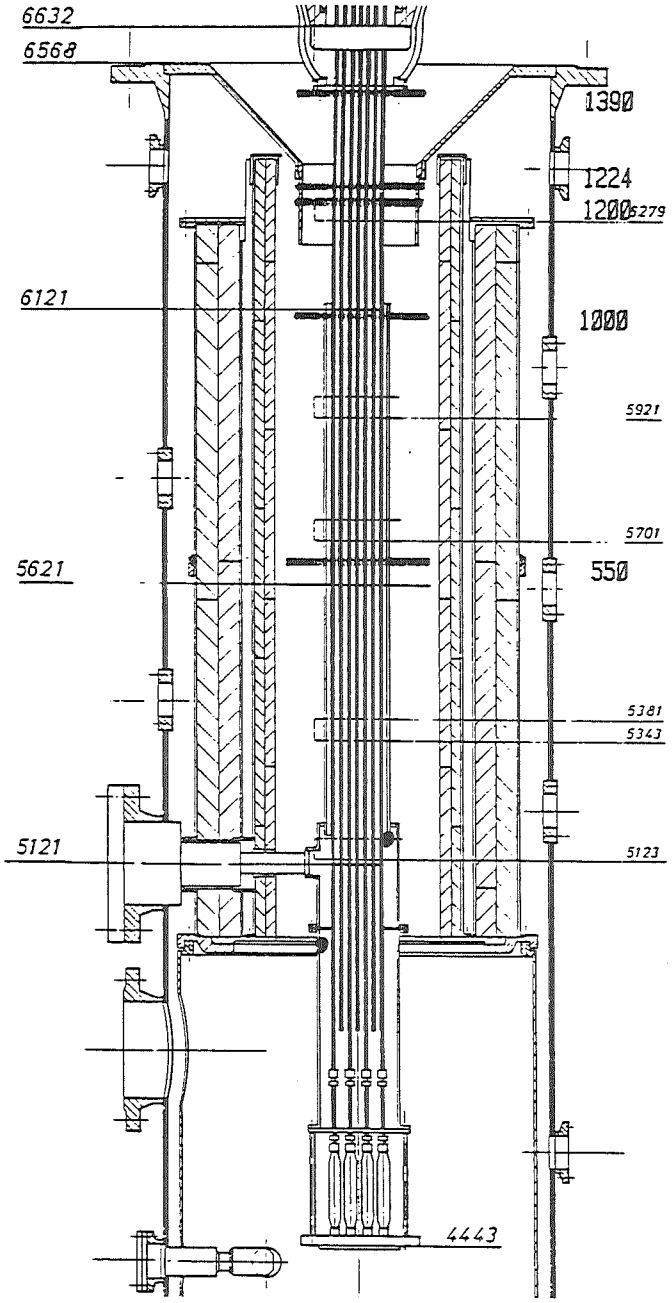

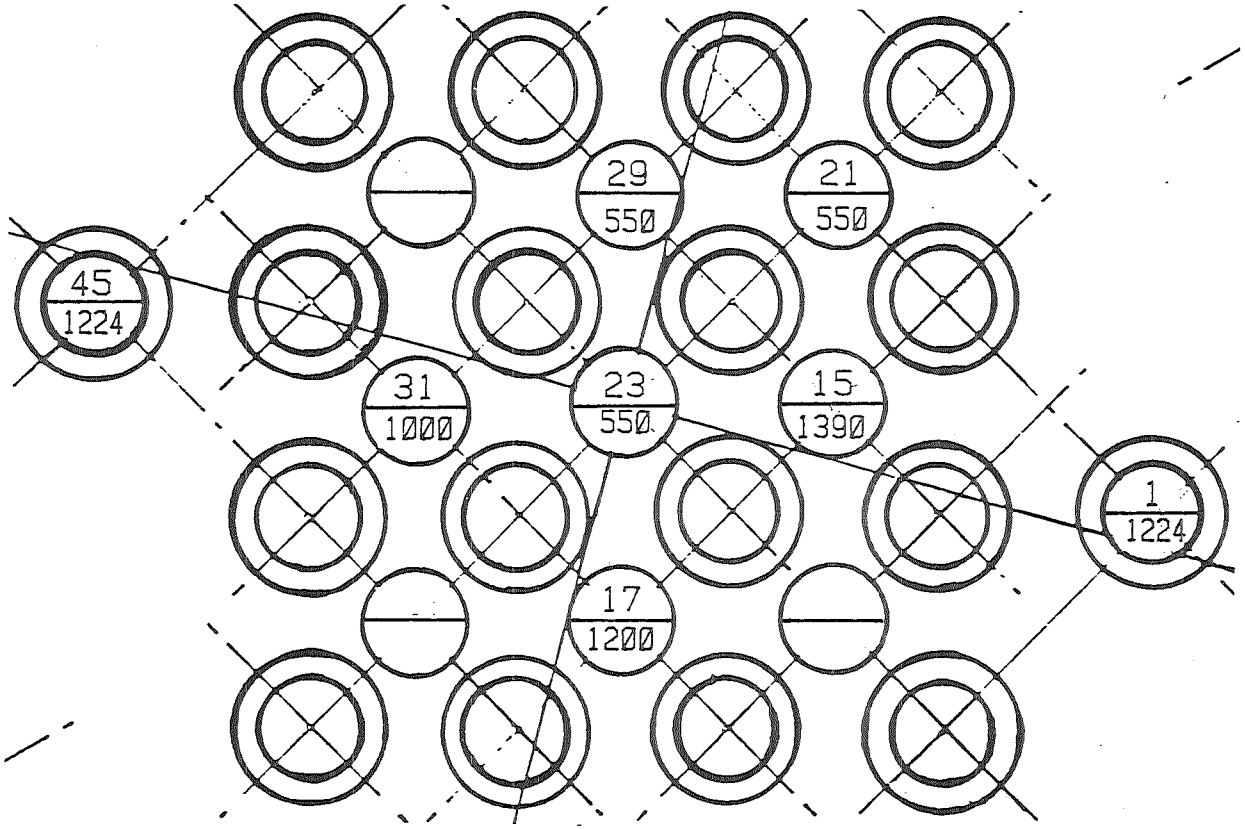

Fig. 36:
Elevations of temperature measurement with thermocouples in CORA bundle B

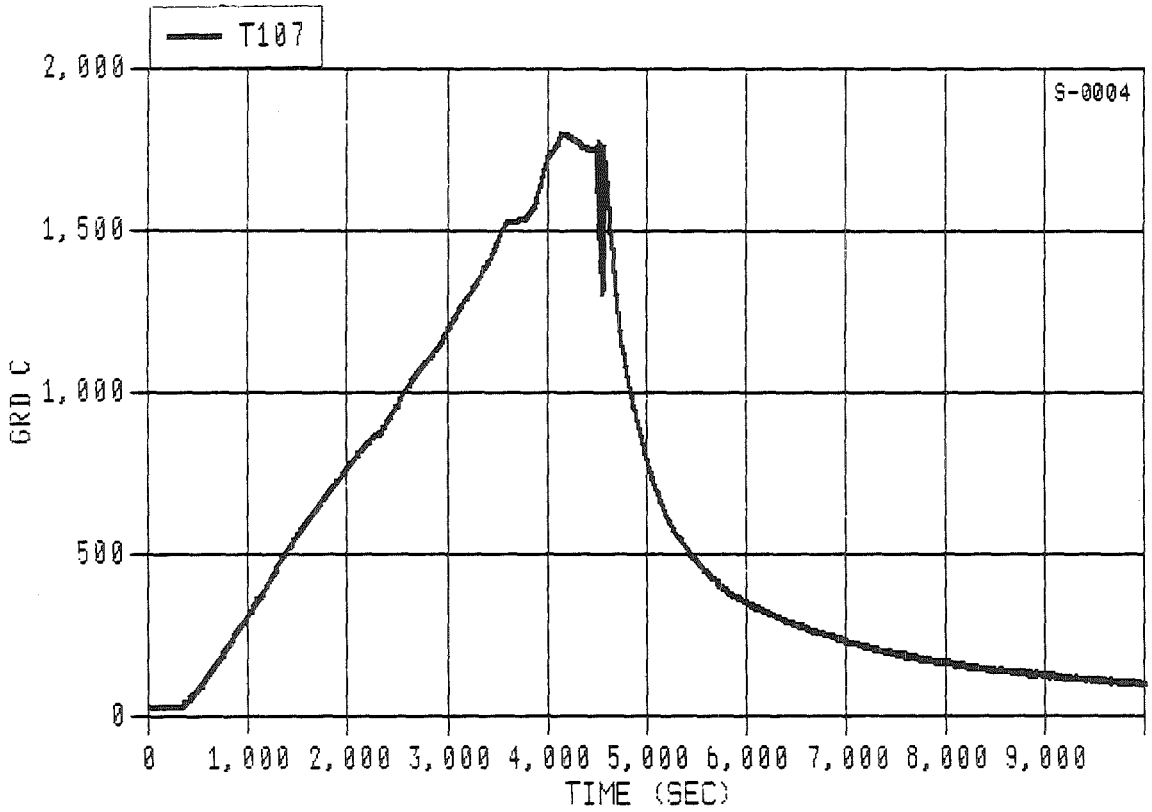

Fig. 37: Temperature of unheated rod 31 at 1000 mm elevation for high temperature test CORA bundle B

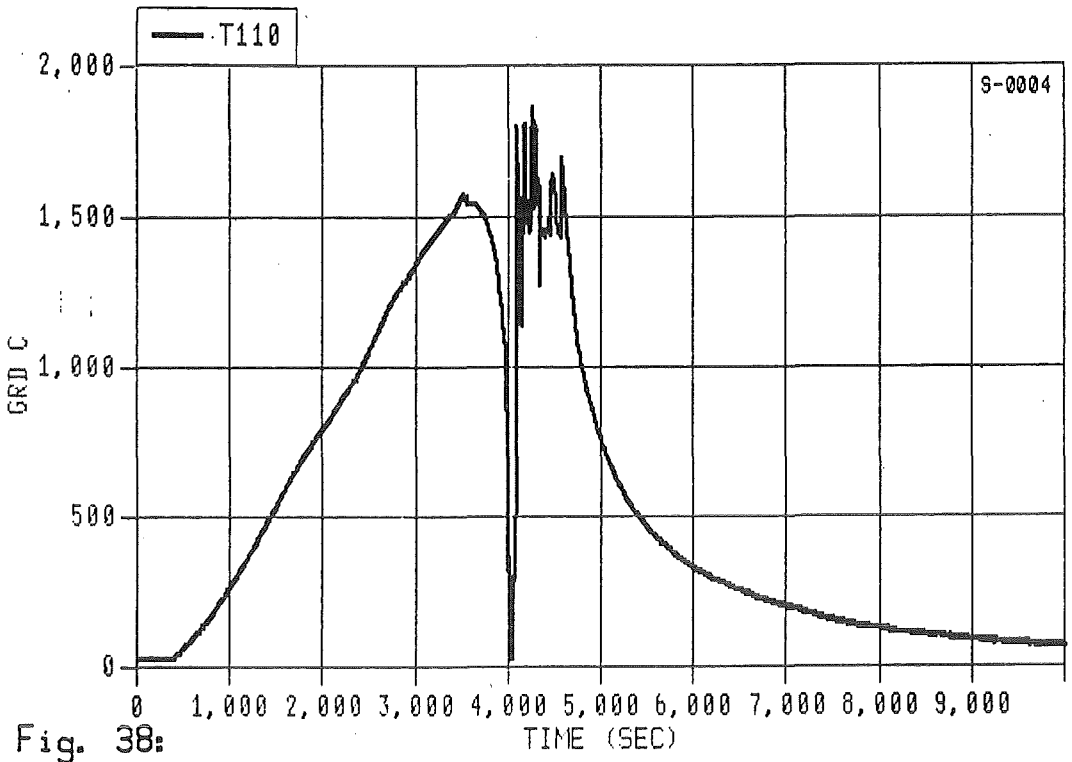

Fig. 38: Temperature of unheated rod 29 at 550 mm elevation for high temperature test CORA bundle B

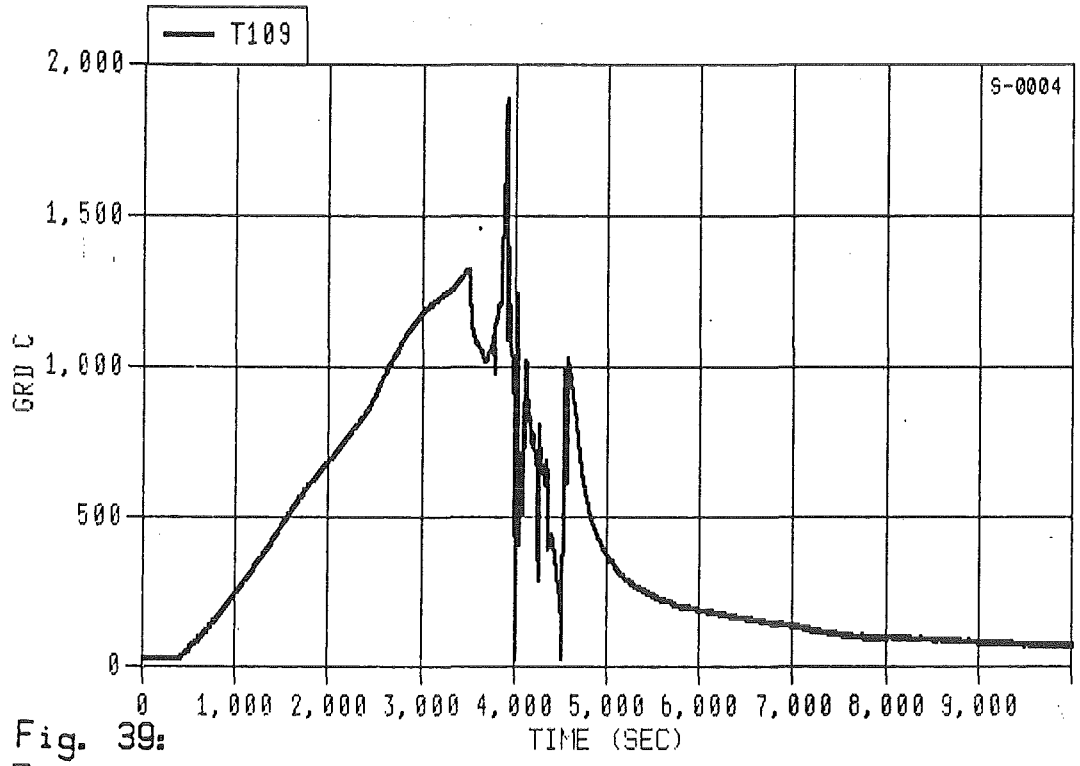

Fig. 39: Temperature of unheated rod 23 at 550 mm elevation for high temperature test CORA bundle B

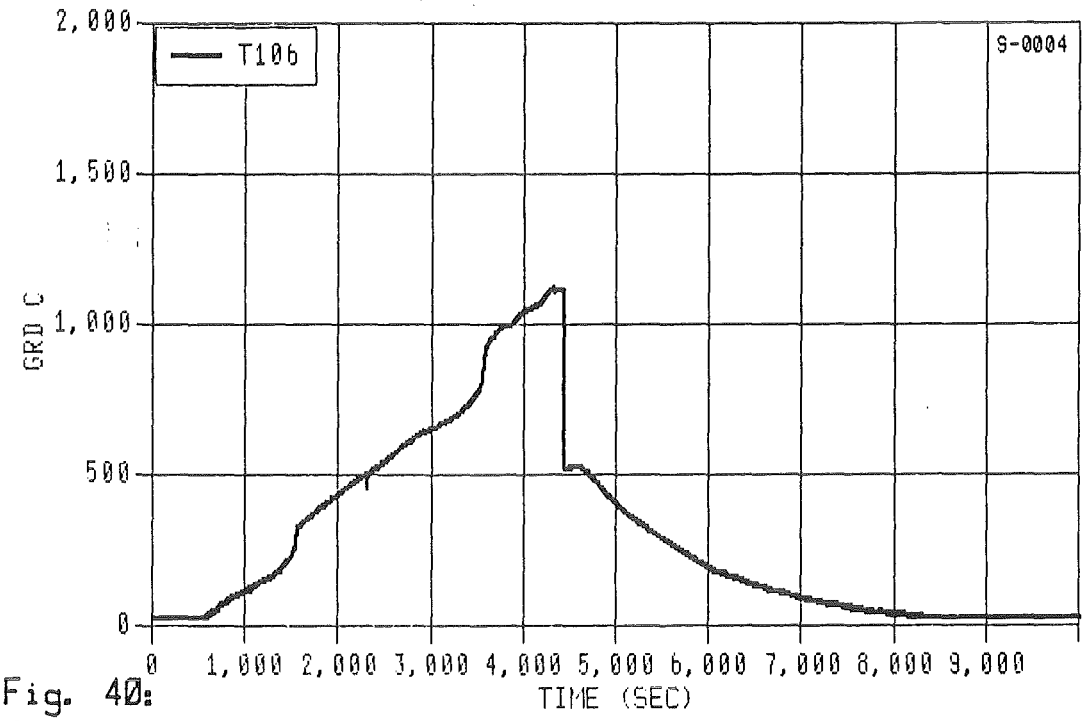

Fig. 40: Temperature of unheated rod 17 at 1200 mm elevation for high temperature test CORA bundle B

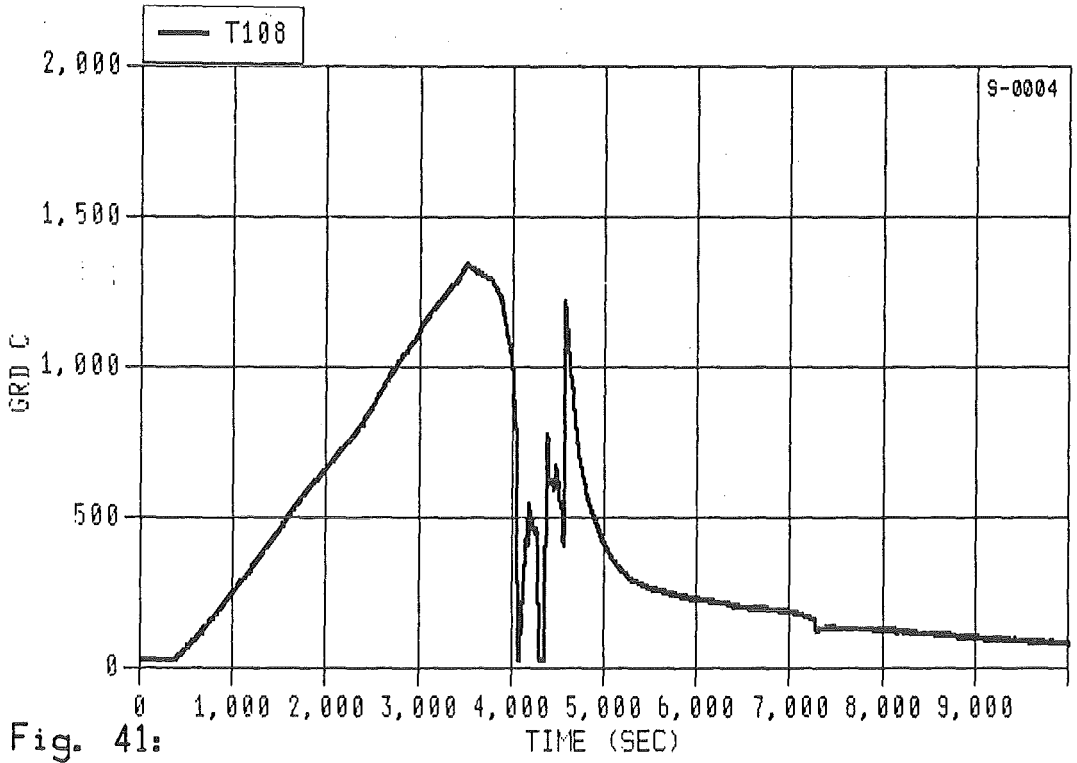

Fig. 41: Temperature of unheated rod 21 at 550 mm elevation for high temperature test CORA bundle B

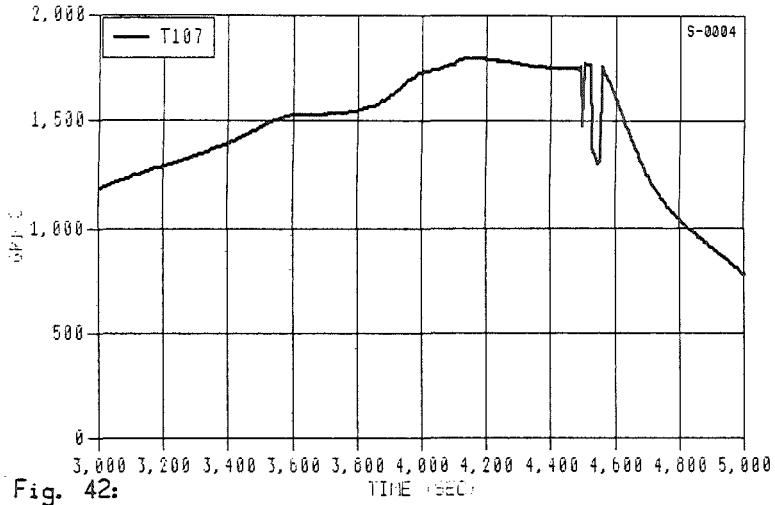

Fig. 42:
Temperature of unheated rod 31 at 1000 mm elevation for high temperature test CORA bundle B

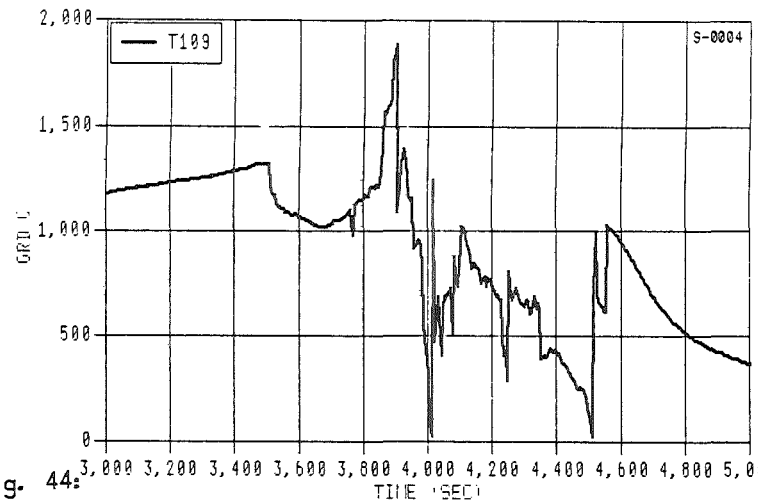

Fig. 44:
Failure of temperature measurement on the unheated rod 23 (550 mm elevation) at about 3500 sec for high temperature test CORA bundle B

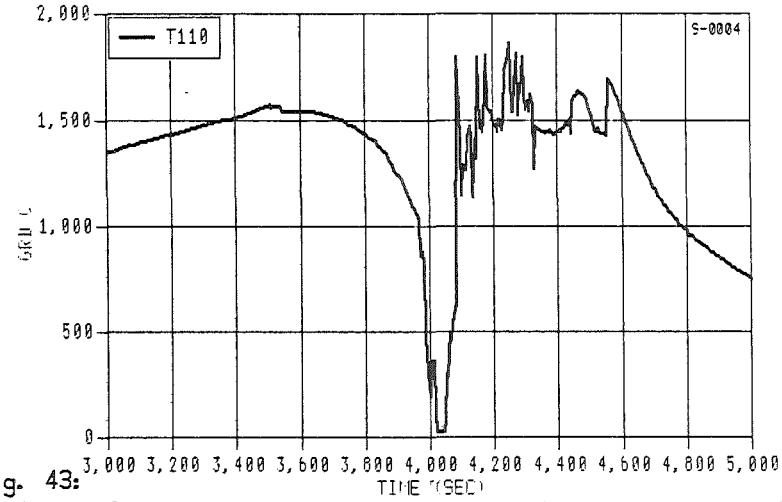

Fig. 43:
Failure of temperature measurement on the unheated rod 29 (550 mm elevation) at about 3500 sec for high temperature test CORA bundle B

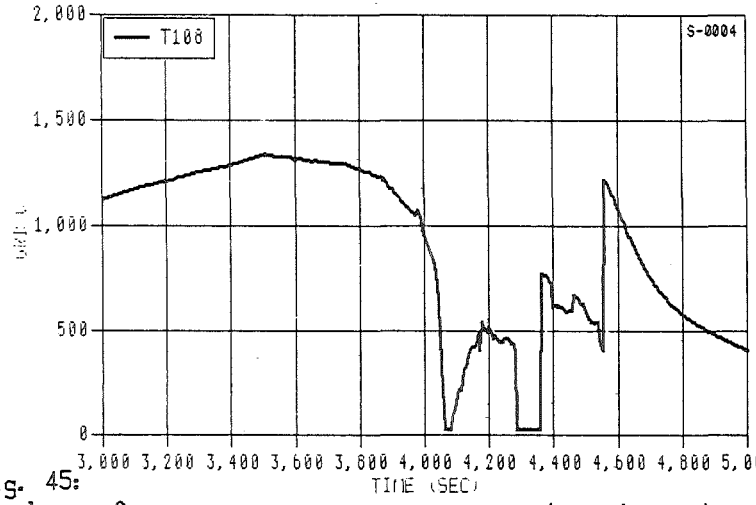

Fig. 45:
Failure of temperature measurement on the unheated rod 21 (550 mm elevation) at about 3500 sec for high temperature test CORA bundle B

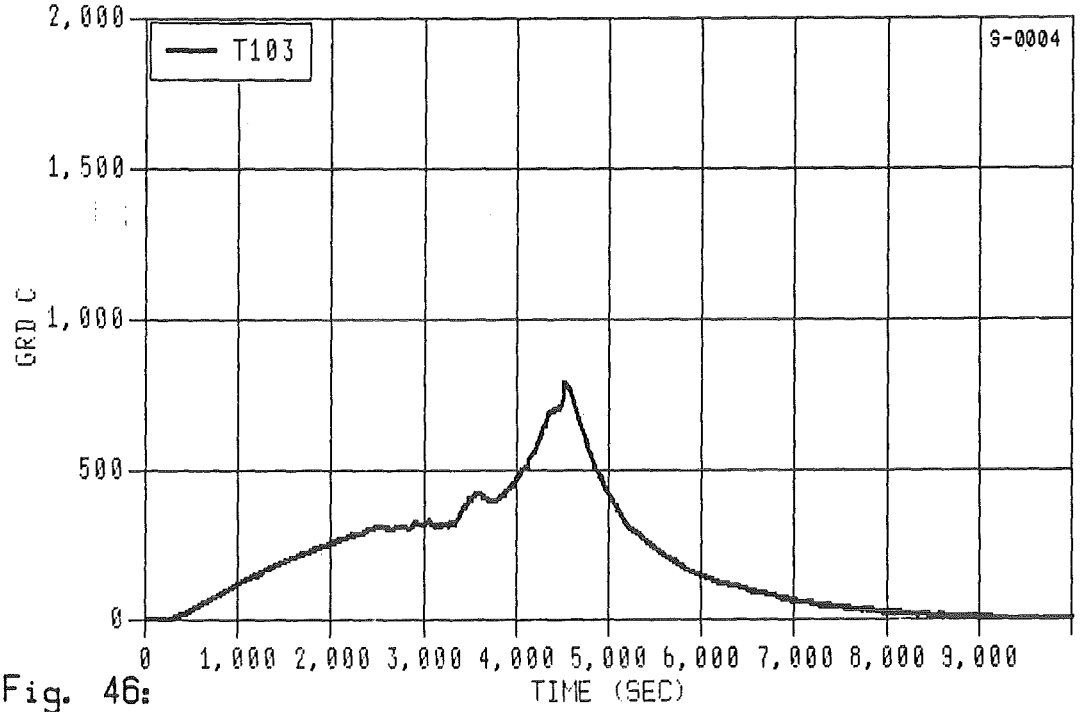

Fig. 46:
Temperature of unheated rod 15 at 1350 mm elevation for high temperature test CORA bundle B

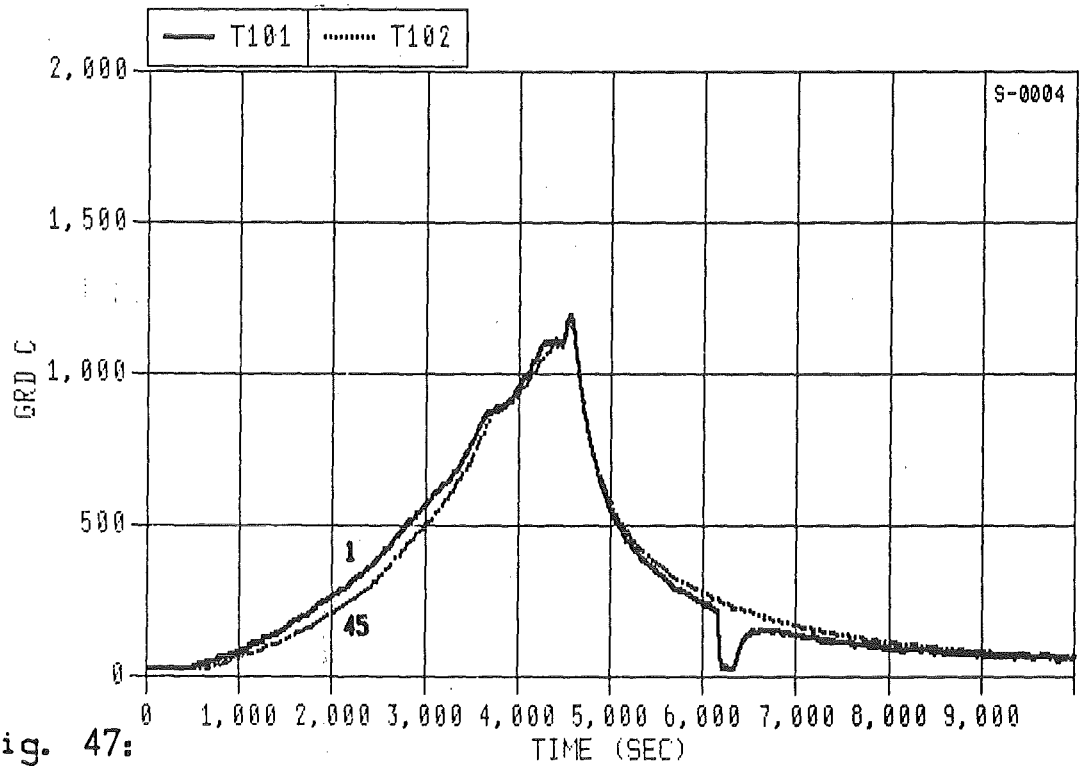

Fig. 47:
Gas temperature measured at position 1 and 45 (1224 mm elevation) for high temperature test CORA bundle B

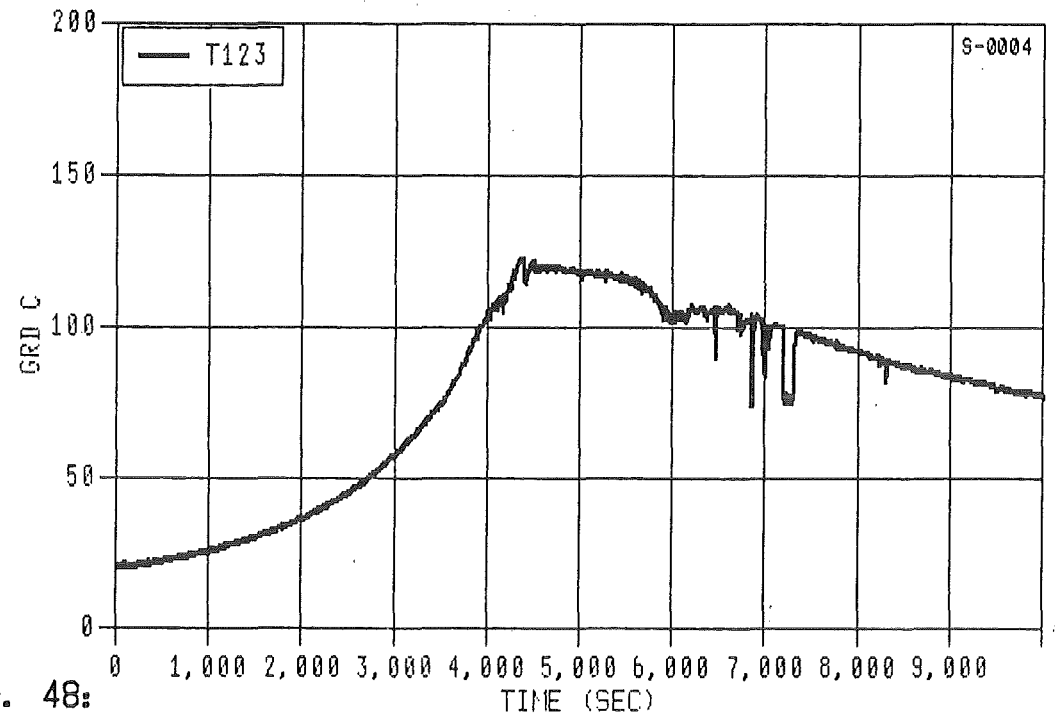

Fig. 48:
Temperature in quench cylinder at -300 mm elevation; 180°; 100 mm radius for high temperature test CORA bundle B

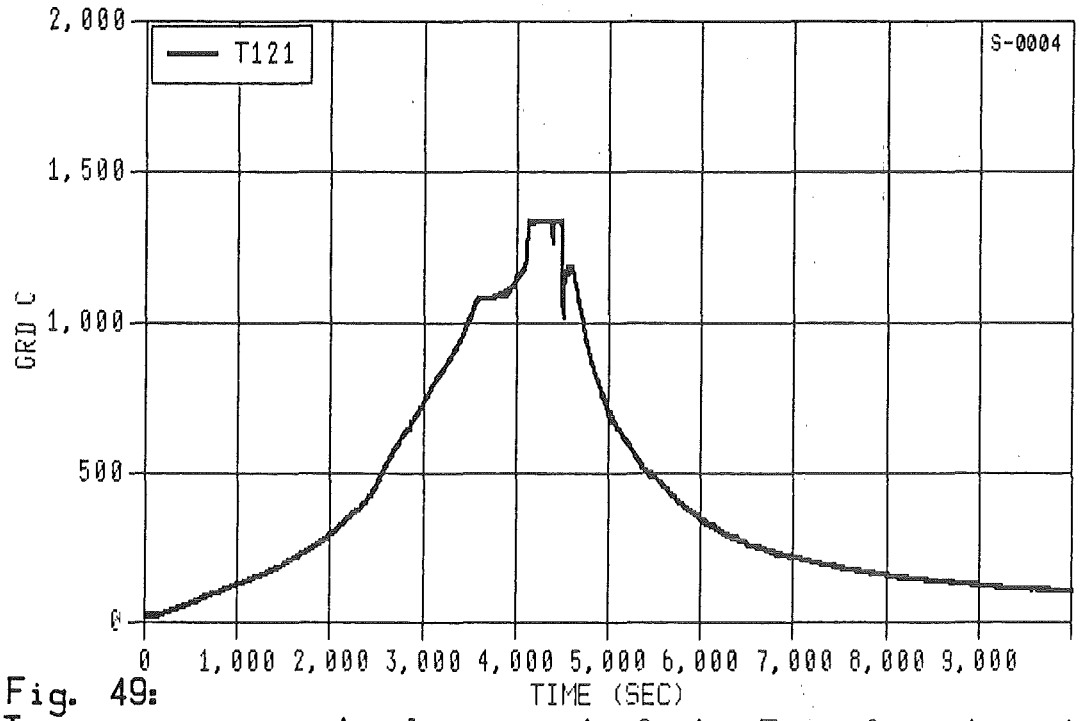

Fig. 49:
Temperature at the lower end of the Zircaloy shroud (35 mm elevation; 0°) for high temperature test CORA bundle B

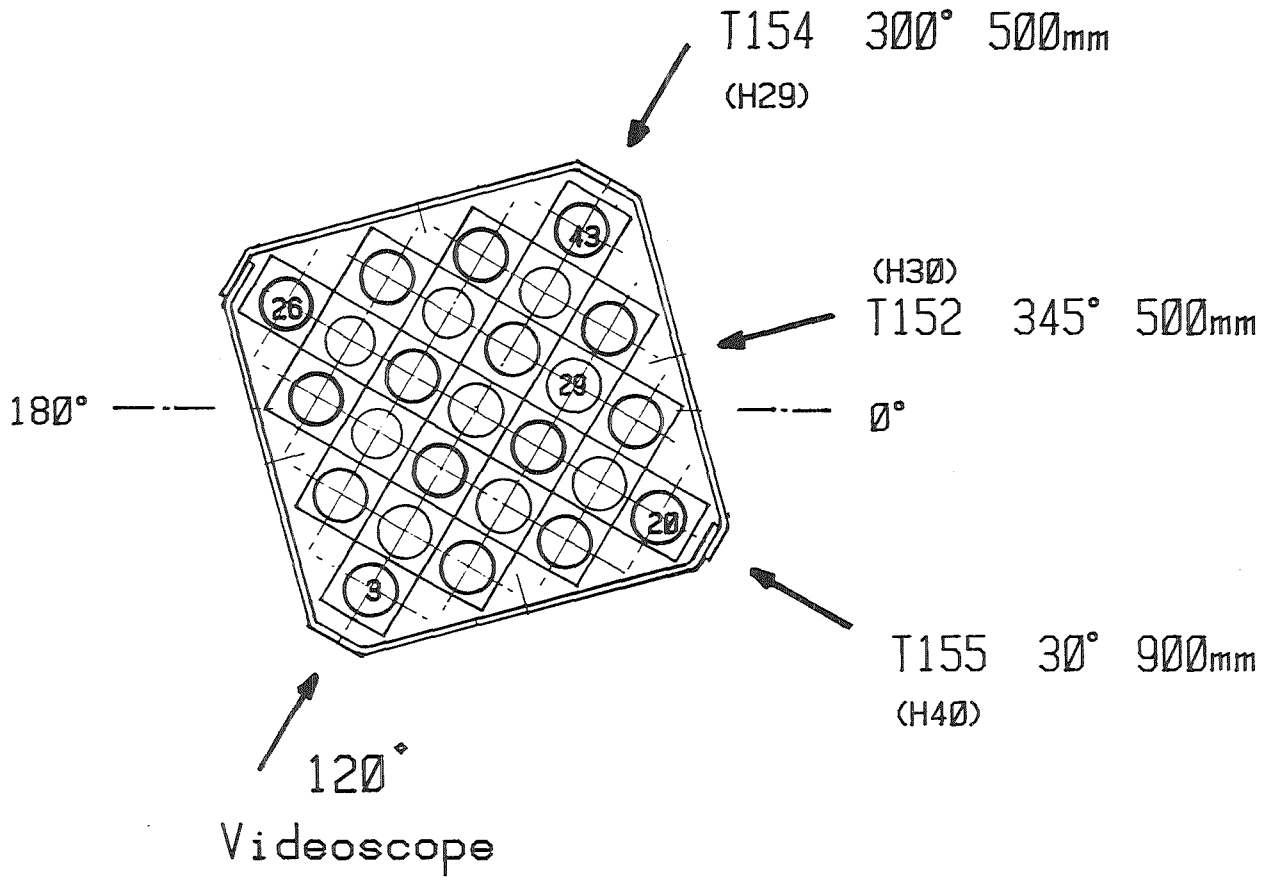

Fig. 50:
Positions of two-color pyrometersfor high temperature test CORA bundle B

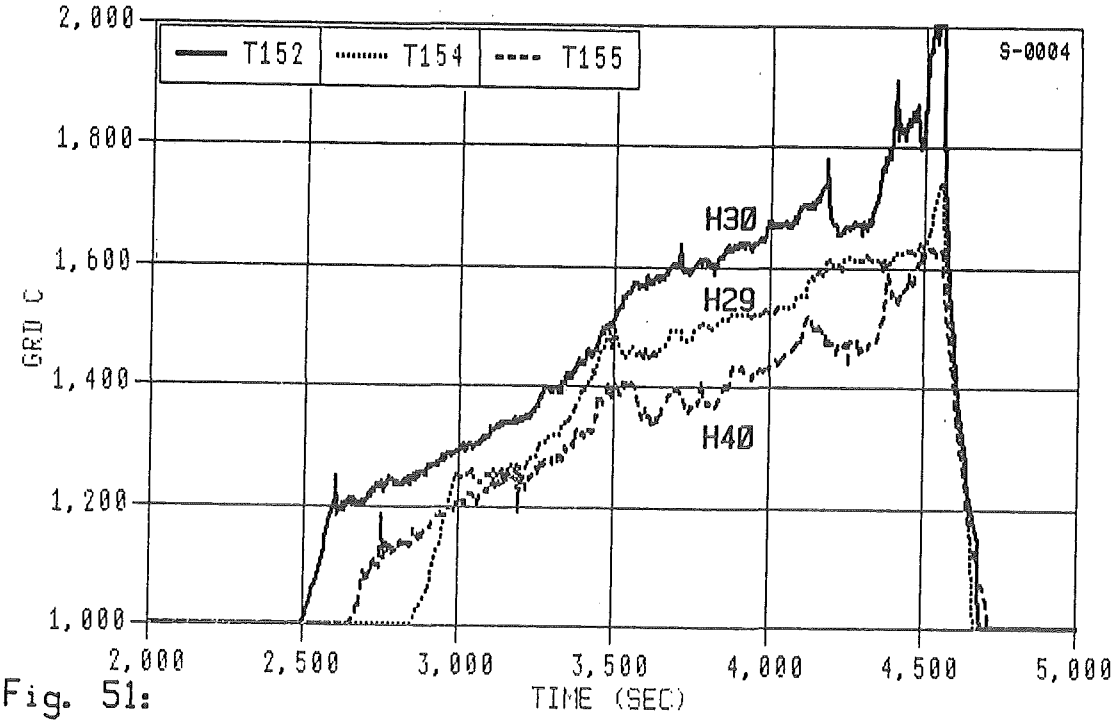

Fig. 51:
Temperatures measured with two color pyrometers at positions H29, H30, H40 for high temperature test CORA bundle B

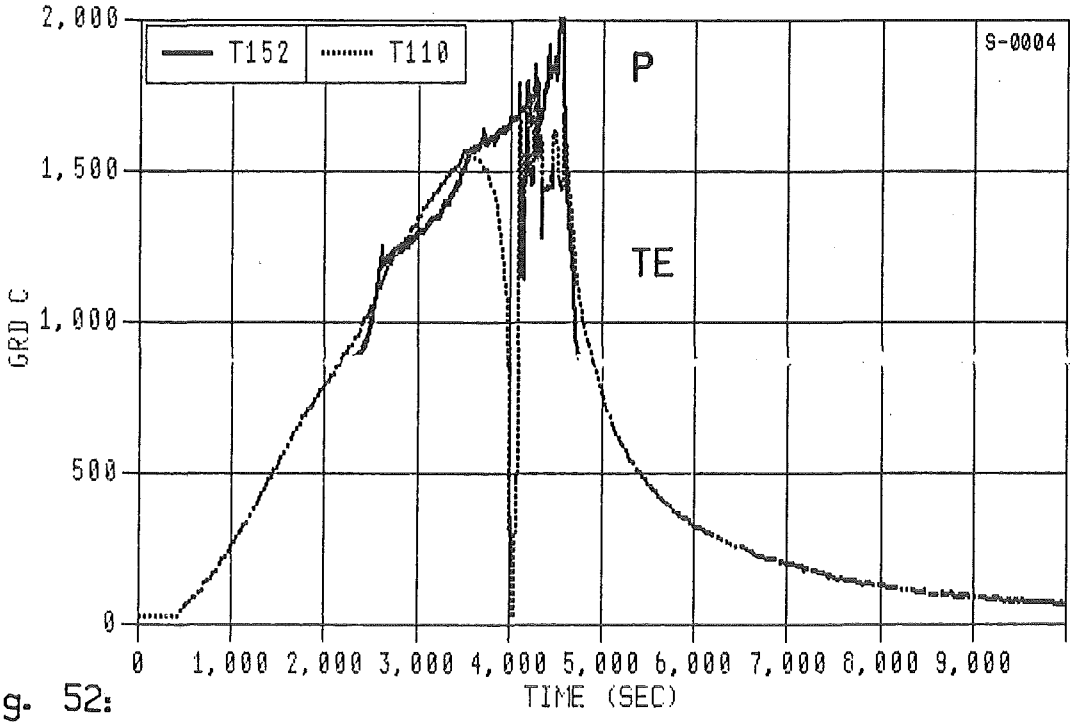

Fig. 52:
Temperature on unheated rod 29 measured with thermocouple at 550mm elevation and with two color pyrometer in H30 at 500mm elevation for high temperature test CORA bundle B

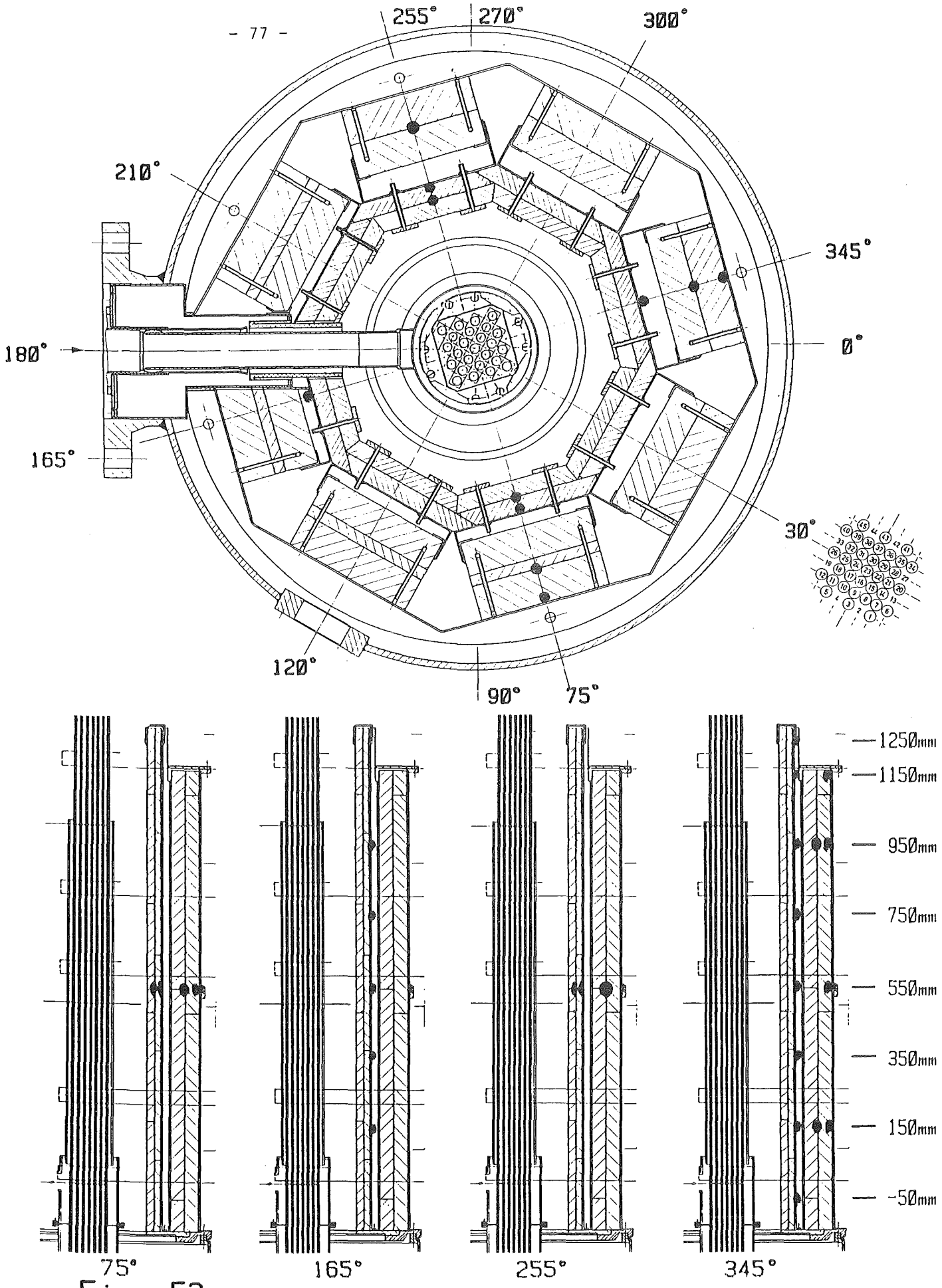

Fig. 53:
Positions of thermocouples in insulation of high temperature shield for CORA bundle B

ORIENTATION		75°				165°	255°			345°		
RADIUS [mm]		172	192	255	293	192	172	192	255	192	255	293
ELEVATION (BUNDLE CODE) [mm]	1250									T234 U73		
	1150									T235 U74		T245 U84
	950					T229 U68				T236 U75	T242 U81	T246 U85
	750					T230 U69				T237 U76		
	550	T124 U22	T126 U24	T130 U28	T244 U83	T231 U70	T125 U23	T127 U25	T131 U29	T238 U77		T247 U86
	350					T232 U71				T239 U78		
	150					T233 U72				T240 U79	T243 U82	T248 U87
	-50									T241 U80		

Fig. 54 : Positions of thermocouples in high temperature shield.
(T = TC-number ; U = UAM-number)

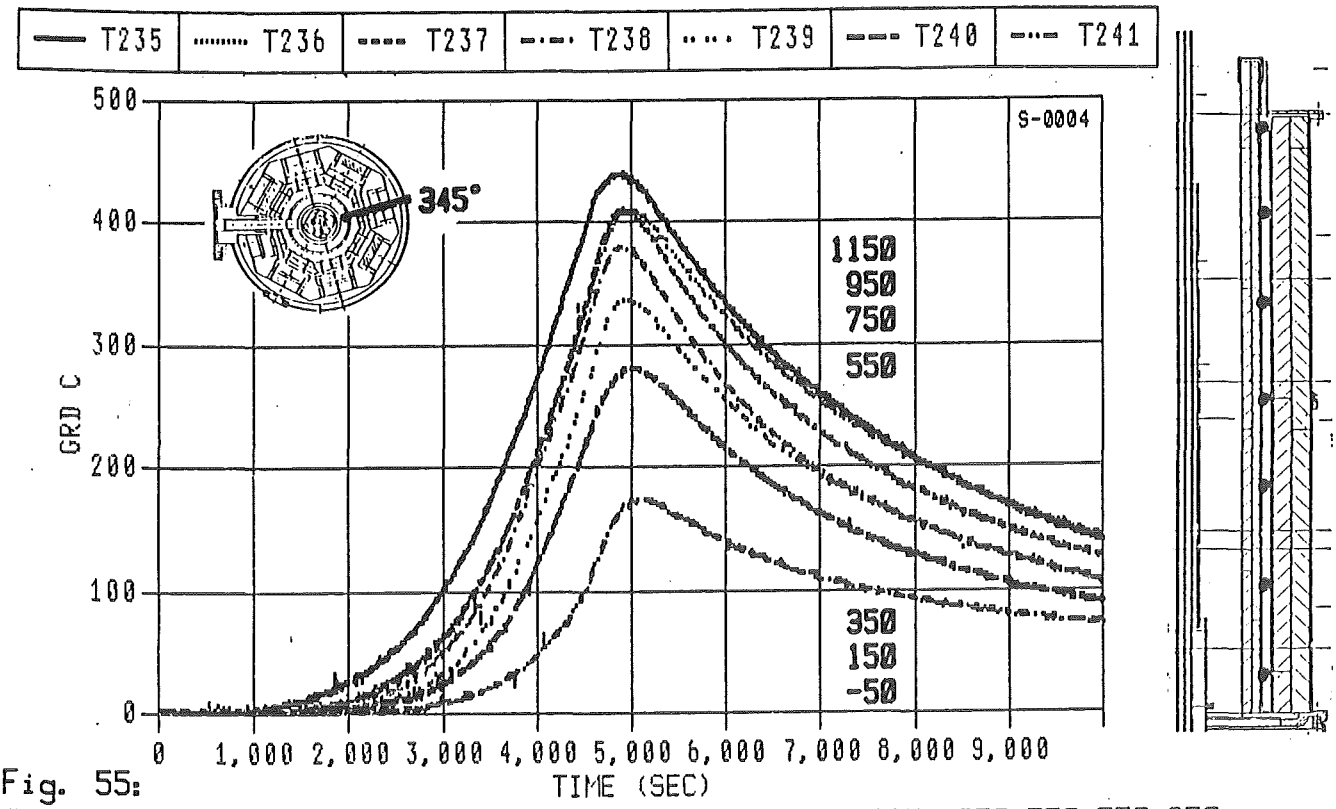

Fig. 55: Temperature in insulation; radius 192mm; elevation 1150, 950, 750, 550, 350, 150, -50 mm ; at 345°; for high temperature test CORA bundle B

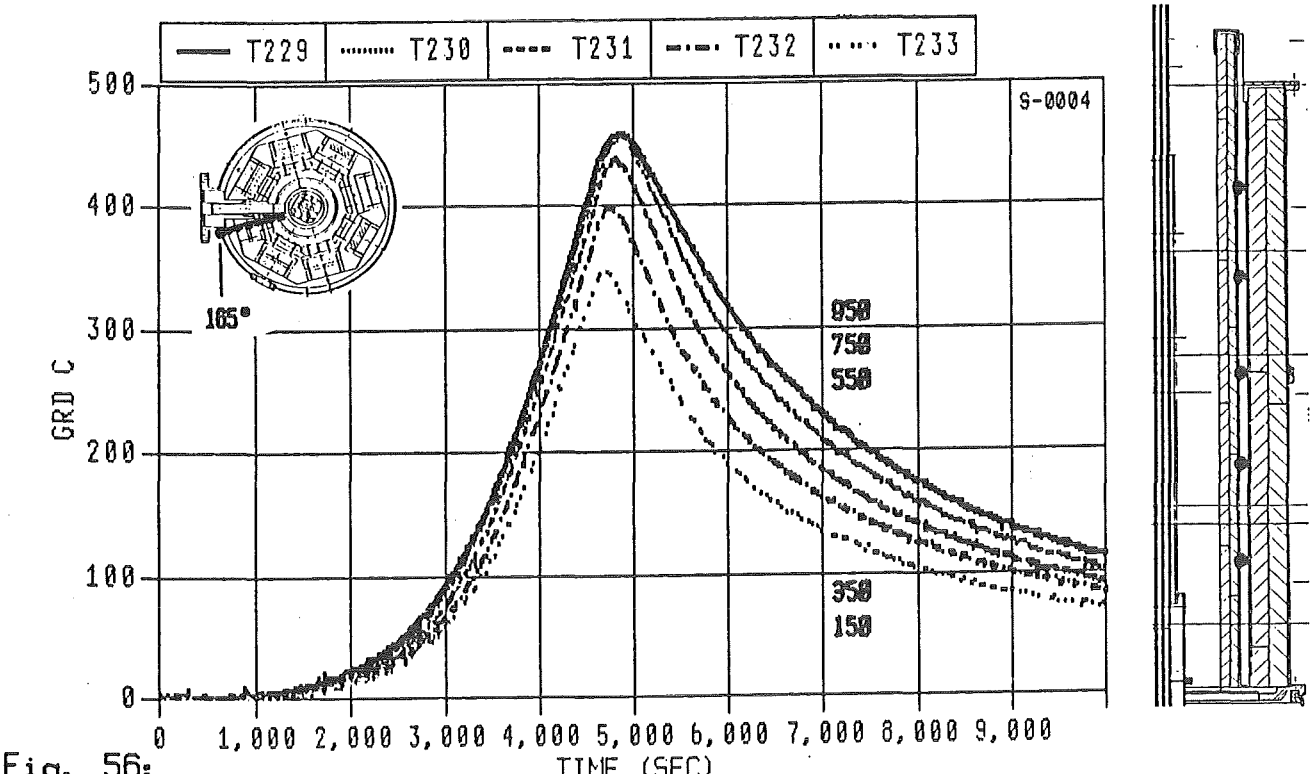

Fig. 56: Temperature in insulation; radius 192 mm; elevation 950, 750, 550, 350, 150 mm; at 165°; for high temperature test CORA bundle B

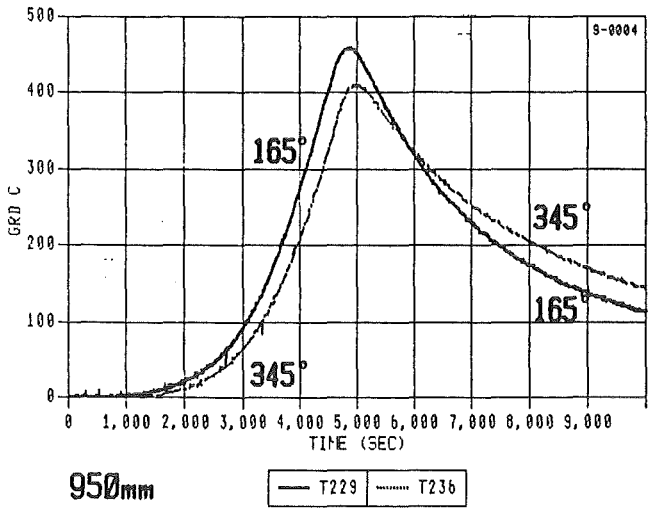

950mm — T229 ····· T236

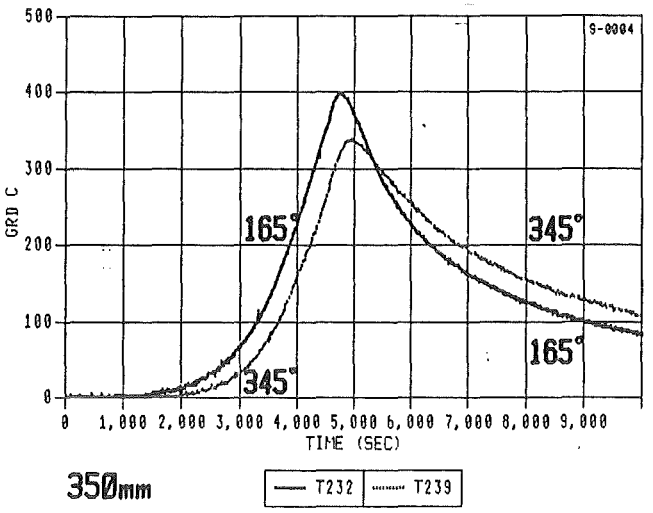

350mm — T232 ····· T239

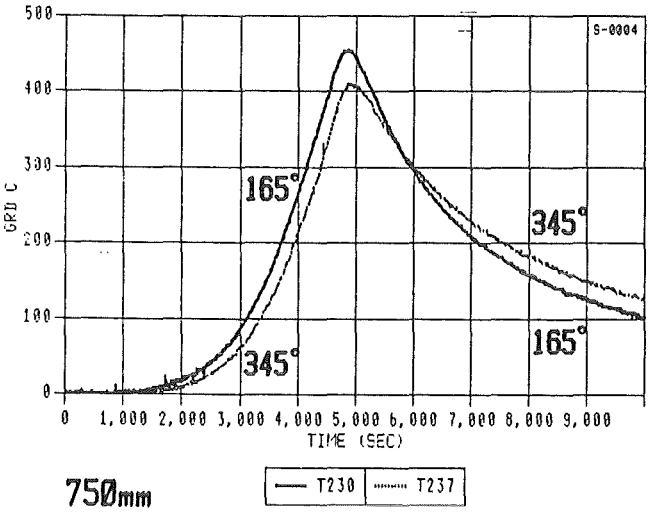

750mm — T230 ····· T237

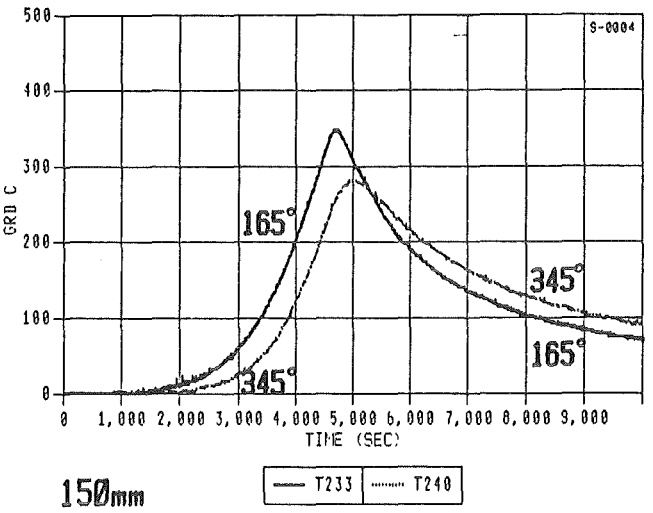

150mm — T233 ····· T240

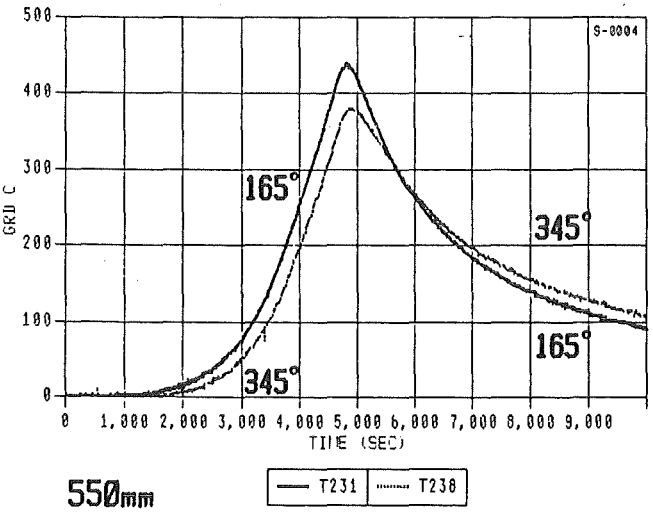

550mm — T231 ····· T238

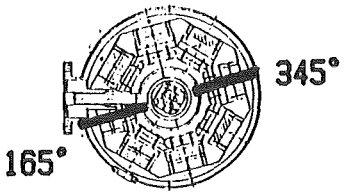

Fig. 57 :
Comparison of temperatures in insulation at 192mm radius for 165° and 345°

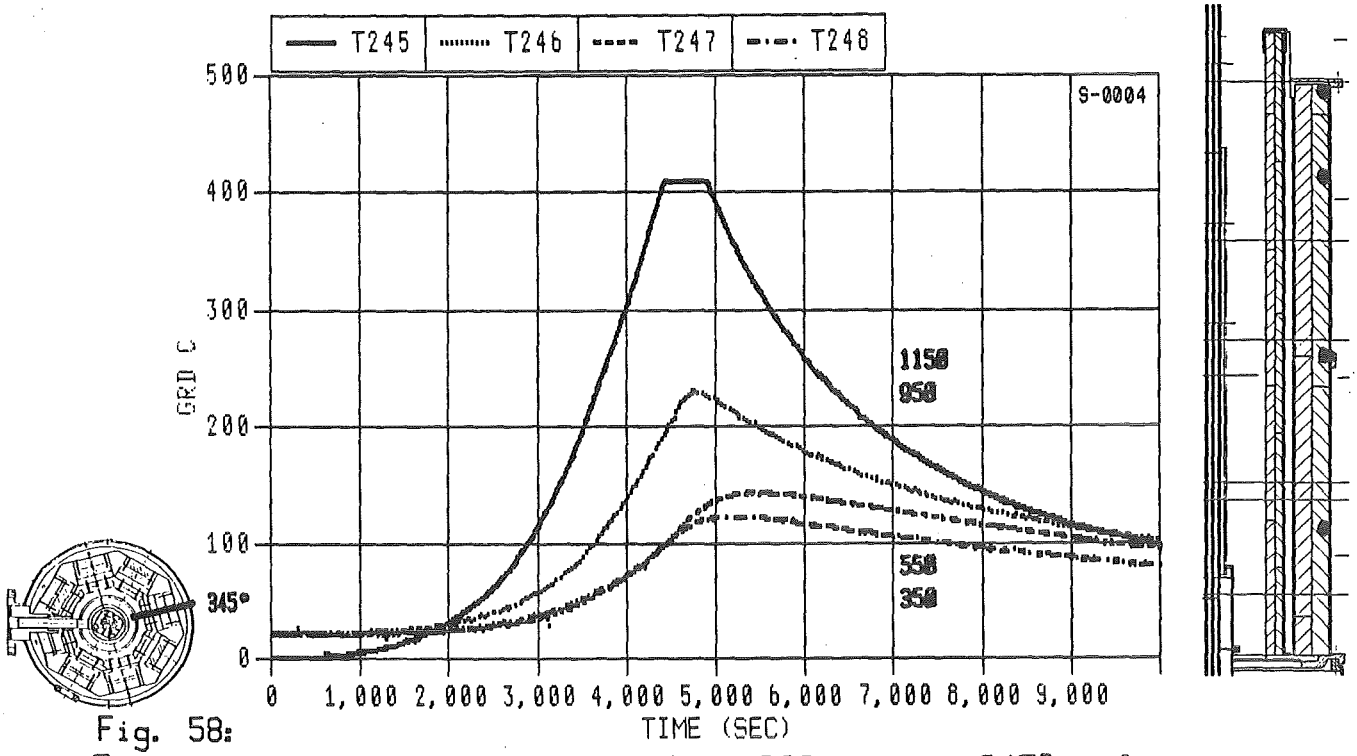

Fig. 58: Temperature in insulation; radius 293 mm; at 345°; elevation 1150, 950, 550, 350 mm; for high temperature test CORA bundle B

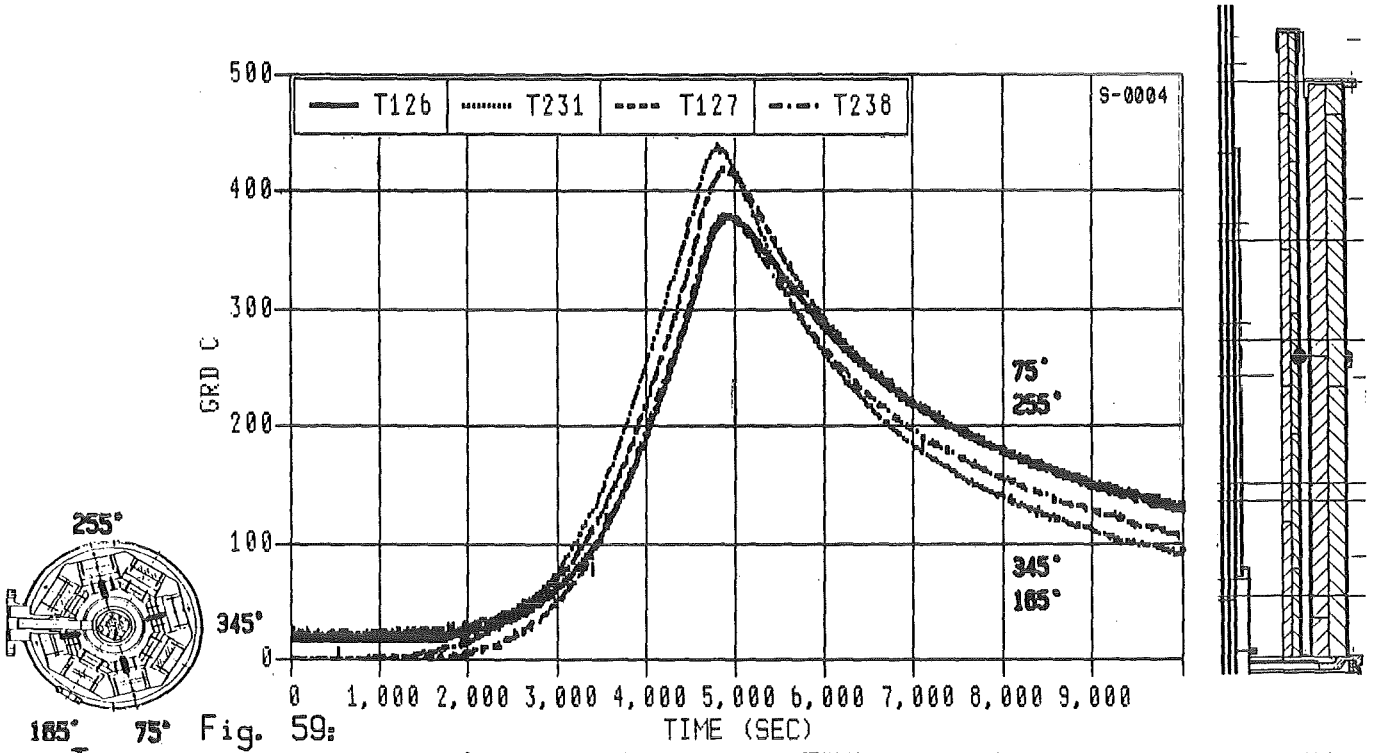

Fig. 59: Temperature in insulation; elevation 550 mm; radius 192 mm; at 75°, 165°, 255° and 345°; for high temperature test CORA bundle B

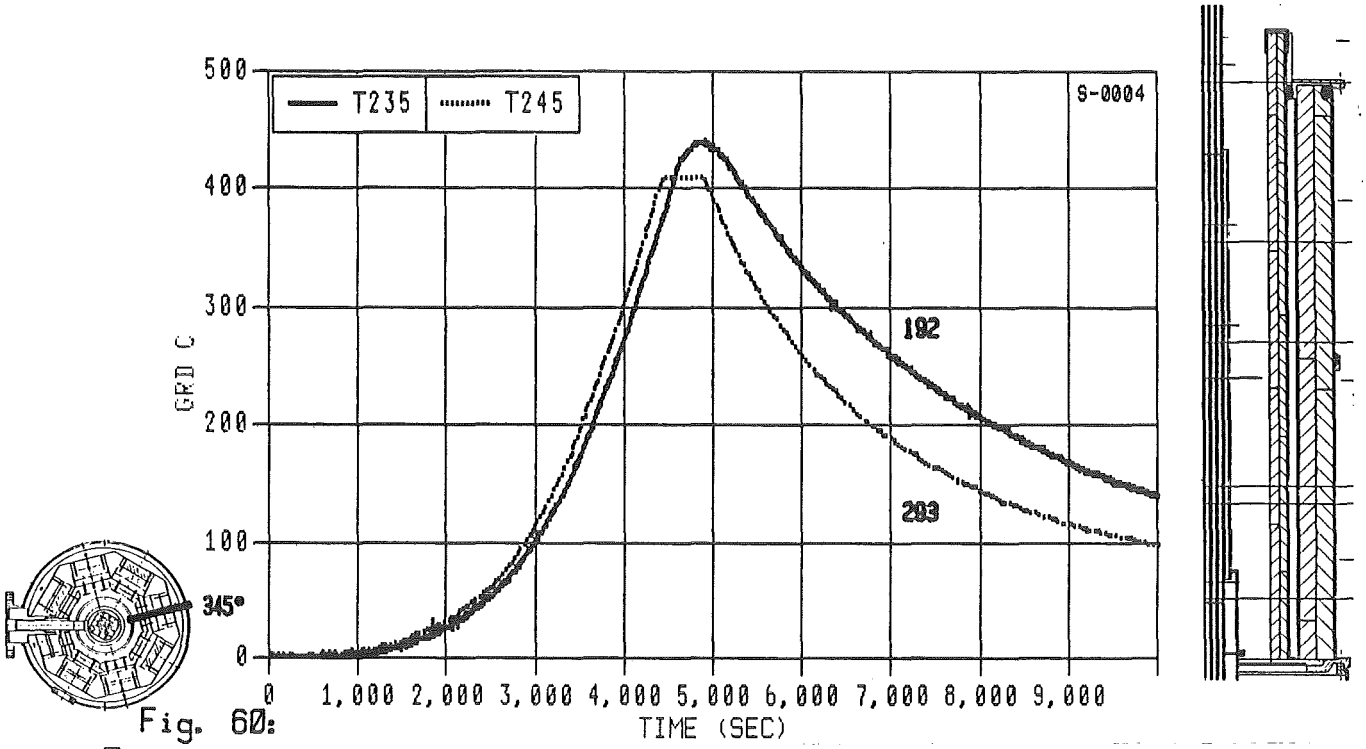

Fig. 60: Temperature in insulation; elevation 1150 mm; at 345°; radius 192 and 293 mm; for high temperature test CORA bundle B

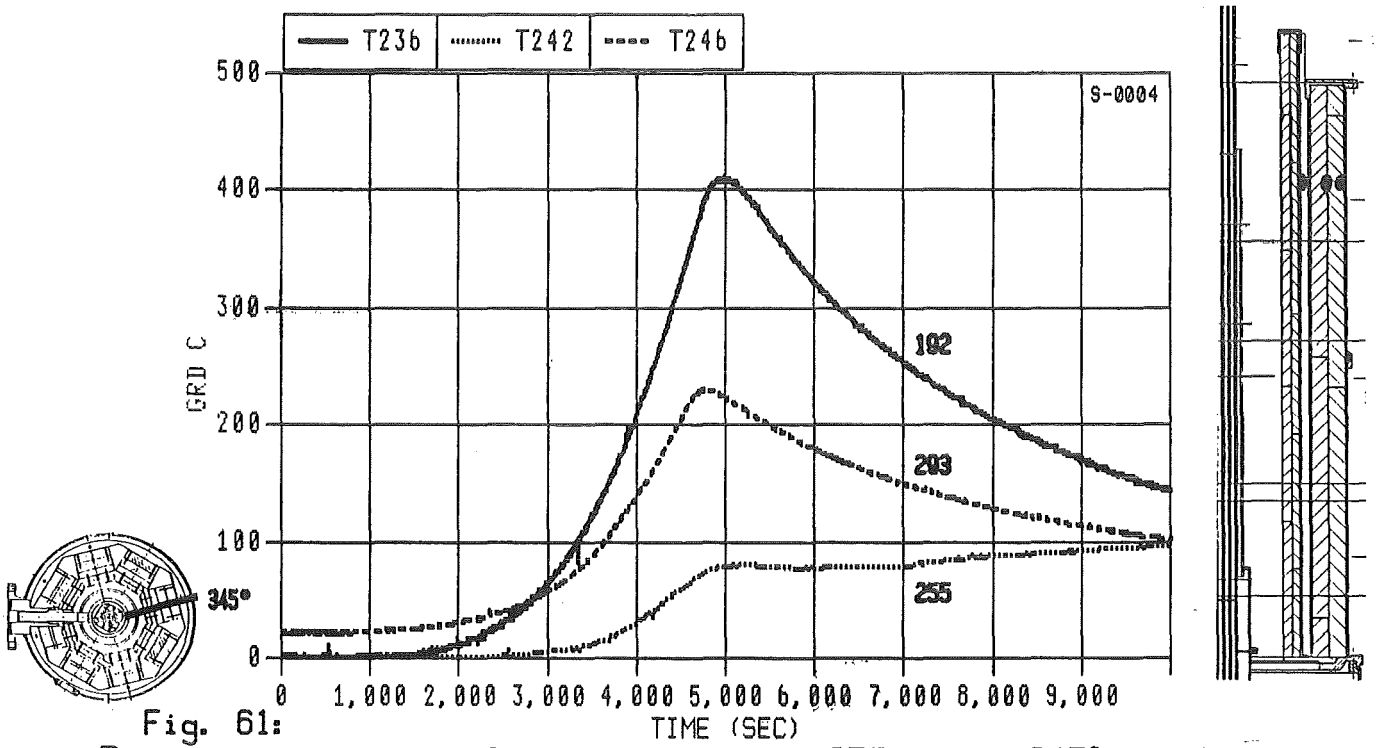

Fig. 61: Temperature in insulation; elevation 950 mm; at 345°; radius 192, 255 and 293 mm; for high temperature test CORA bundle B

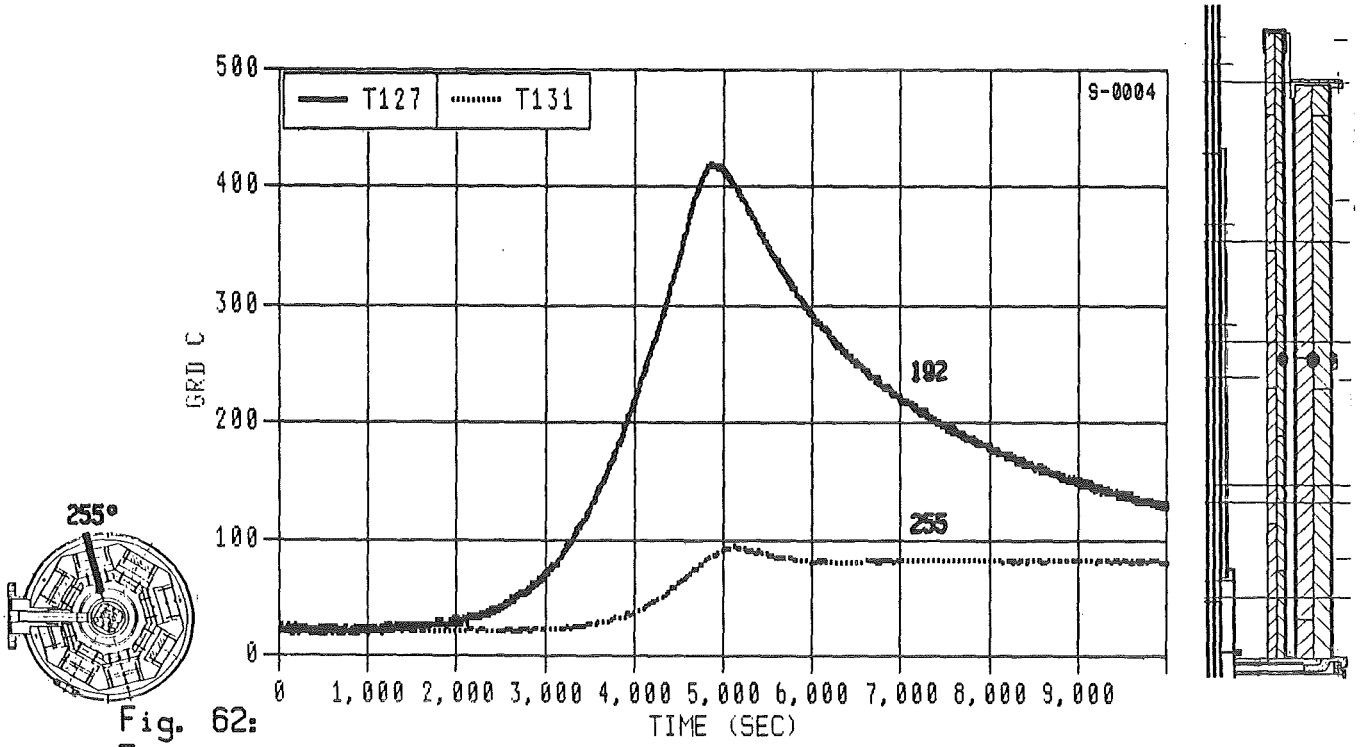

Fig. 62: Temperature in insulation; elevation 550 mm; at 255°; radius 192 and 255 mm; for high temperature test CORA bundle B

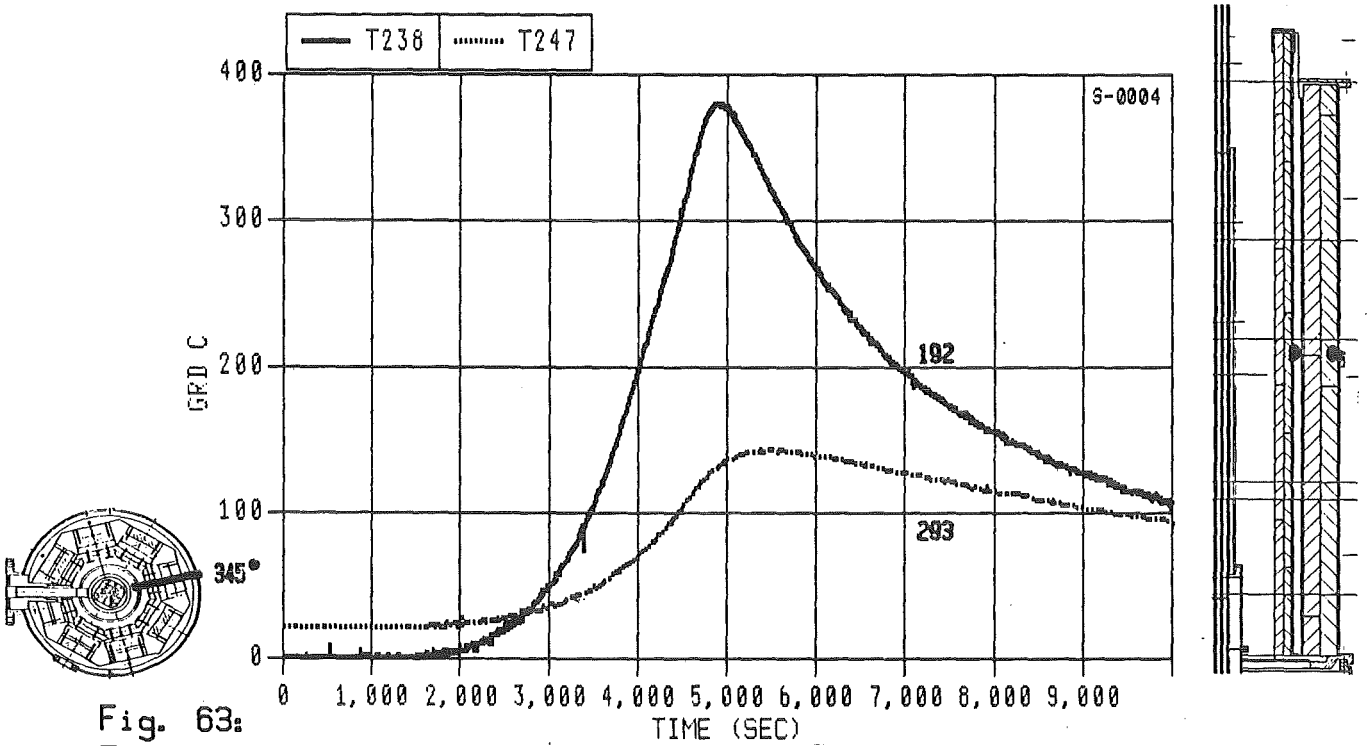

Fig. 63: Temperature in insulation; elevation 550 mm; at 345°; radius 192 and 293 mm; for high temperature test CORA bundle B

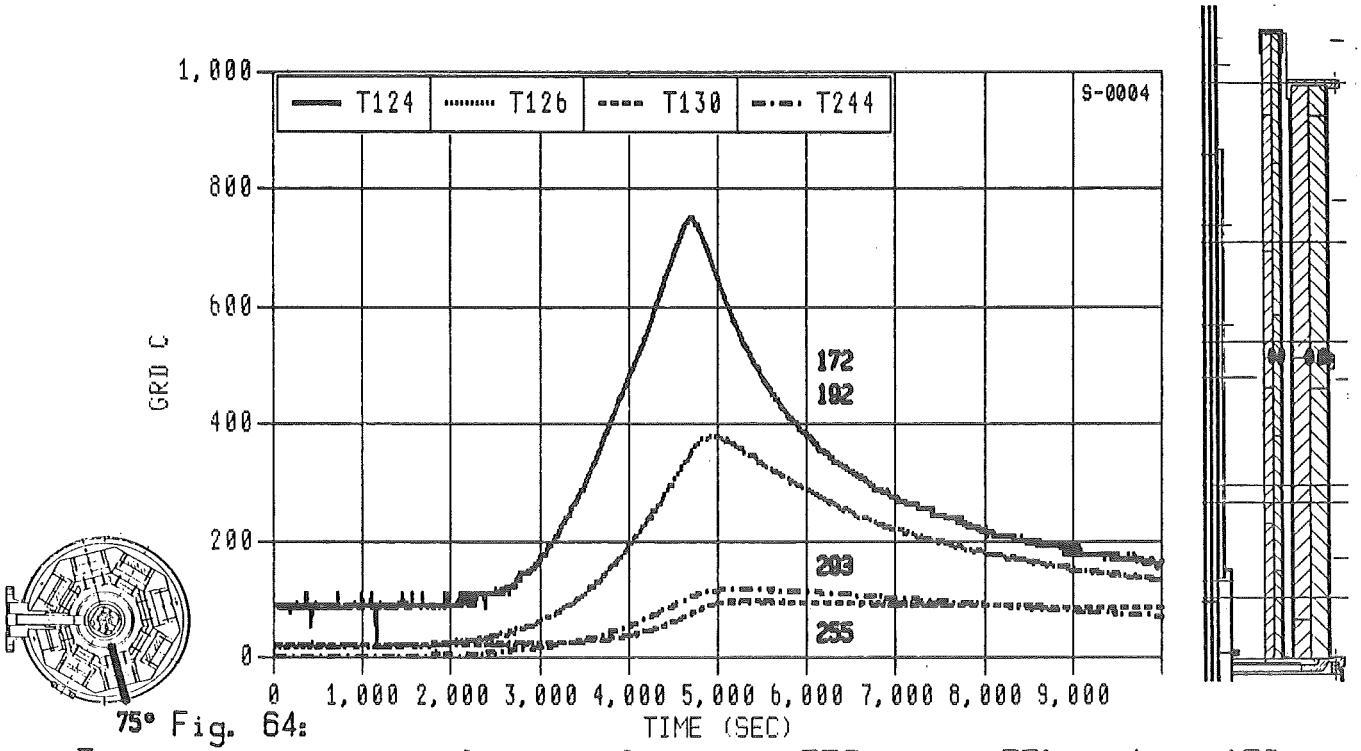

Fig. 64: Temperature in insulation; elevation 550 mm; at 75°; radius 172, 192, 255 and 293 mm; for high temperature test CORA bundle B

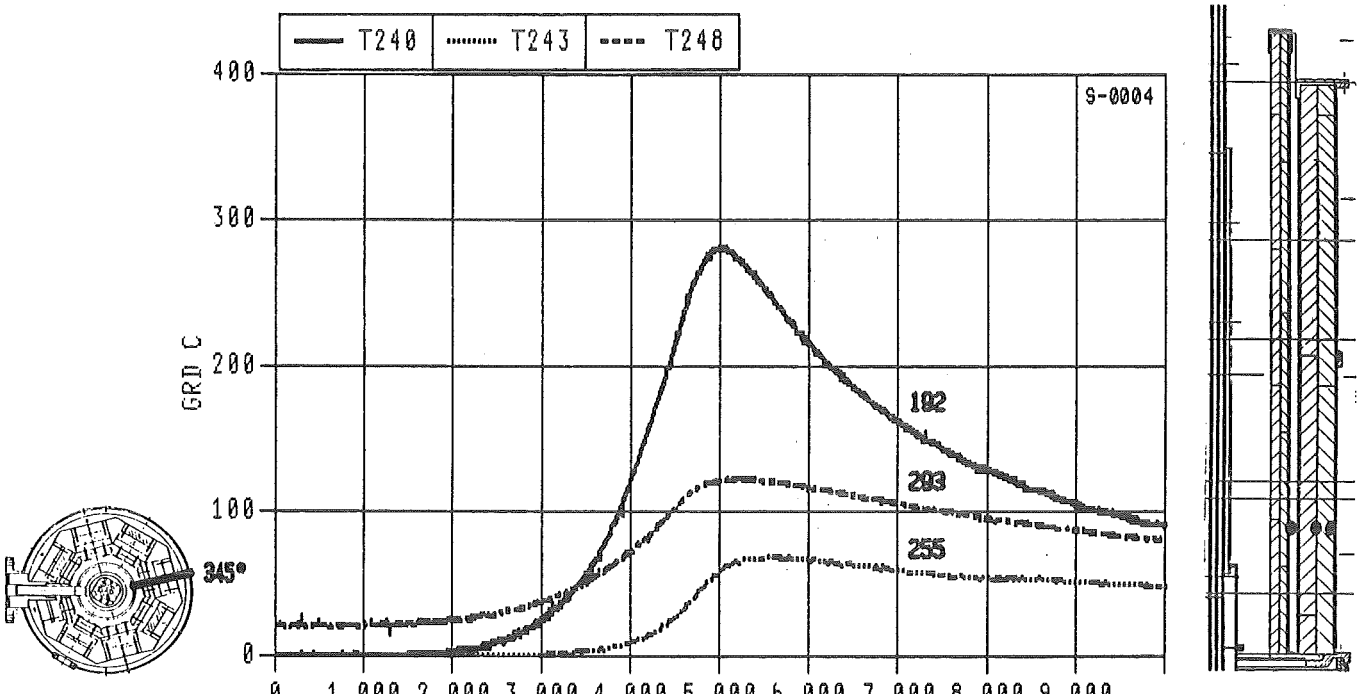

Fig. 65: Temperature in insulation; elevation 150 mm; at 345°; radius 192, 255 and 293 mm; for high temperature test CORA bundle B

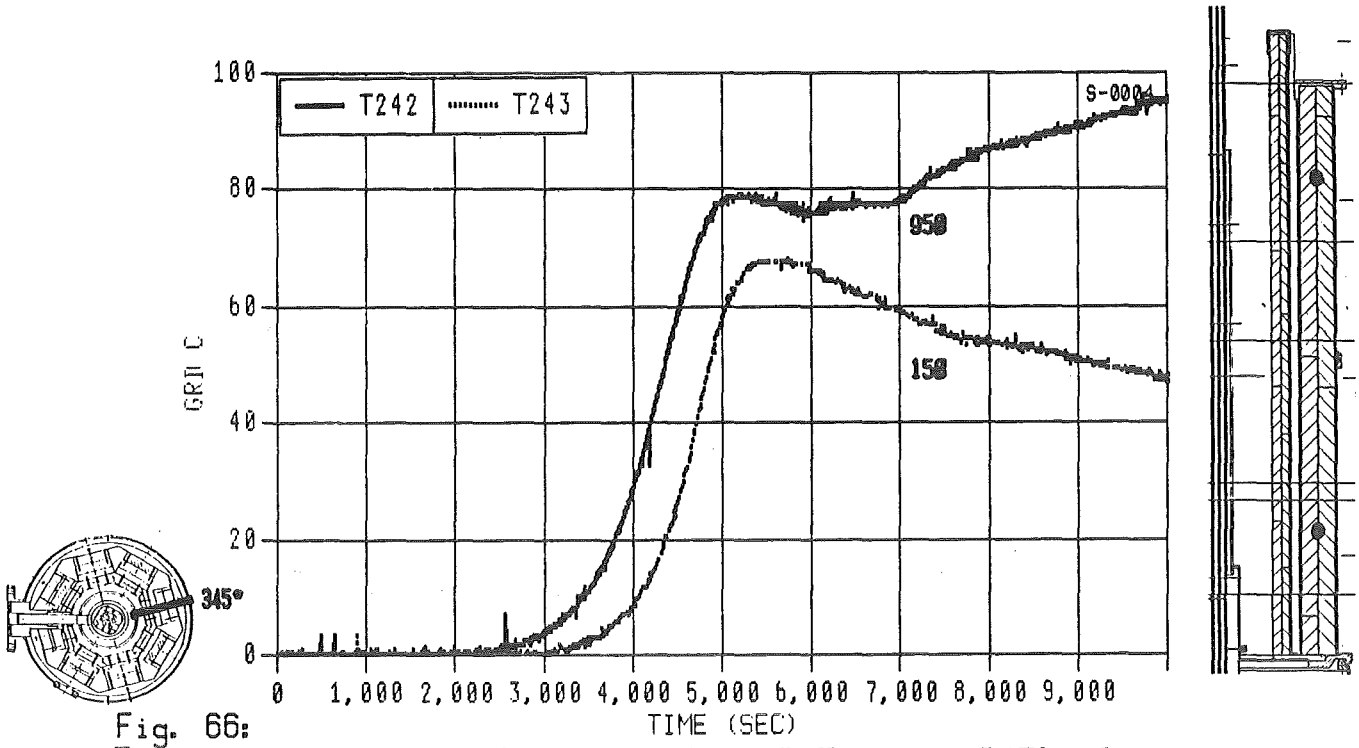

Fig. 66: Temperature in insulation; radius 255 mm; at 345°; elevation 950 and 150 mm; for high temperature test CORA bundle B

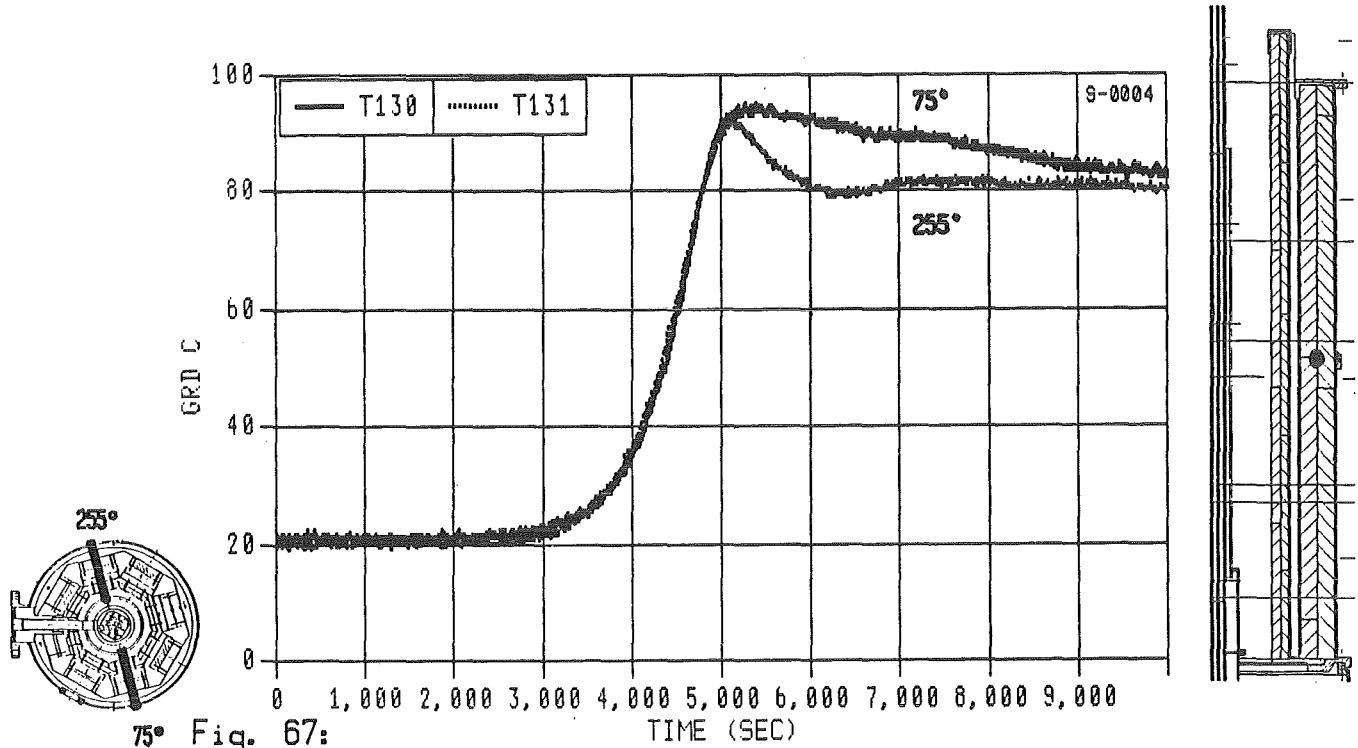

Fig. 67: Temperature in insulation; radius 255 mm; elevation 550 mm; at 75° and 255°; for high temperature test CORA bundle B

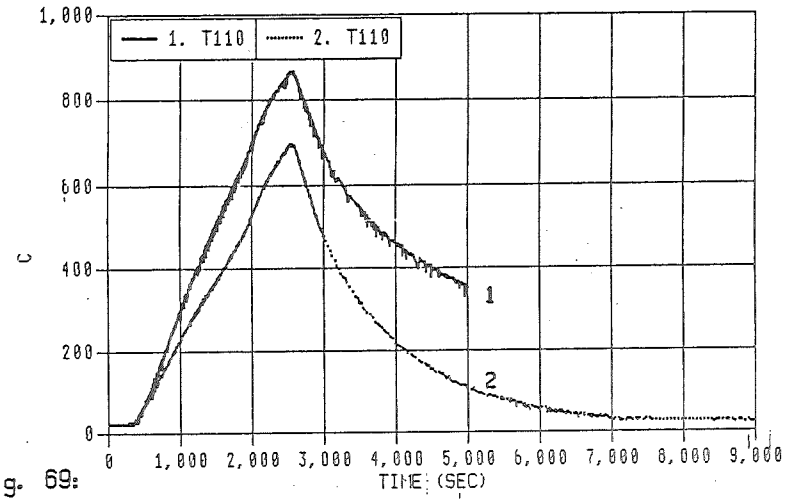

Fig. 69: Temperatures of unheated rod 29 at 550 mm elevation for heatup in vacuum (1) and Argon (2) of CORA bundle B

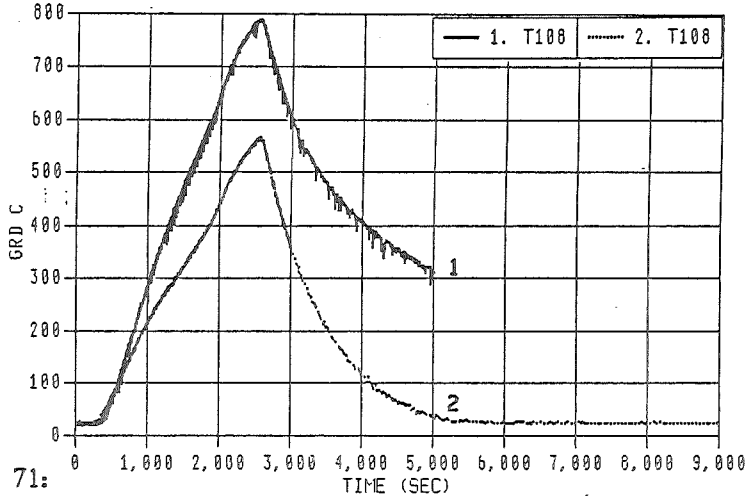

Fig. 71: Temperatures of unheated rod 21 at 550 mm elevation for heatup in vacuum (1) and Argon (2) of CORA bundle B

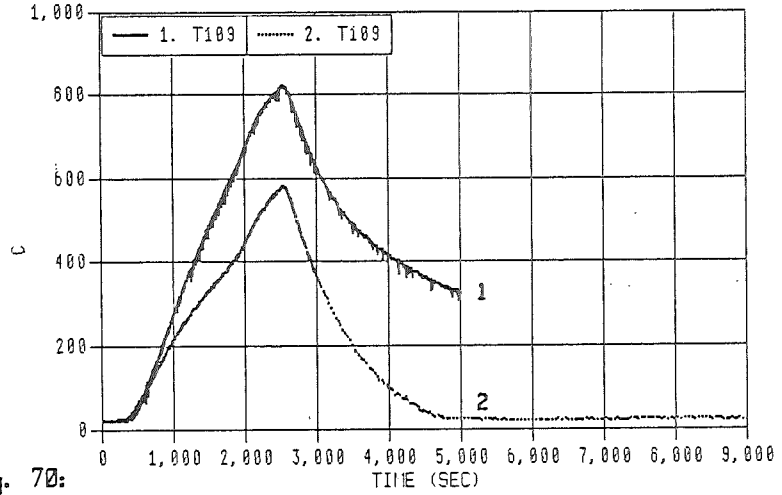

Fig. 70: Temperatures of unheated rod 23 at 550 mm elevation for heatup in vacuum (1) and Argon (2) of CORA bundle B

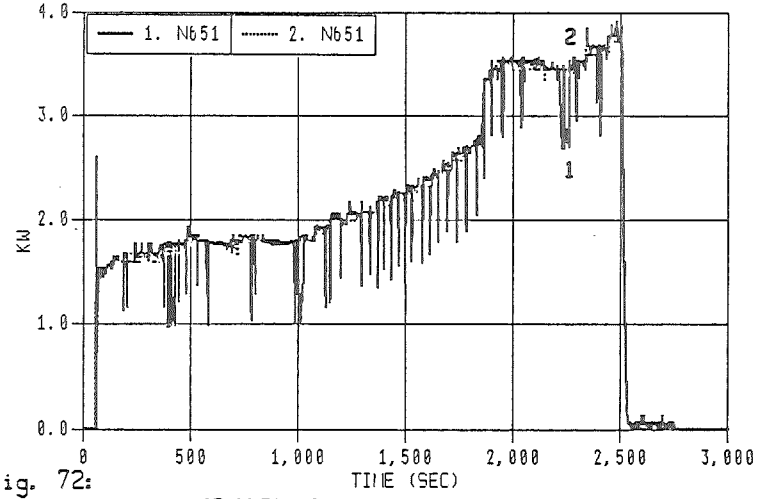

Fig. 72: Power inputs (6/16) for heatup in vacuum (1) and Argon (2) of CORA bundle B

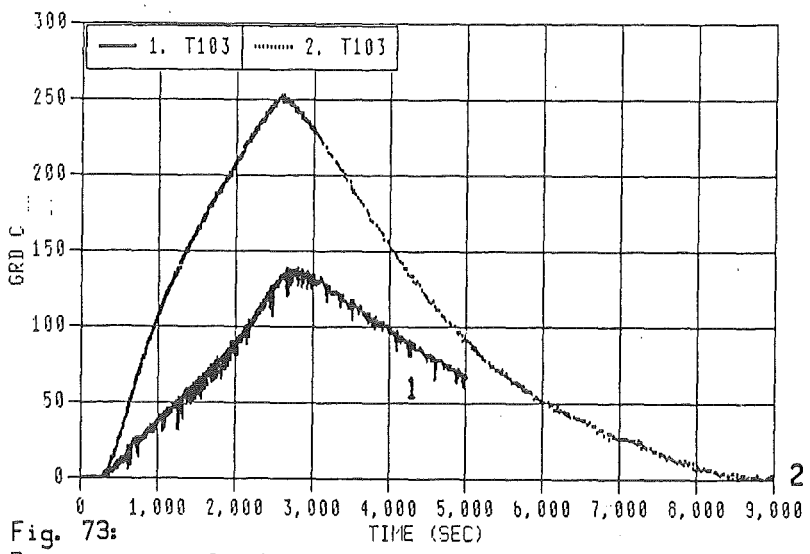

Fig. 73: Temperatures of unheated rod 15 at 1390 mm elevation for heatup in vacuum (1) and Argon (2) of CORA bundle B

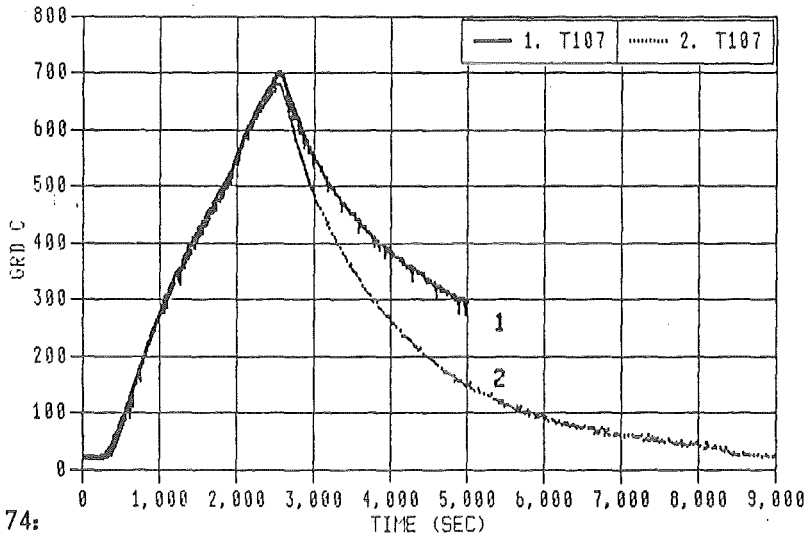

Fig. 74: Temperatures of unheated rod 31 at 1000 mm elevation for heatup in vacuum (1) and Argon (2) of CORA bundle B

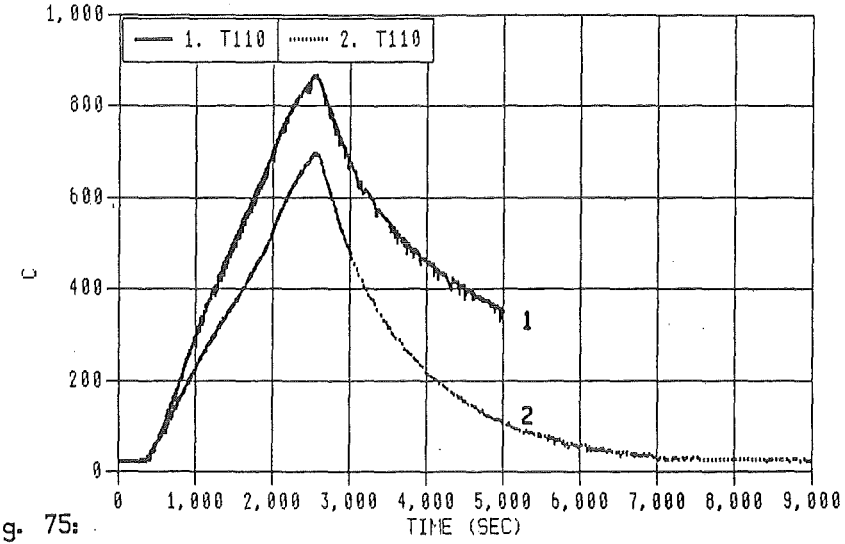

Fig. 75: Temperatures of unheated rod 29 at 550 mm elevation for heatup in vacuum (1) and Argon (2) of CORA bundle B

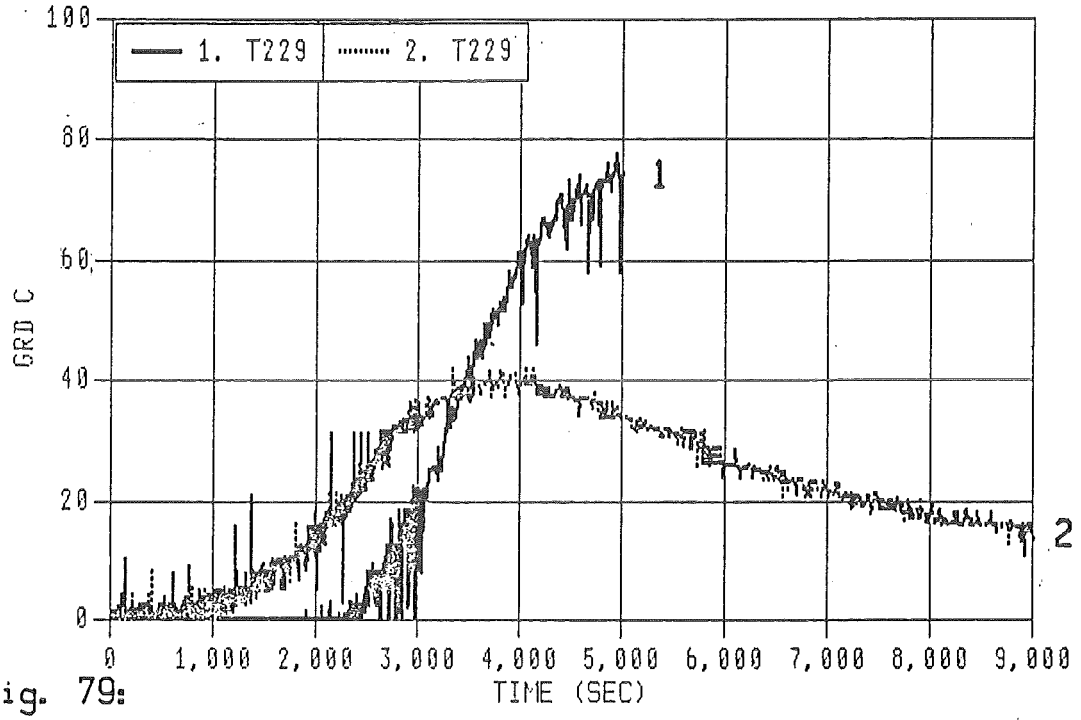

Fig. 79:
Temperatures in insulation at 950 mm elevation; radius 192 mm for heatup in vacuum (1) and Argon (2) of CORA bundle B

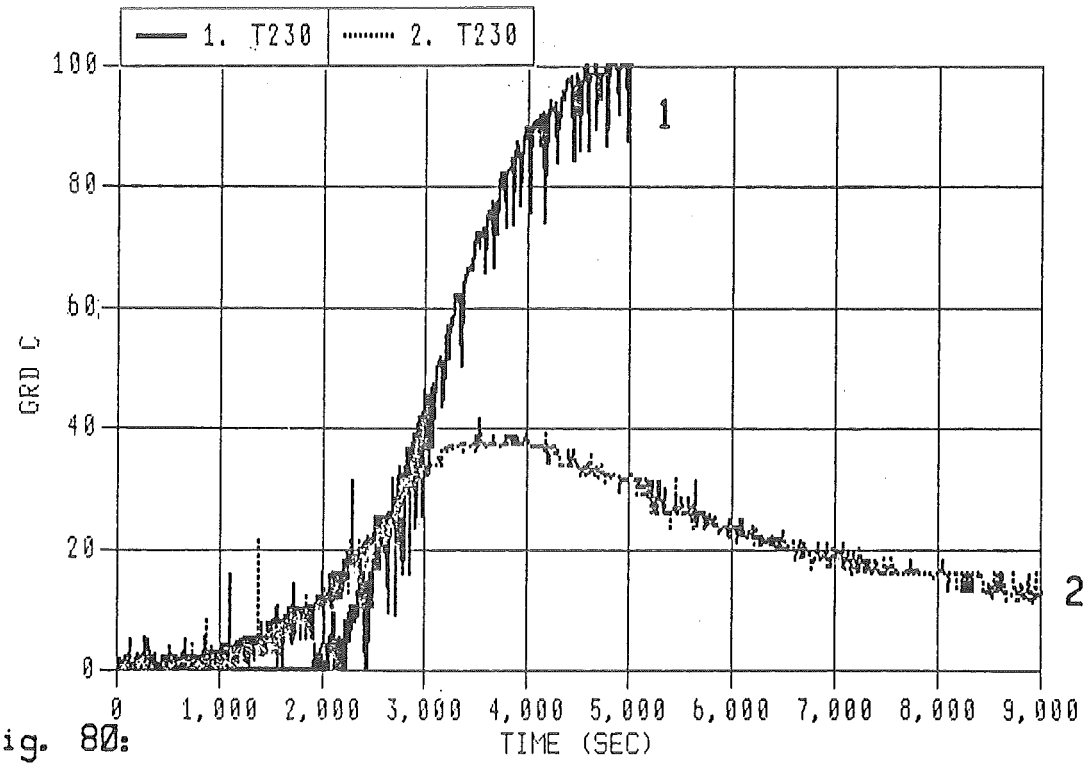

Fig. 80:
Temperatures in insulation at 750 mm elevation; radius 192 mm for heatup in vacuum (1) and Argon (2) of CORA bundle B

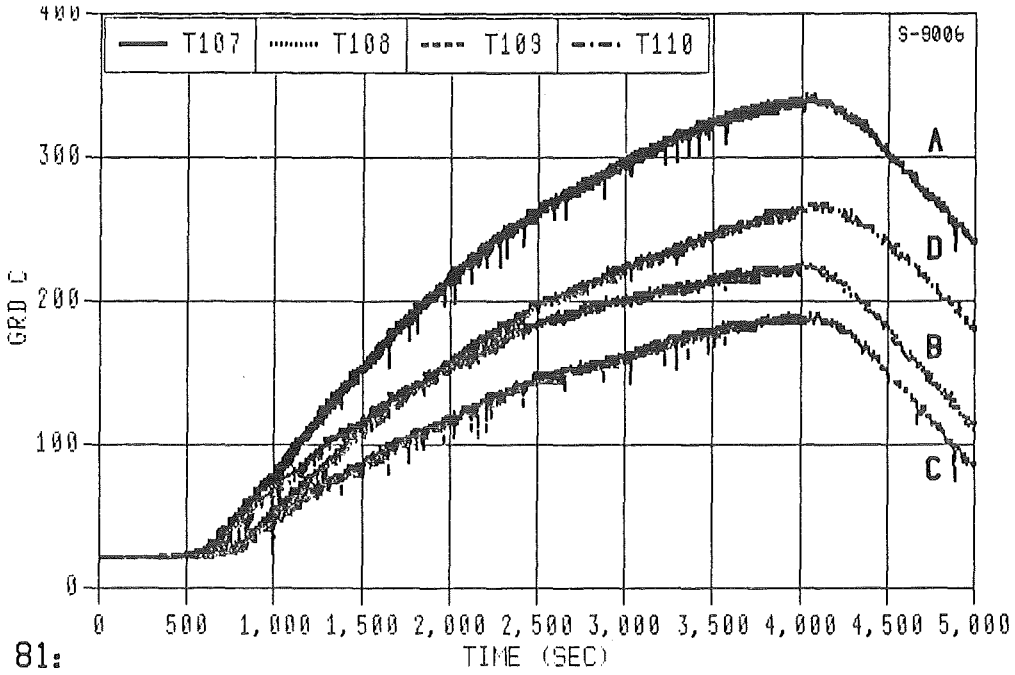

Fig. 81: Temperature increase of unheated rod 31 (A) at 1000 mm and unheated rods 21 (B), 23 (C) and 29 (D) at 550 mm due to constant power input (CORA bundle B)

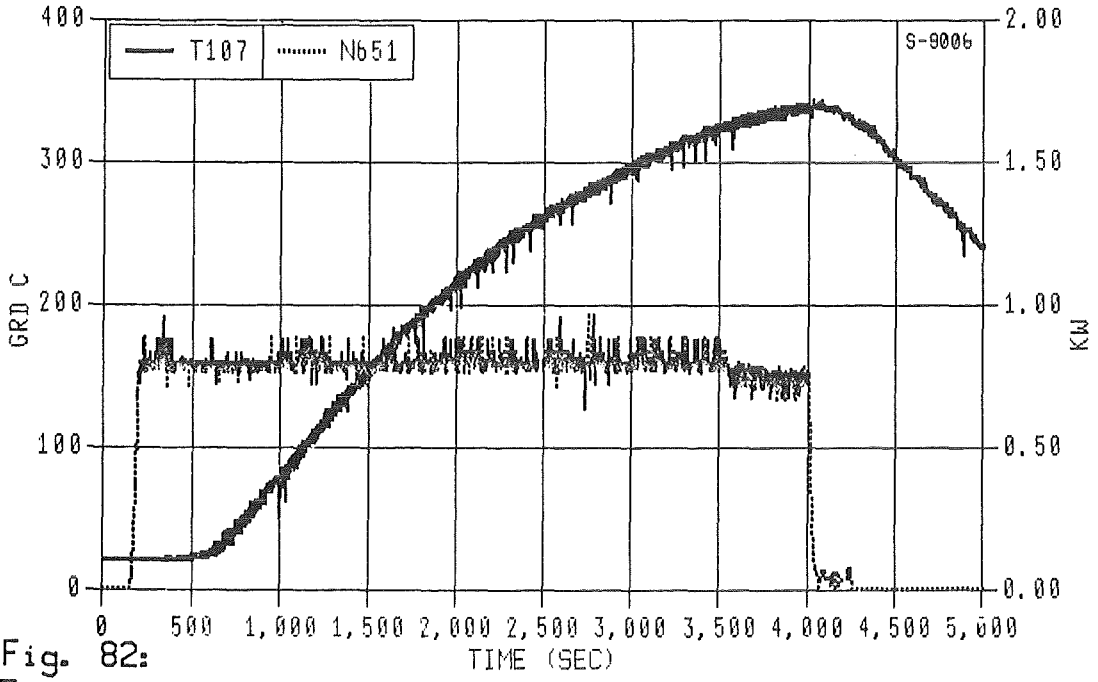

Fig. 82: Temperature increase of unheated rod 31 at 1000 mm elevation due to constant power input (6/16; CORA bundle B)

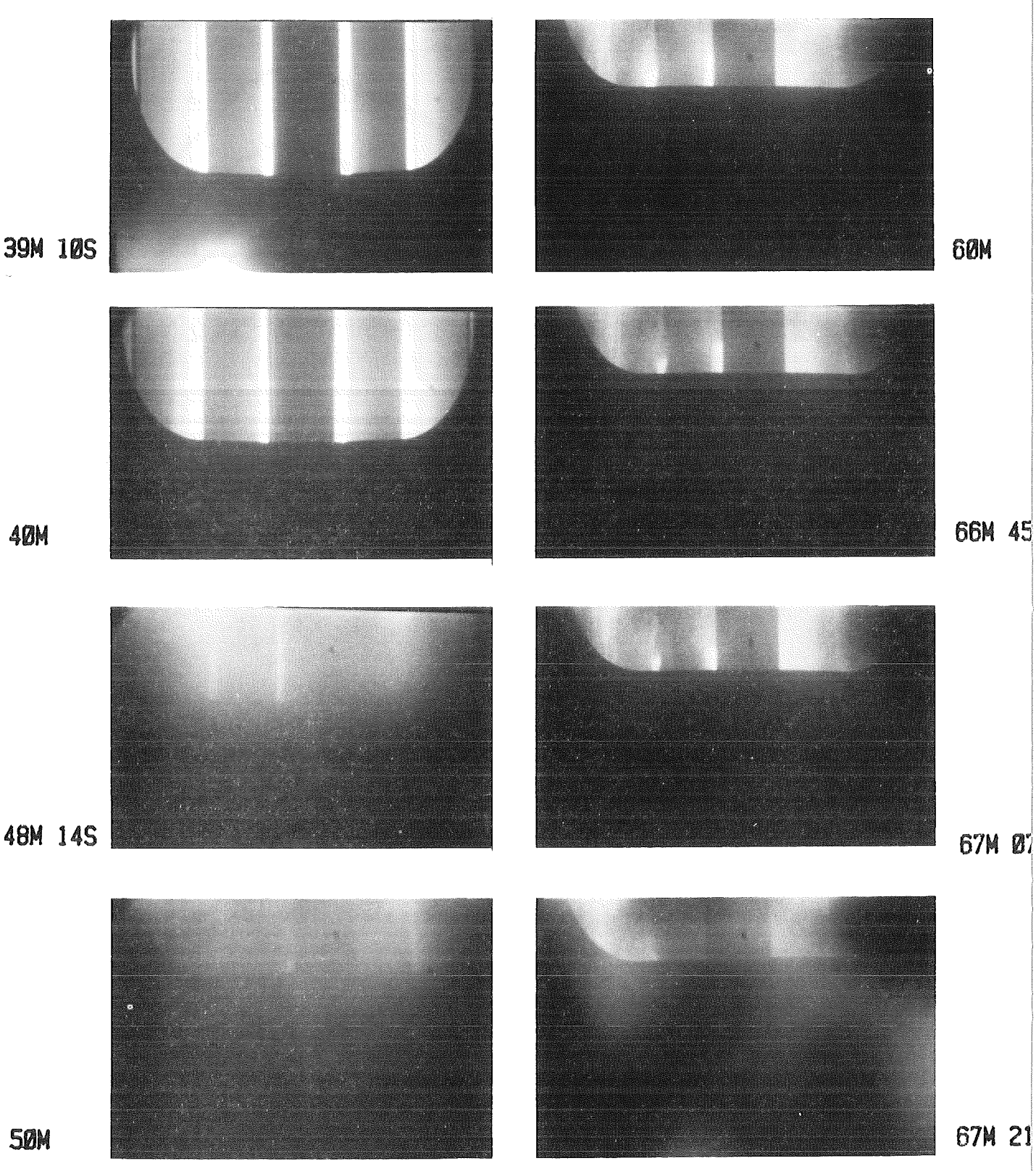

Fig. 83: CORA scoping test B: Pictures taken at H35 (120 , 590mm) for test time given

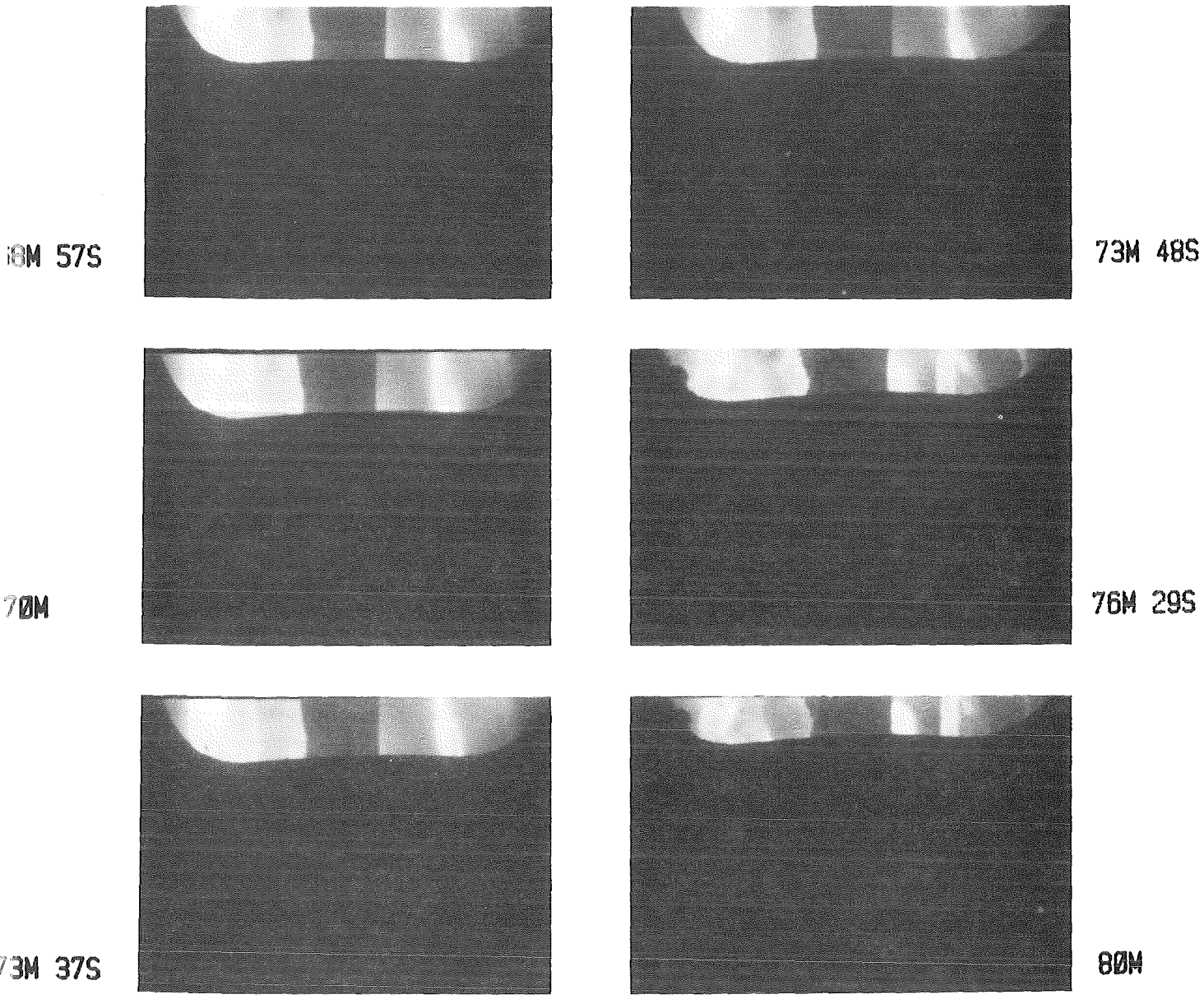

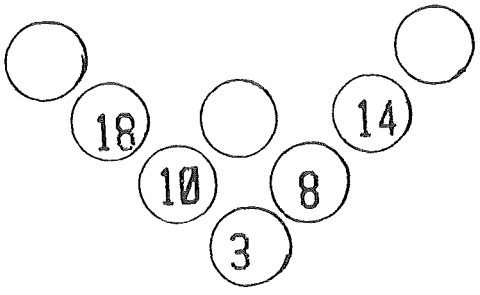

Fig. 84: CORA scoping test B: Pictures taken at H35 (120°, 590mm) for test time given.

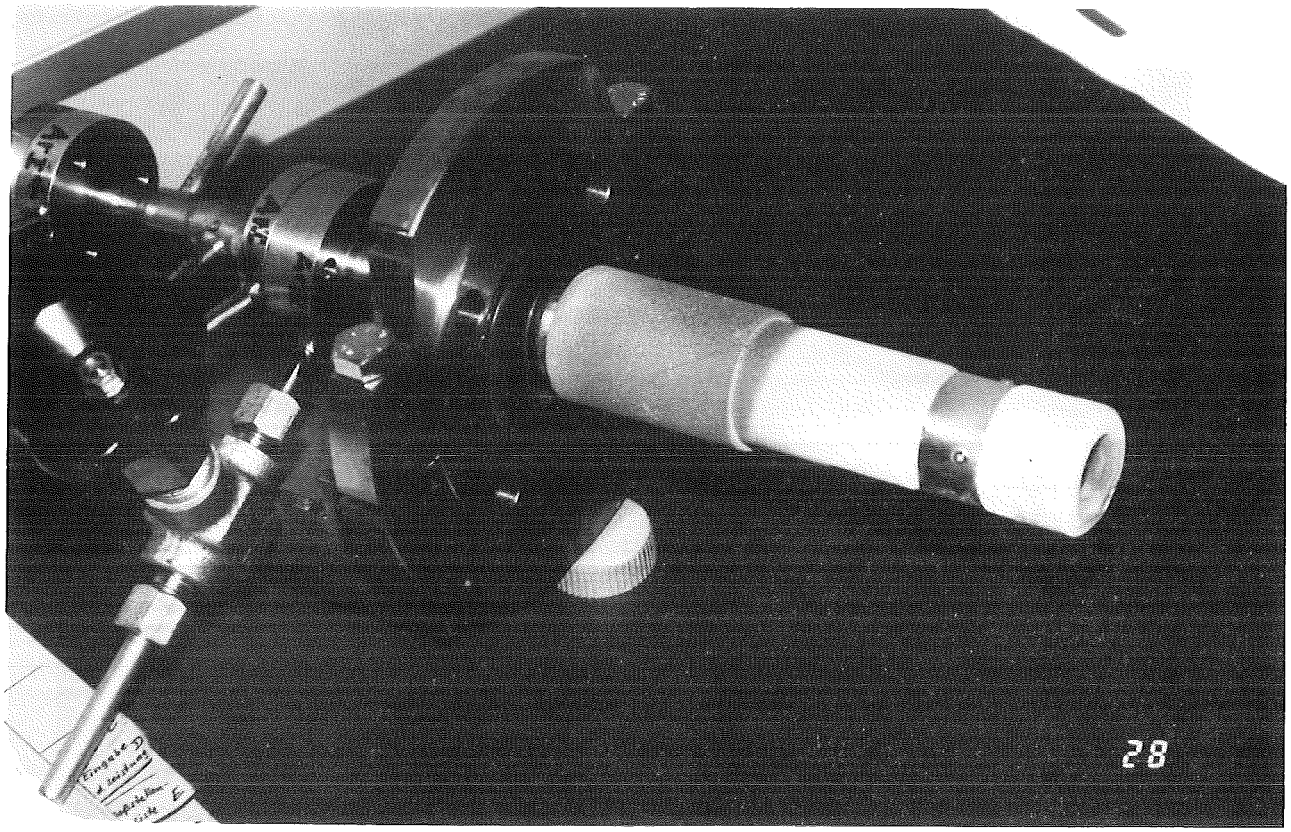

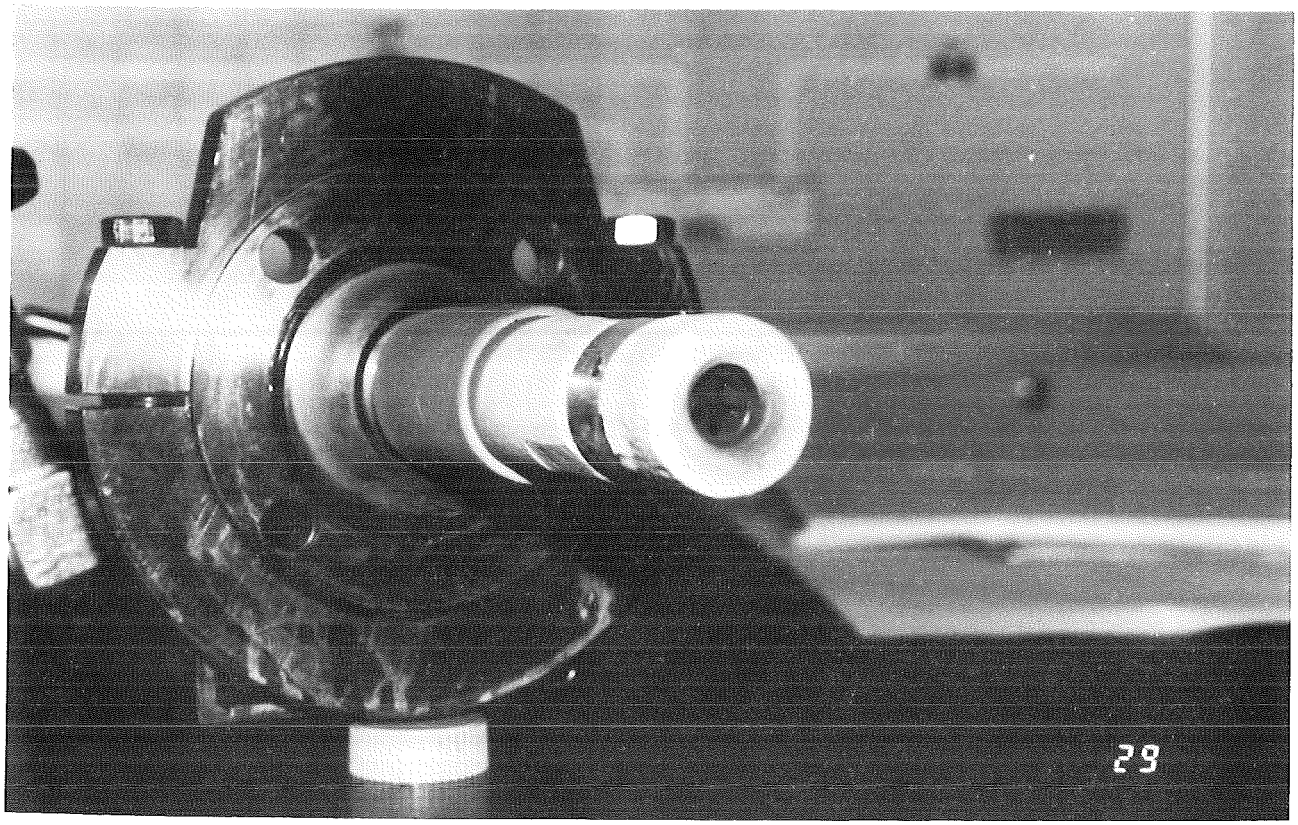

Fig. 85: Endoscope position H35 CORA bundle B

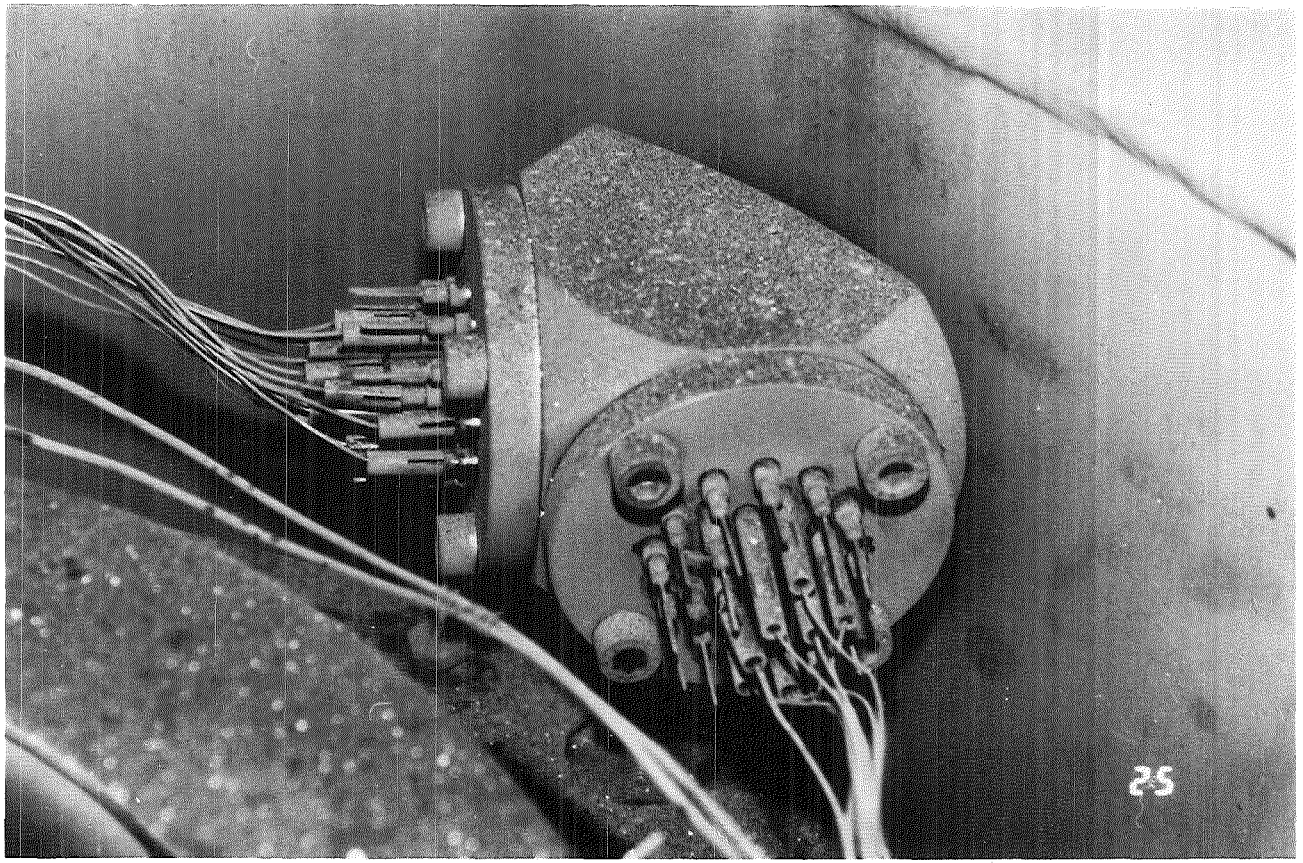

Fig. 86:
Aerosol deposition after high temperature test CORA bundle B

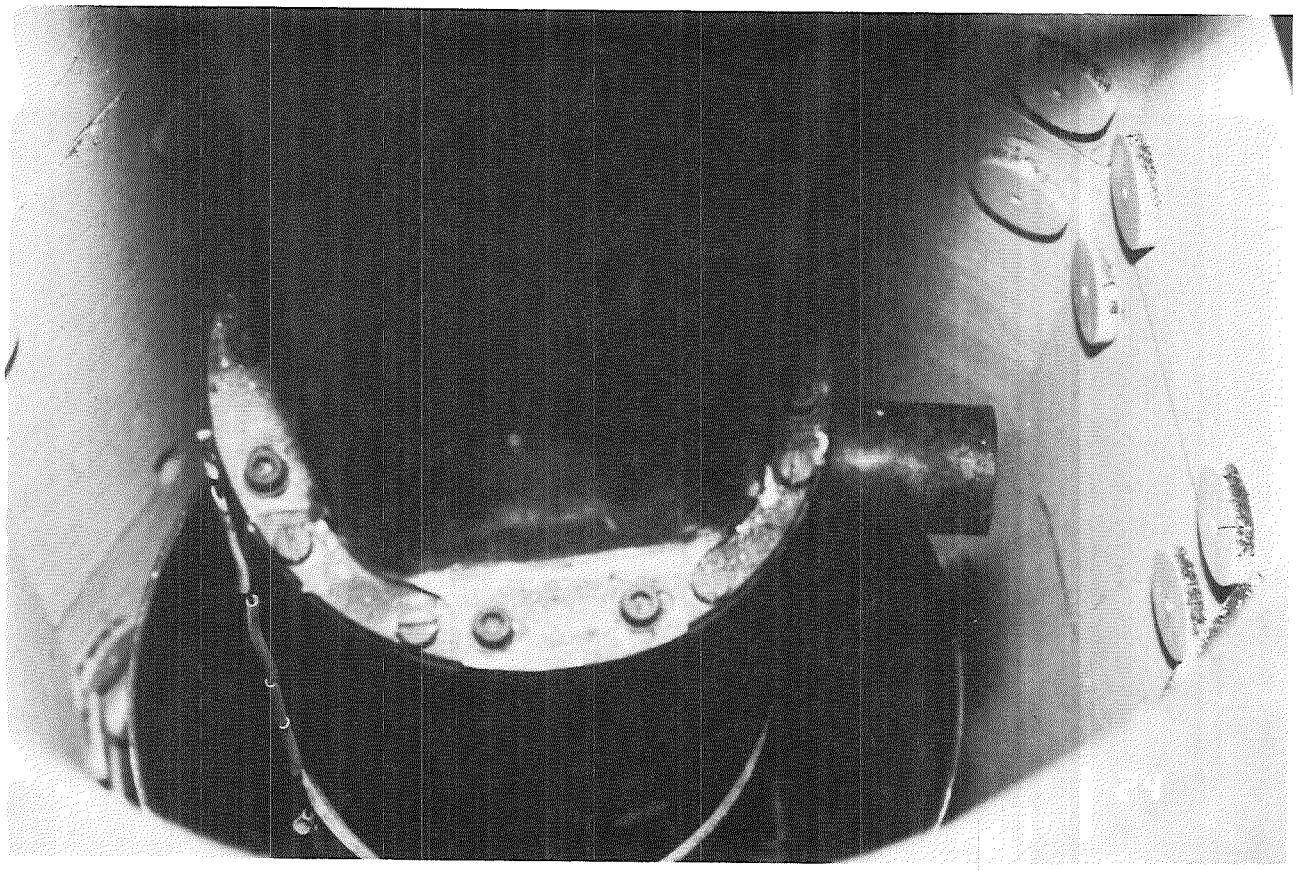

Fig. 87:
Aerosol deposition on insulation buttons after high temperature test
CORA bundle B

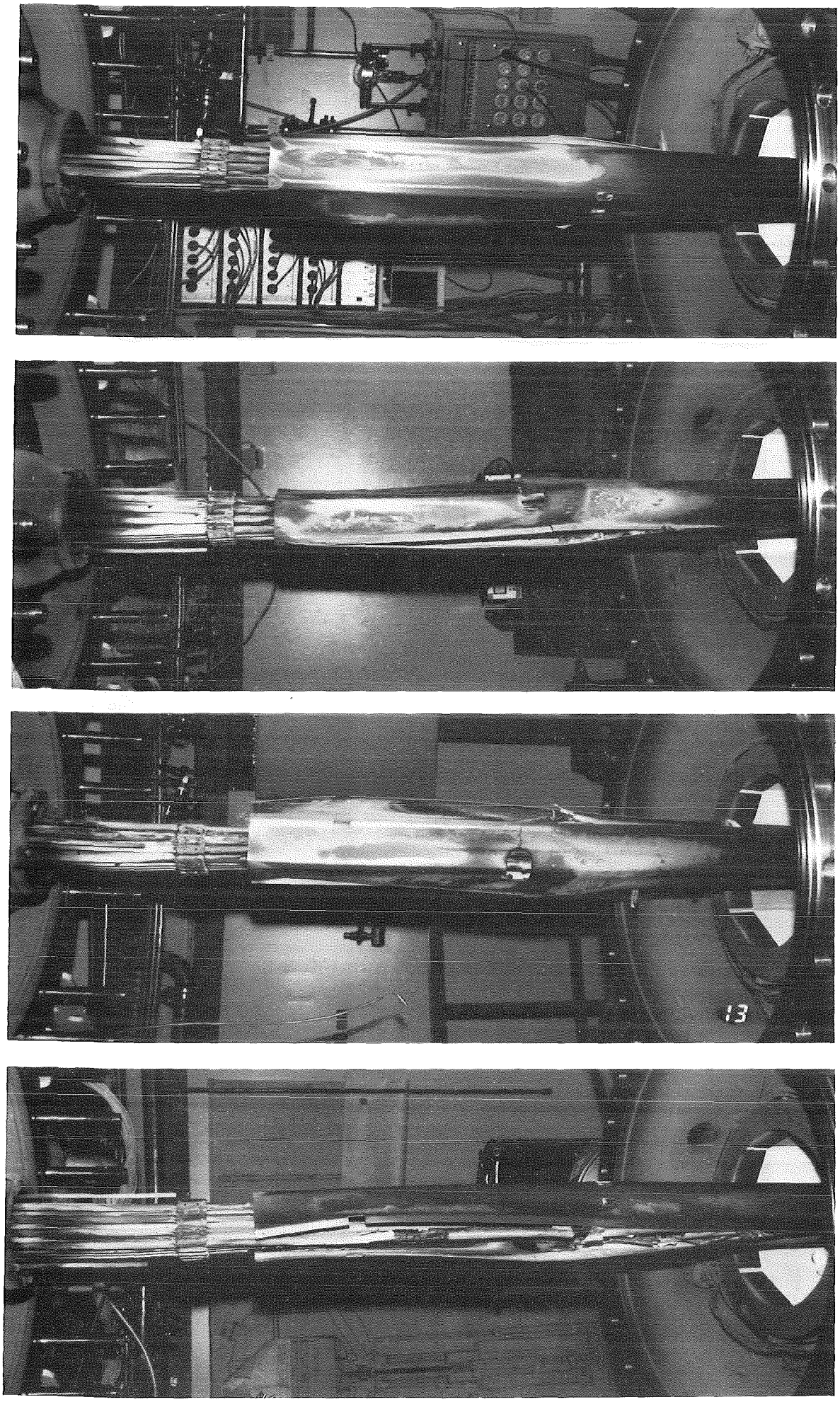

Fig. 88: Post test appearance CORA bundle B

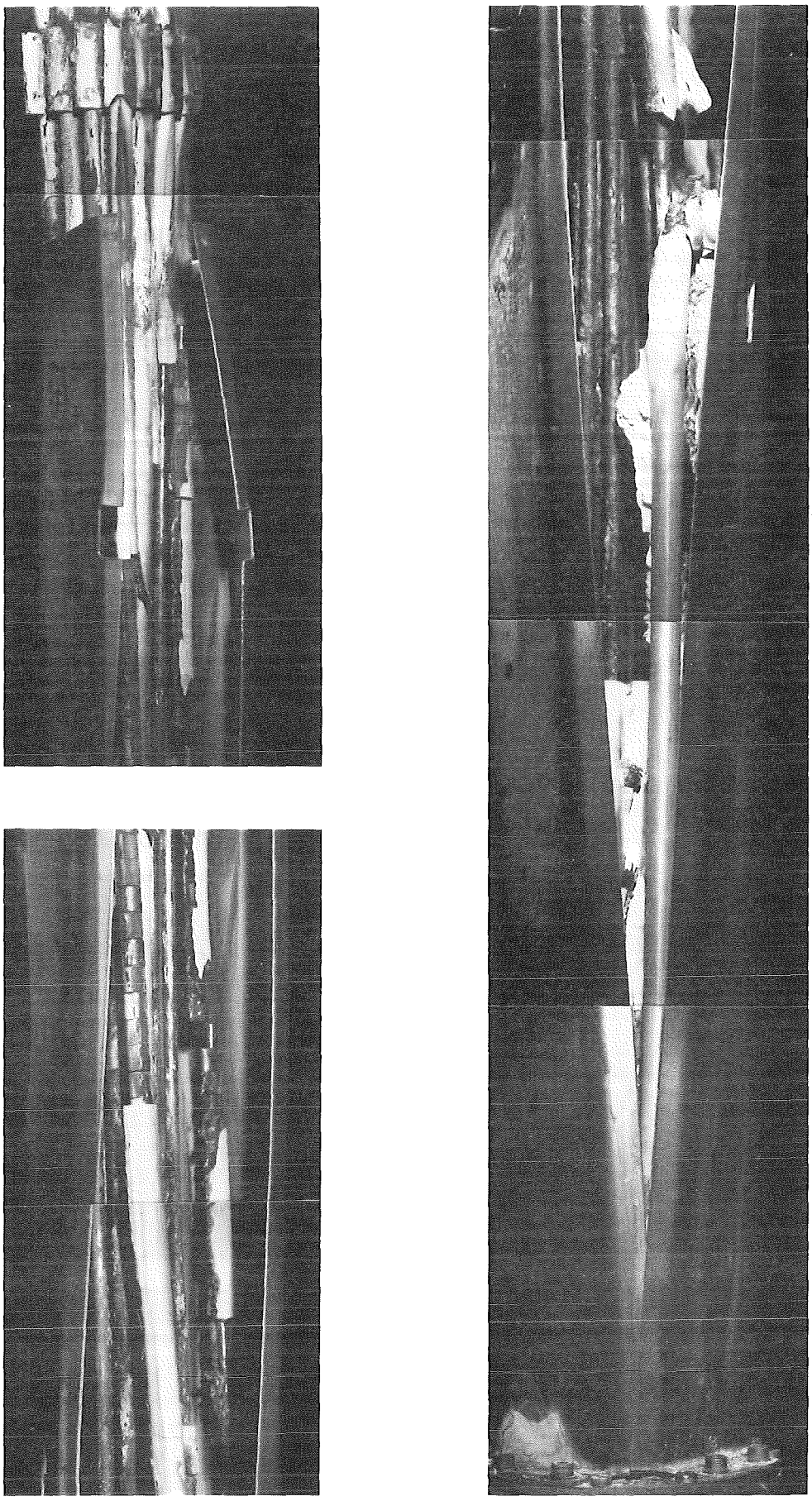

Fig. 89:
CORA Scoping Test B
Posttest appearance with shroud, 37.5° orientation

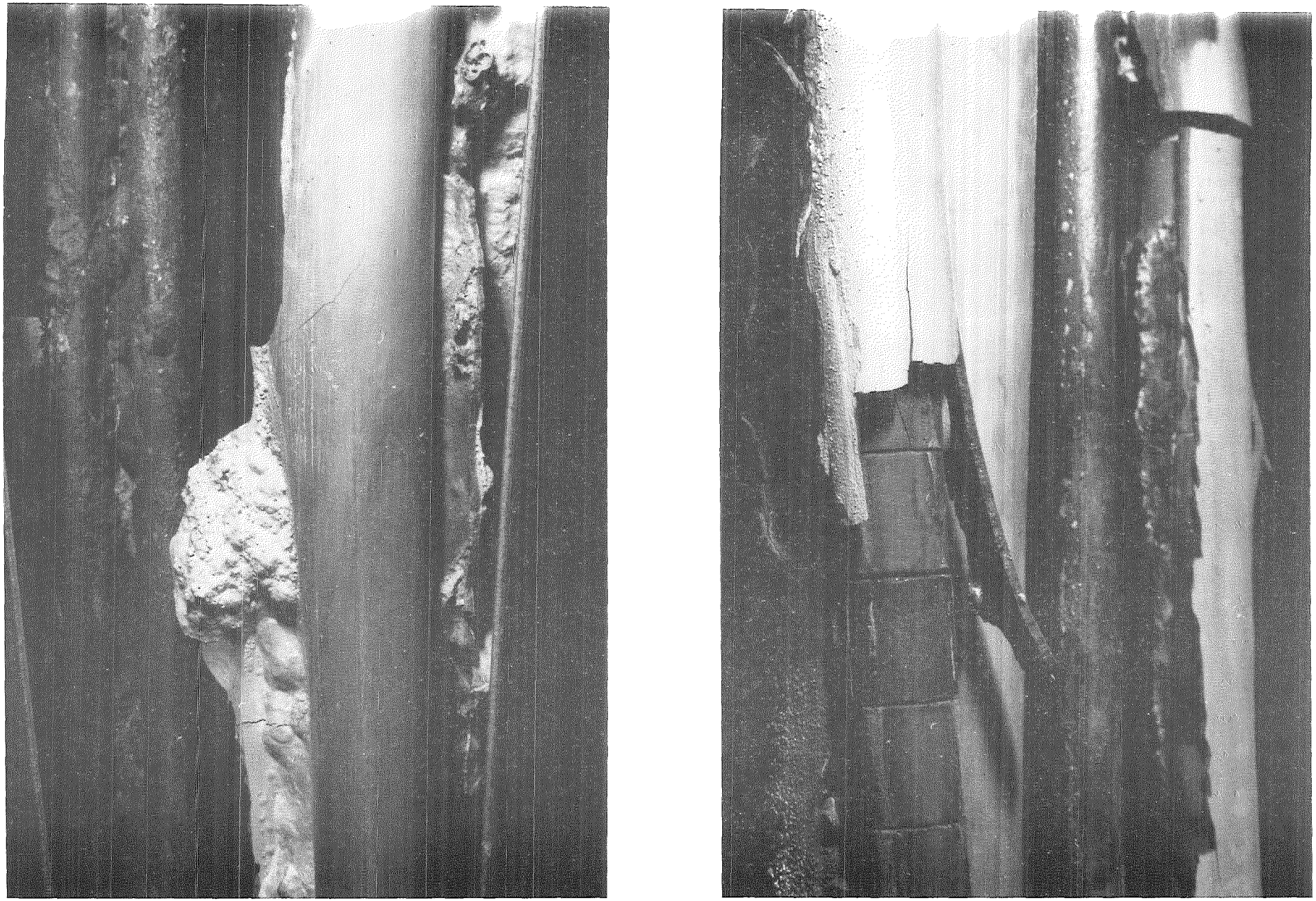

Fig. 90: Details of middle region CORA bundle B

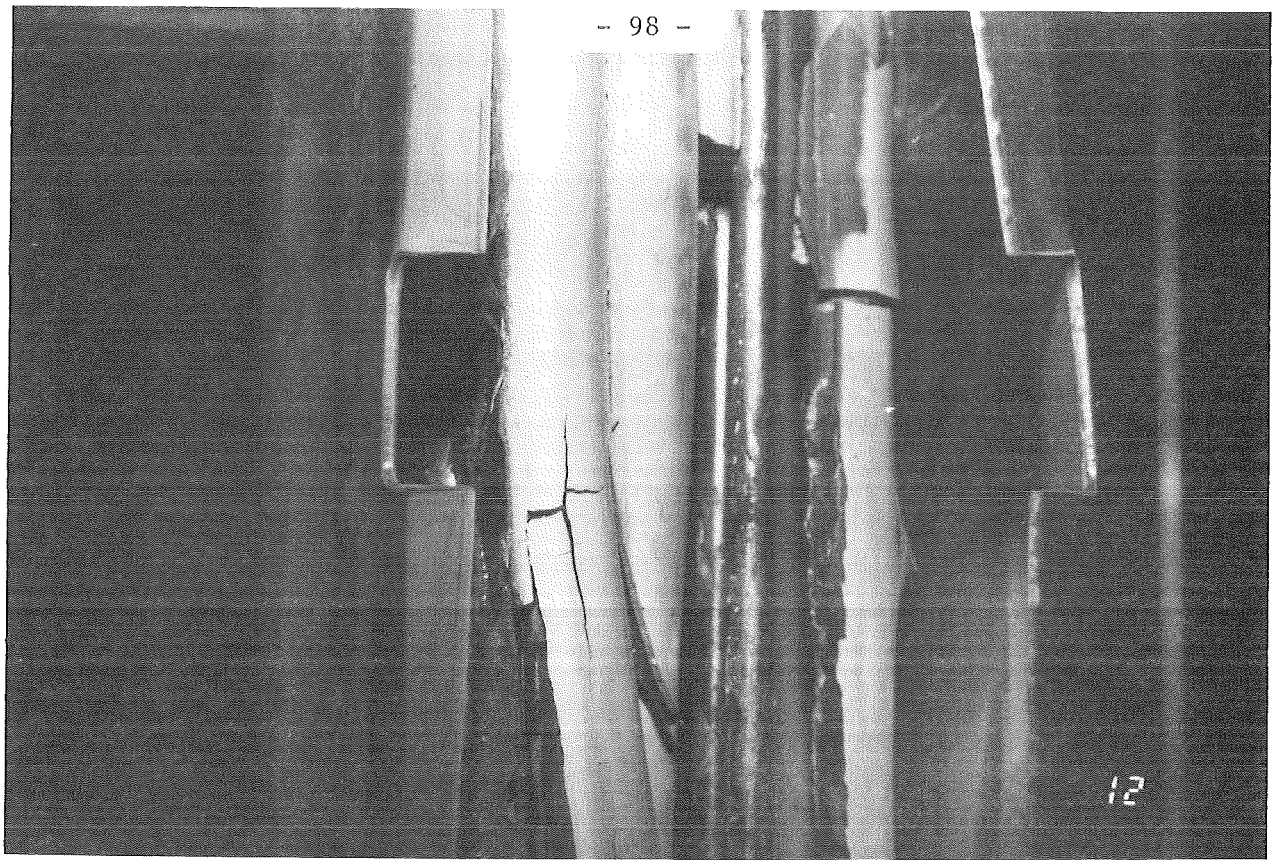

Fig. 91a: Bundle at 900mm elevation
Hole in shroud at H29

Fig. 91b: Bundle at 600mm elevation
CORA bundle B

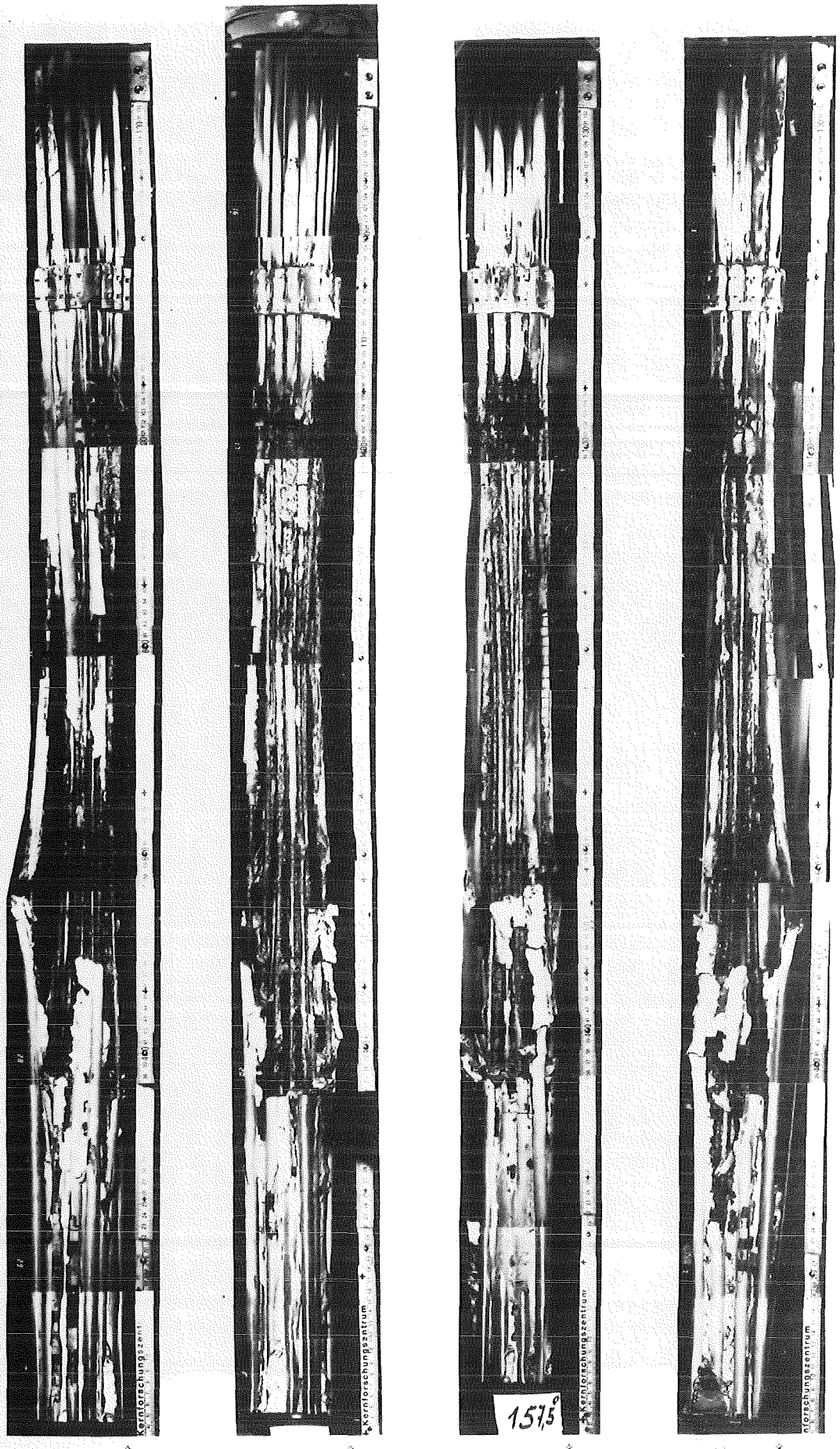

Fig. 92: **Post test appearance CORA bundle B**

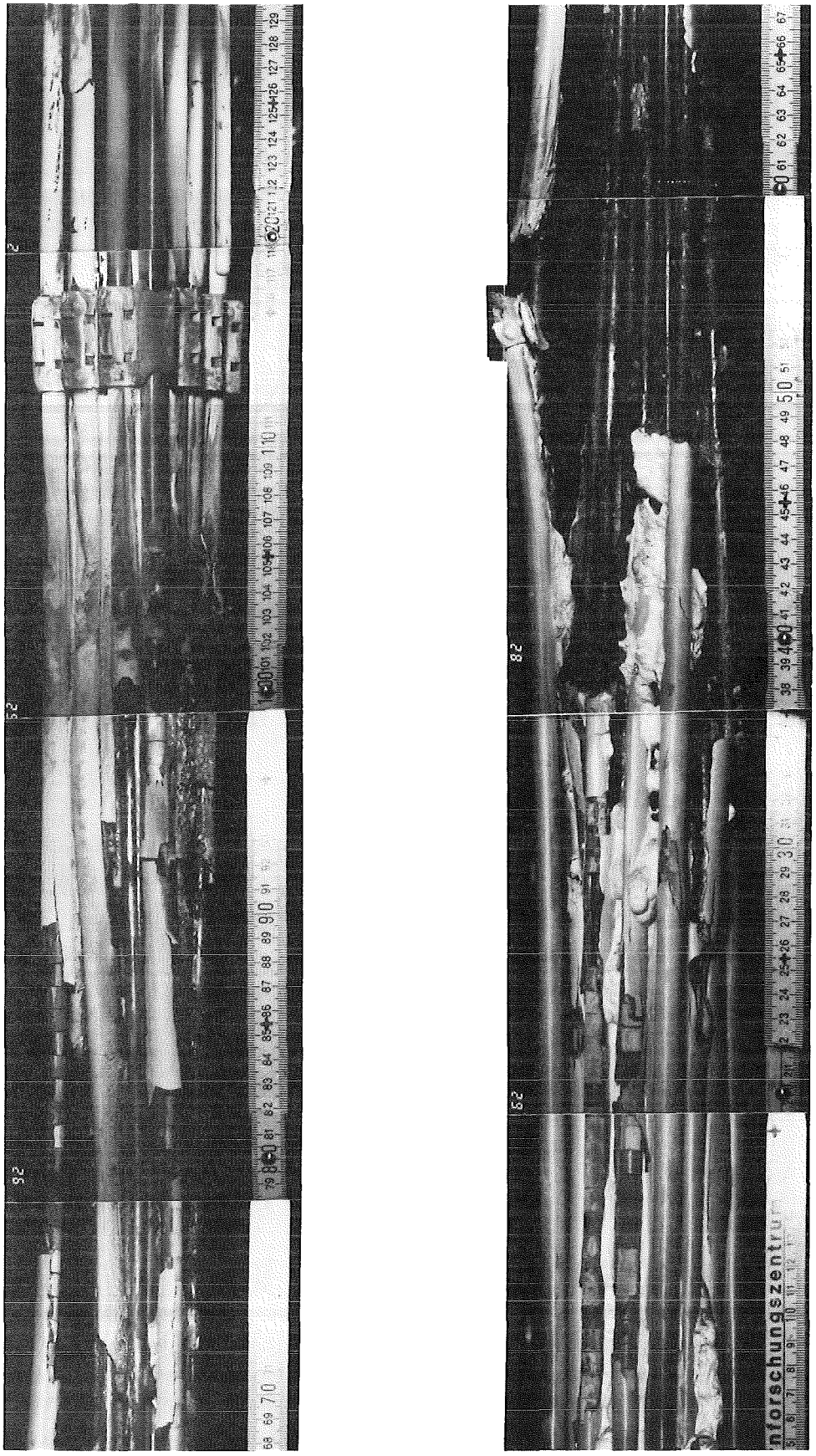

Fig. 93:
CORA Scoping Test B
Posttest view of the bundle, 307.5-degree orientation

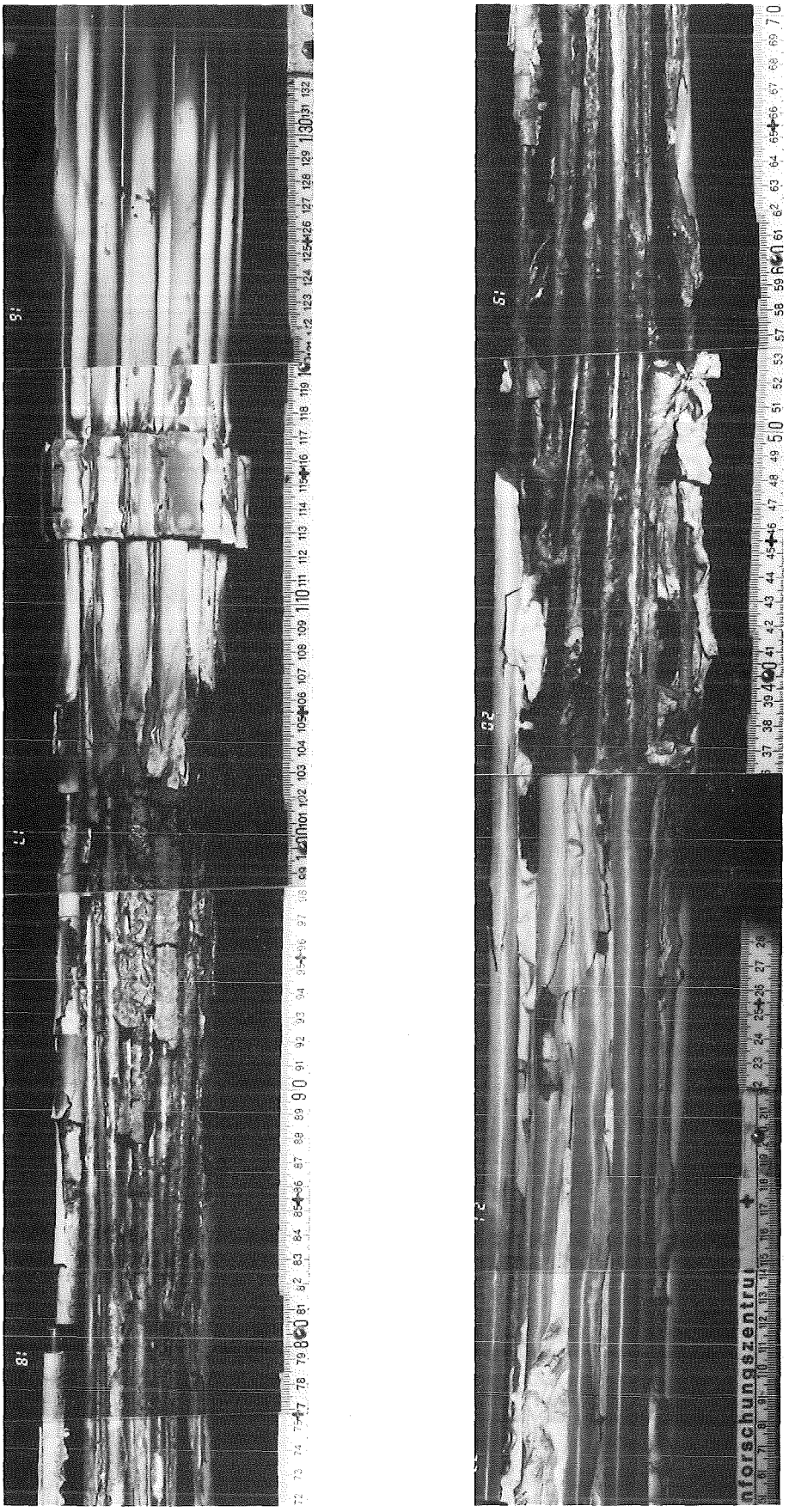

Fig. 94:
CORA Scoping Test B
Posttest view of the bundle, 232.5-degree orientation

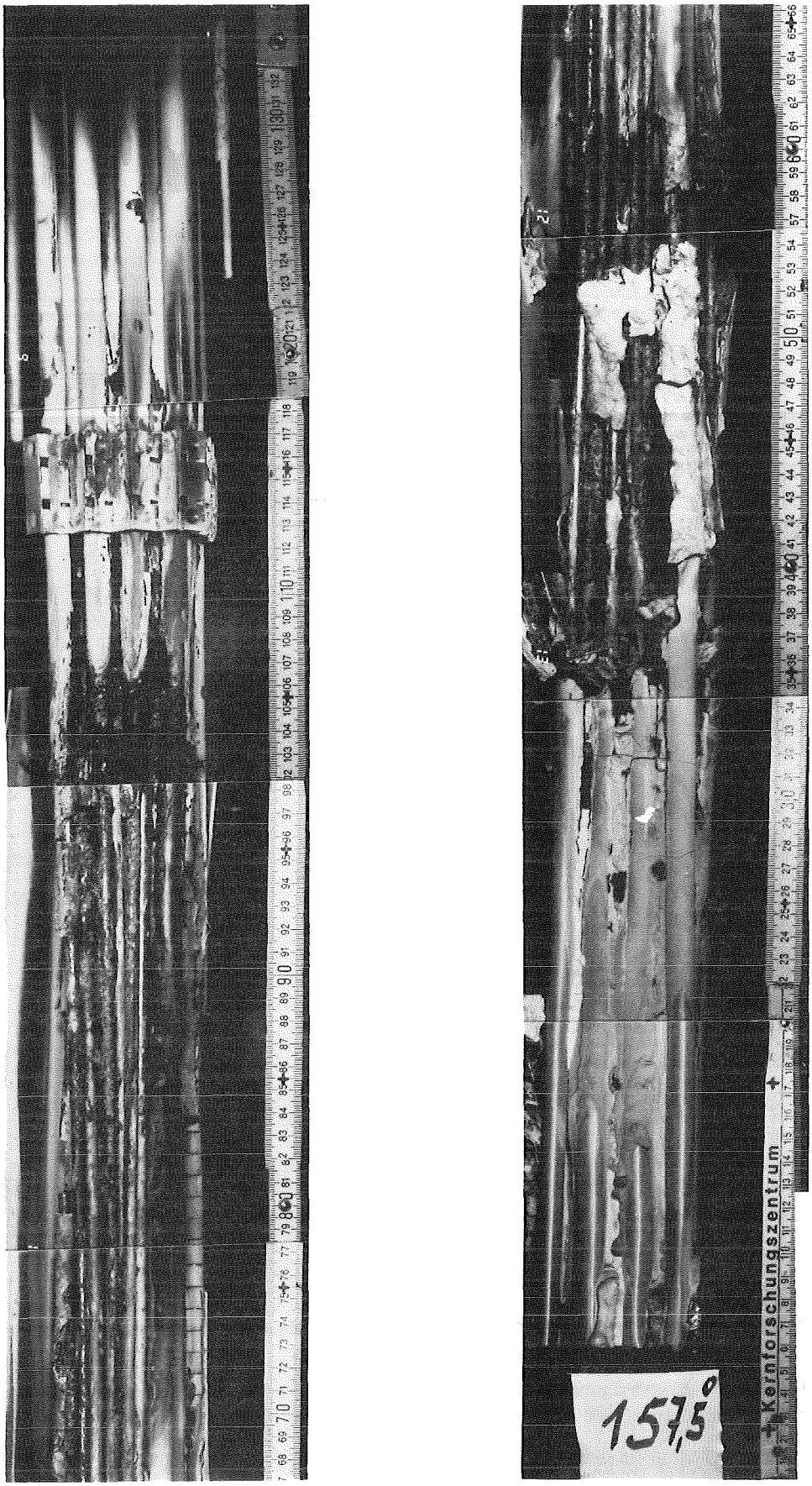

Fig. 95:
CORA Scoping Test B
Posttest view of the bundle, 157.5-degree orientation

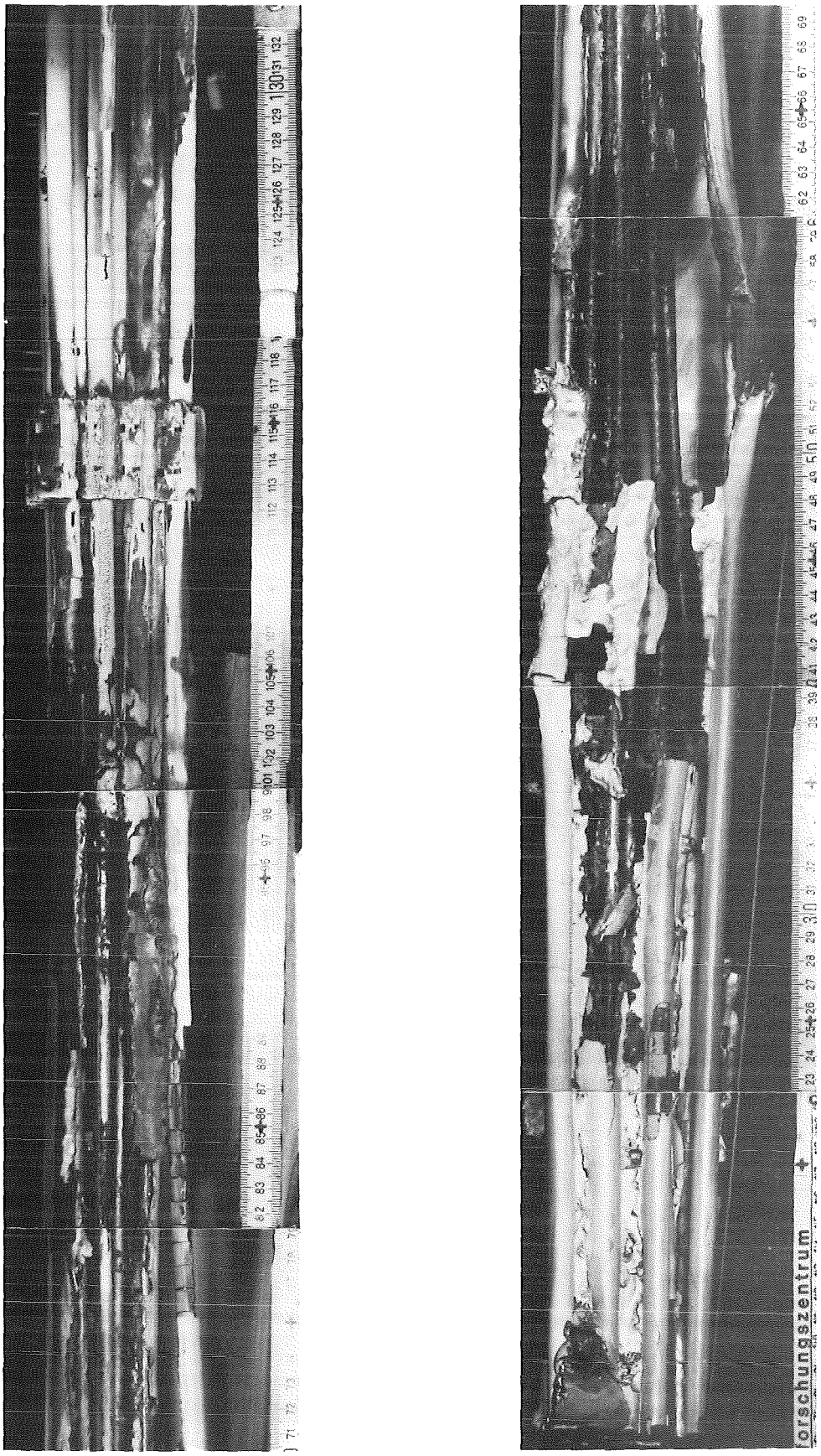

Fig. 96:
CORA Scoping Test B
Posttest view of the bundle, 82.5-degree orientation

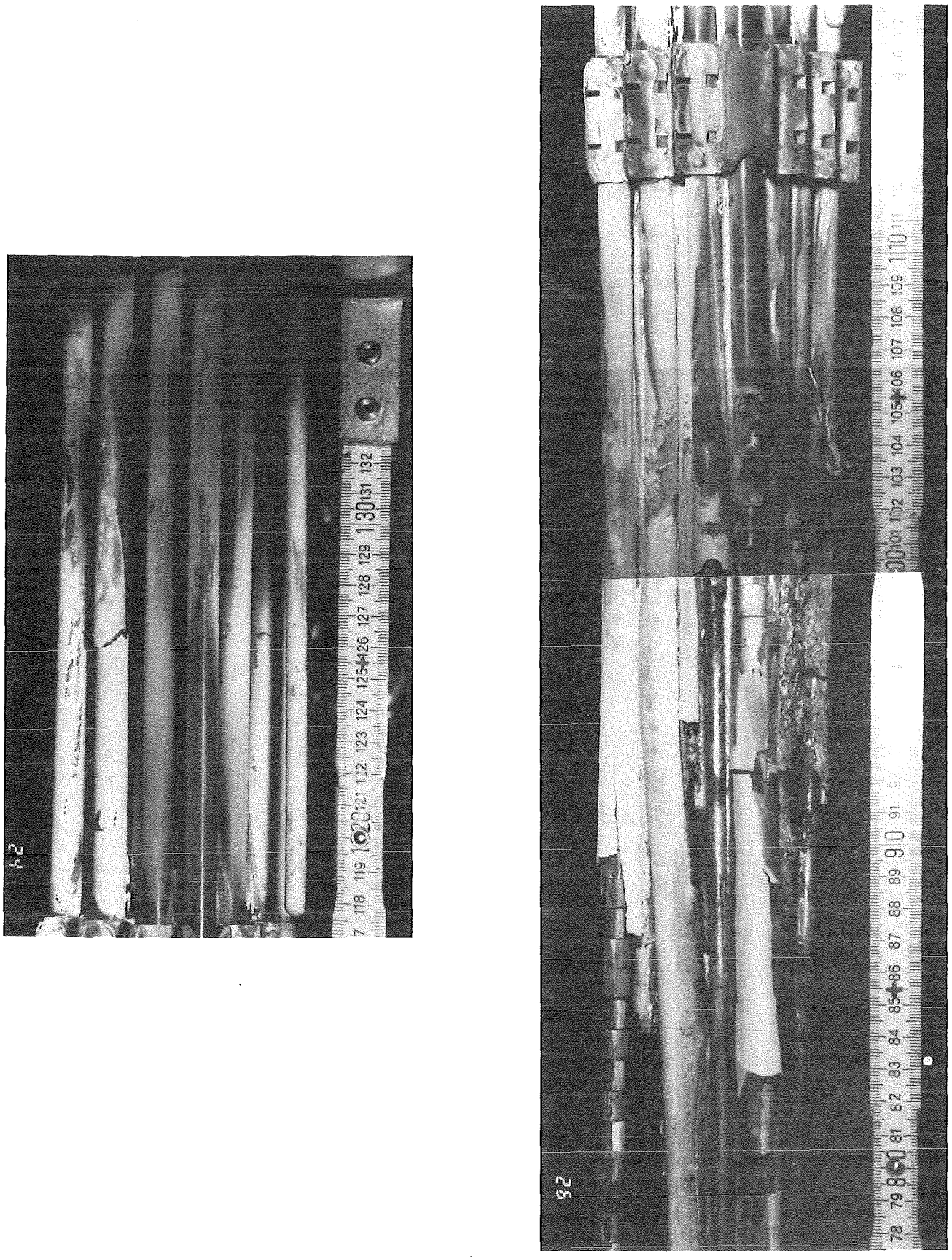

Fig. 97:
CORA Scoping Test B
Upper part of the bundle, 307,5-degree orientation

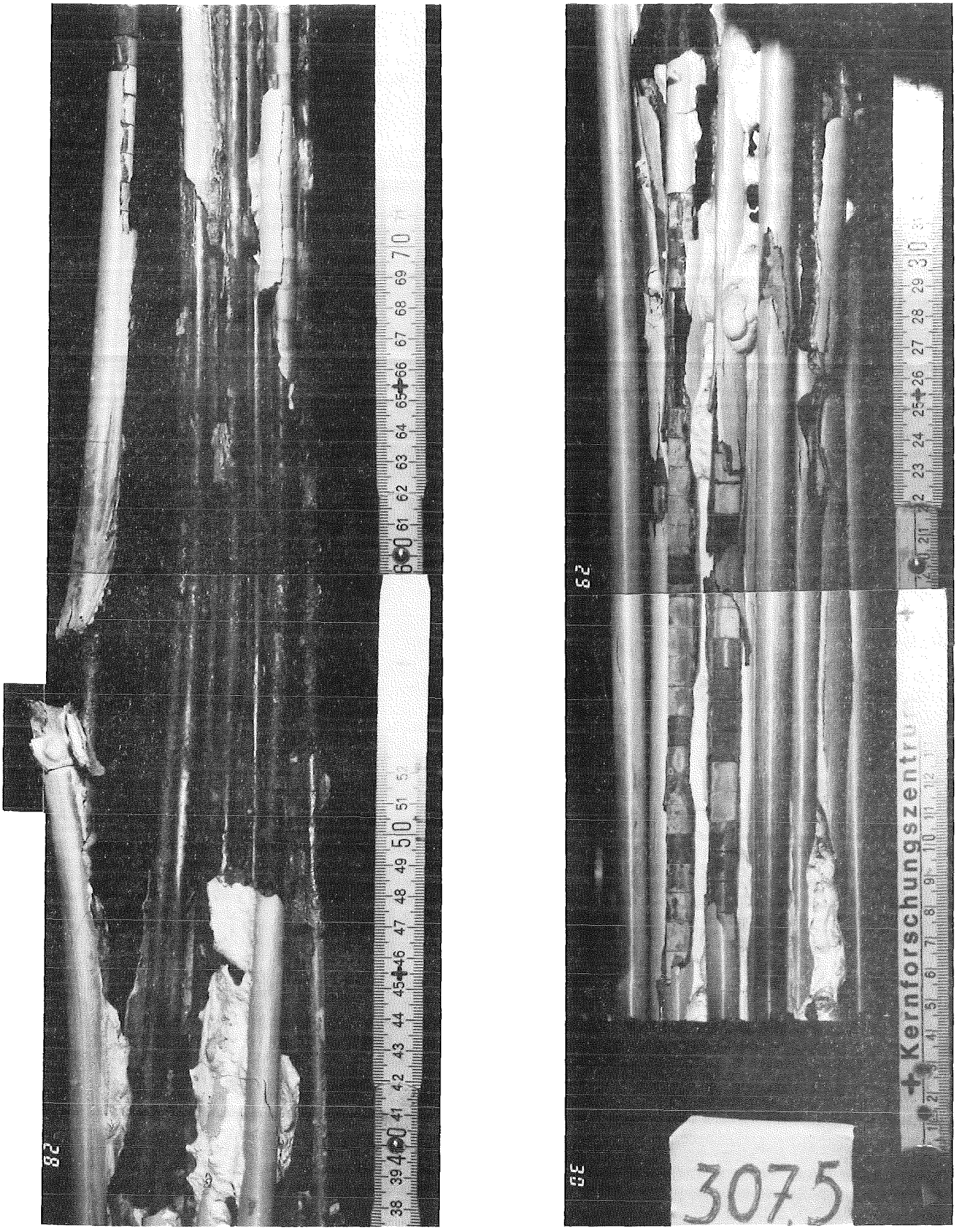

Fig. 98:
CORA Scoping Test B
Lower part of the bundle, 307, 5-degree orientation

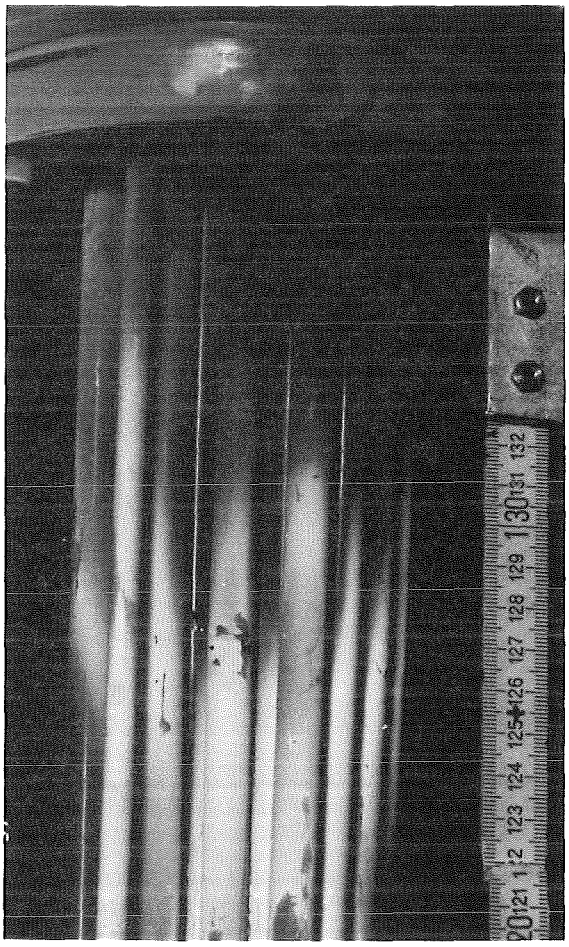

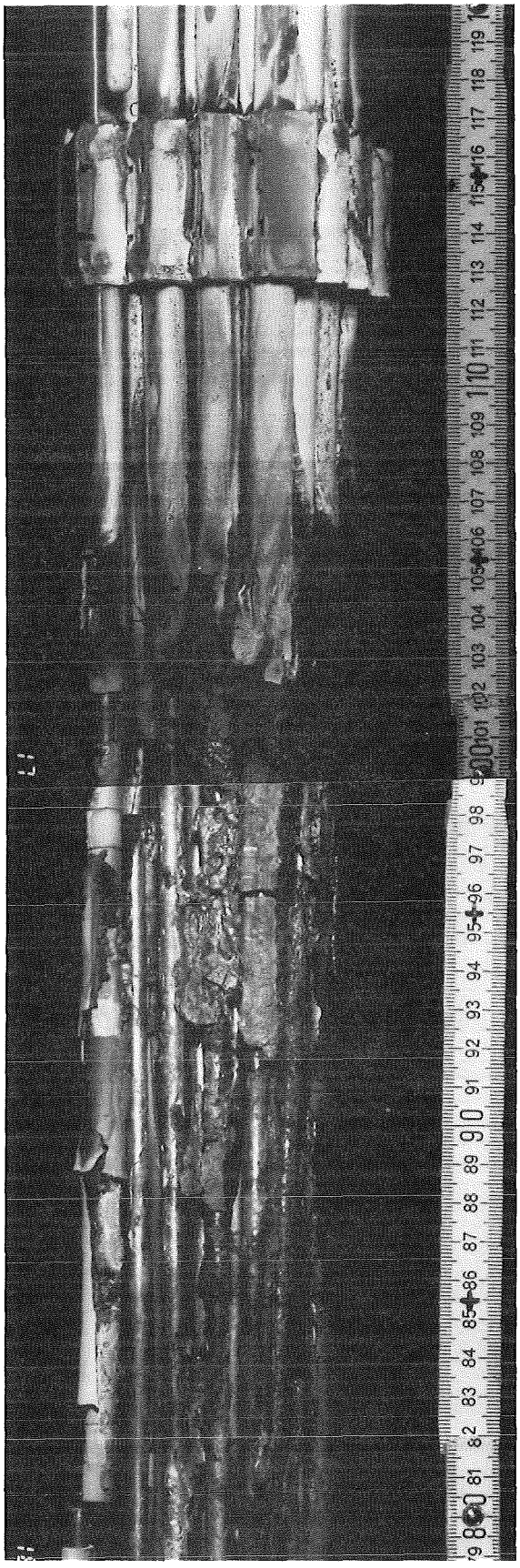

Fig. 99:
CORA Scoping Test B
Upper part of the bundle, 232,5-degree orientation

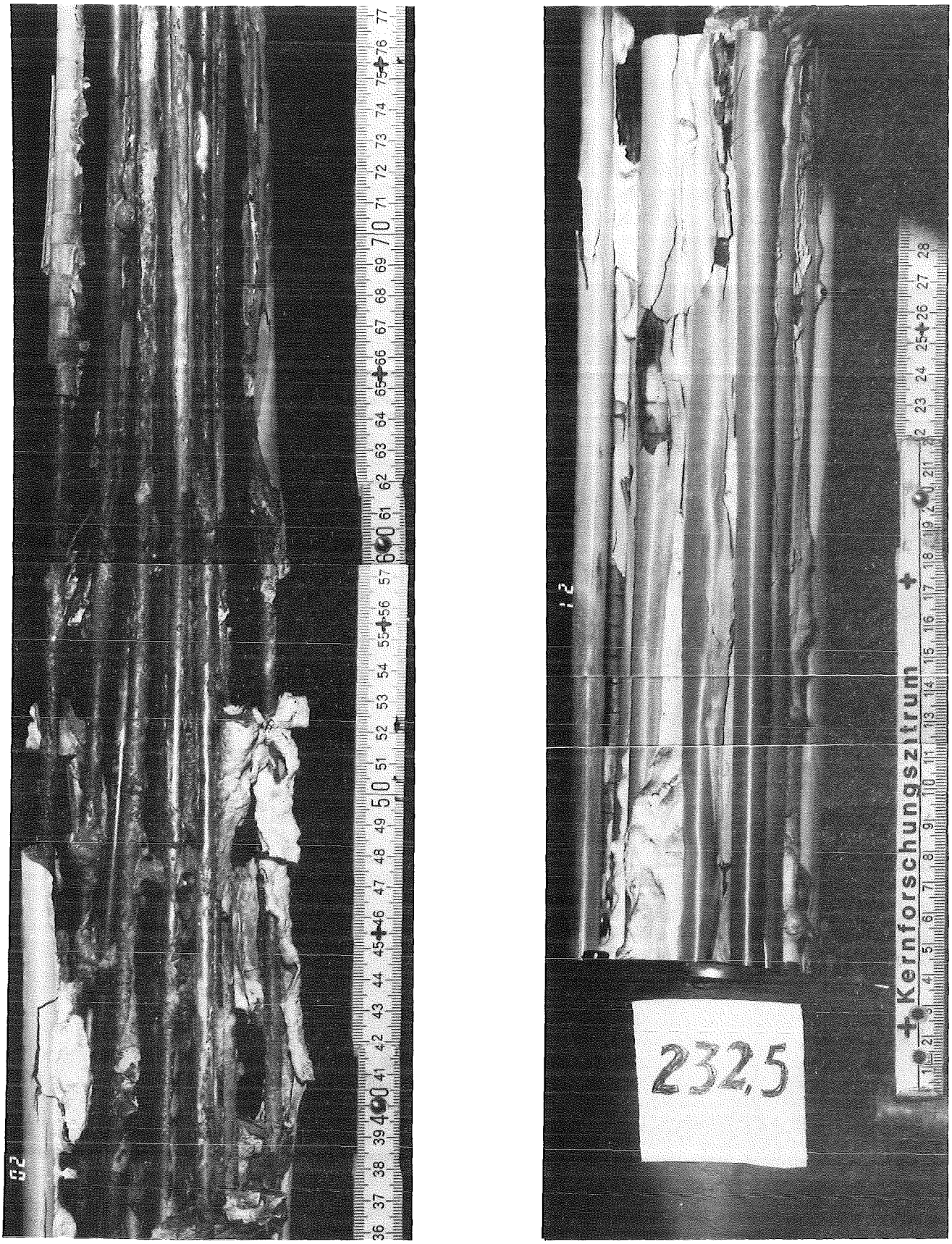

Fig. 100:
CORA Scoping Test B
Middle and lower part of the bundle
232.5-degree orientation

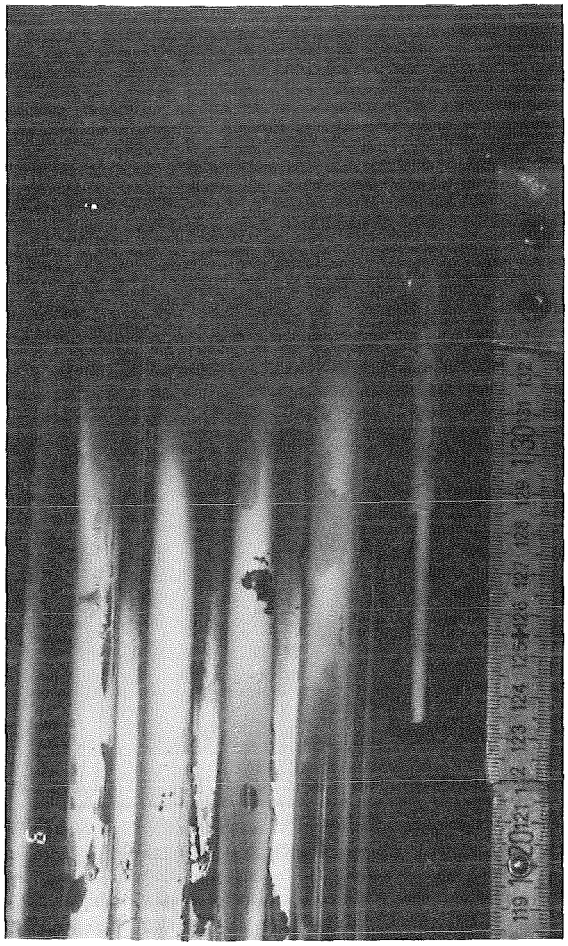

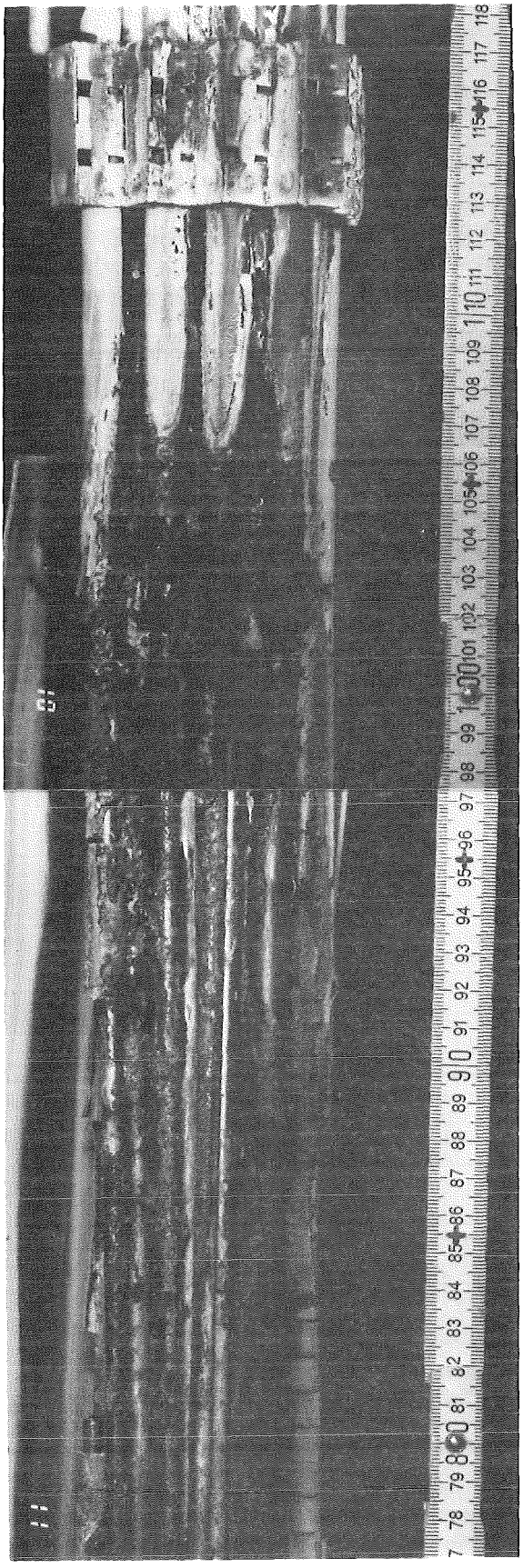

Fig. 101:
CORA Scoping Test B
Upper part of the bundle, 157,5-degree orientation

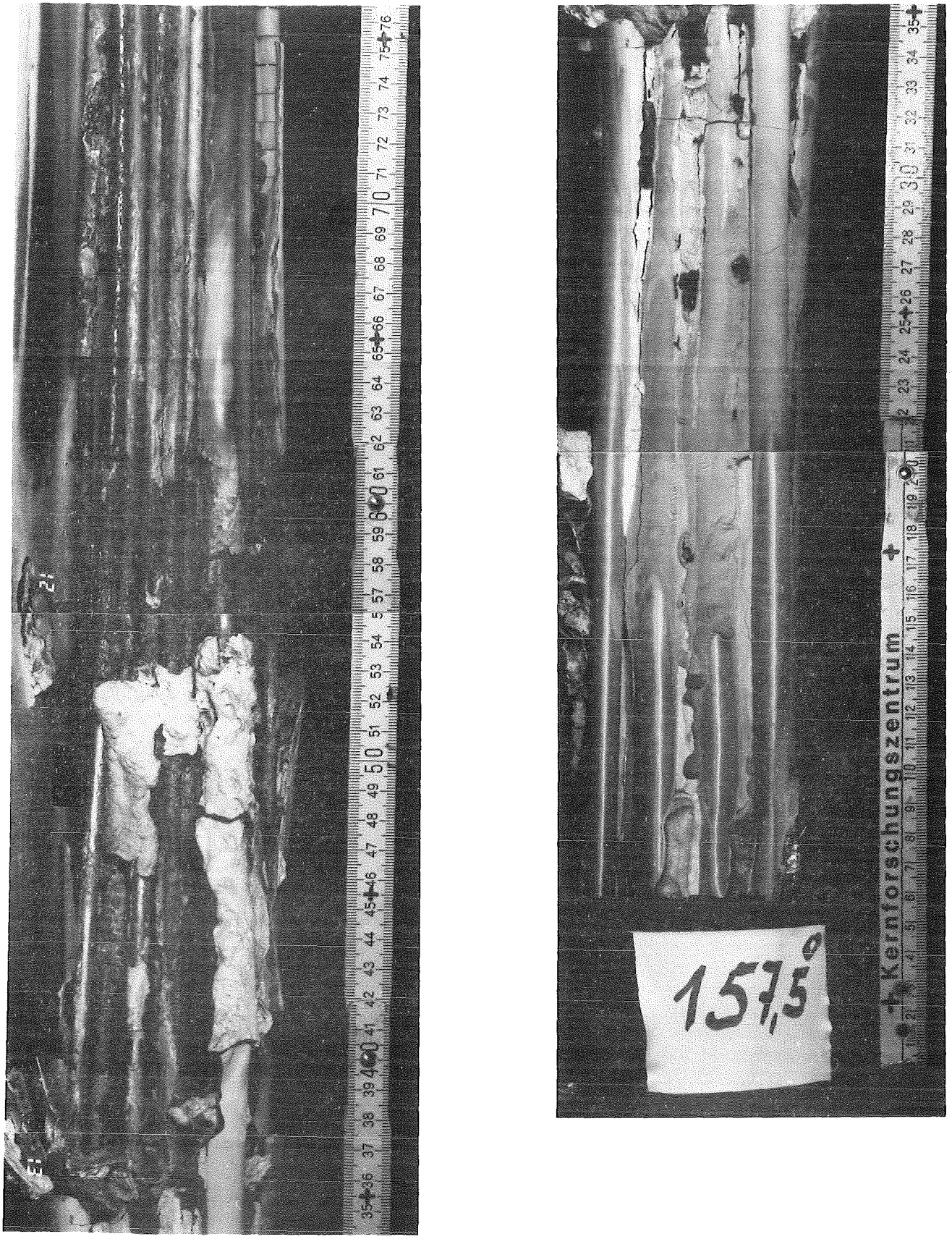

Fig. 102:
CORA Scoping Test B
Lower part of the bundle, 157,5-degree orientation

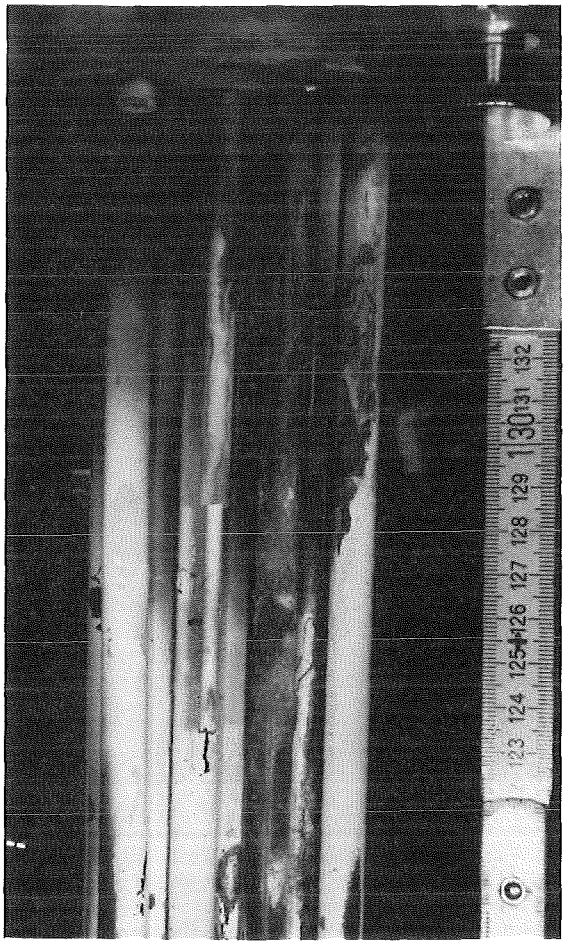

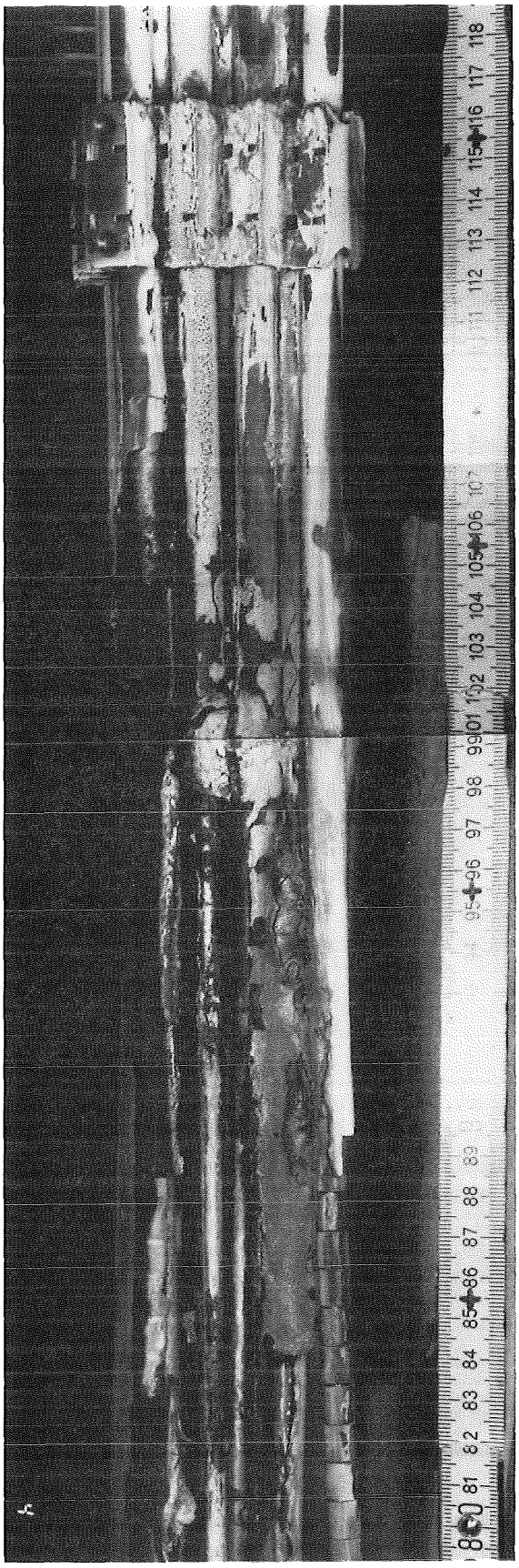

Fig. 103:
CORA Scoping Test B
Upper part of the bundle, 82,5-degree orientation

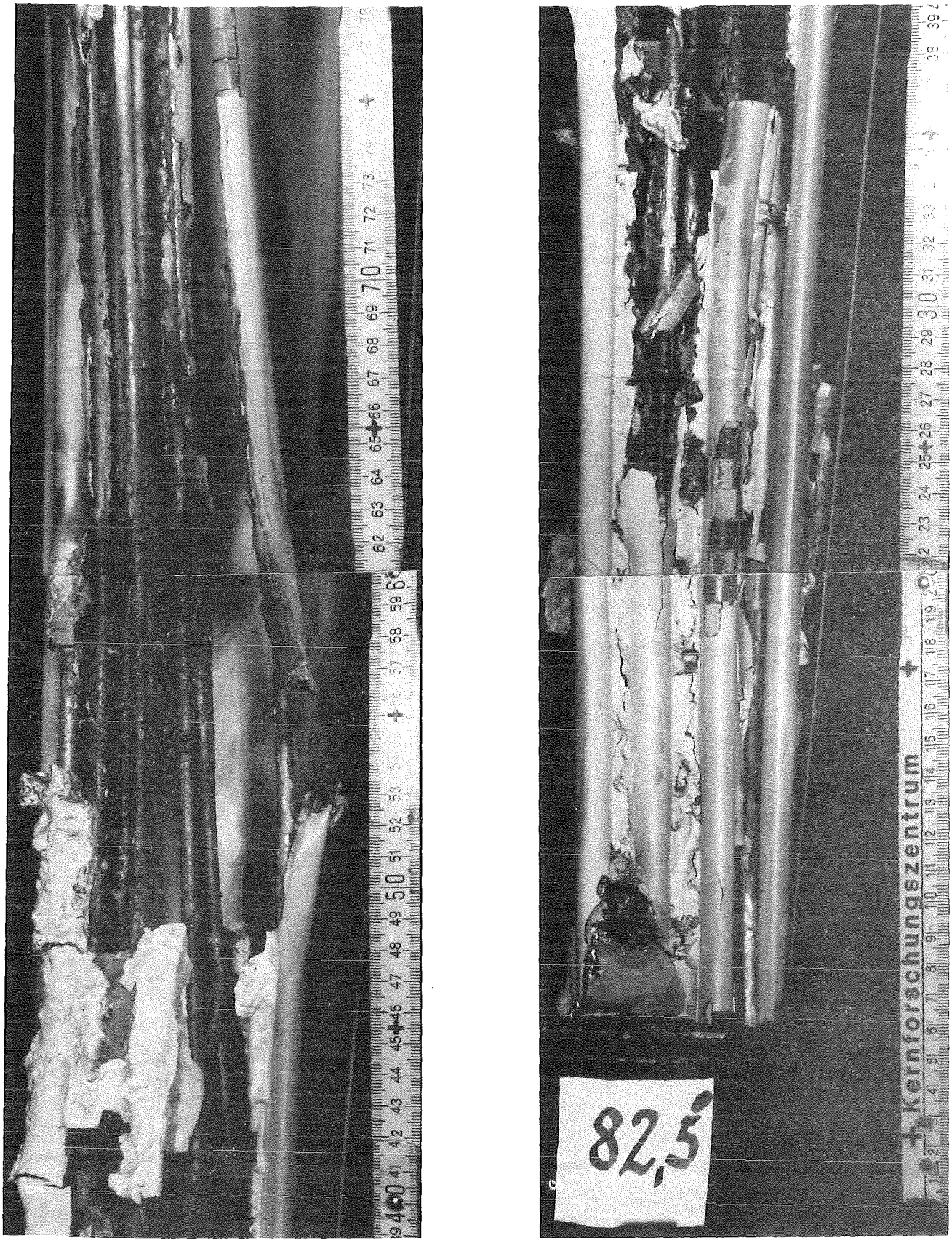

Fig. 104:
CORA Scoping Test B
Lower part of the bundle, 82,5-degree orientation

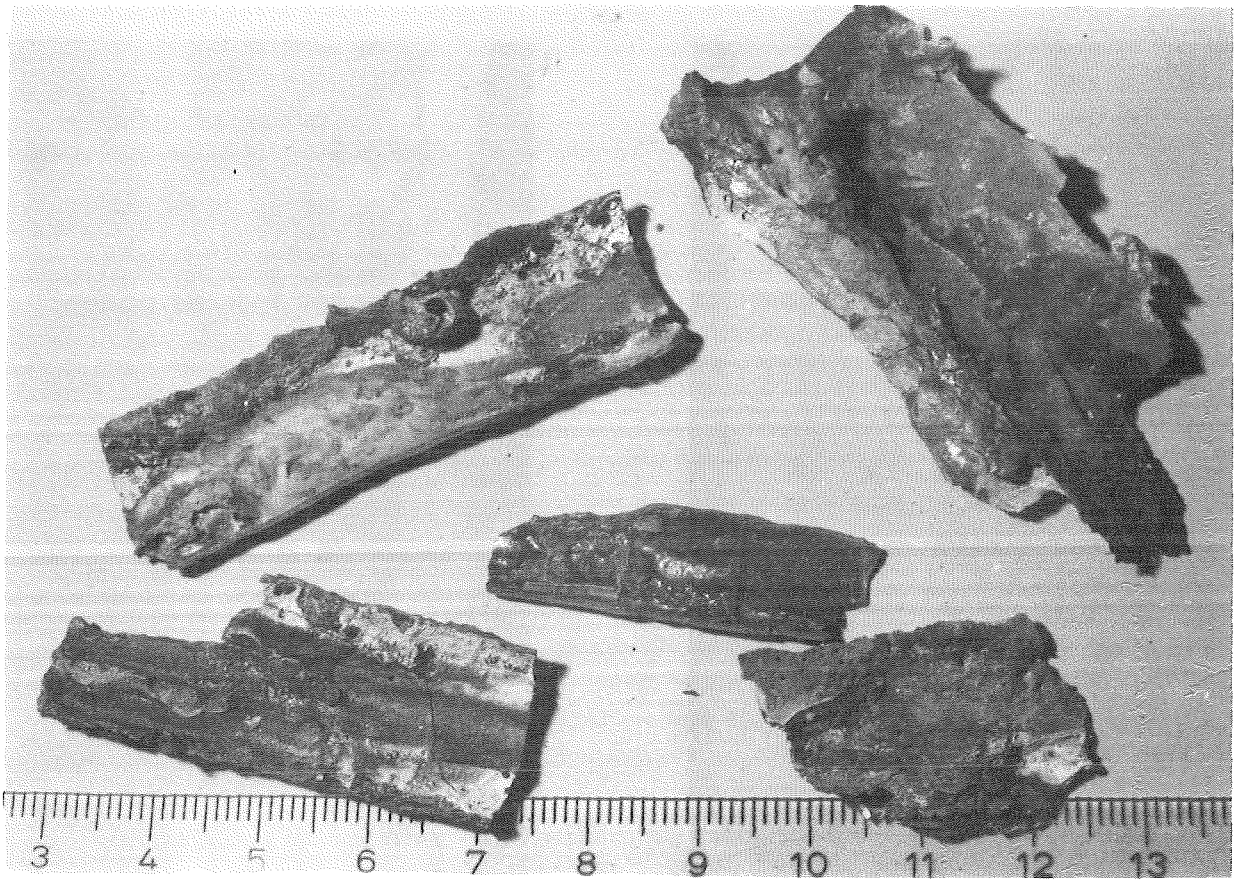

Fig.105a Pieces of cladding CORA bundle B

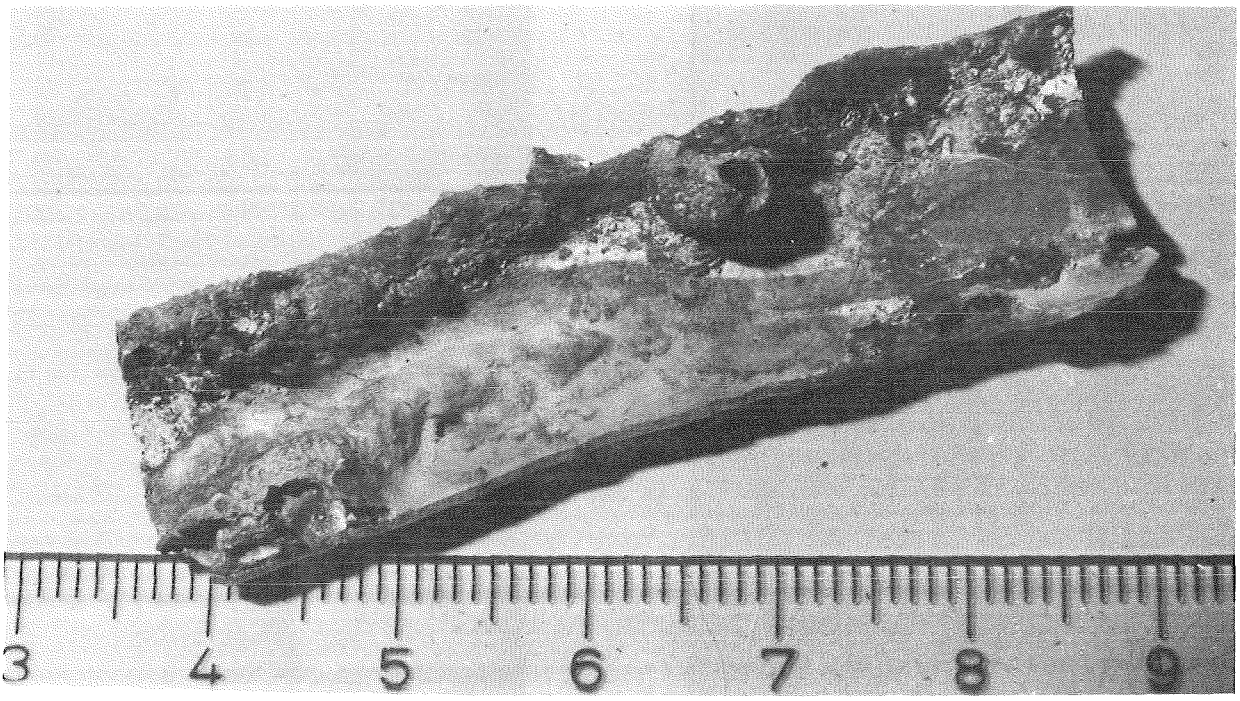

Fig.105b Piece of cladding from heated zone CORA bundle B

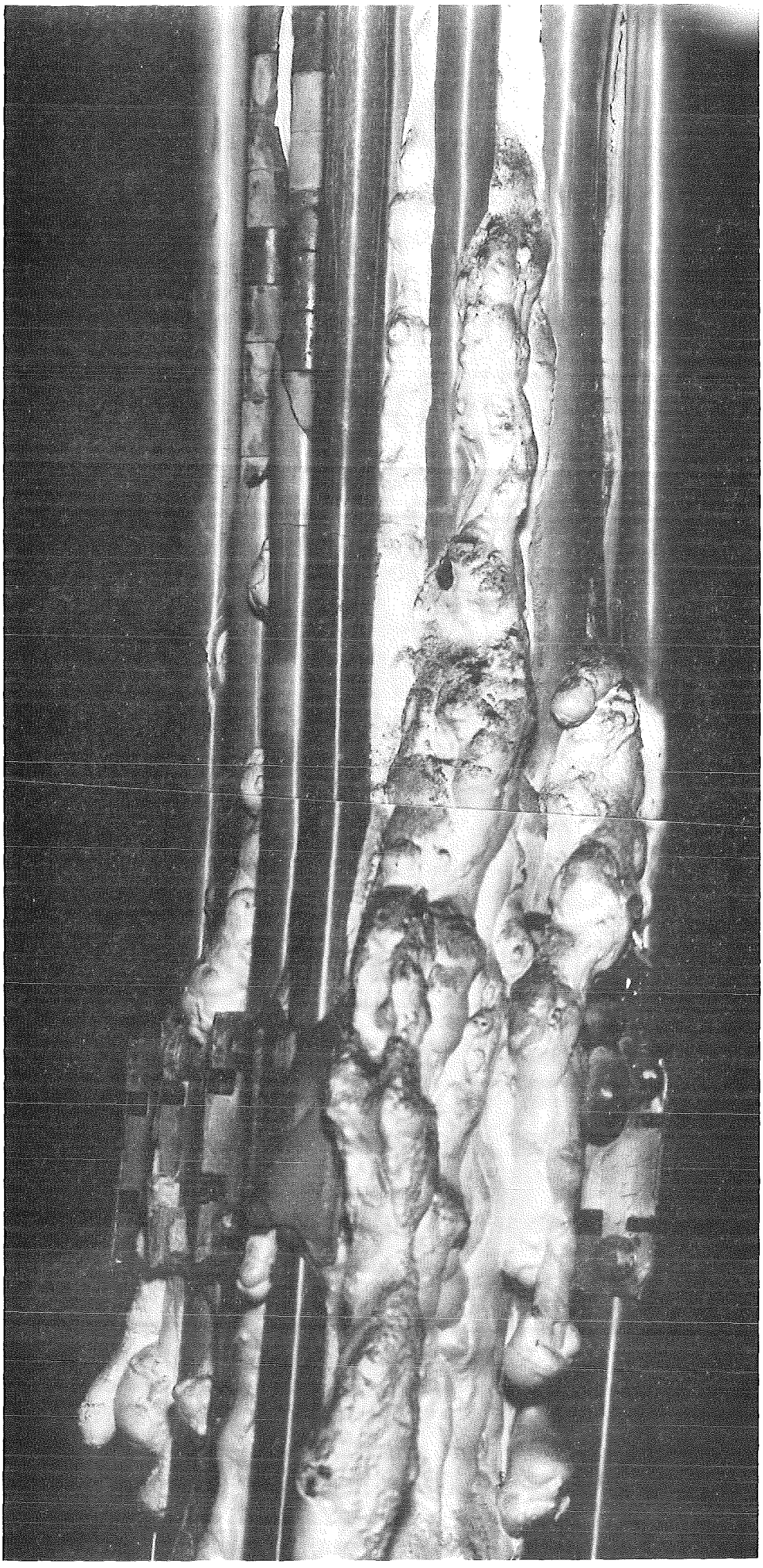

Fig. 106:
Refrozen melt at lower end of CORA bundle B (277,5°)

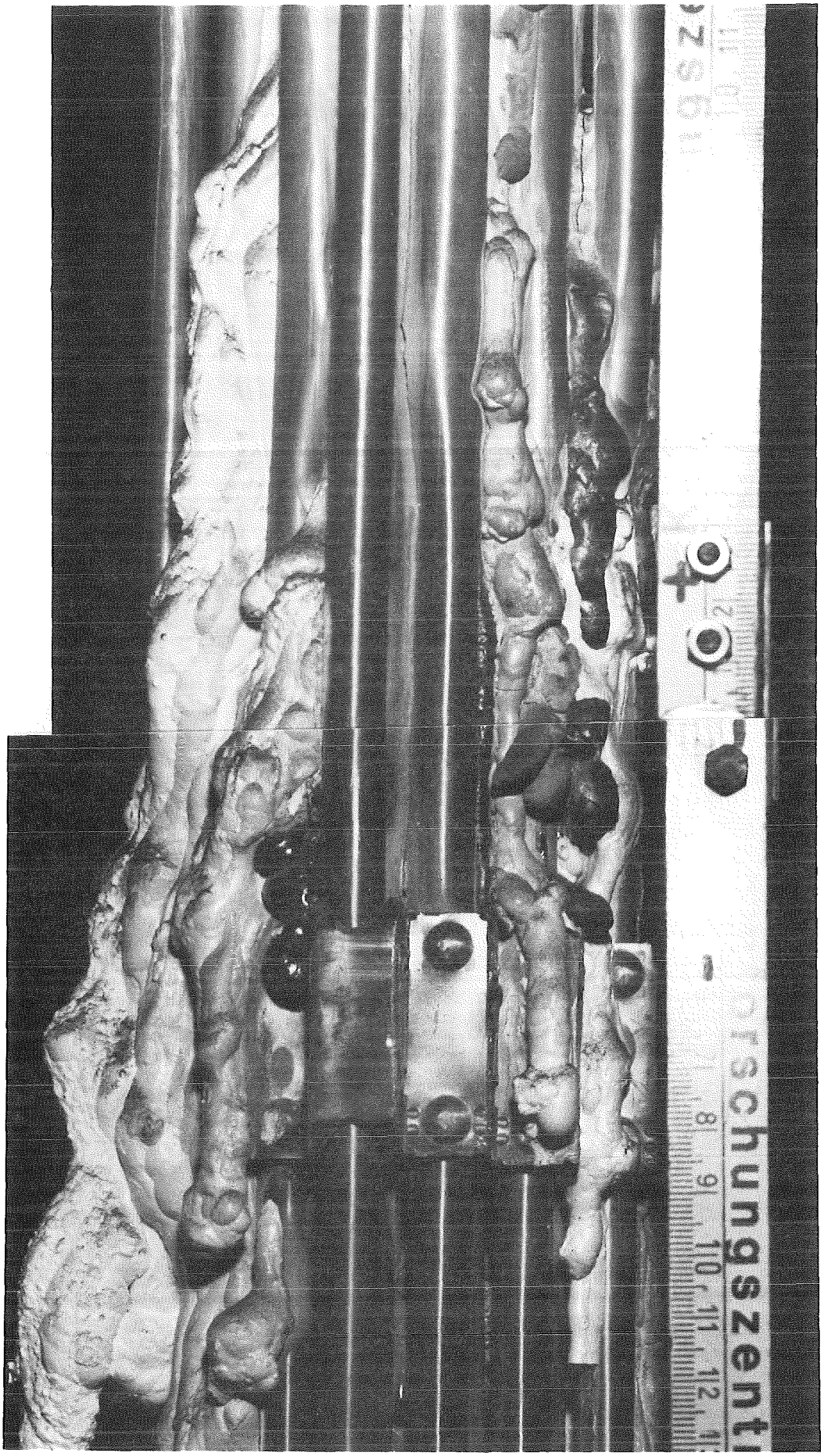

Fig. 107:
Refrozen melt at lower end of CORA bundle B (202,5°)

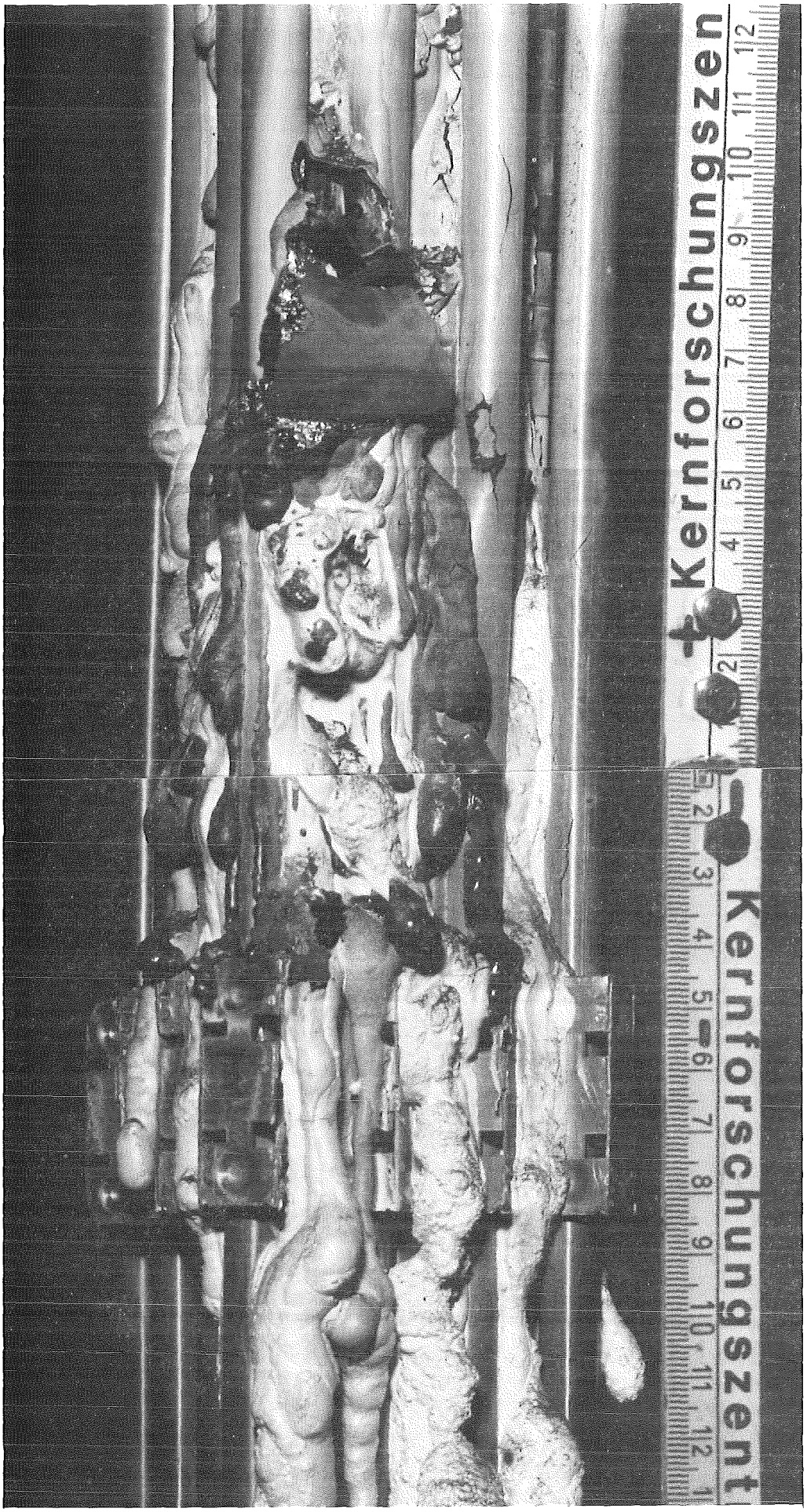

ig. 108:
efrozen melt at lower end of CORA bundle B (97.5°)

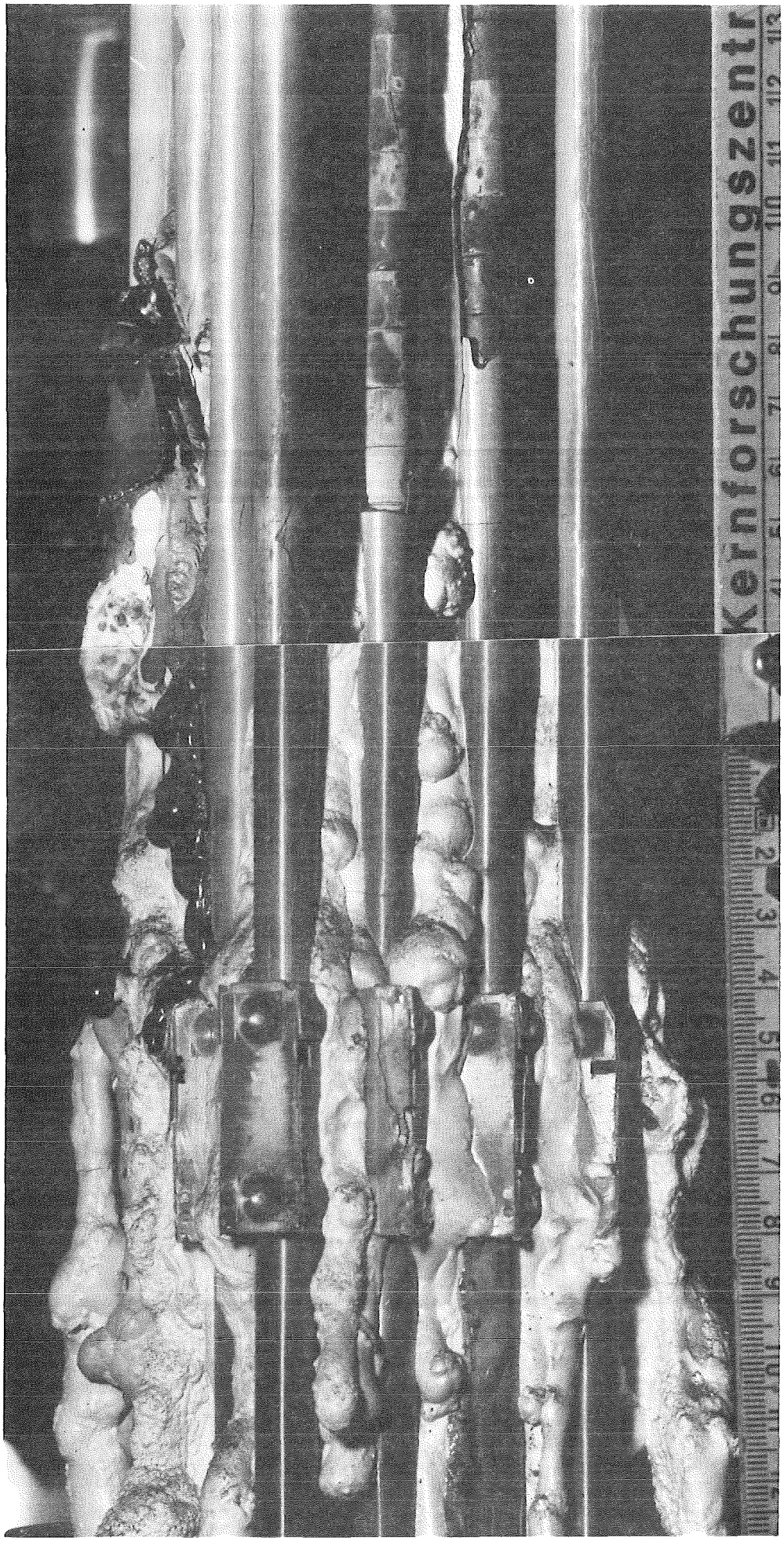

Fig. 109:
Refrozen melt at lower end of CORA bundle B (0°)

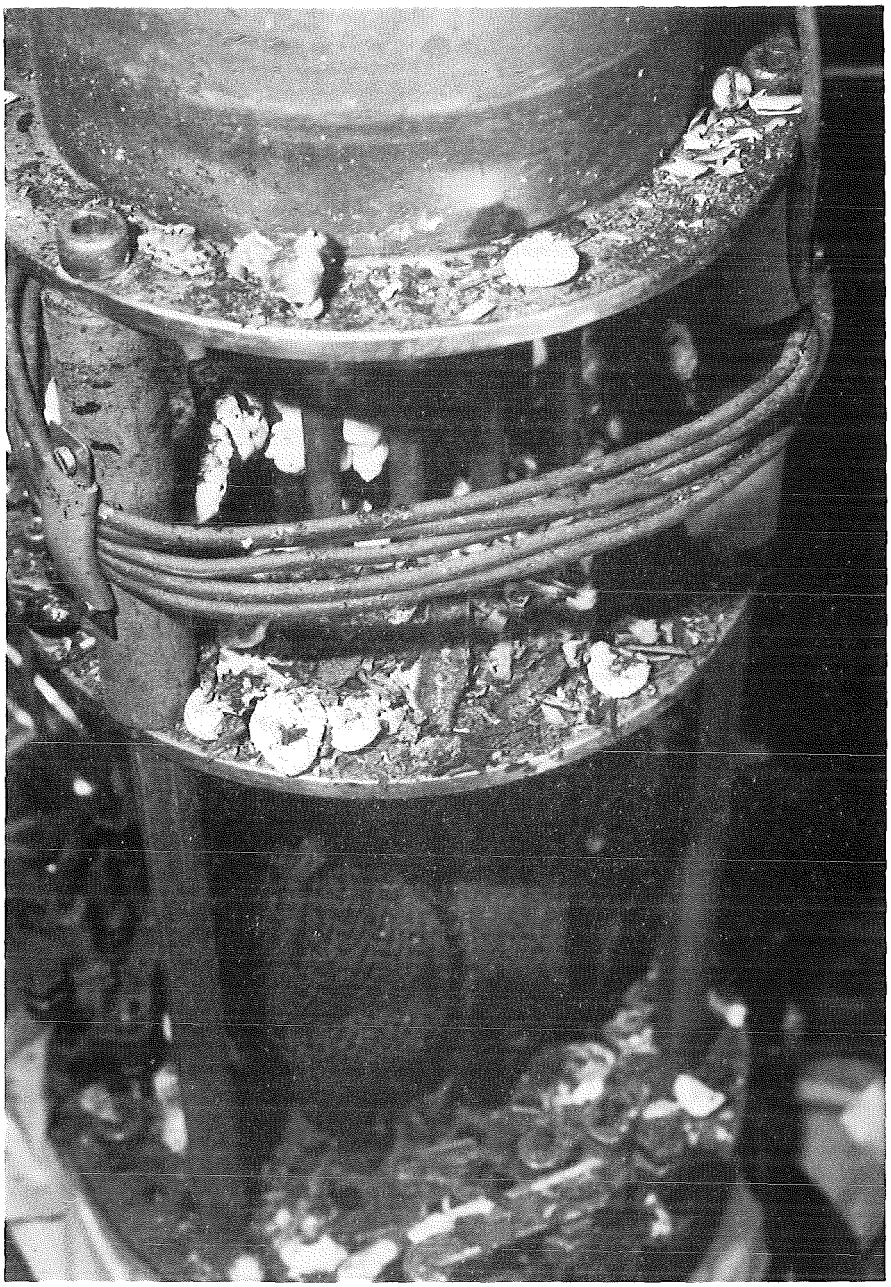

Fig. 110: Lower end of test arrangement CORA bundle B

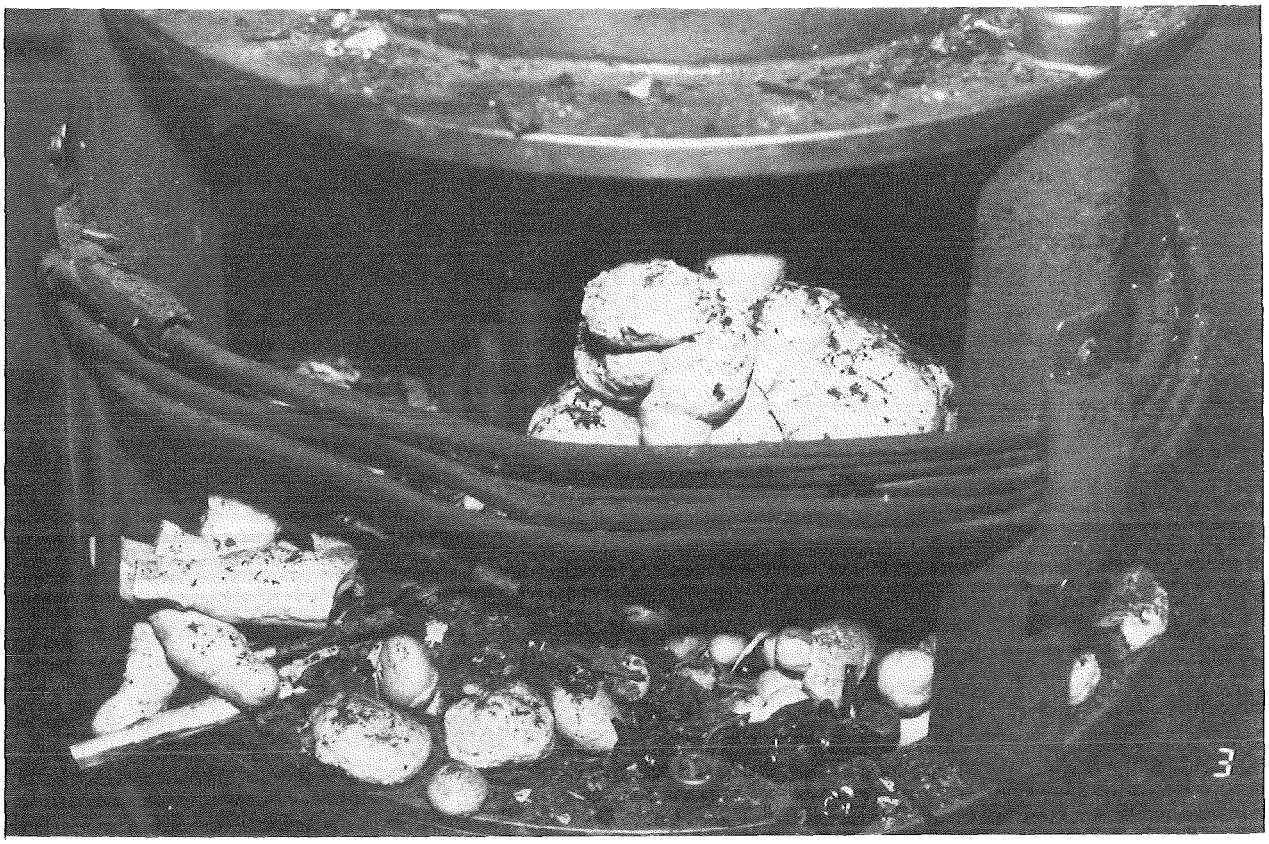

Fig. 111: Refrozen melt on "comb"-plate CORA bundle B

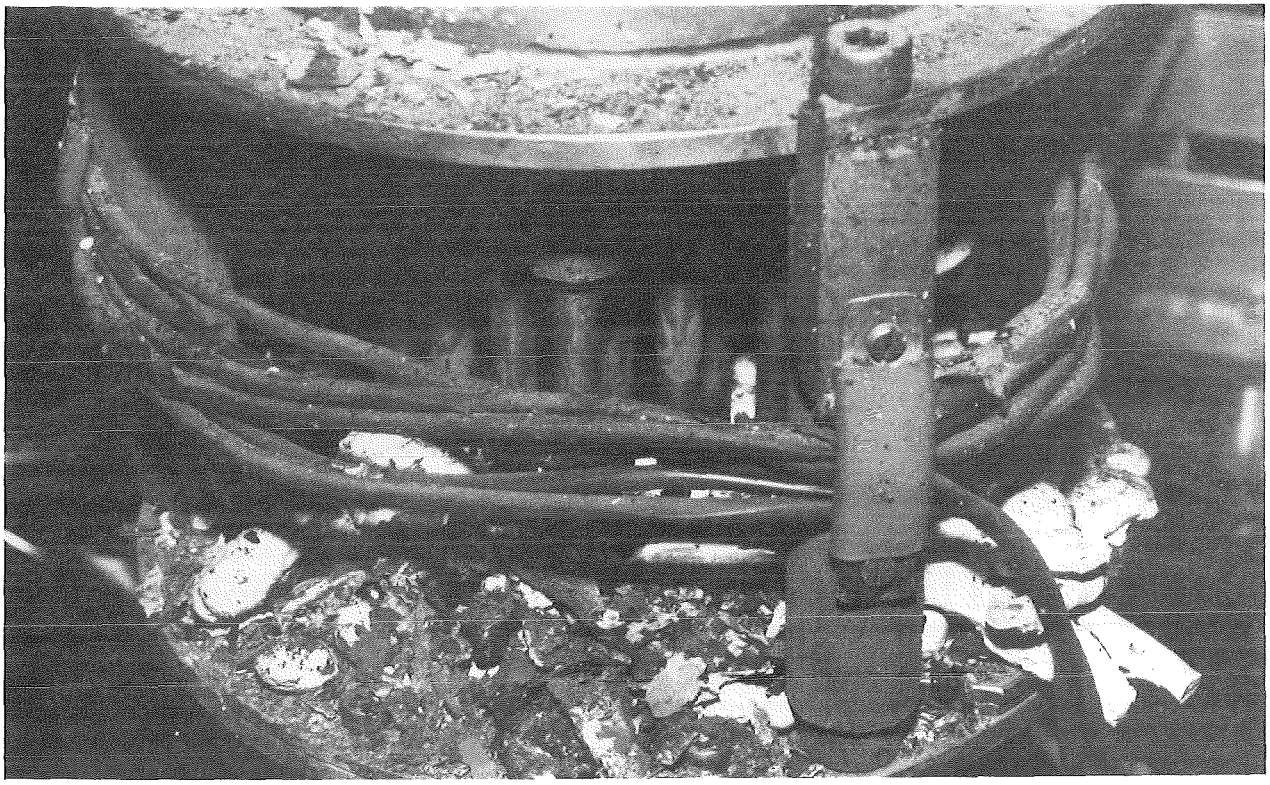

Fig. 112: Rubble on "comb"-plate CORA bundle B

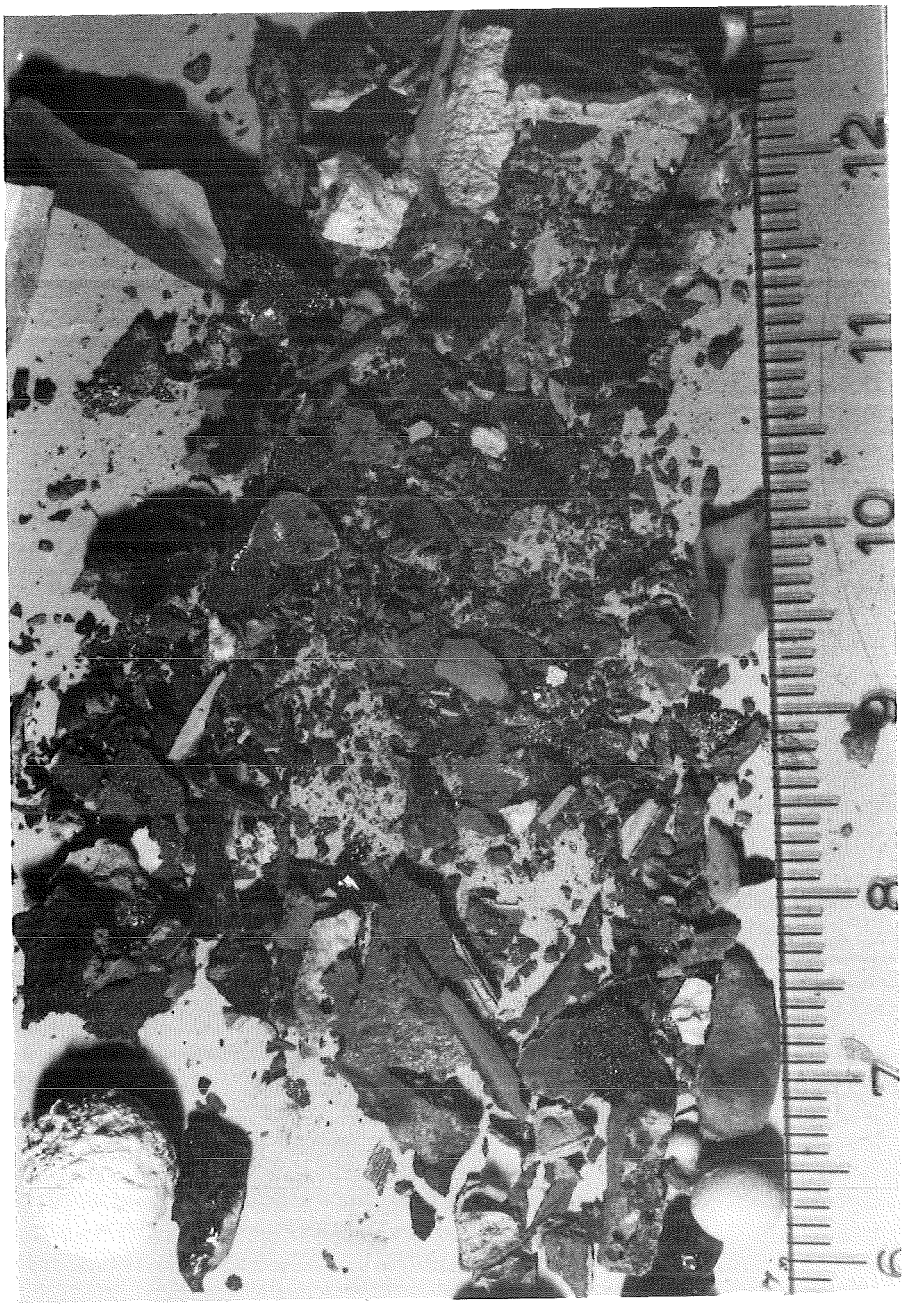

Fig. 113: Rubble from lower plates of CORA bundle B

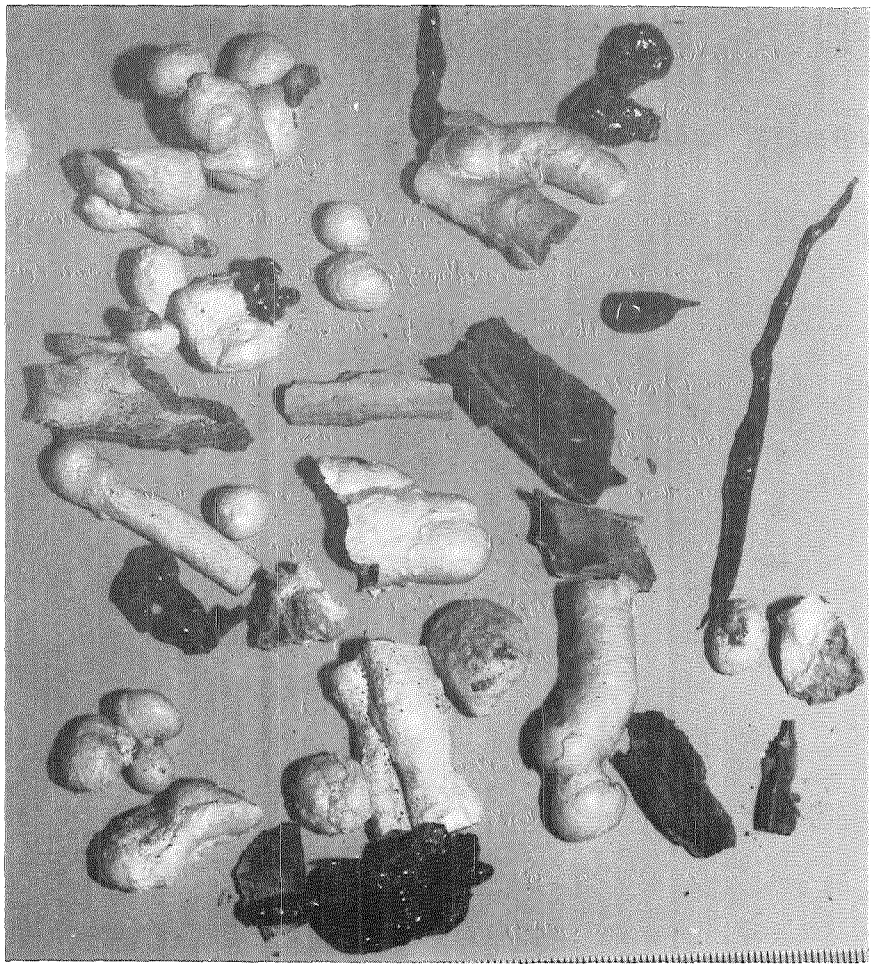

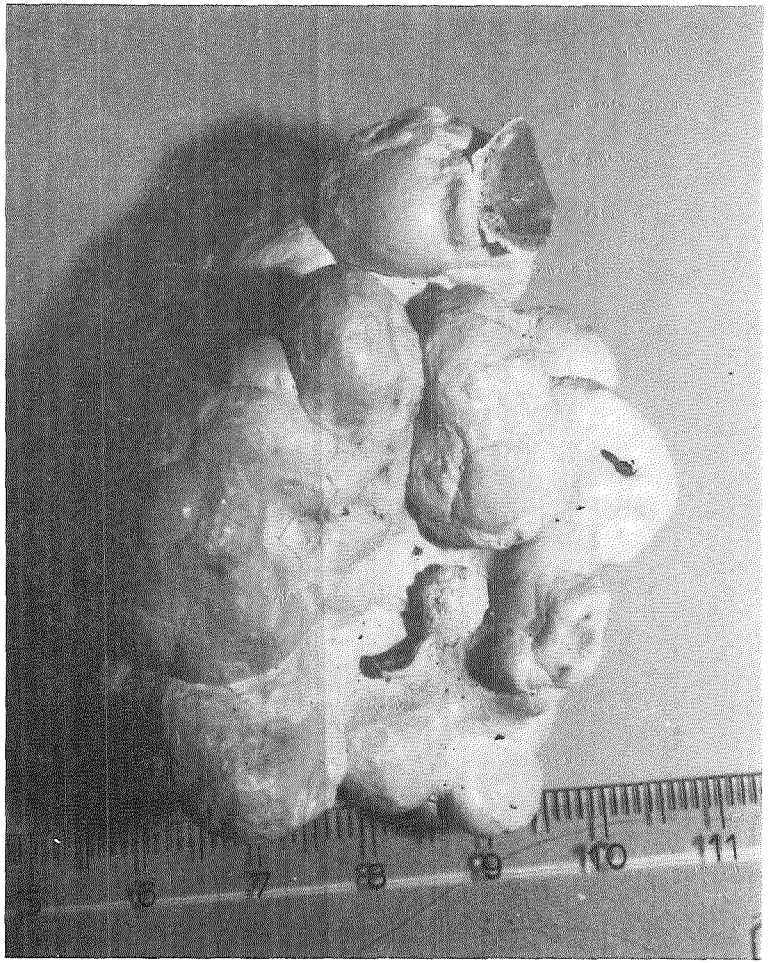

Fig. 114: Refrozen melt found in region of lower plates CORA bundle B

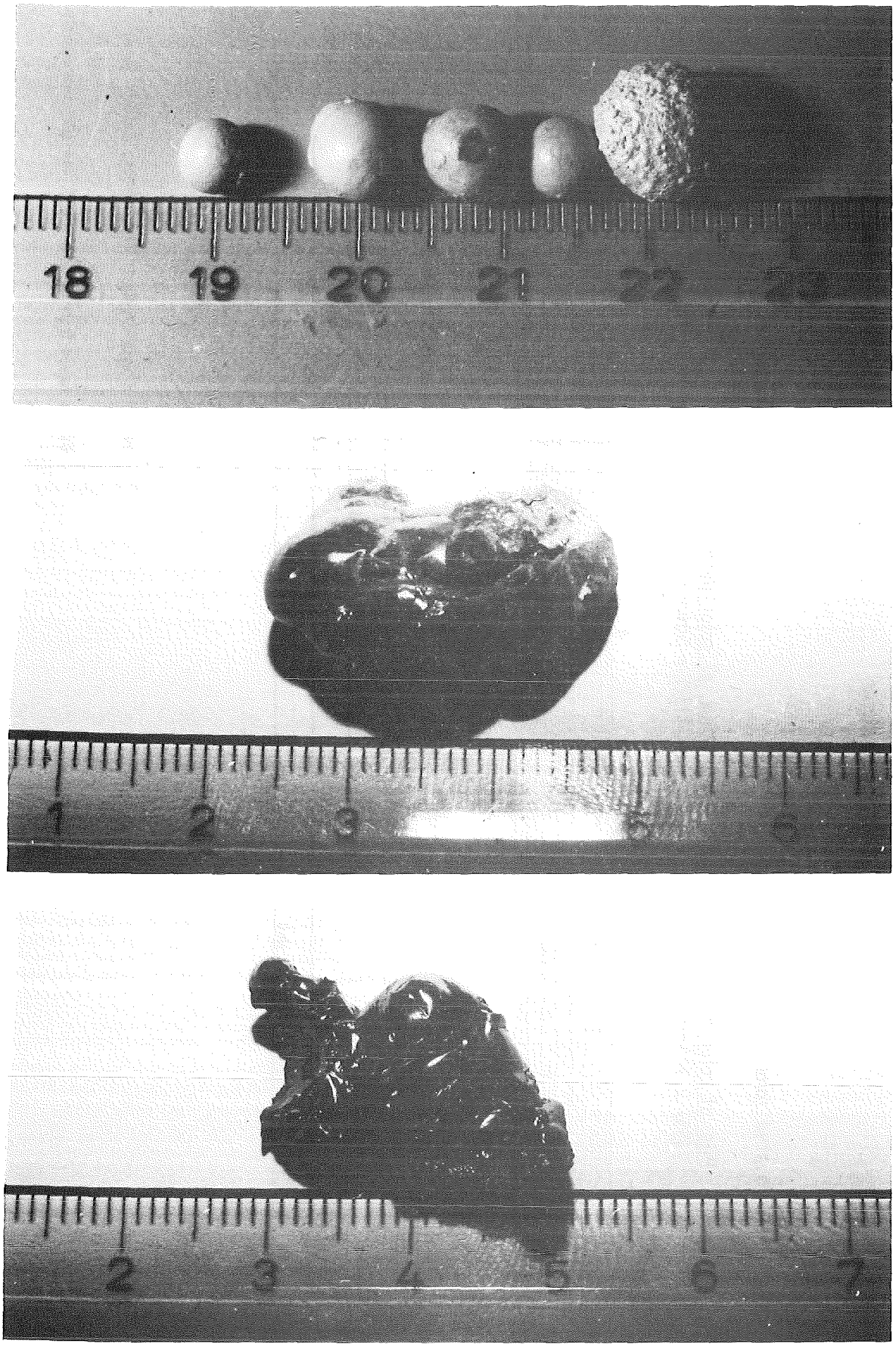

Fig. 115: Refrozen melt found in region of lower plates CORA bundle B

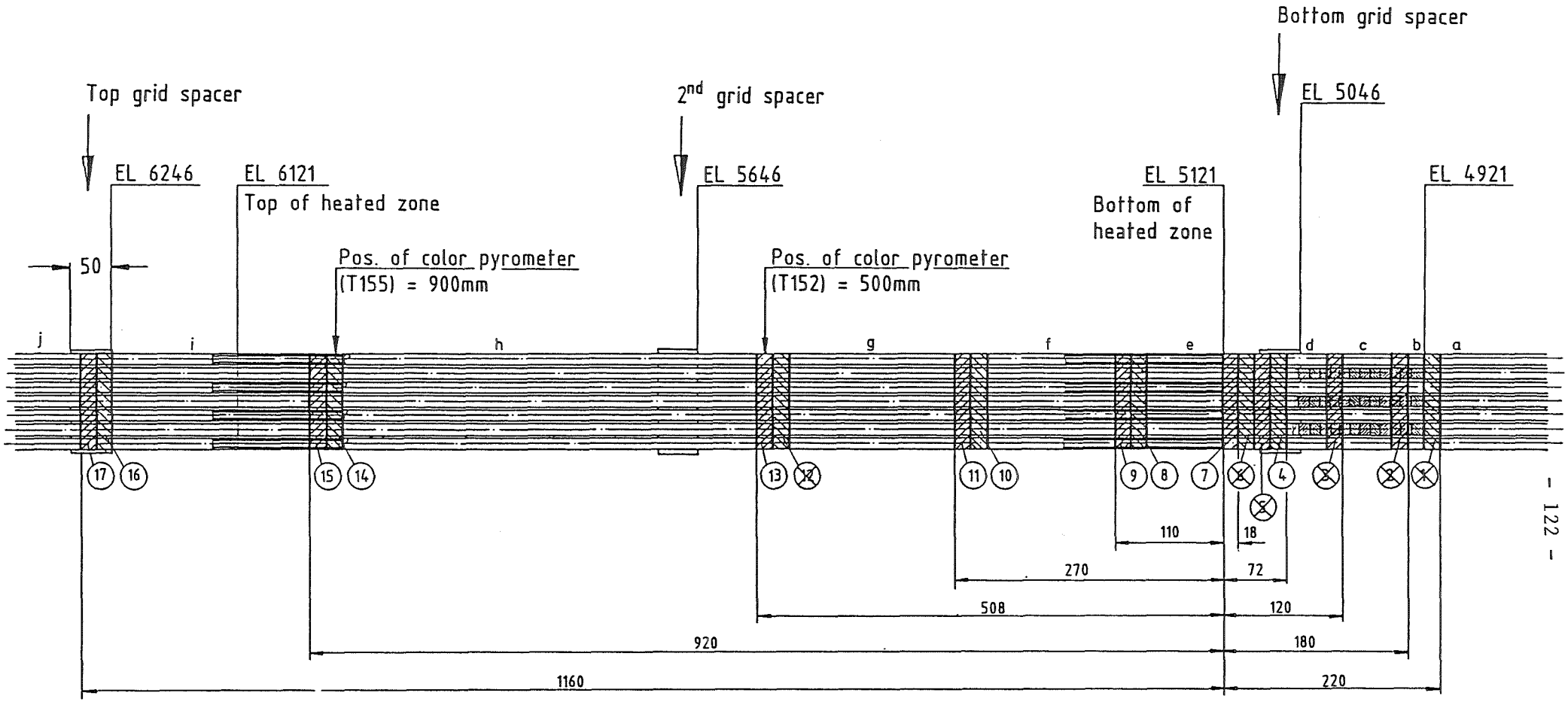

Fig.: 116
CORA Test B
Bundle Sectioning

Height of each sample : 16mm (Marking distance 18mm)

Bundle viewed from 30°, 120°, 210°, and 300°, respectively

31.3.87

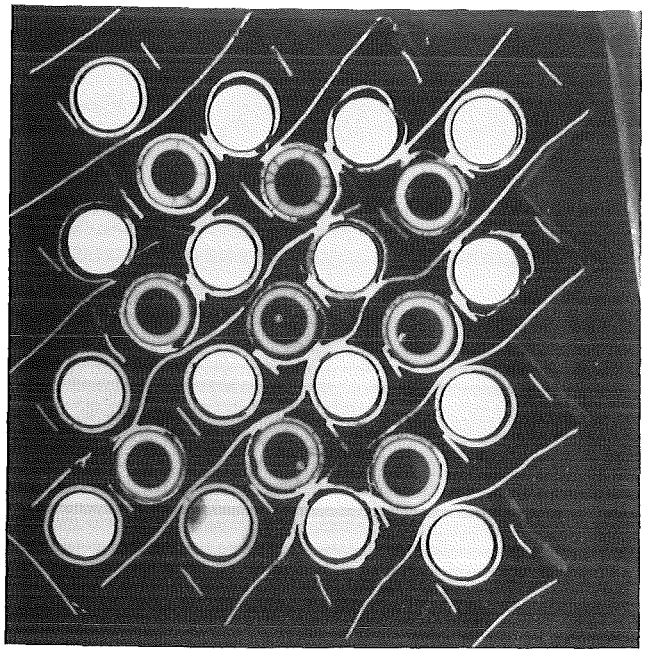

1159mm upper

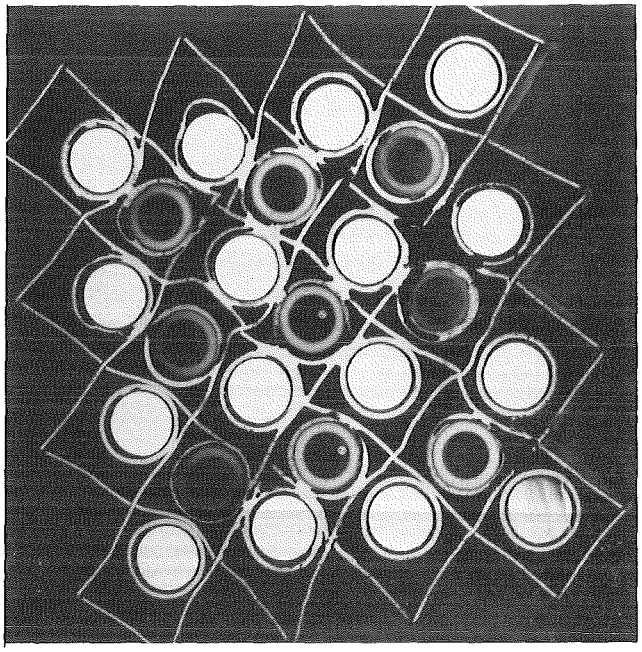

1143mm lower

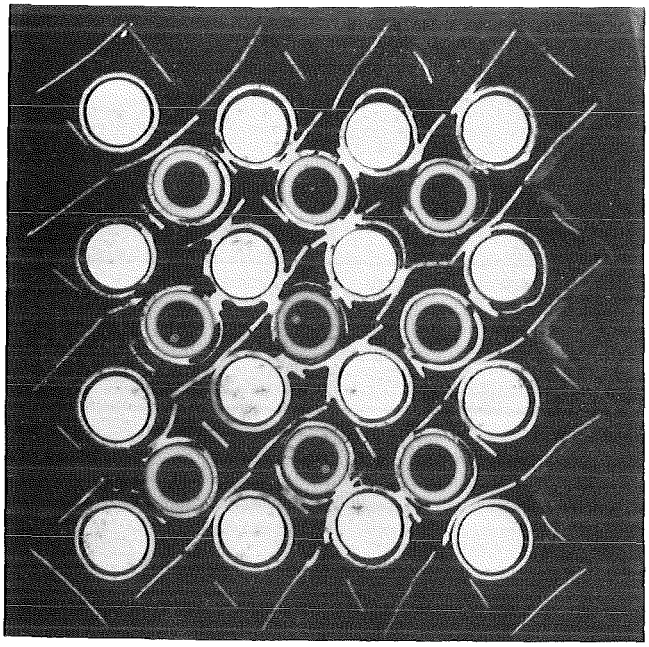

1141mm upper

20 14 8 3
21 15 9
28 22 16 10
29 23 17
36 30 24 18
37 31 25
43 38 32 26

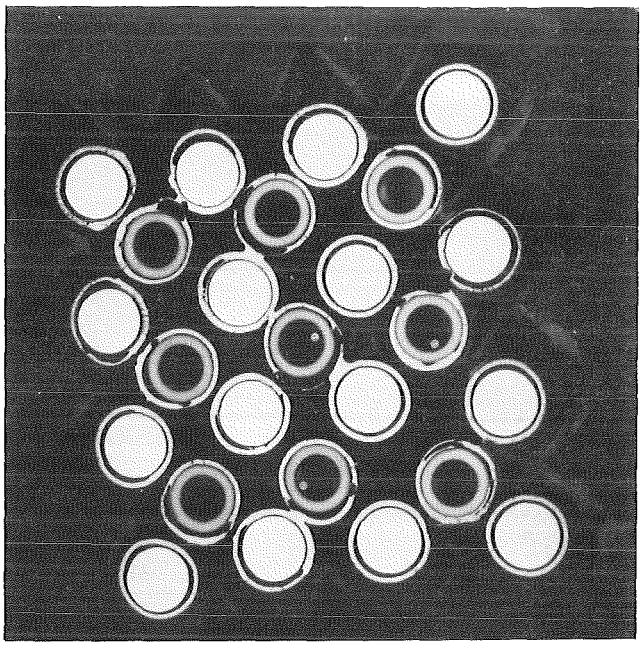

1125mm lower

3 8 14 20
9 15 21
10 16 22 28
17 23 29
18 24 30 36
25 31 37
26 32 38 43

Fig.117: Cross sections of CORA bundle B at elevations given (bundle code)

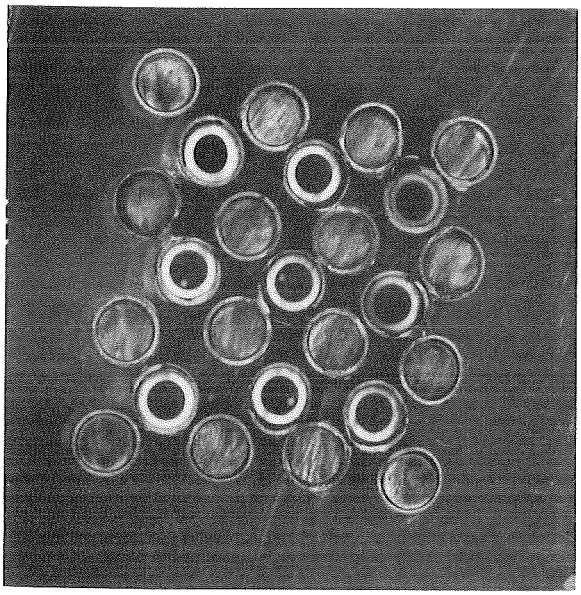

1123 upper

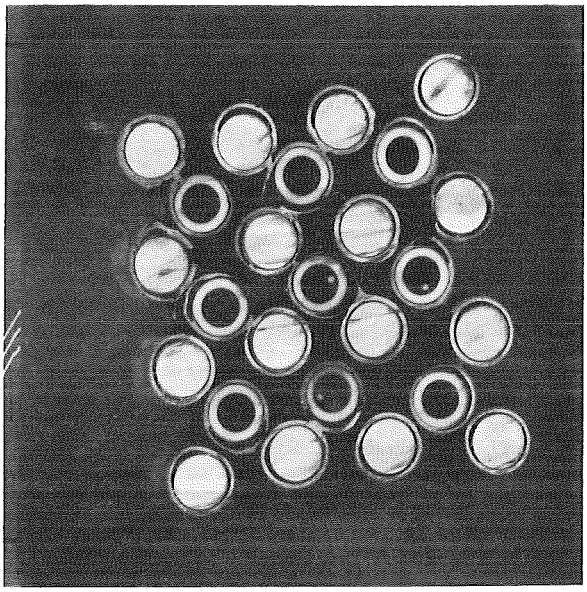

1112 lower

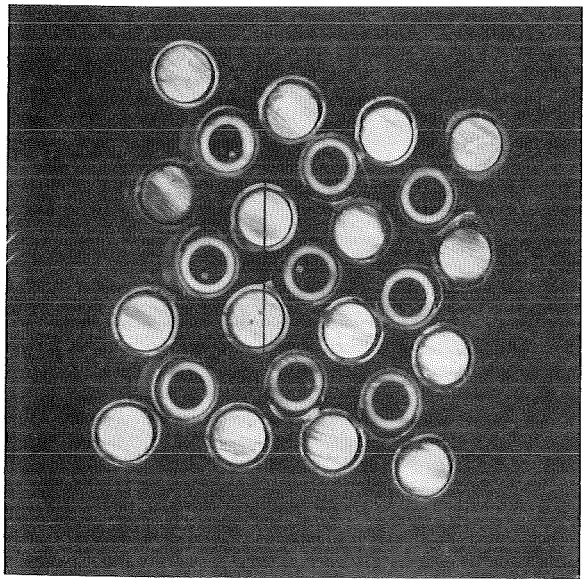

1108

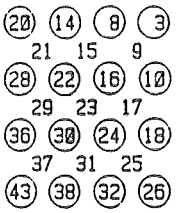

upper

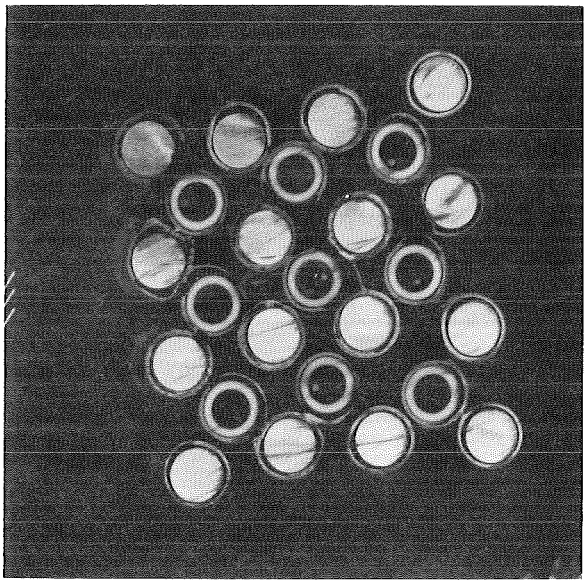

1097

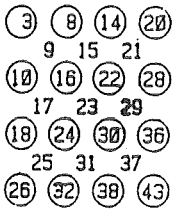

lower

Fig.: 117a Cross section of CORA bundle B

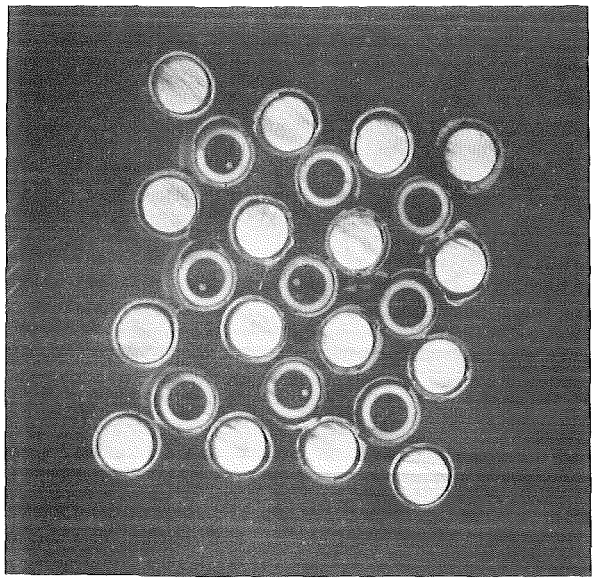

1Ø93 upper

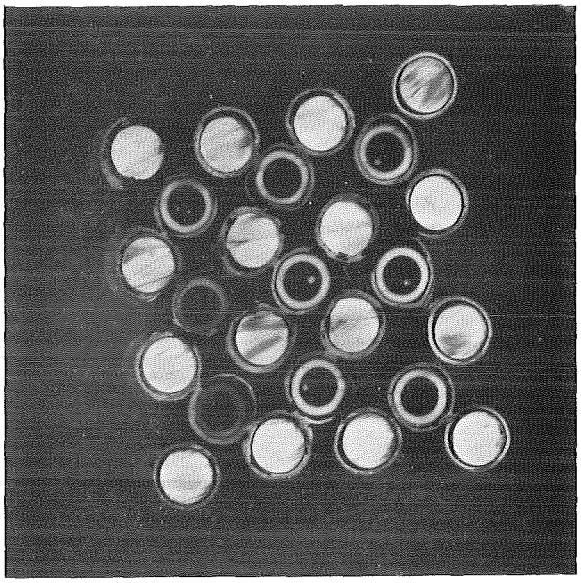

1Ø82 lower

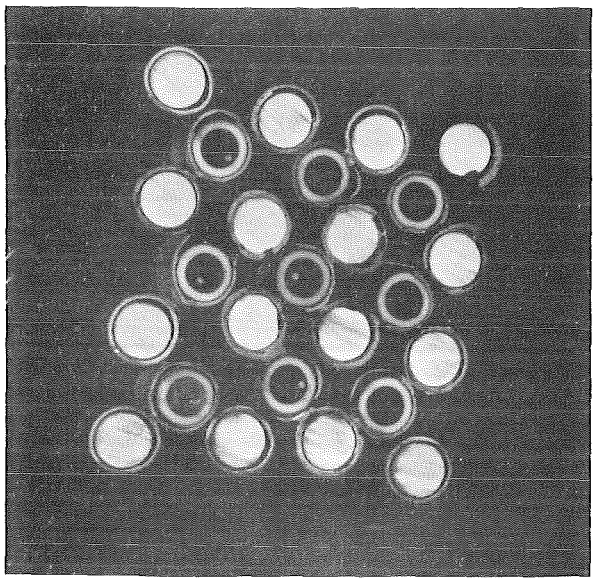

1Ø78

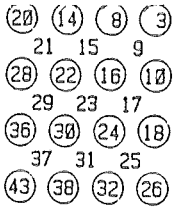

upper

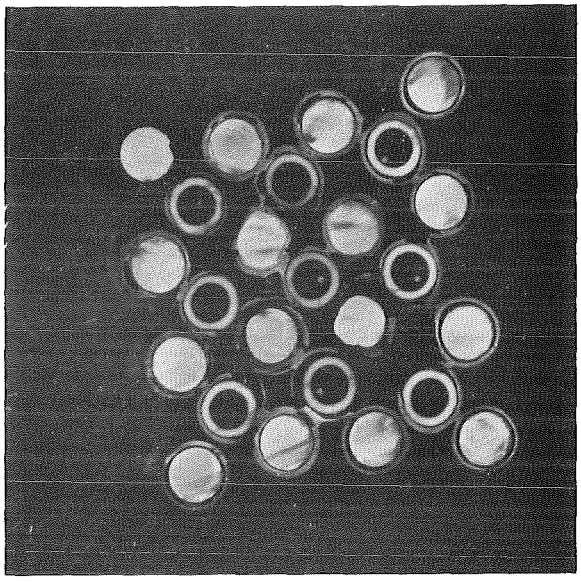

1Ø67

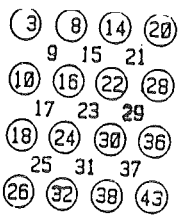

lower

Fig.: 117b Cross section of CORA bundle B

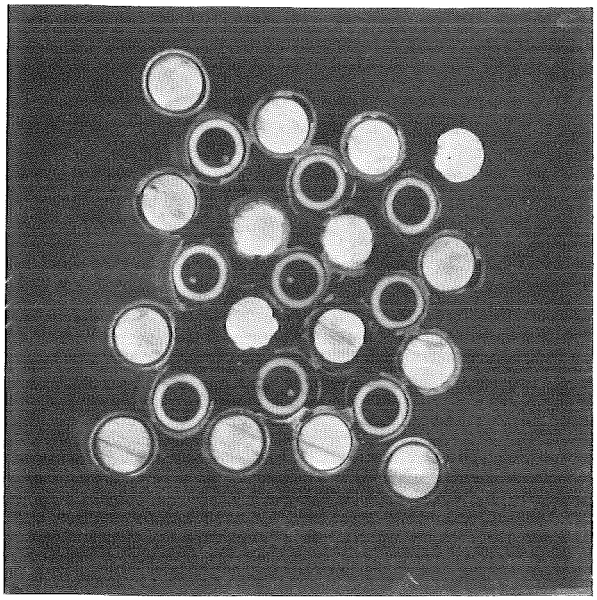

1063 upper

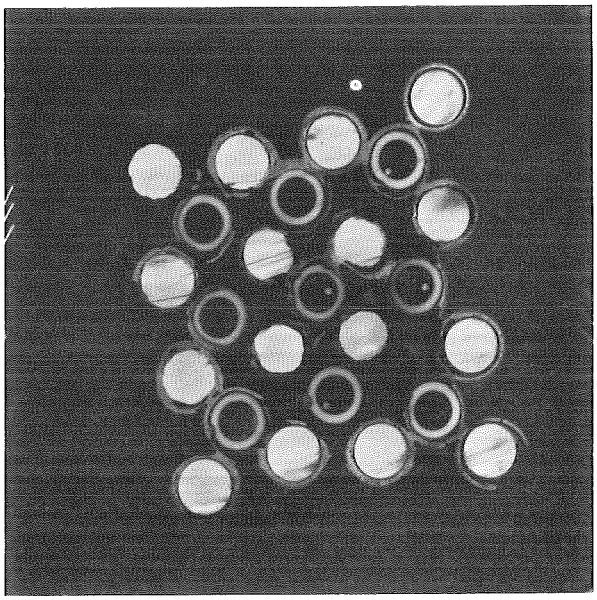

1052 lower

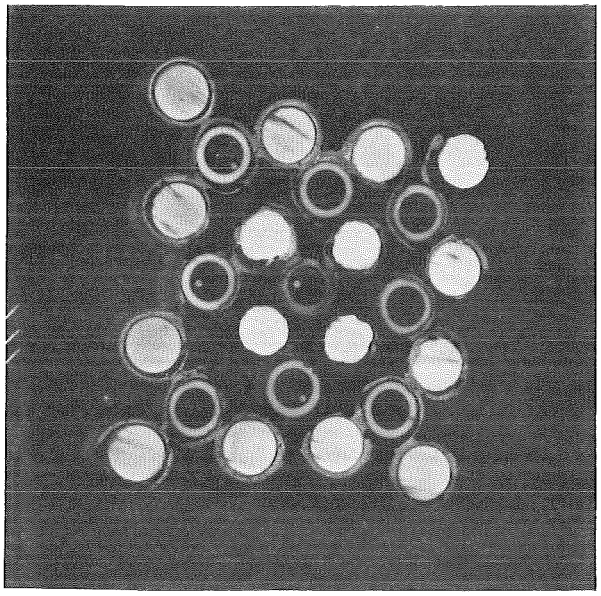

1048

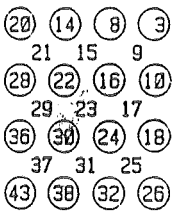

upper

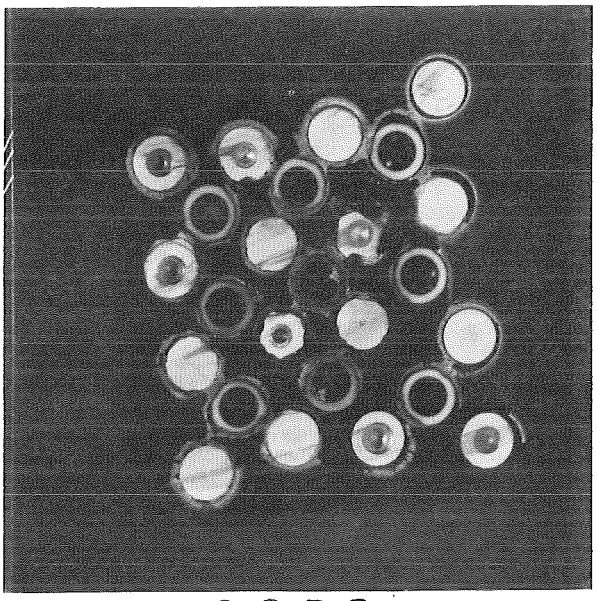

1037

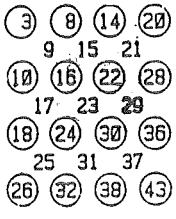

lower

Fig.: 117c Cross section of CORA bundle B

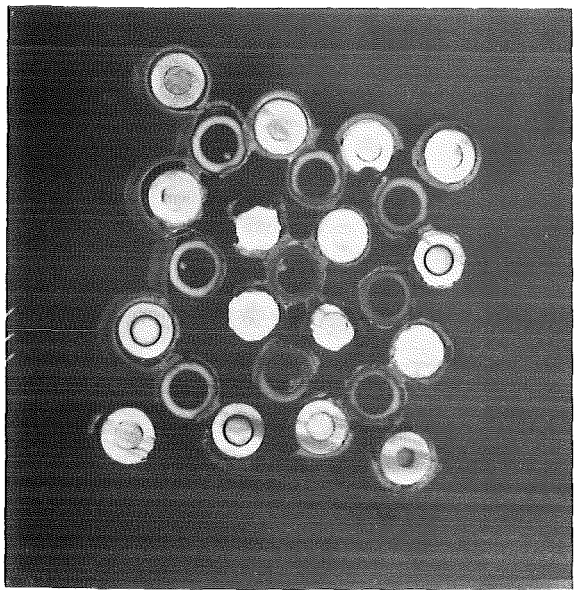

1033 mm

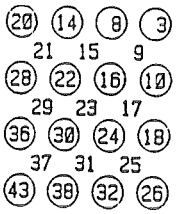

upper

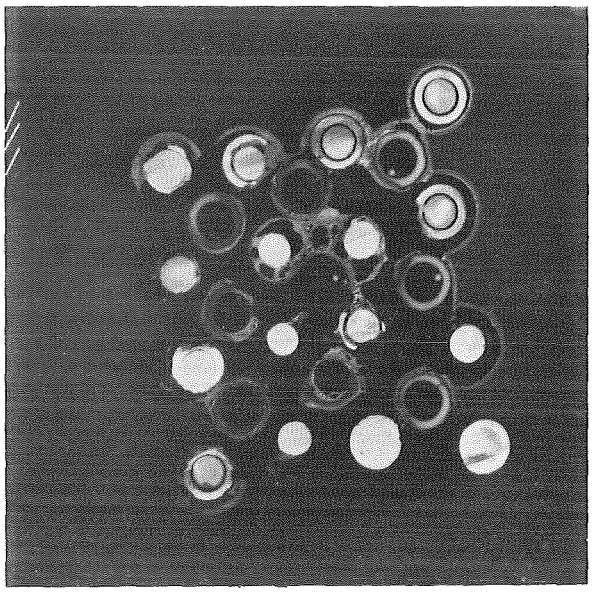

1022 mm

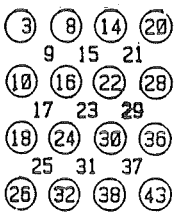

lower

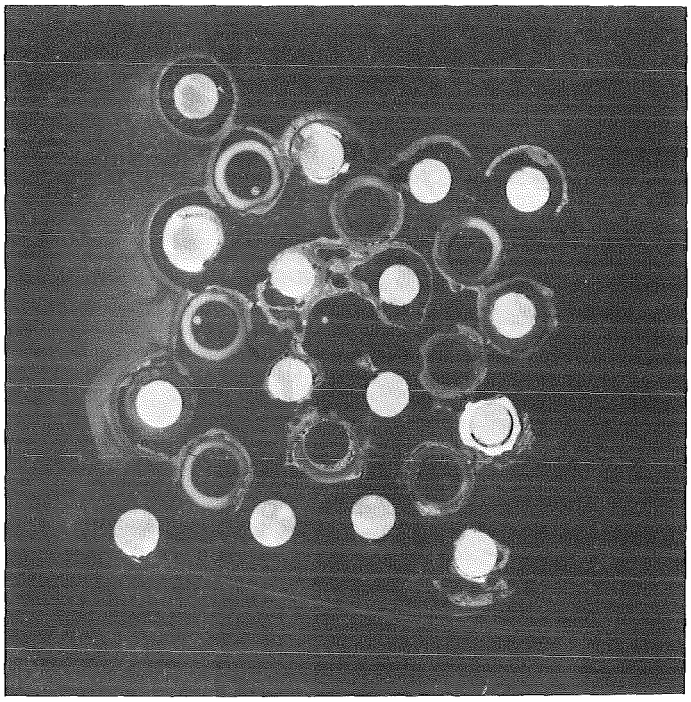

1018 mm

Fig.: 117d Cross section of CORA bundle B

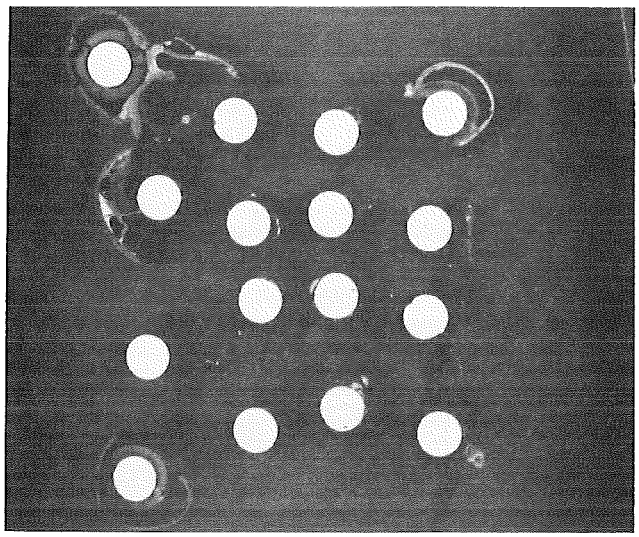

919mm

upper

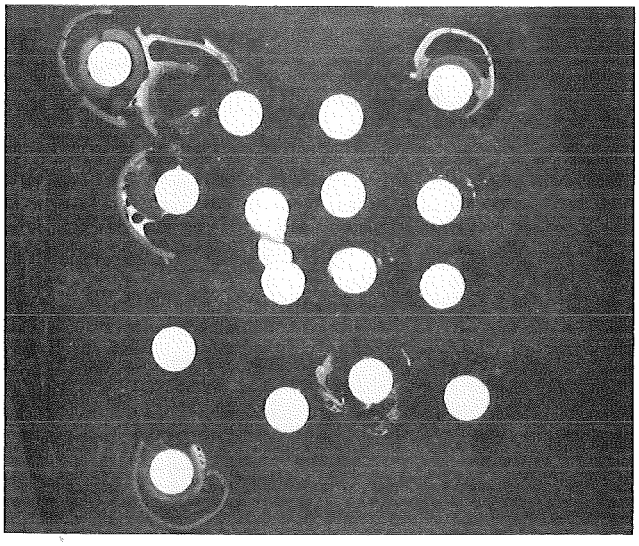

901mm

upper

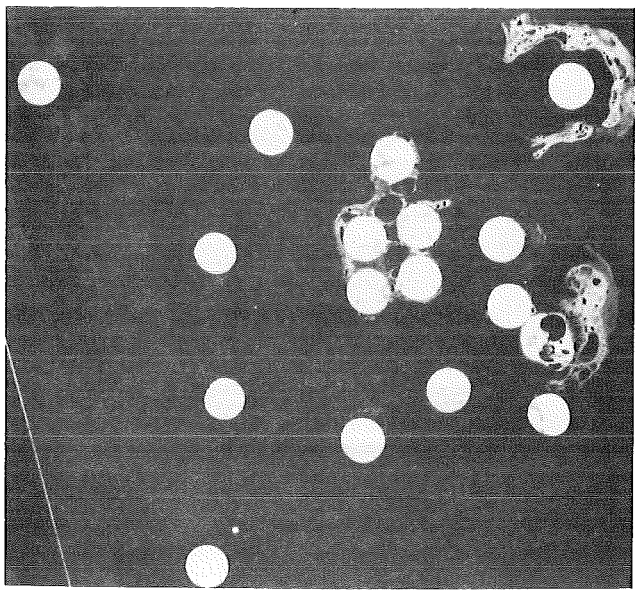

507mm

upper

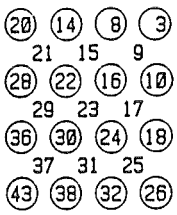

Fig. 118: Cross sections of CORA bundle B at elevations given (bundle code)

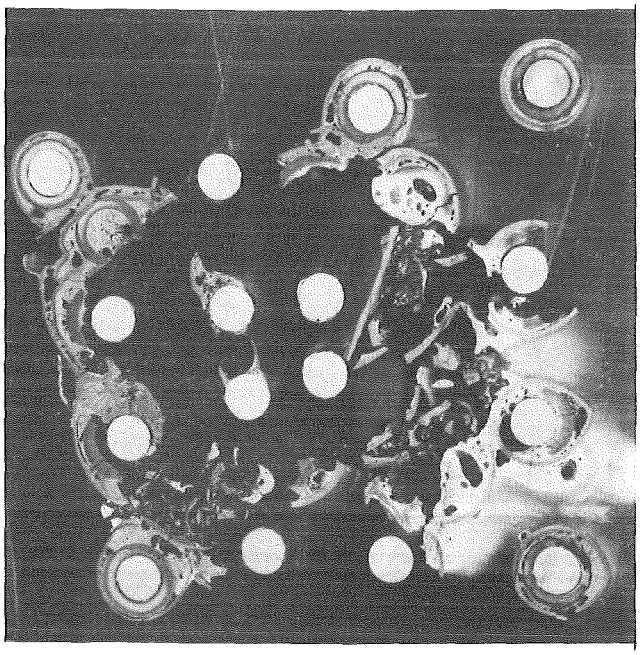

271mm lower

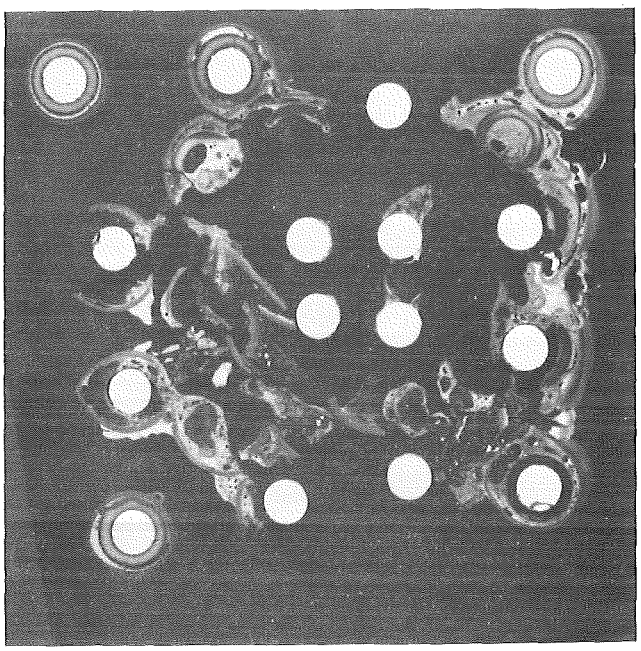

269mm upper

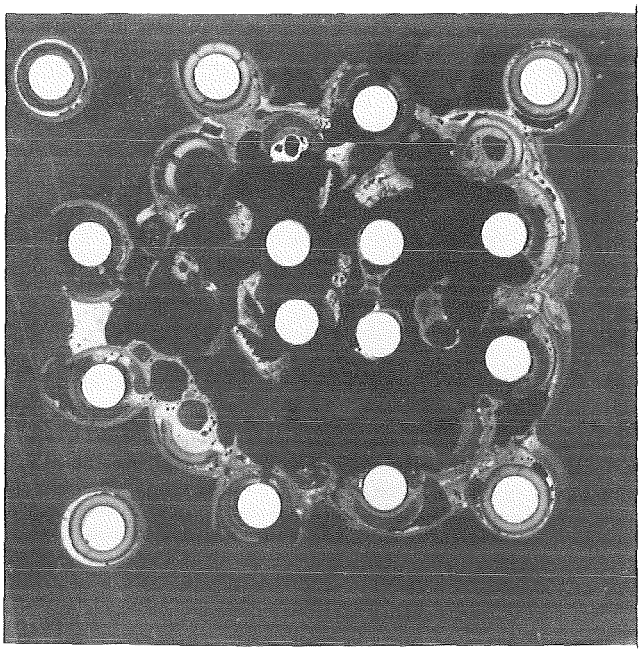

251mm upper

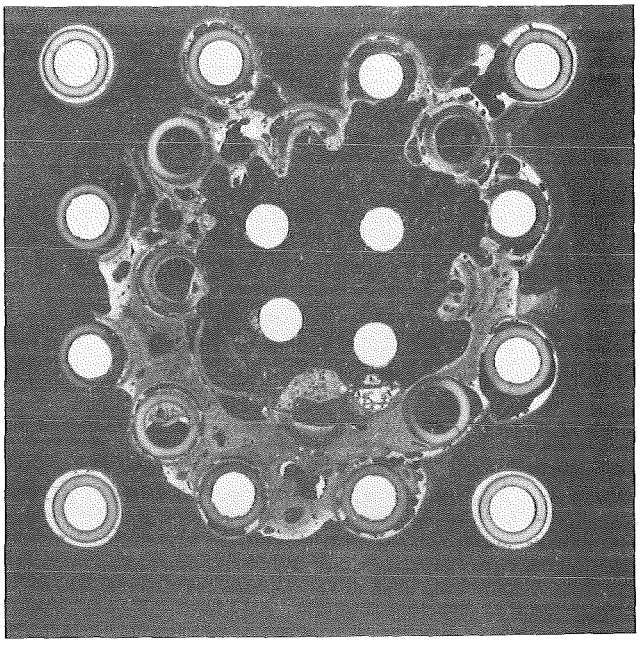

109mm upper

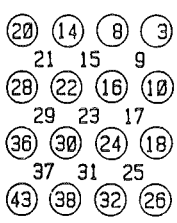

upper

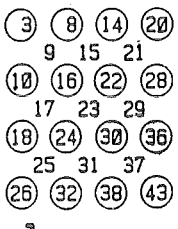

lower

Fig. 119: Cross sections of CORA bundle B at elevations given (bundle code)

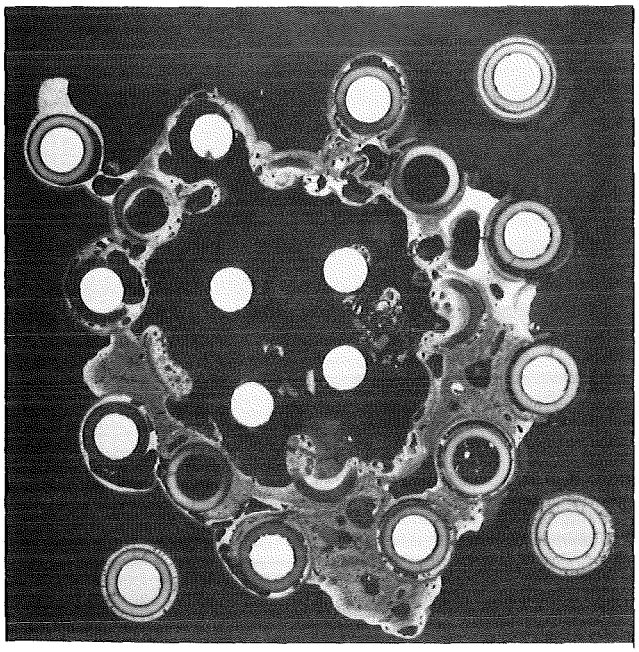

93mm lower

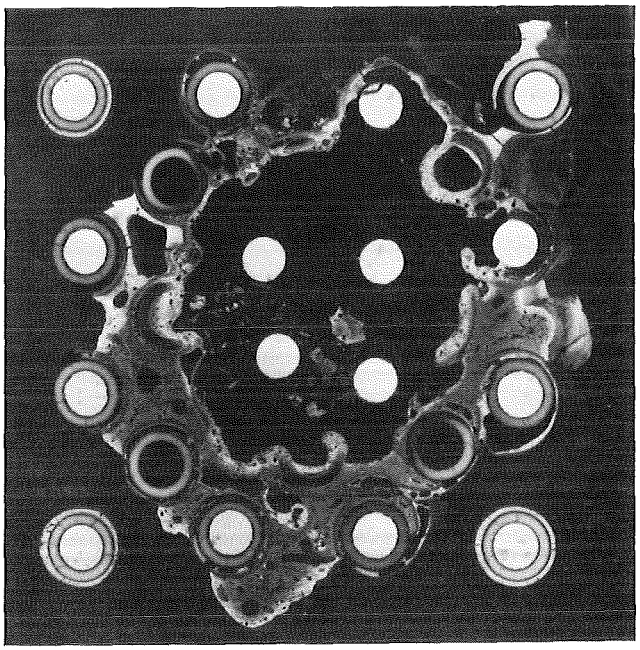

91mm upper

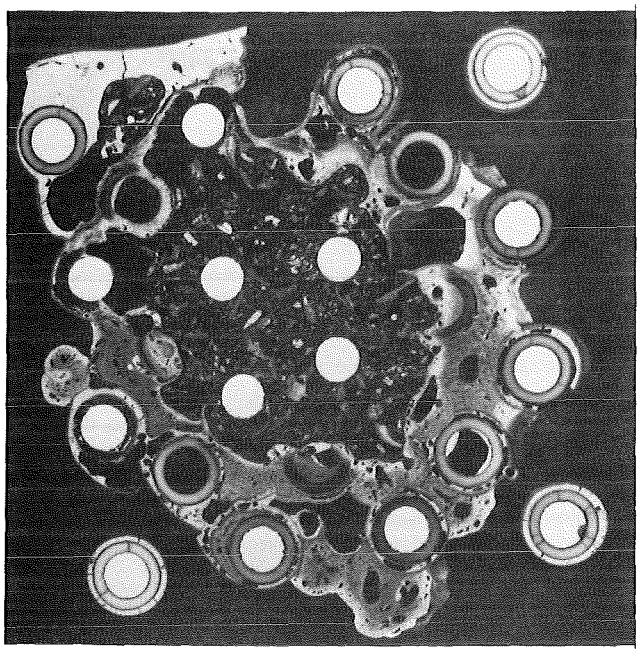

75mm lower

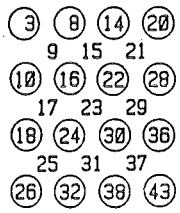

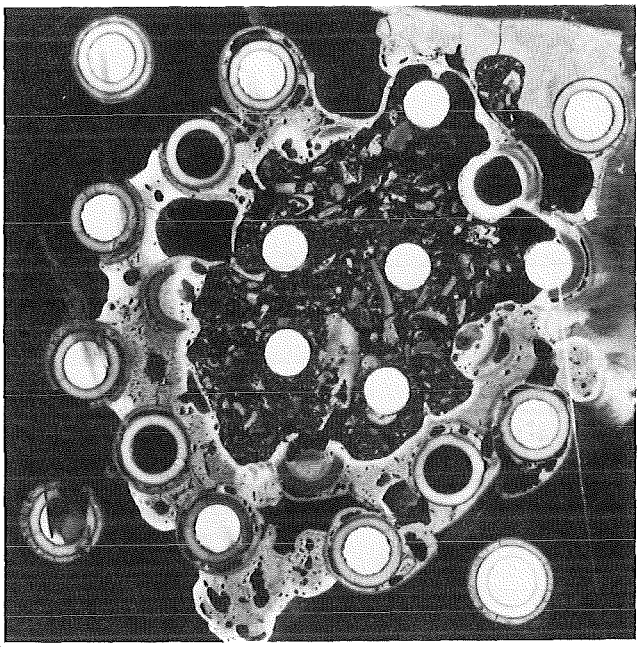

73mm upper

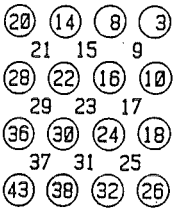

Fig. 120: Cross sections of CORA bundle B at elevations given (bundle code)

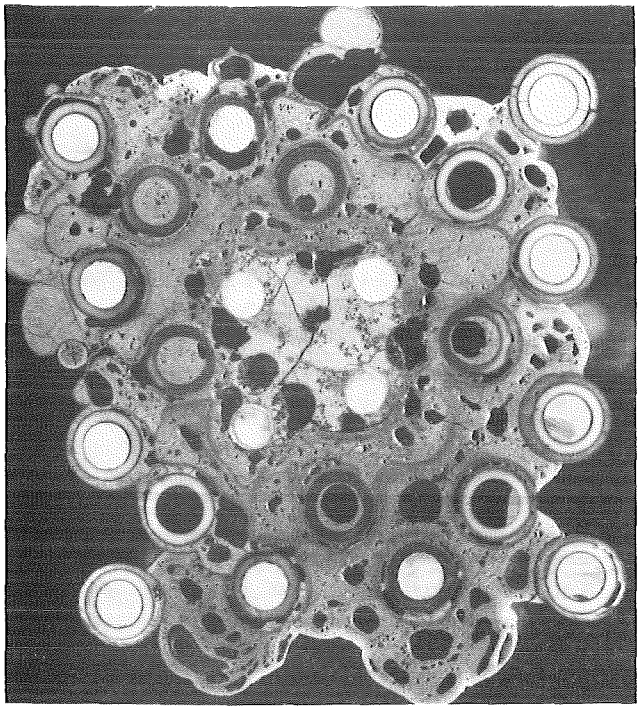

1mm lower

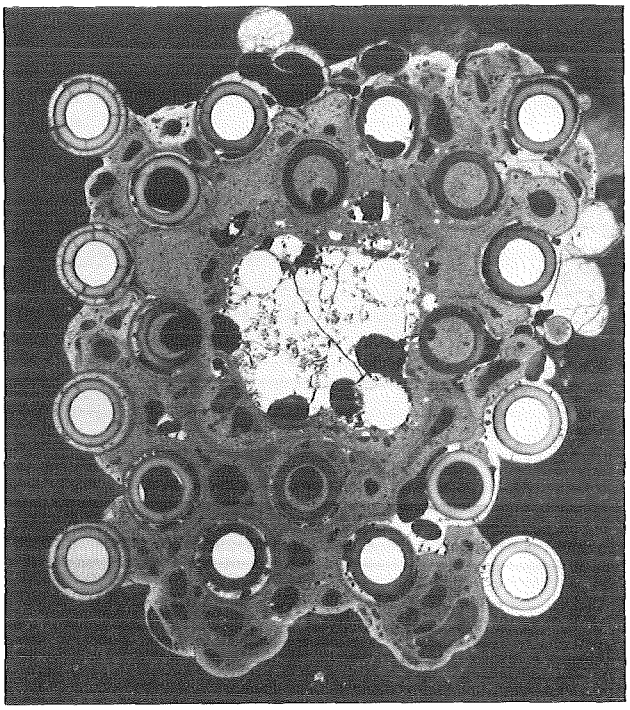

0mm upper

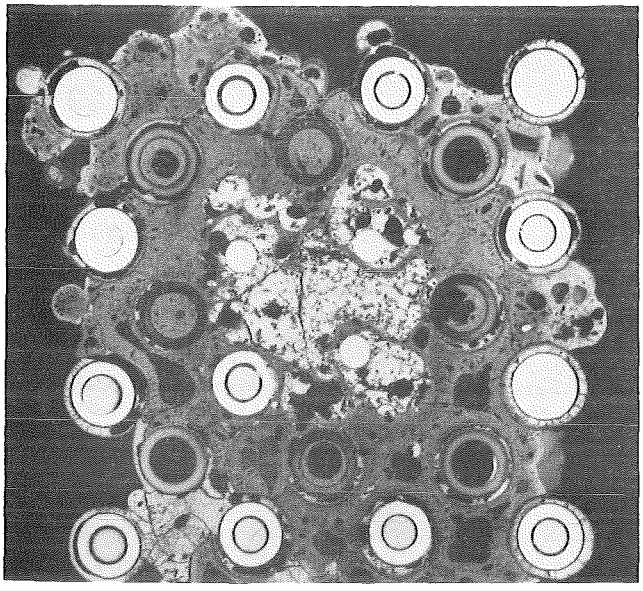

-16mm

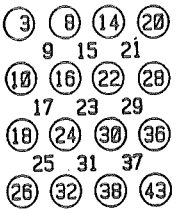

lower

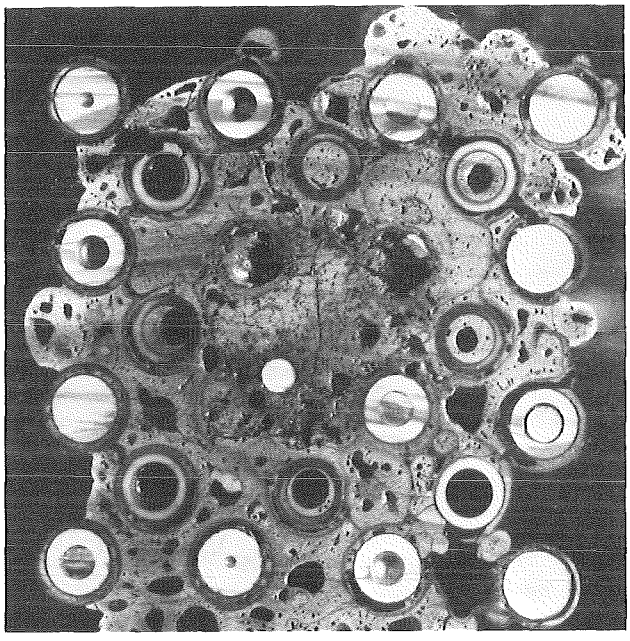

-18mm

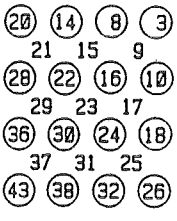

upper

Fig. 121: Cross sections of CORA bundle B at elevations given (bundle code)

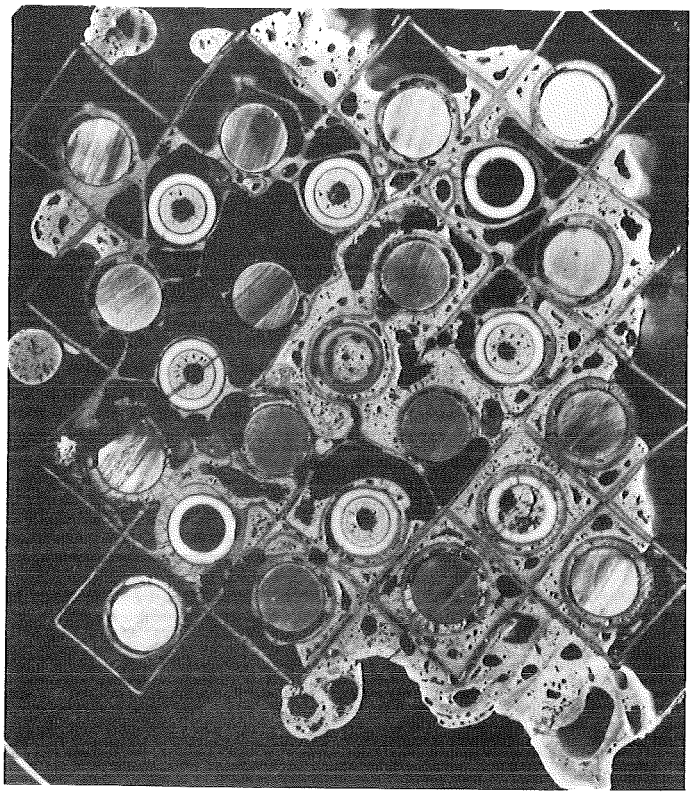

-53mm lower

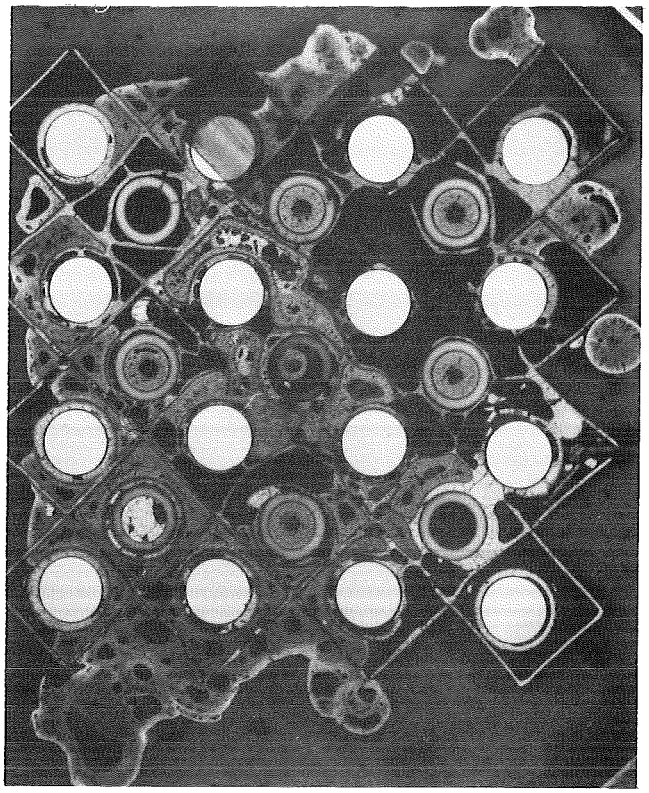

-55mm upper

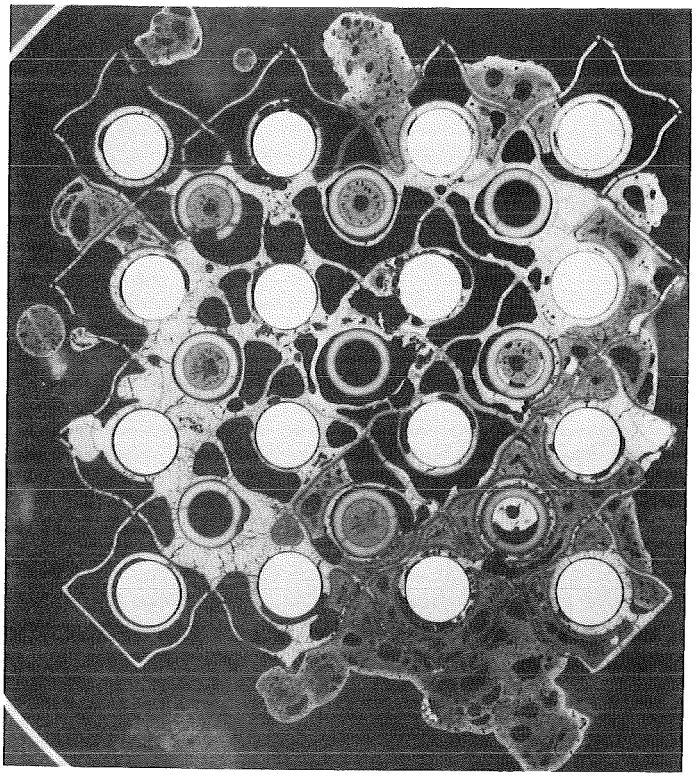

-71mm

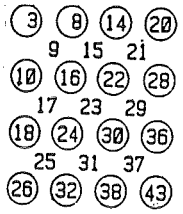

lower

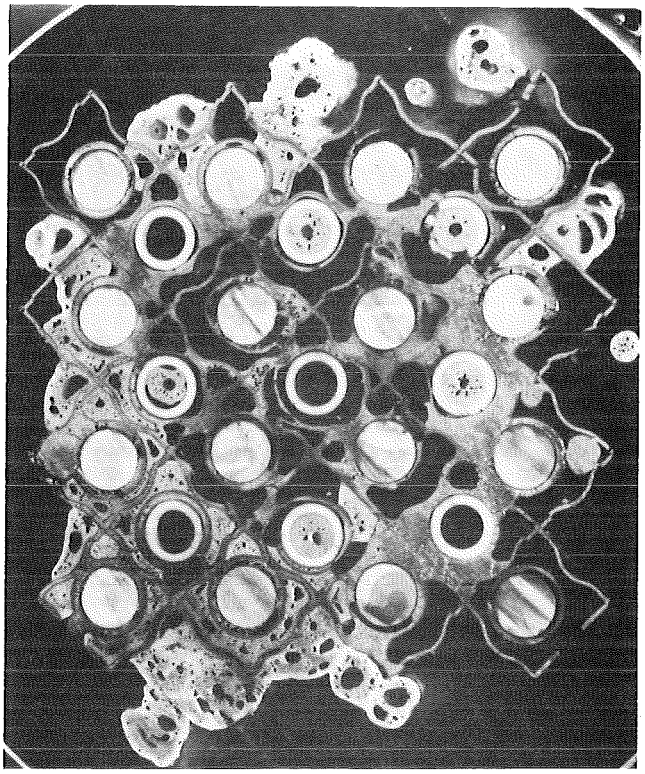

-73mm

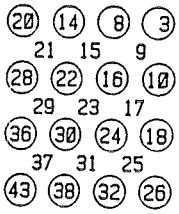

upper

Fig.122: Cross sections of CORA bundle B at elevations given (bundle code)

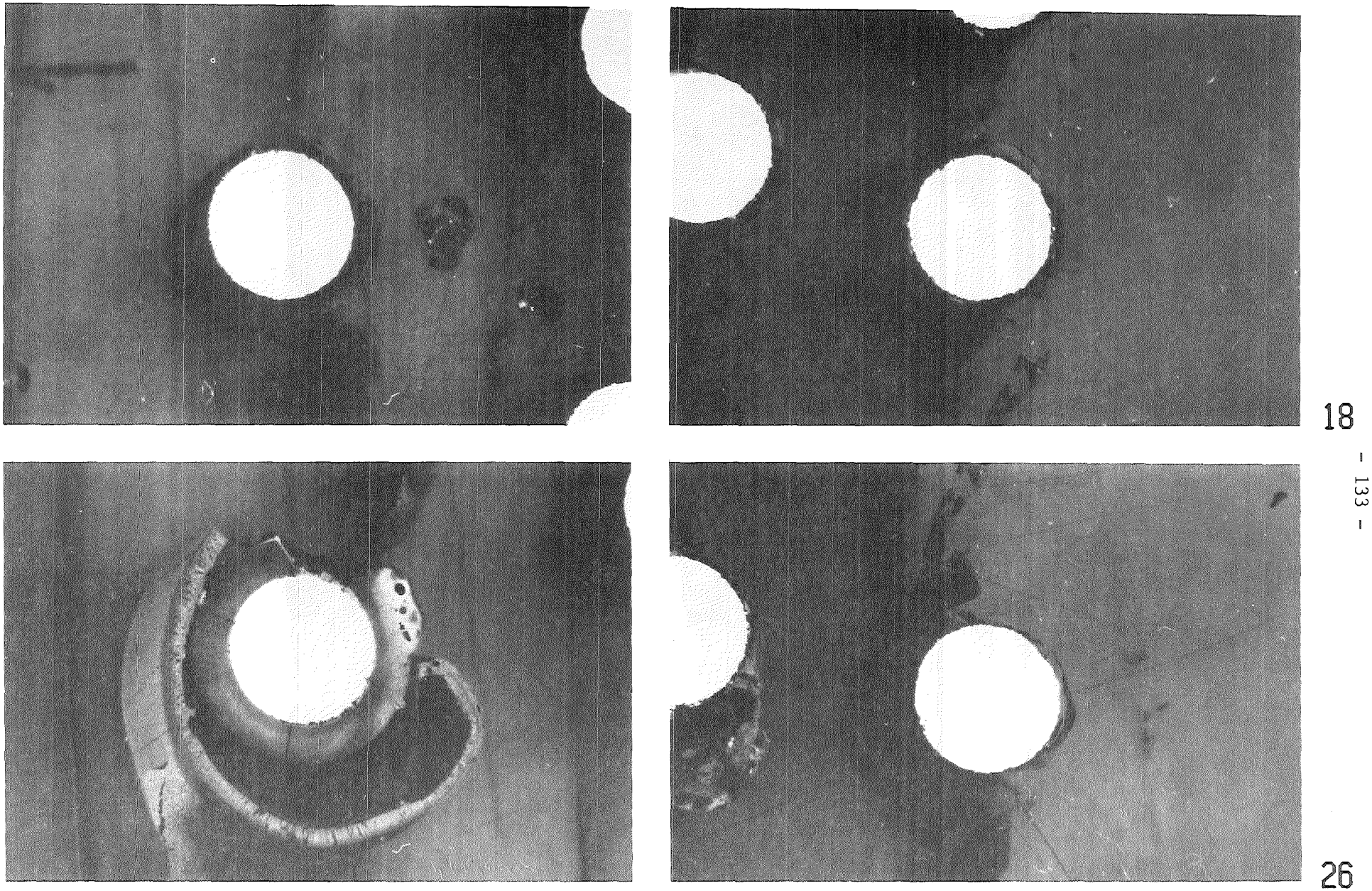

Fig. 123: Enlarged cross sections of heated rods at 901 mm elevation (CORA bundle B)

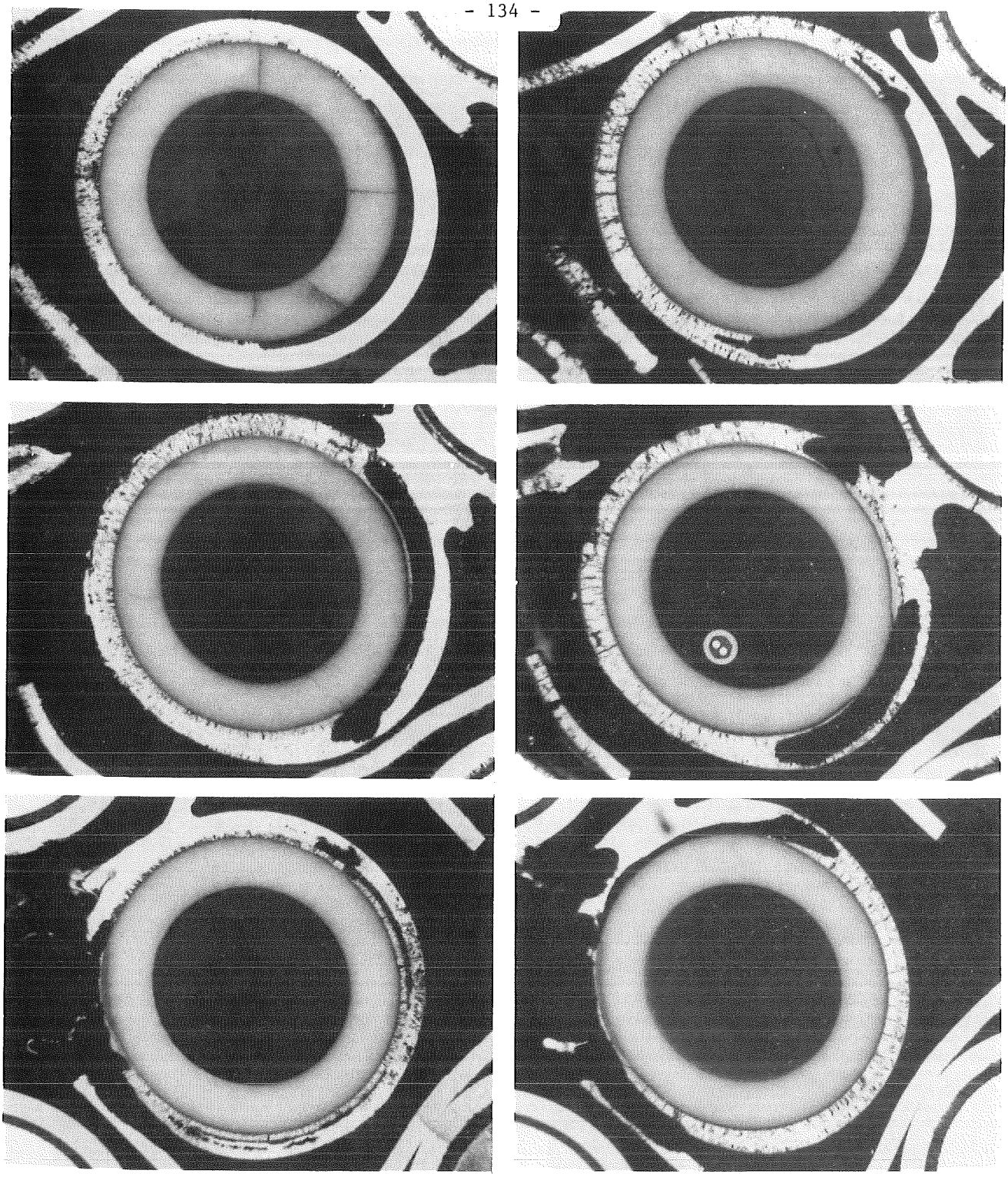

1159 mm

1141 mm

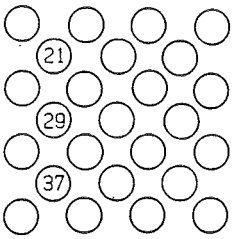

Fig. 123 a: Cross section of unheated rods 21, 29 and 37 at 1159 mm and 1141 mm (CORA-B)

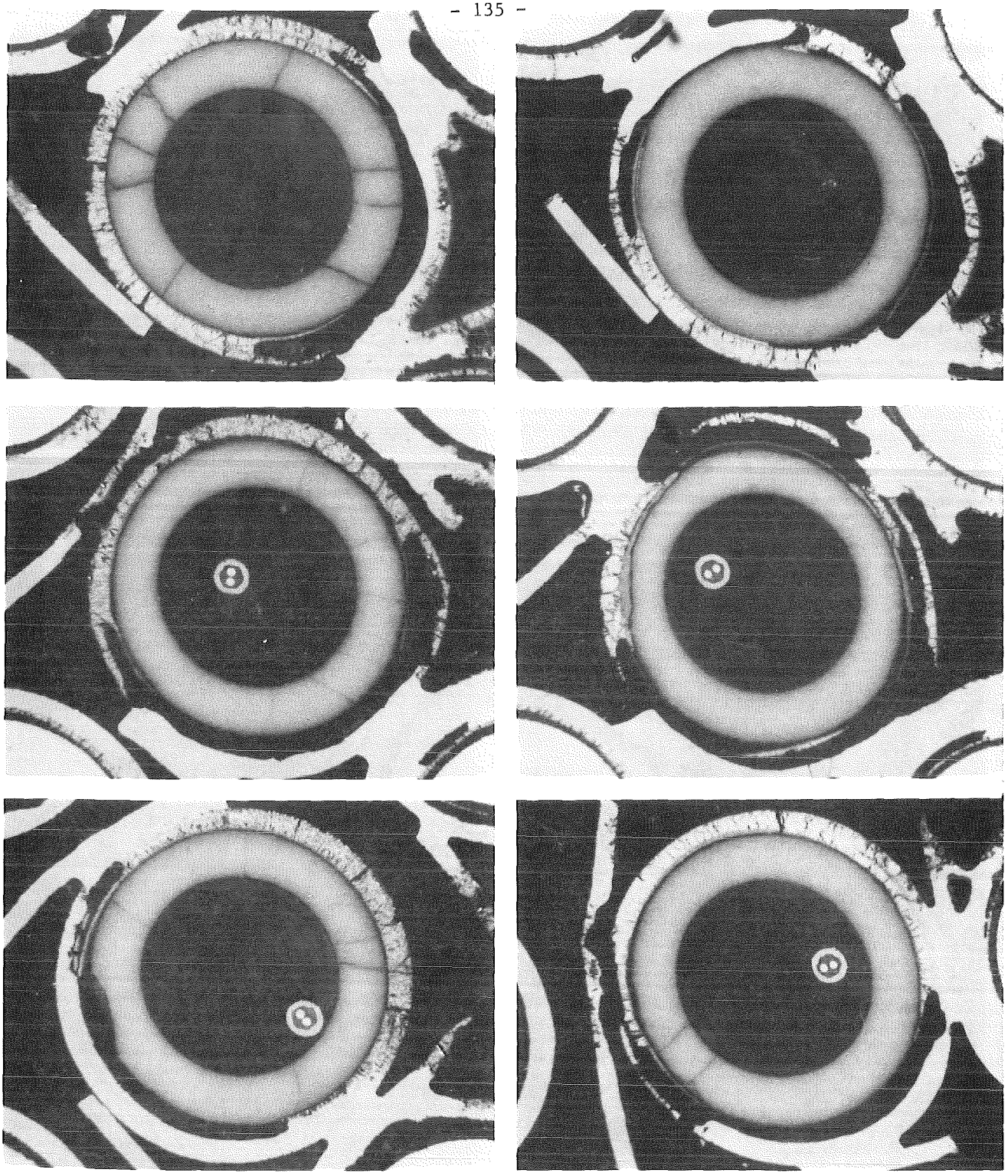

1159 mm

1141 mm

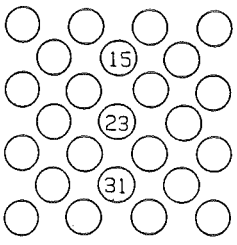

Fig. 123 b: Cross section of unheated rods 15, 23 and 31 at 1159 mm and 1141 mm (CORA-B)

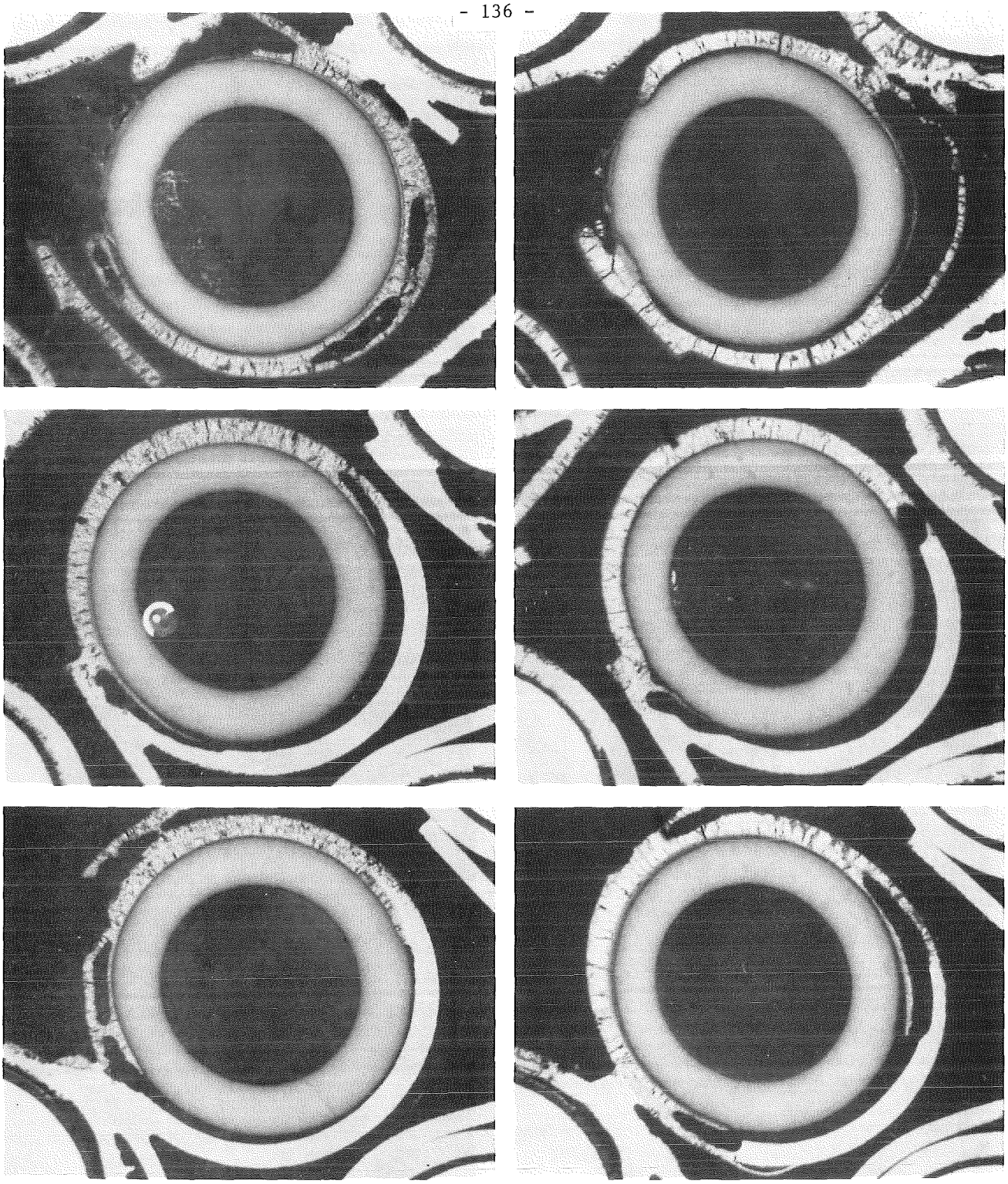

1159 mm

1141 mm

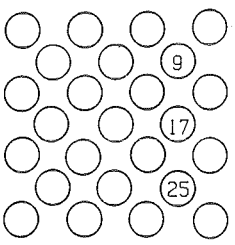

Fig. 123 c: Cross sections of unheated rods 9, 17 and 25 at 1159mm and 1141mm (CORA-B)

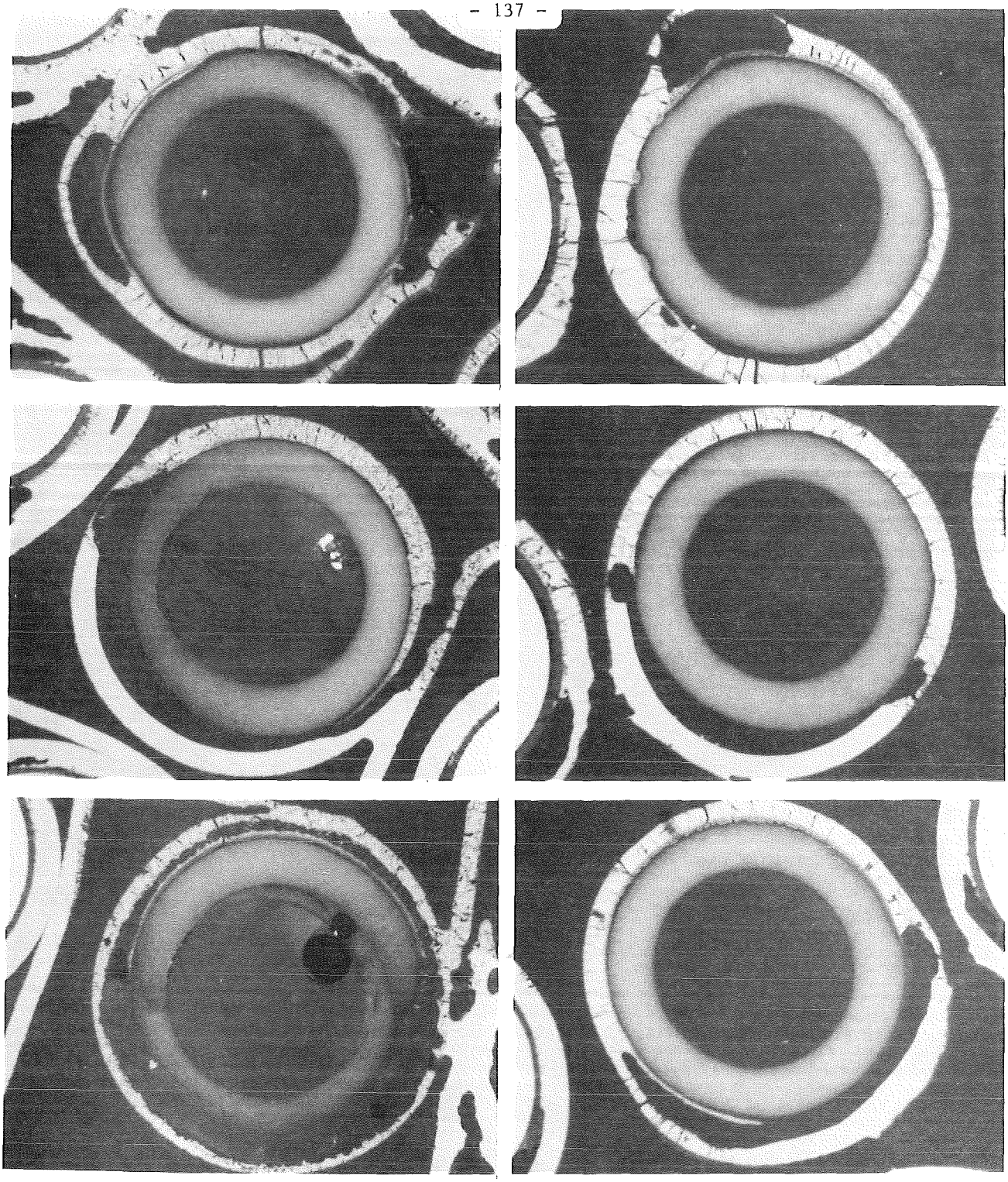

1143 mm 1125 mm

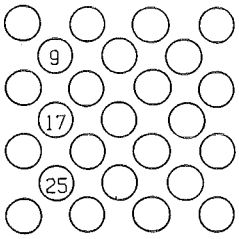

Fig. 123 d: Cross sections of unheated rods 9, 17 and 25 at 1143mm and 1125mm (CORA-B)

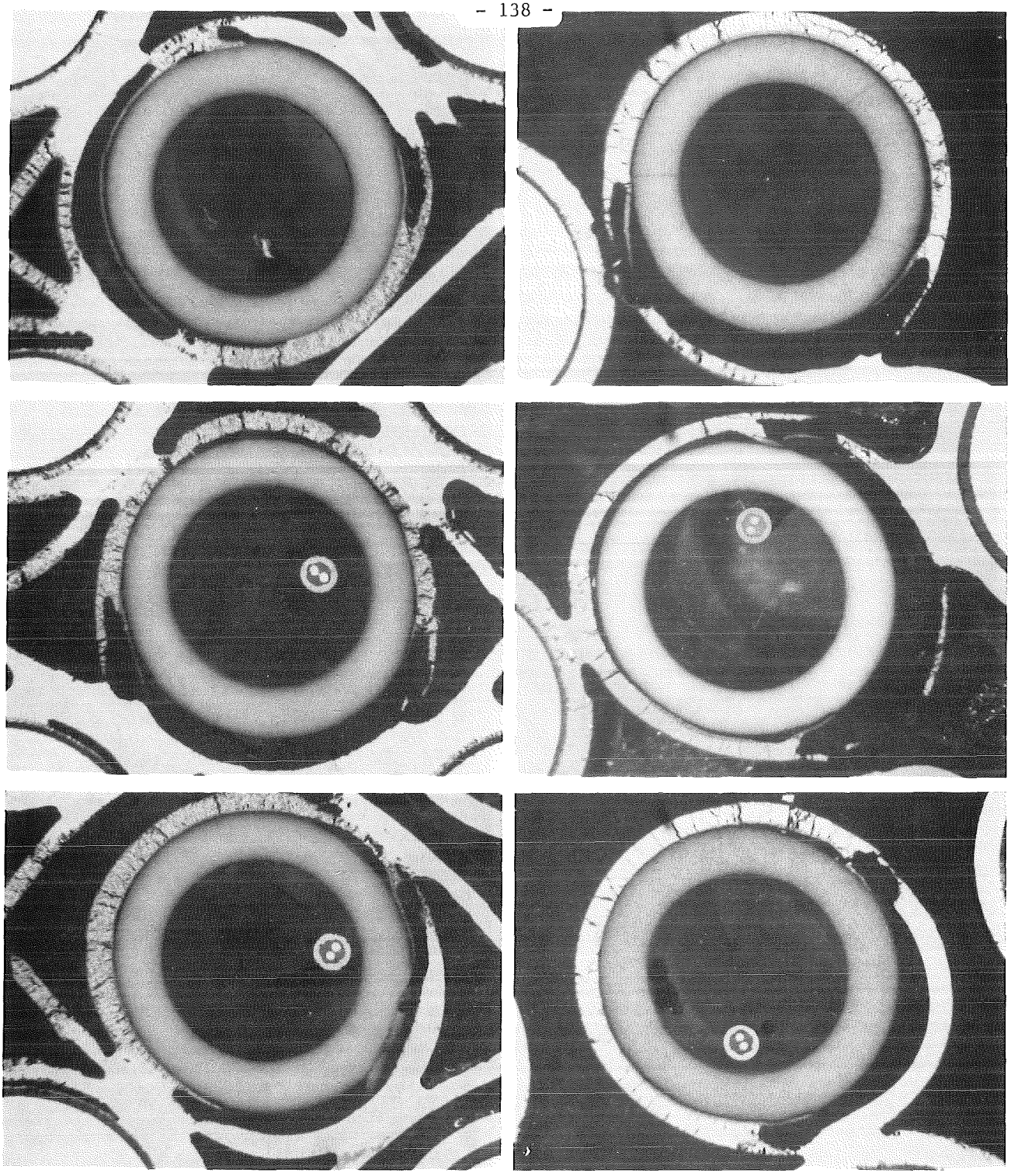

1143 mm

1125 mm

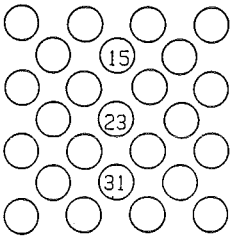

Fig. 123 e: Cross sections of unheated rods 15, 23 and 31 at 1143mm and 1125mm (CORA-B)

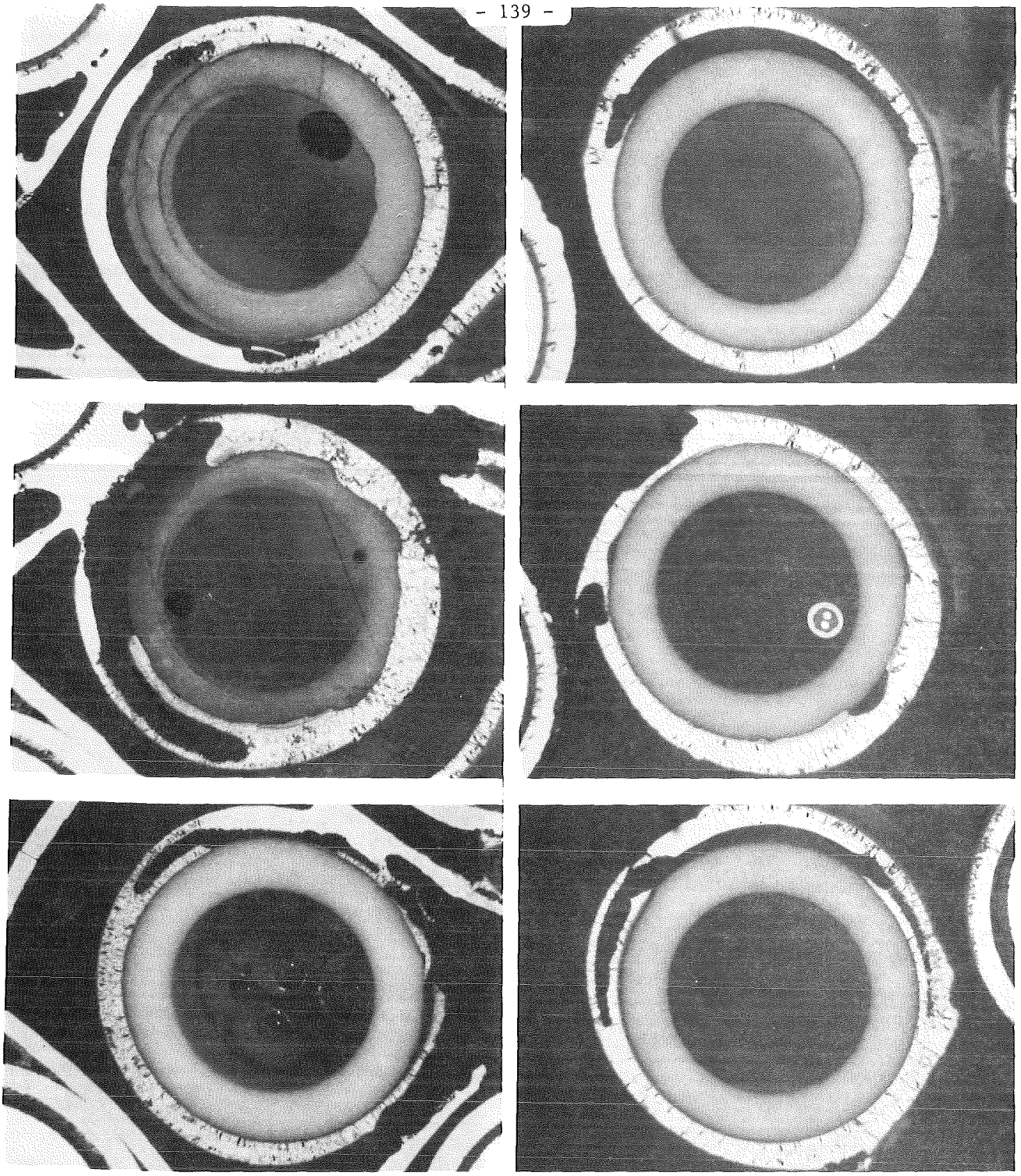

1143 mm

1125 mm

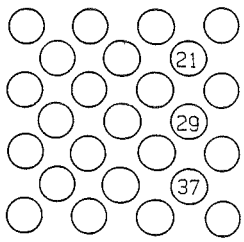

Fig. 123 f: Cross sections of unheated rods 21, 29 and 37 at 1143mm and 1125mm (CORA-B)

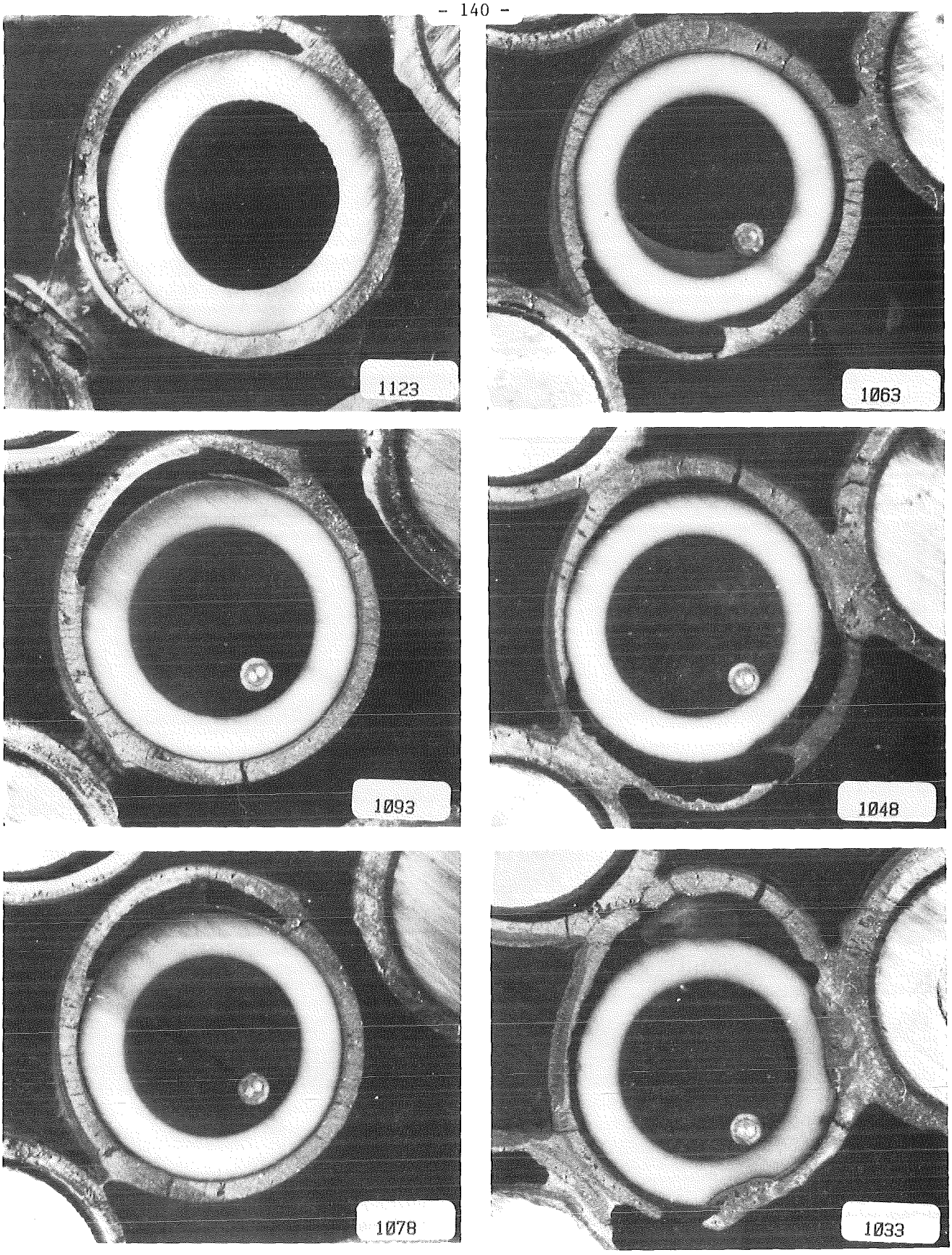

Fig. 123g Cross sections at upper end of unheated fuel rod simulator 21 CORA-B)

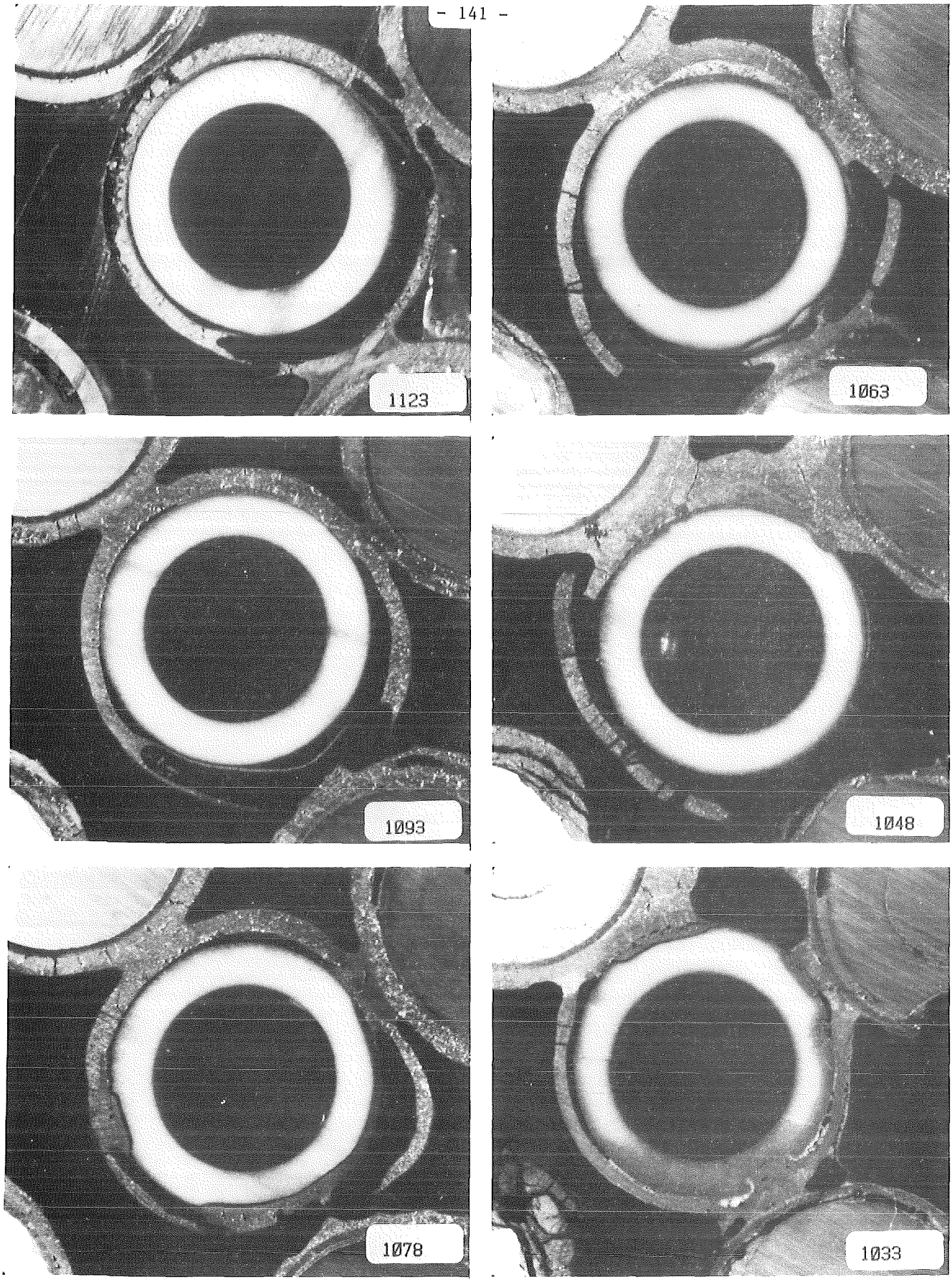

Fig. 123h : Cross sections at upper end of unheated fuel rod simulator 15 (CORA-B)

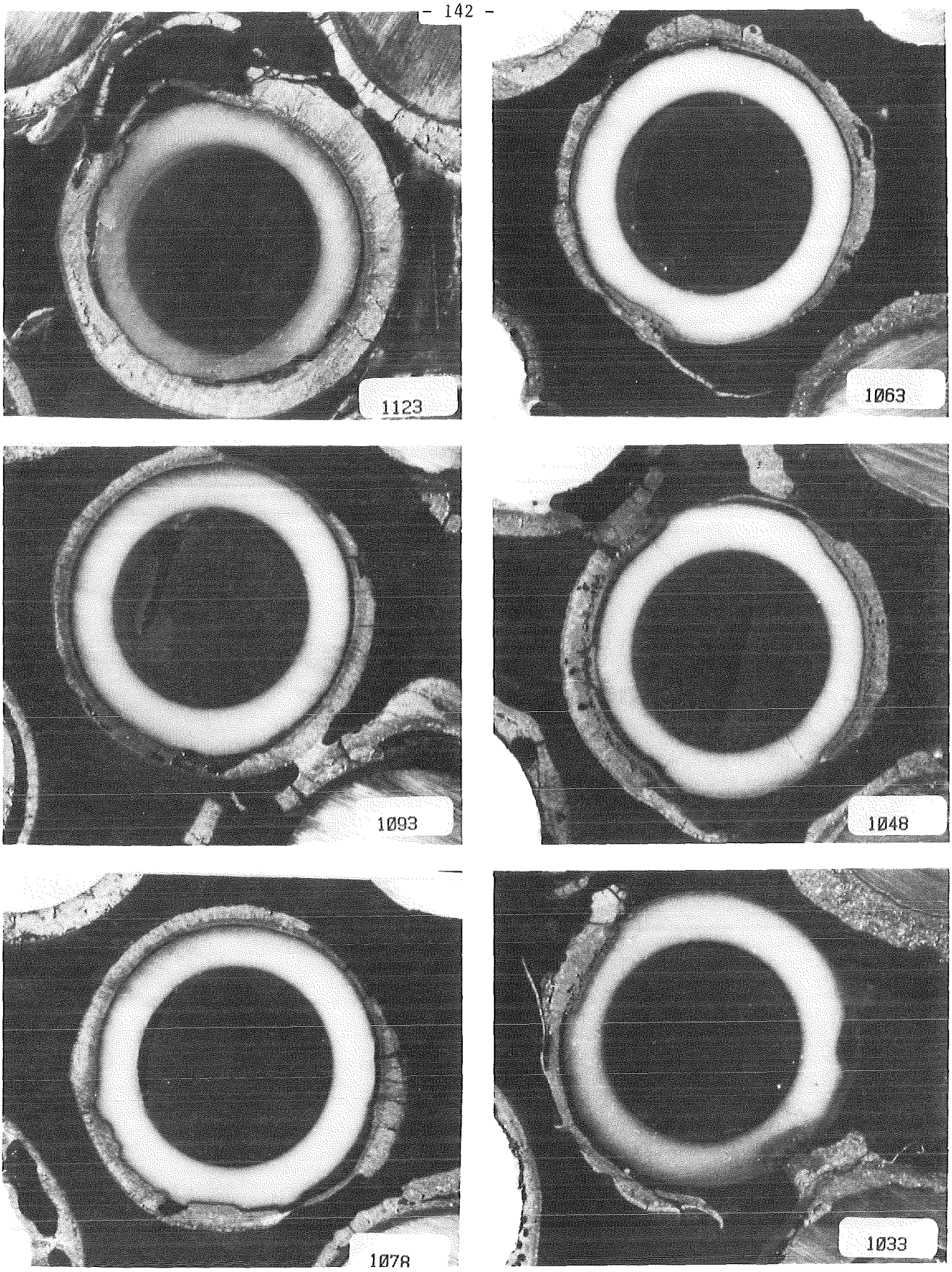

Fig. 123: Cross sections at upper end of unheated fuel rod simulator 9 (CORA-B)

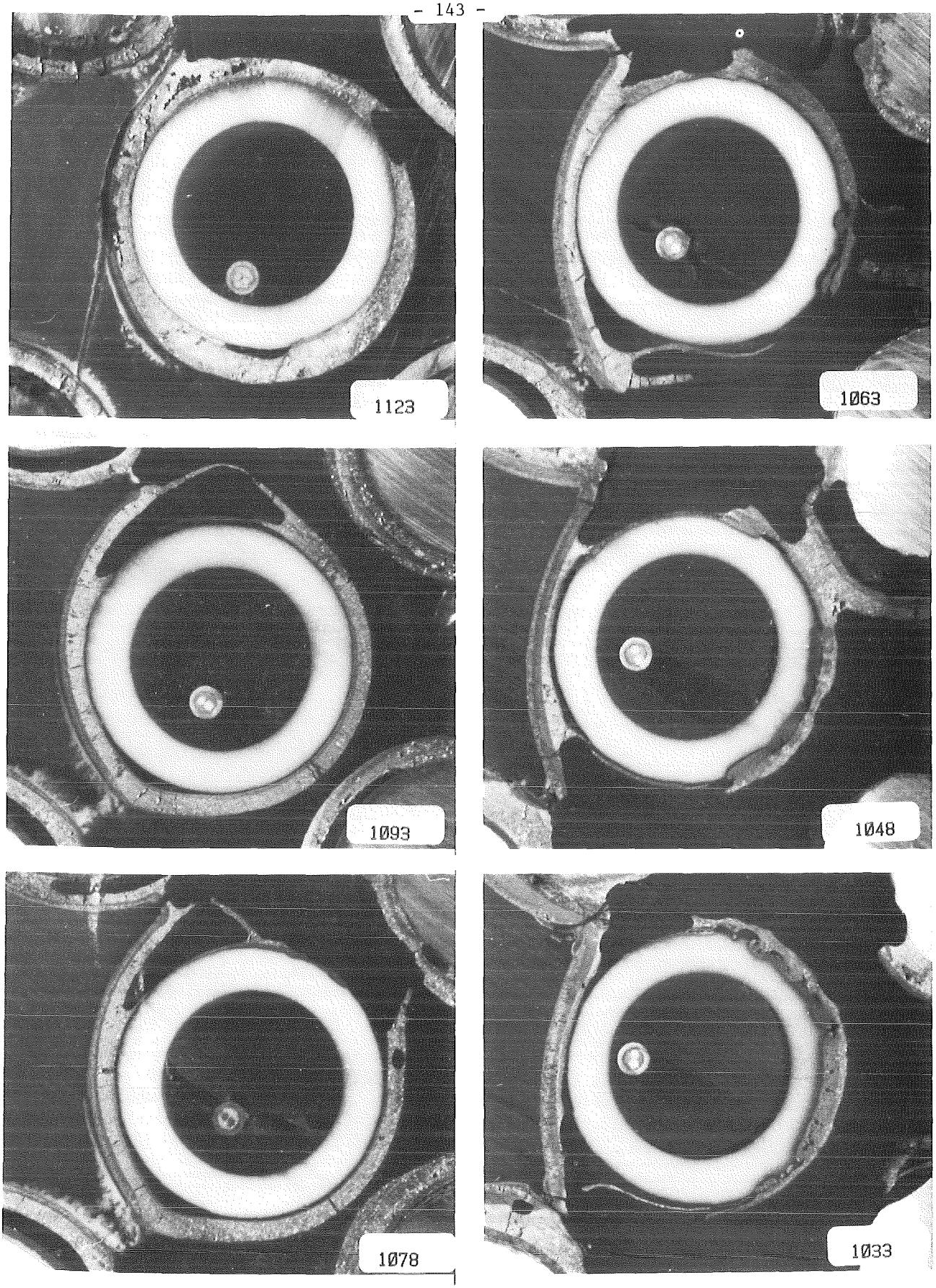

Fig. 123 j : Cross sections at upper end of unheated fuel rod simulator 29 (CORA-B)

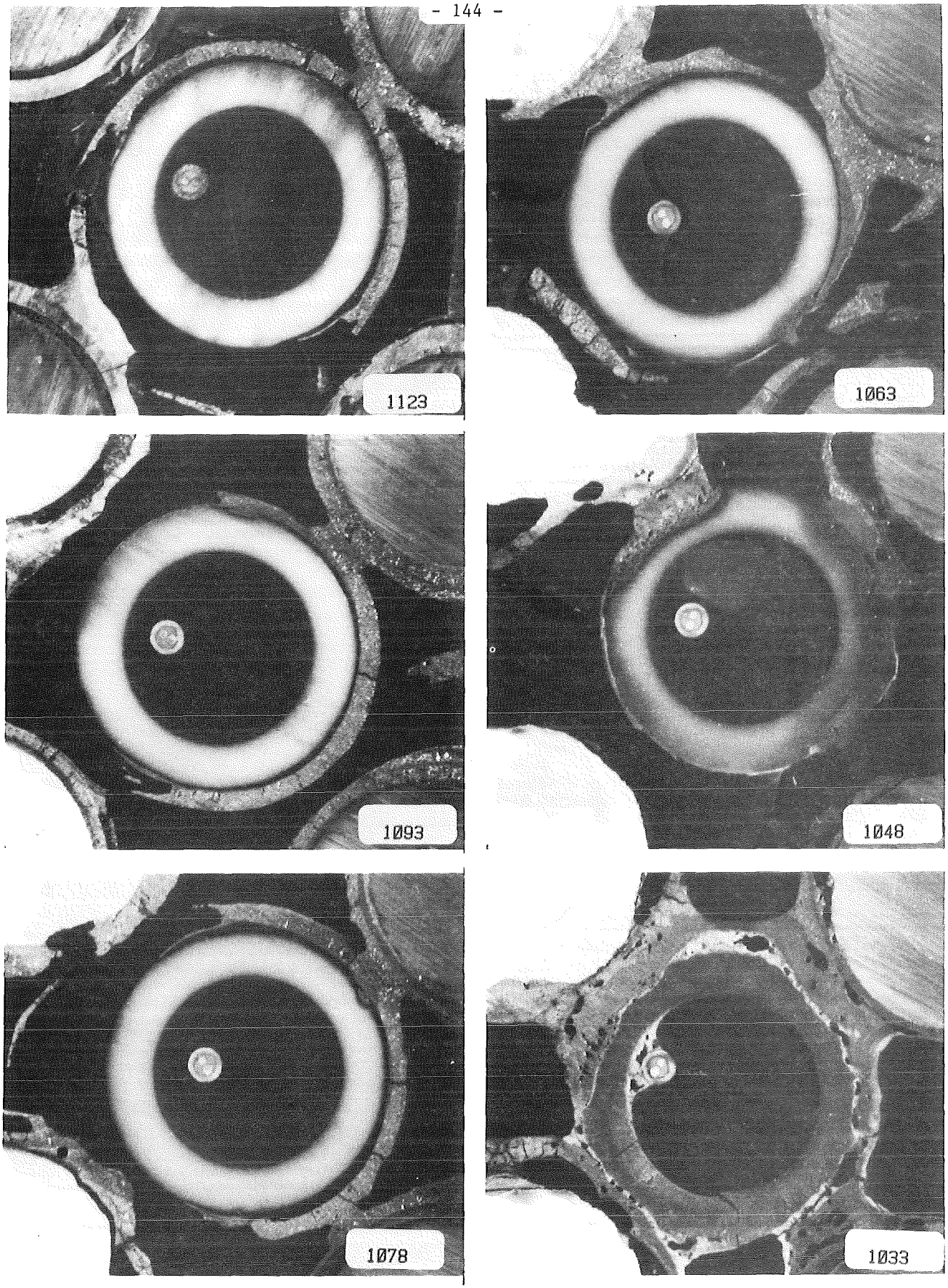

Fig. 123k : Cross sections at upper end of unheated fuel rod simulator 23 (CORA-B)

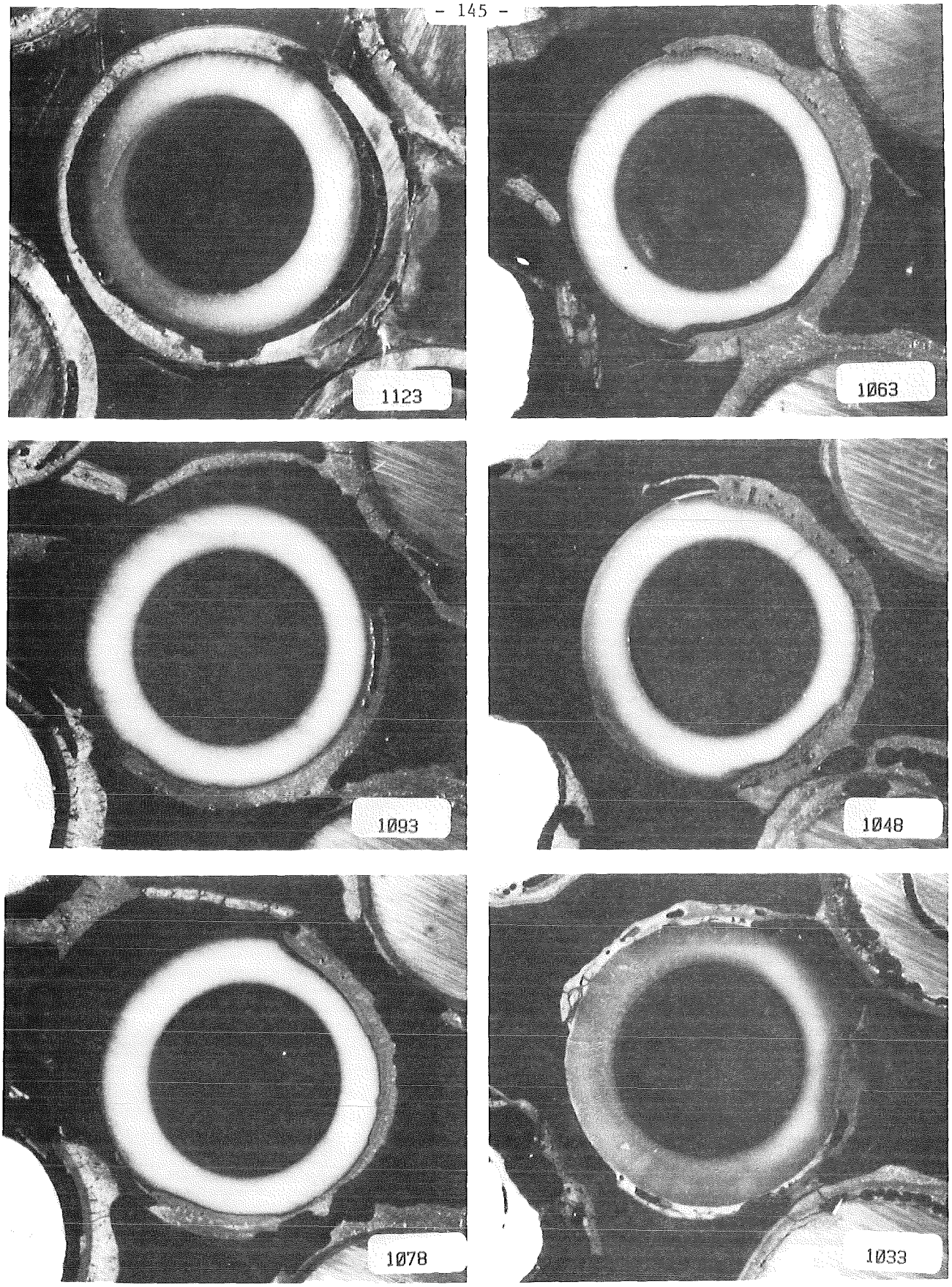

Fig. 1231 : Cross sections at upper end of unheated fuel rod simulator 17 (CORA-B)

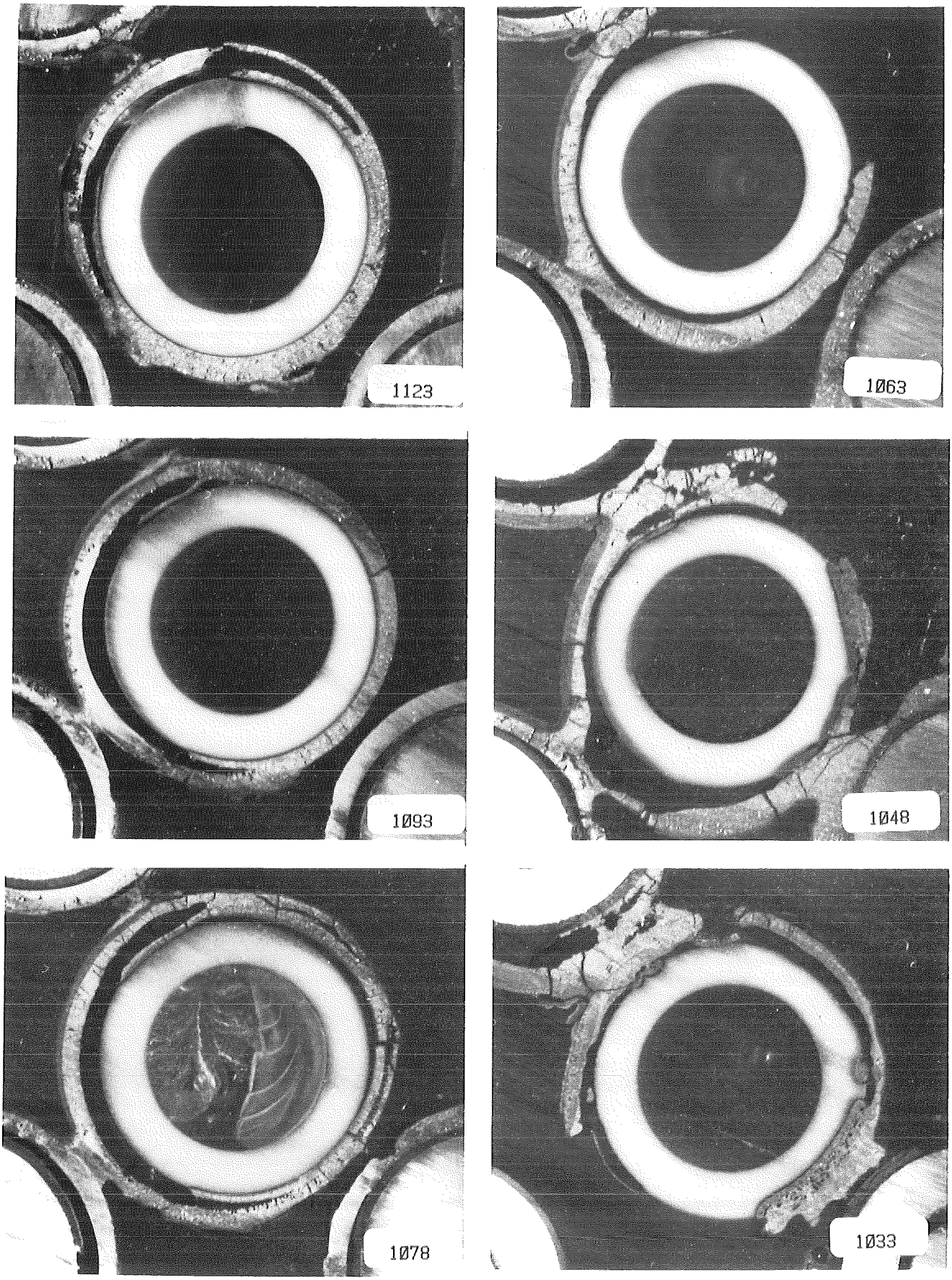

Fig. 123m : Cross sections at upper end of unheated fuel rod simulator 37 (CORA-B)

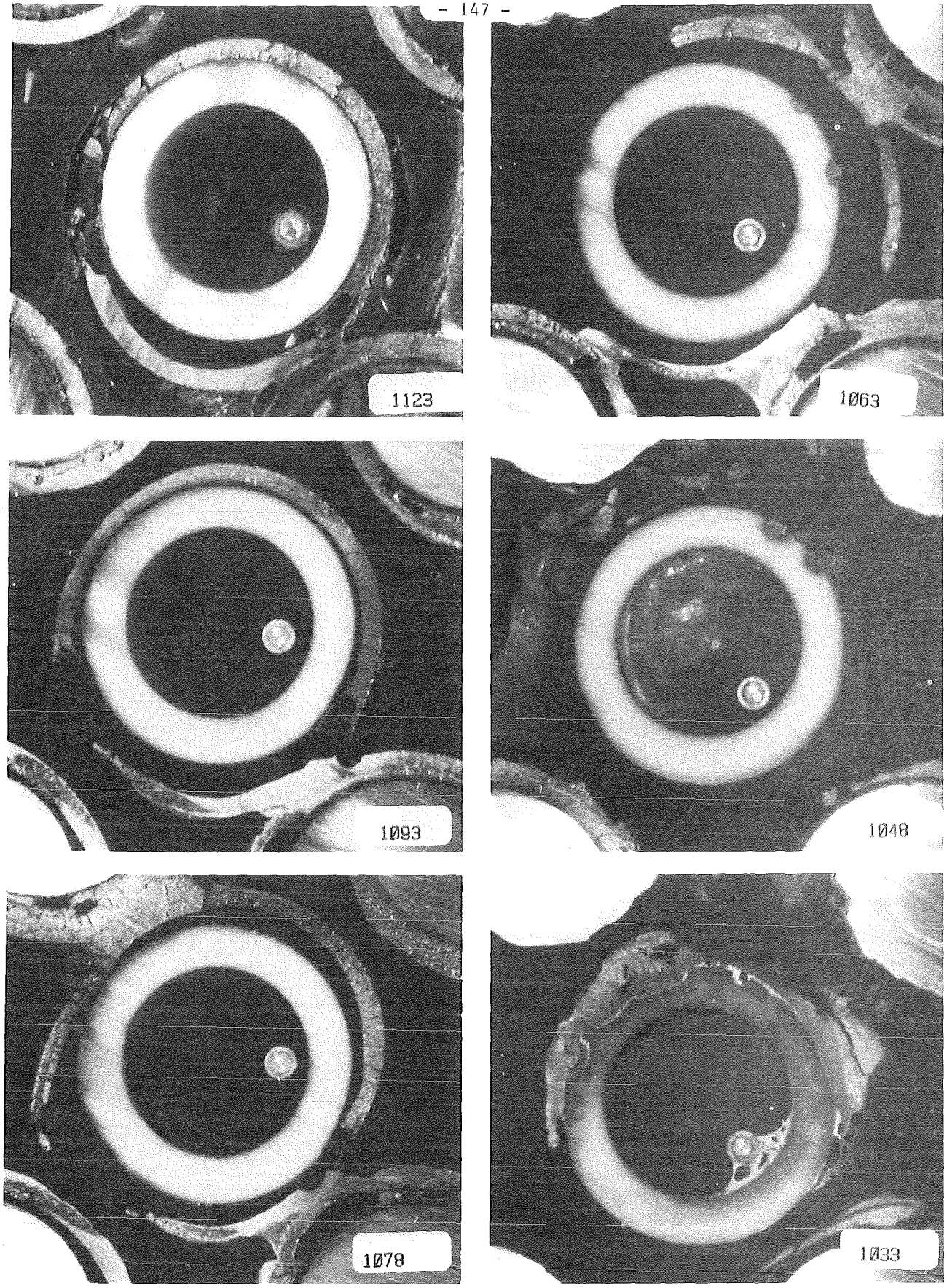

Fig. 123n : Cross sections at upper end of unheated fuel rod simulator 31 (CORA-B)

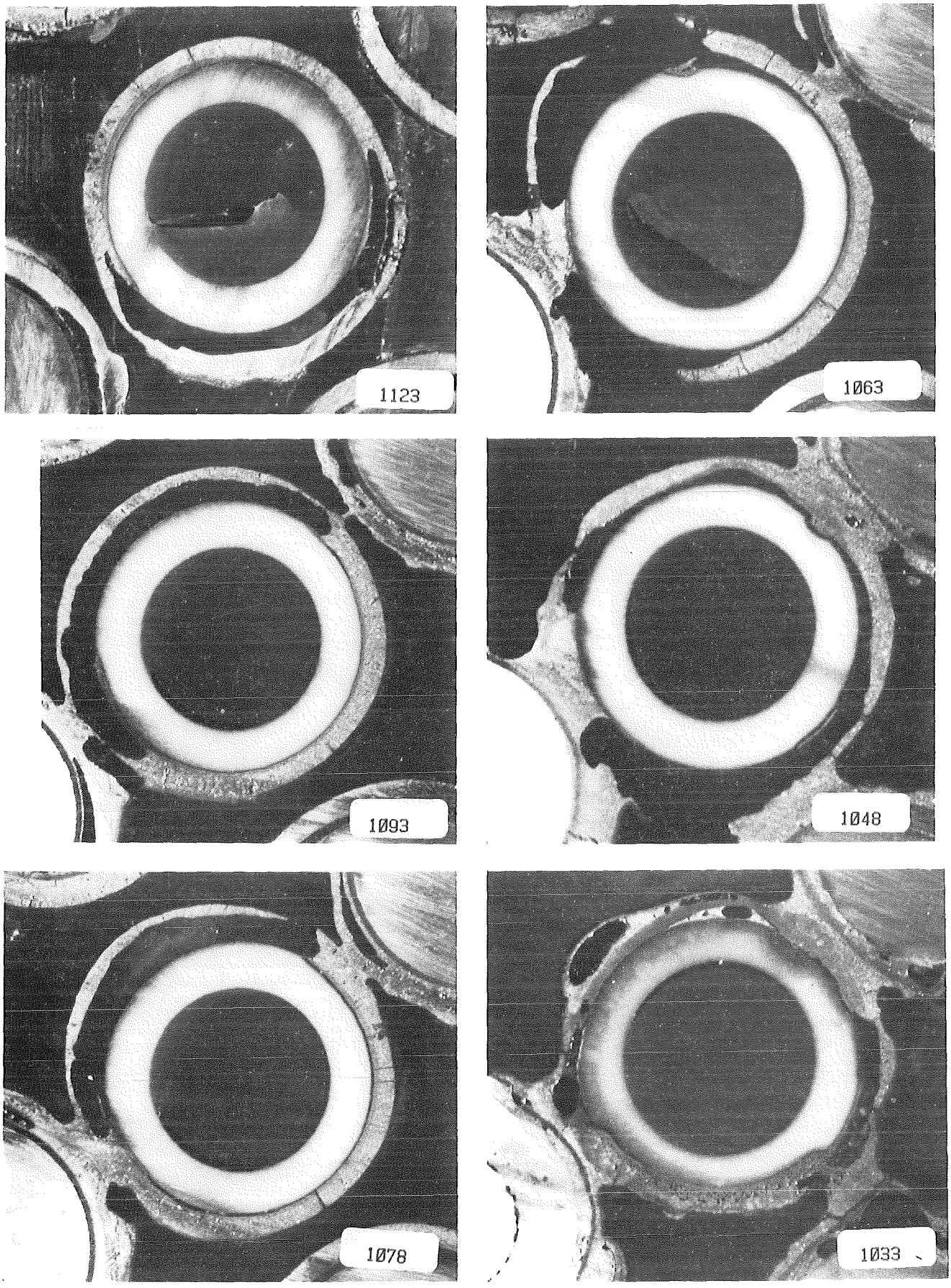

Fig. 123: Cross sections at upper end of unheated fuel rod simulator 25 (CORA-B)

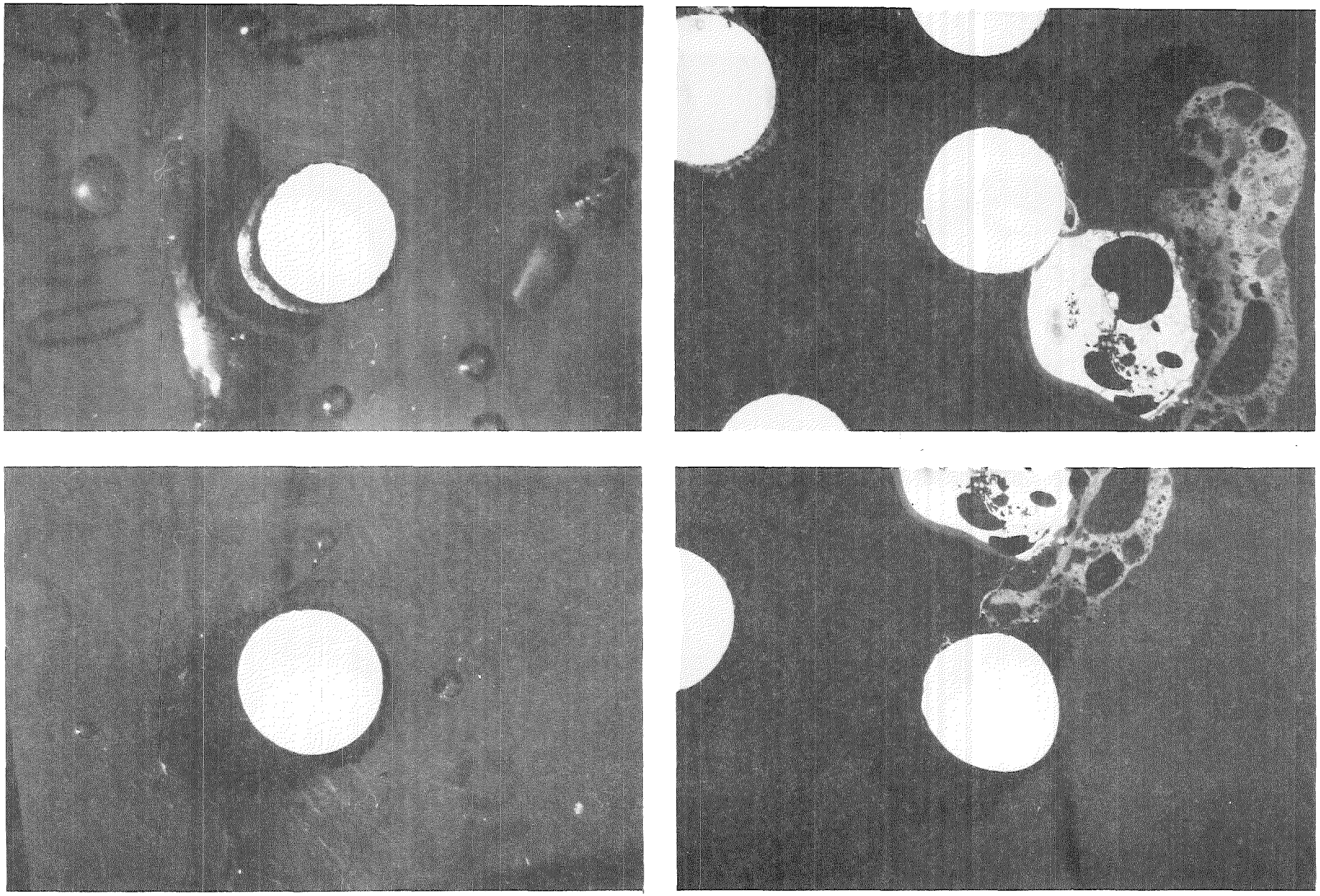

Fig. 124: Enlarged cross sections of heated rods at 507 mm elevation (CORA bundle B)

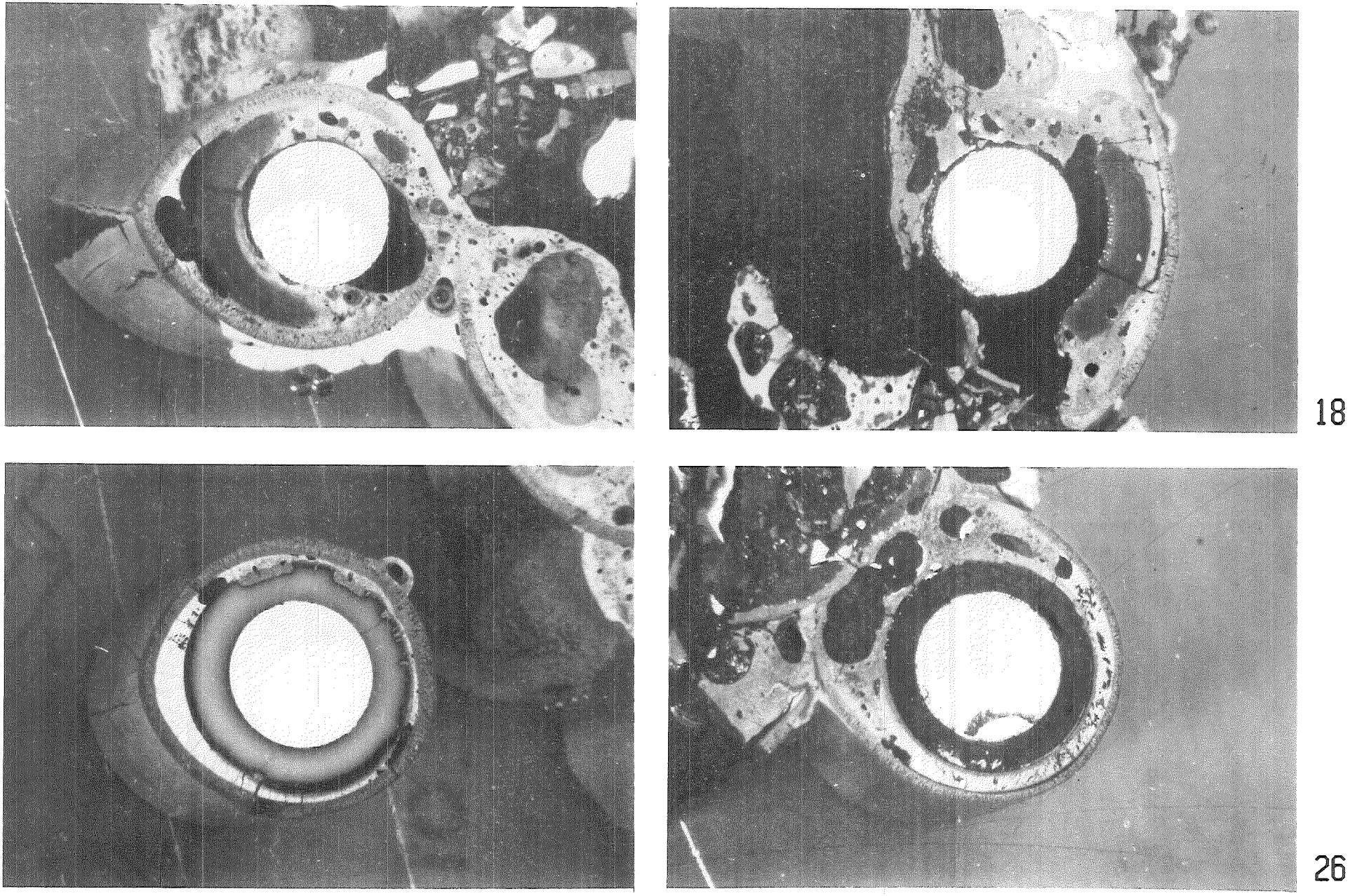

Fig. 125: Enlarged cross sections of heated rods at 269 mm elevation (CORA bundle B)

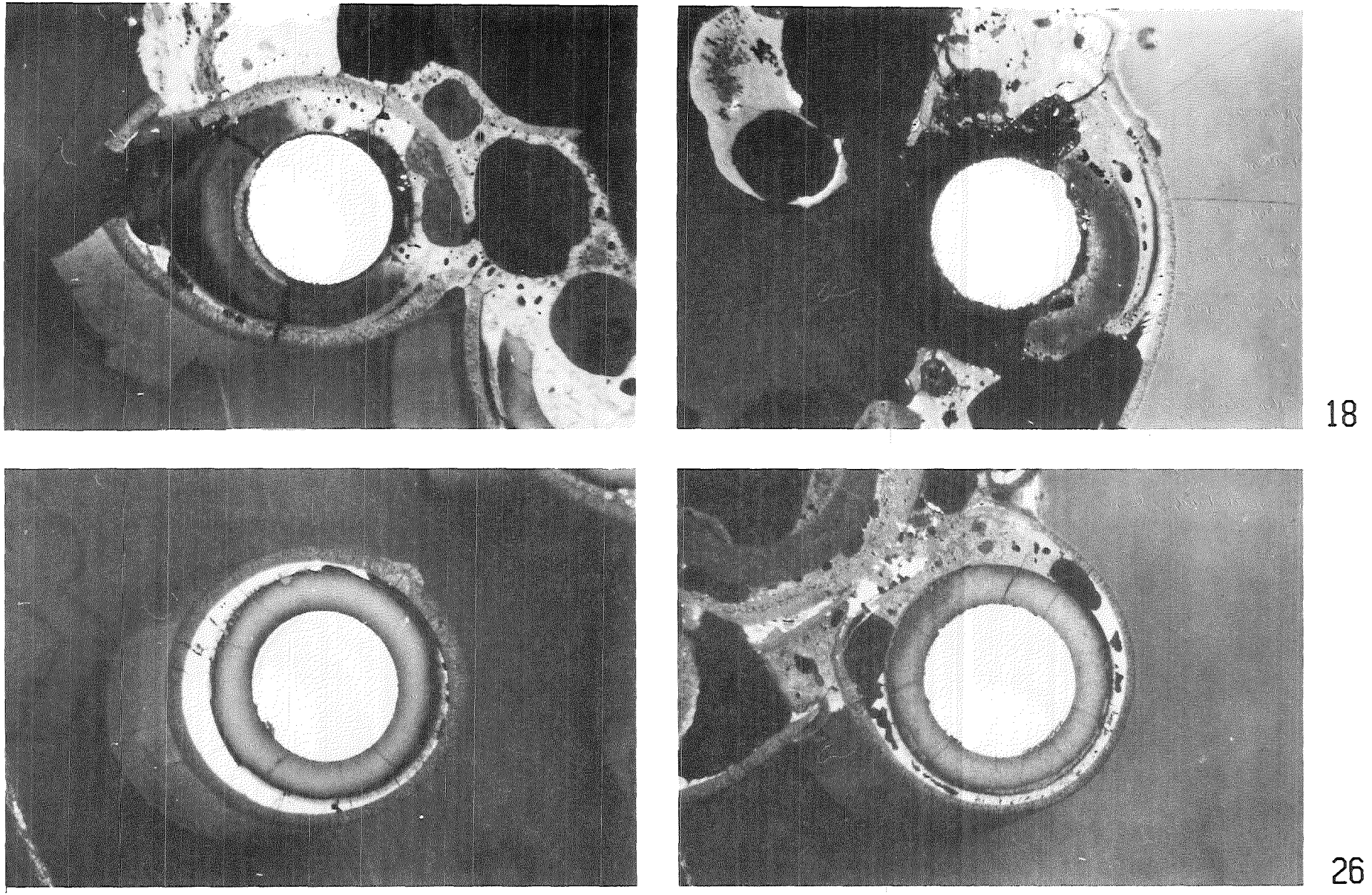

Fig. 126: Enlarged cross sections of heated rods at 251 mm elevation (CORA bundle B)

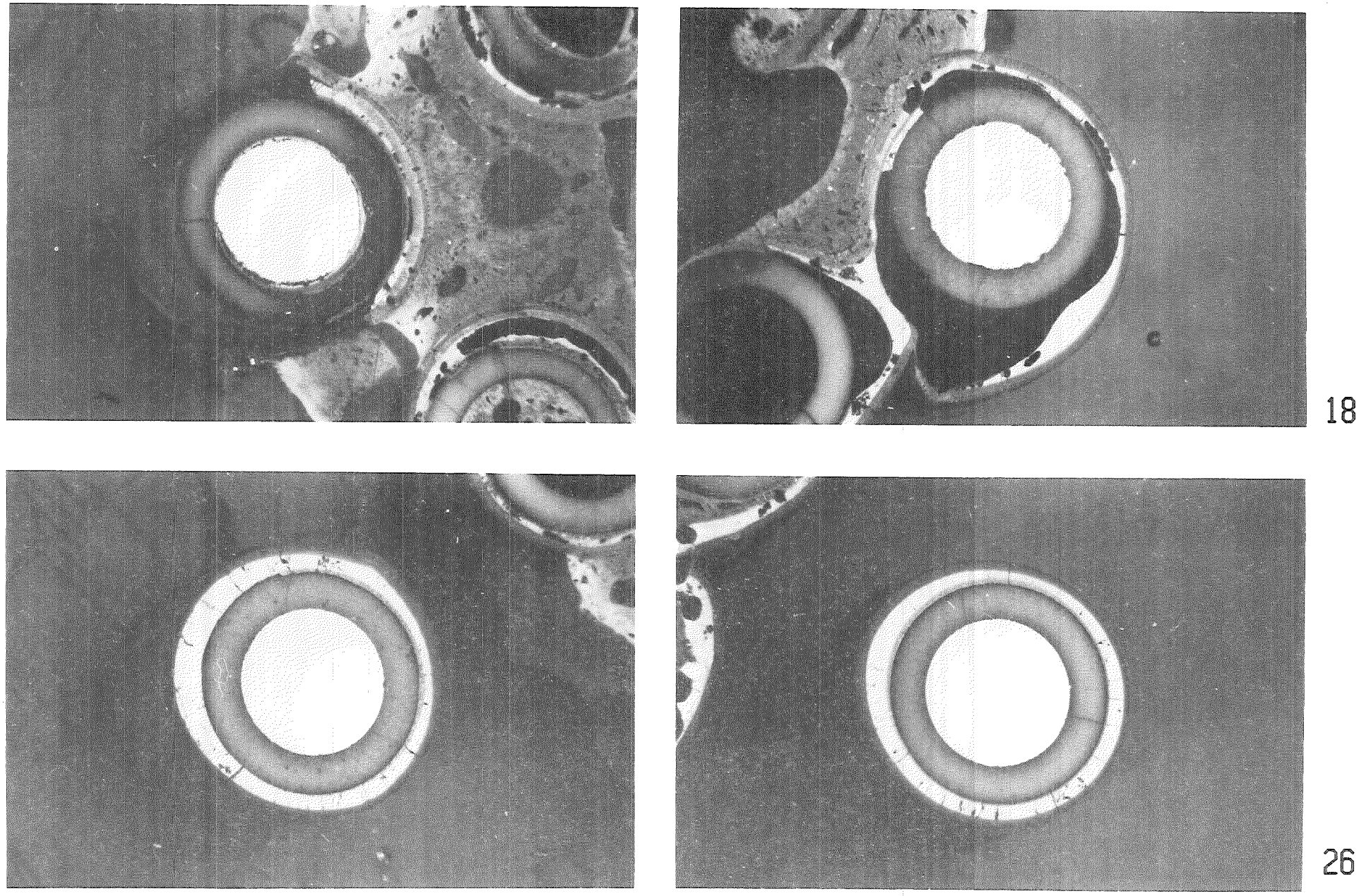

Fig. 127: Enlarged cross sections of heated rods at 109 mm elevation (CORA bundle B)

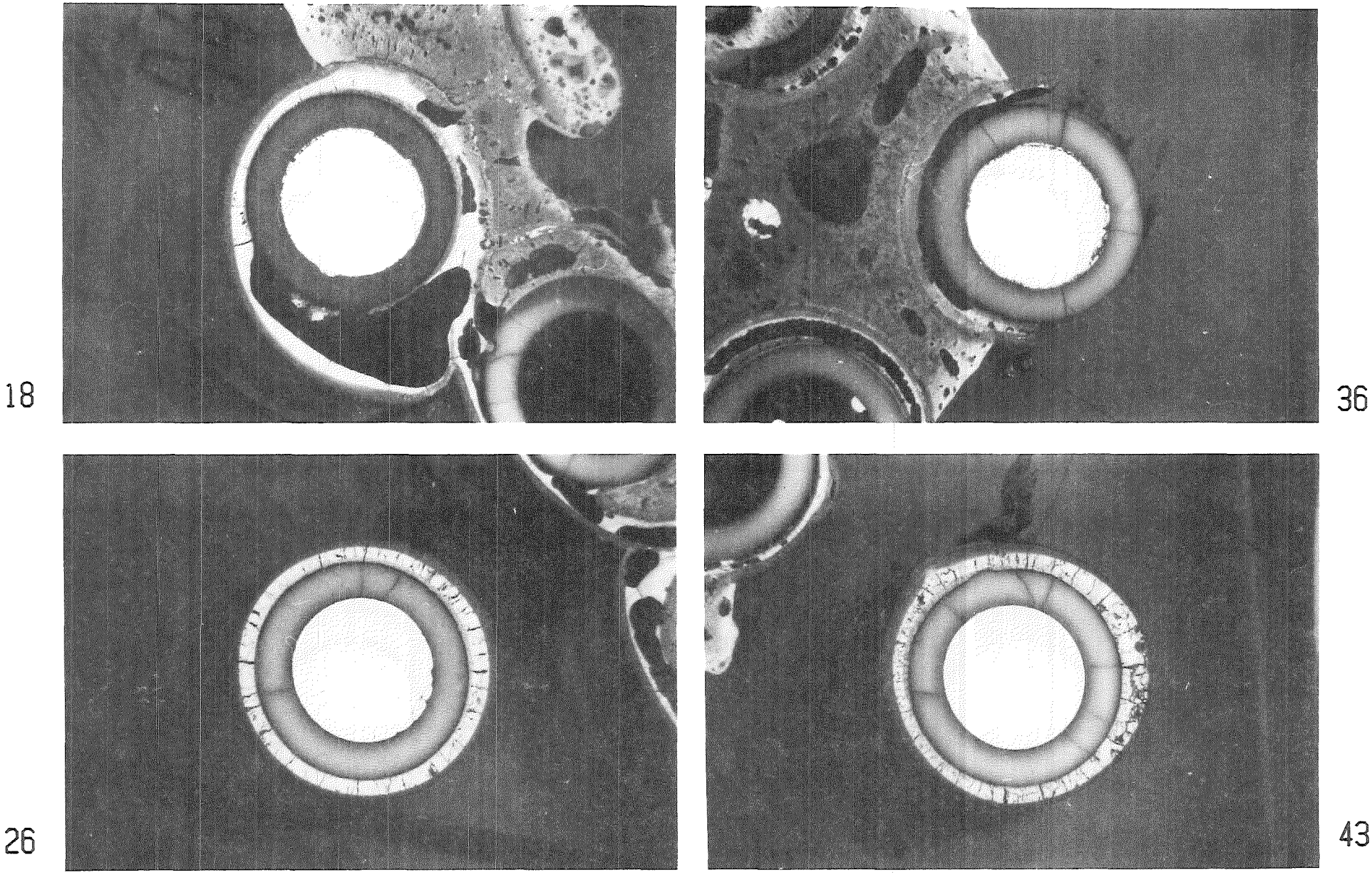

Fig. 128: Enlarged cross sections of heated rods at 93 mm elevation (CORA bundle B)

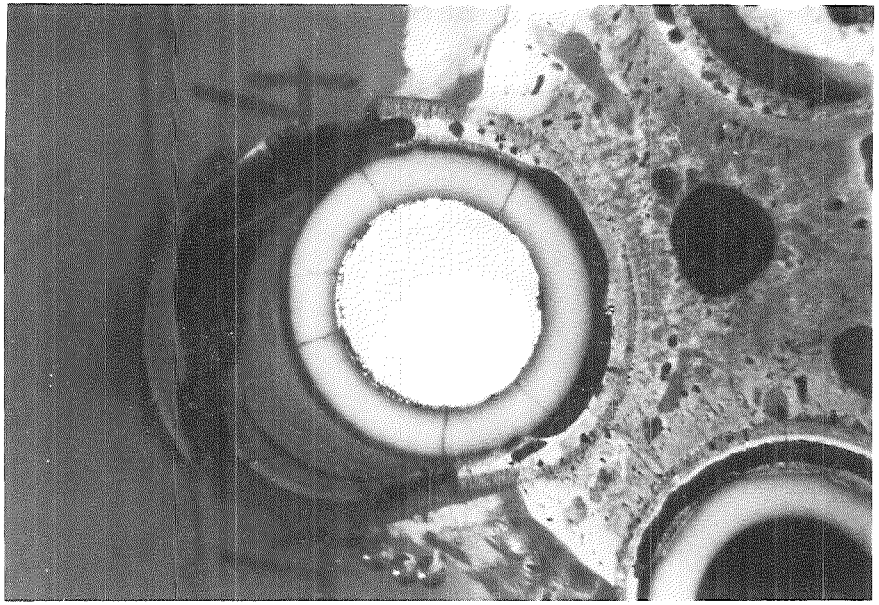

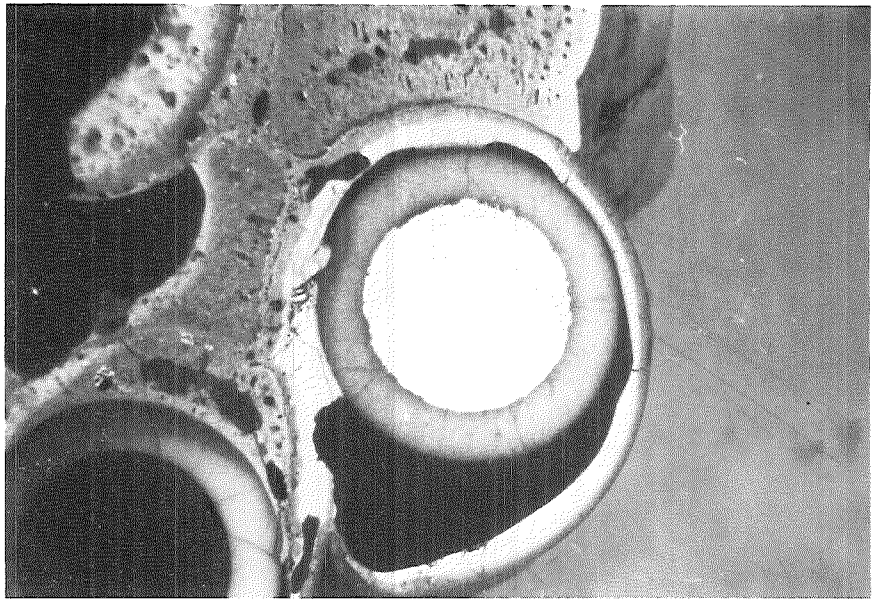

36

18

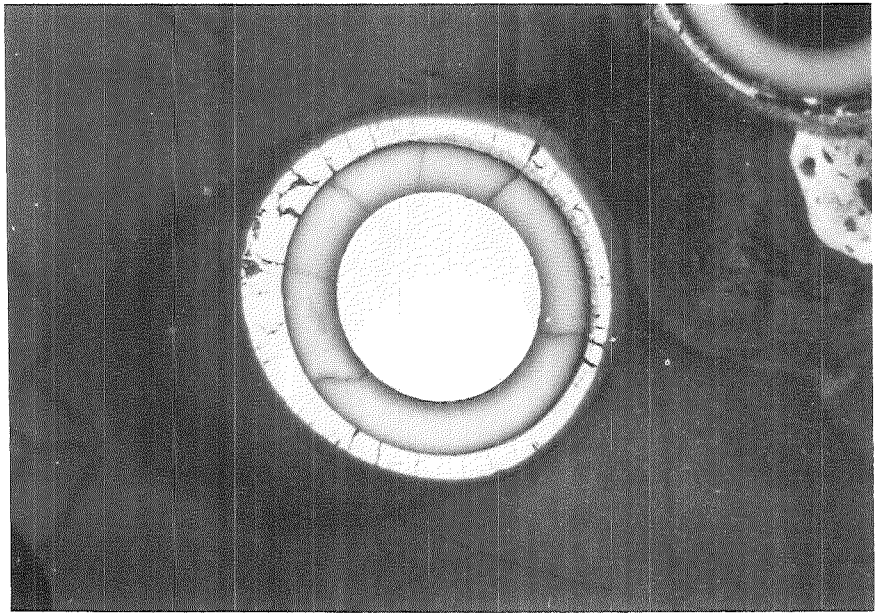

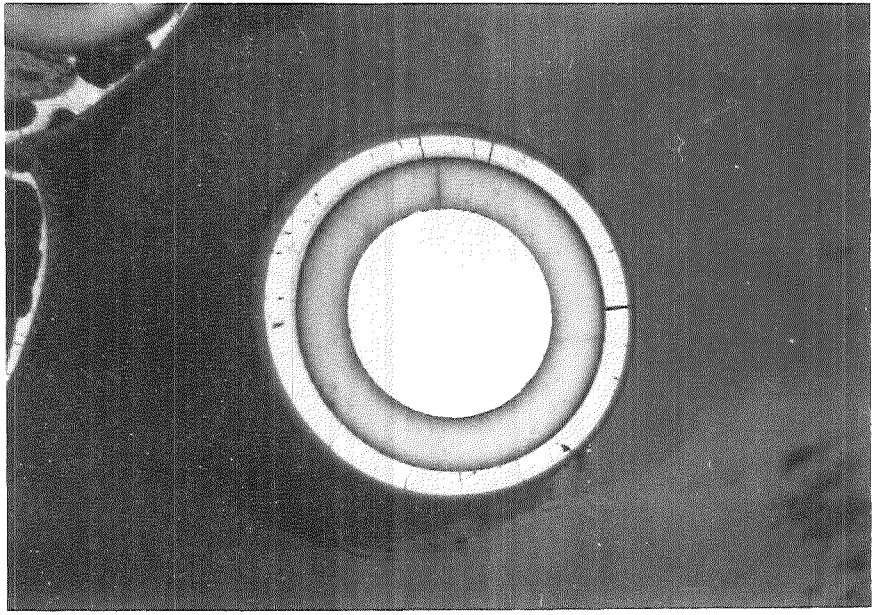

43

26

Fig. 129: Enlarged cross sections of heated rods at 91 mm elevation (CORA bundle B)

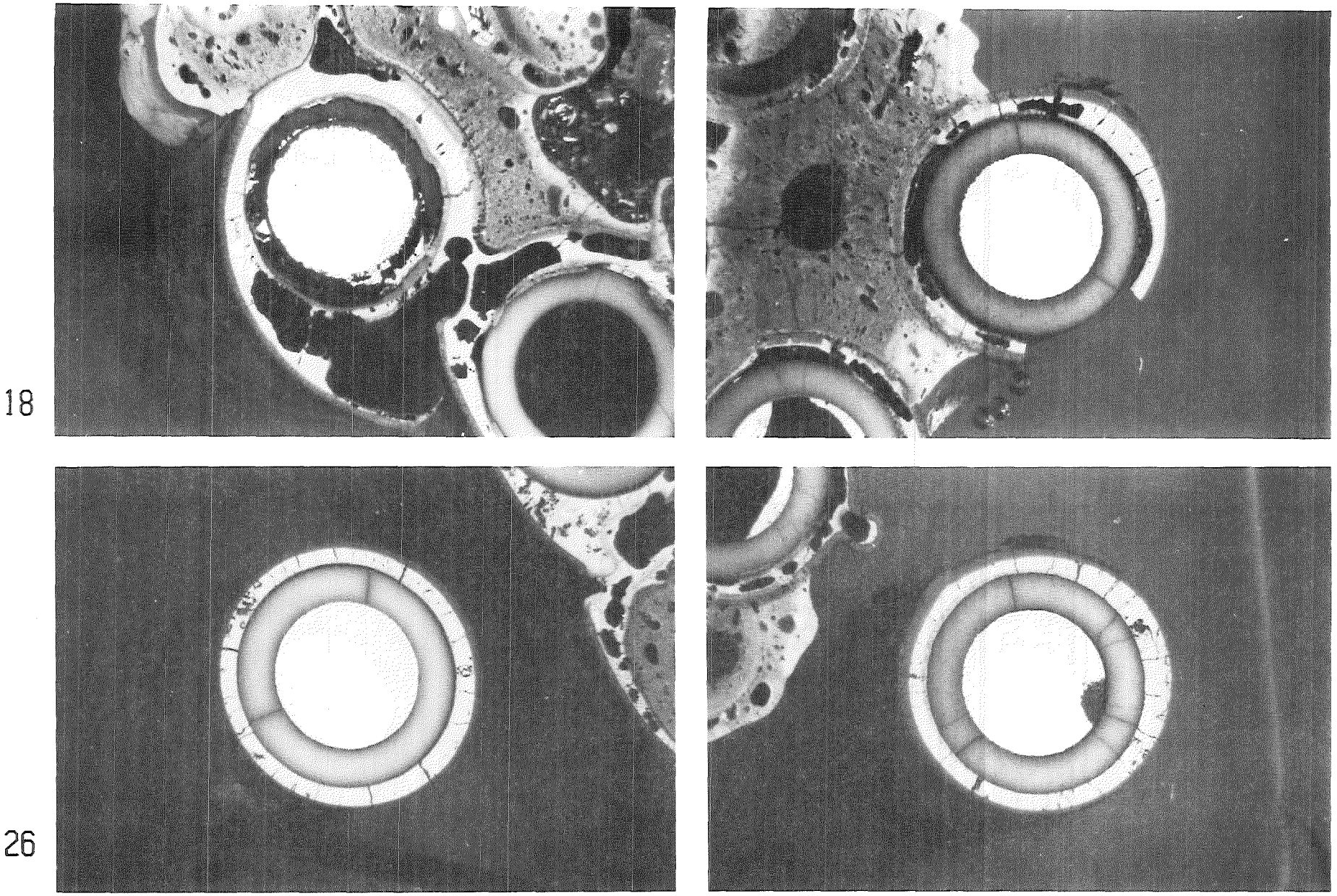

Fig. 130: Enlarged cross sections of heated rods at 75 mm elevation (CORA bundle B)

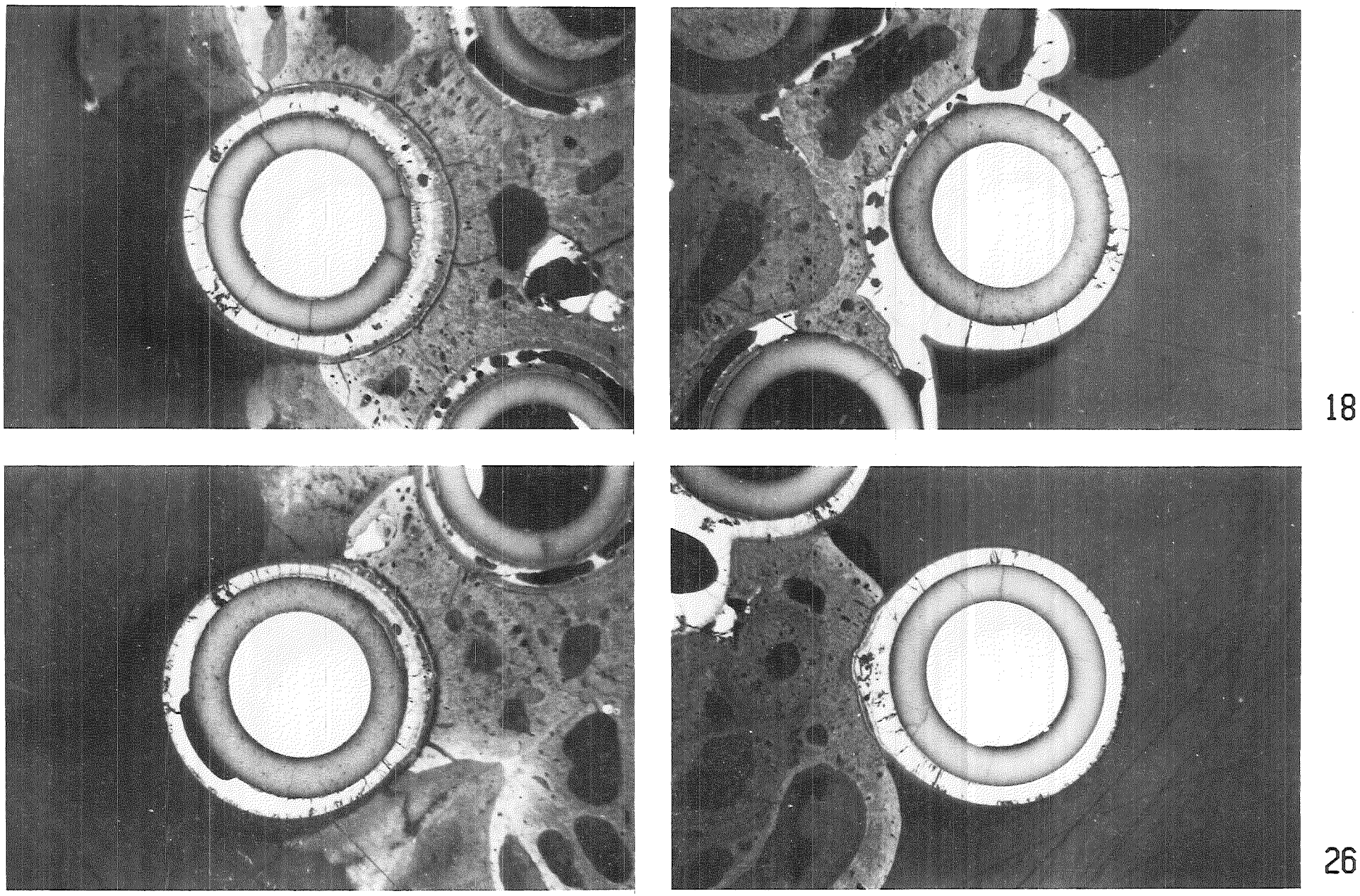

Fig. 131: Enlarged cross sections of heated rods at 0 mm elevation (CORA bundle B)

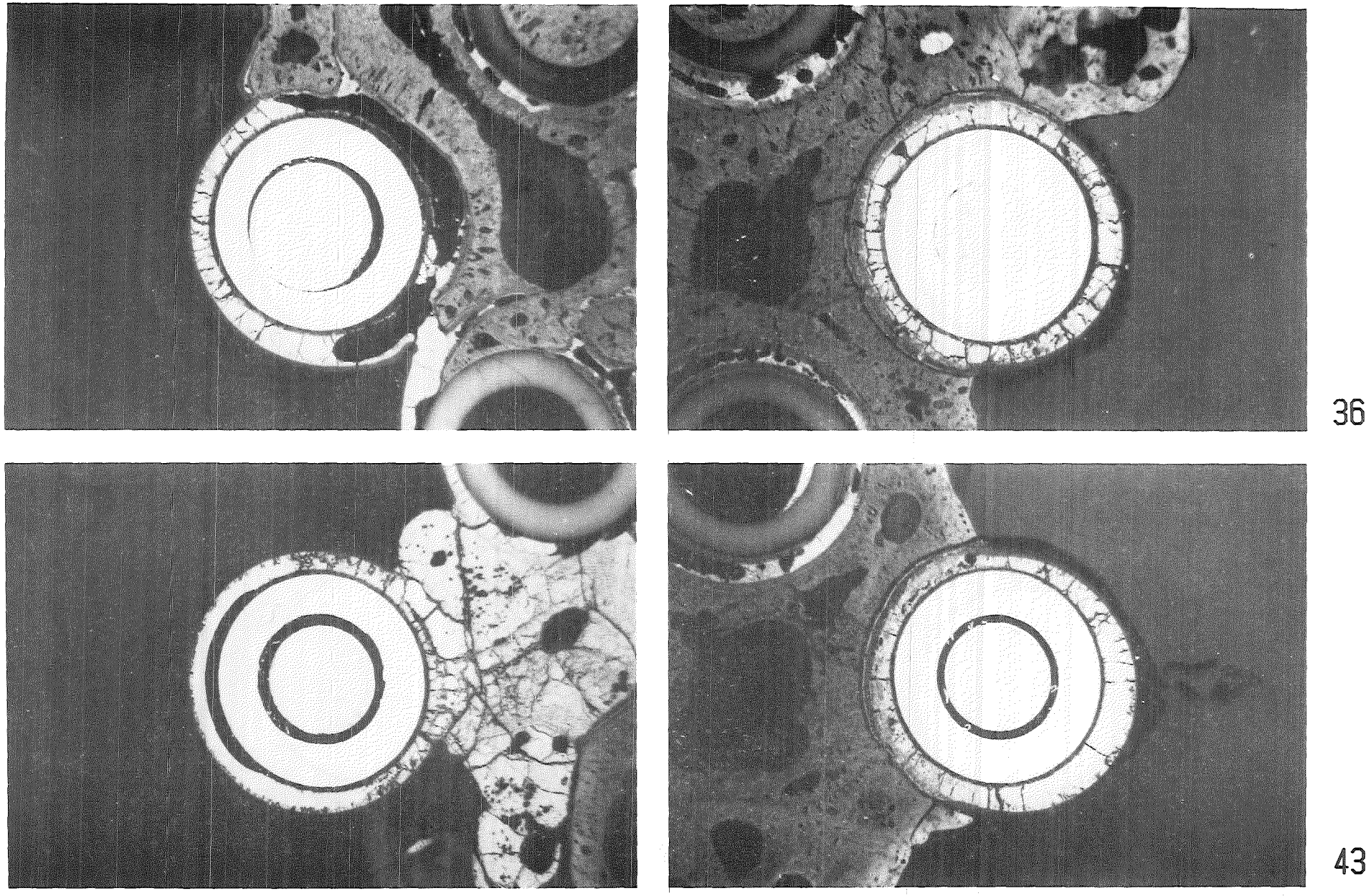

Fig. 132: Enlarged cross sections of heated rods at -16 mm elevation (CORA bundle B)

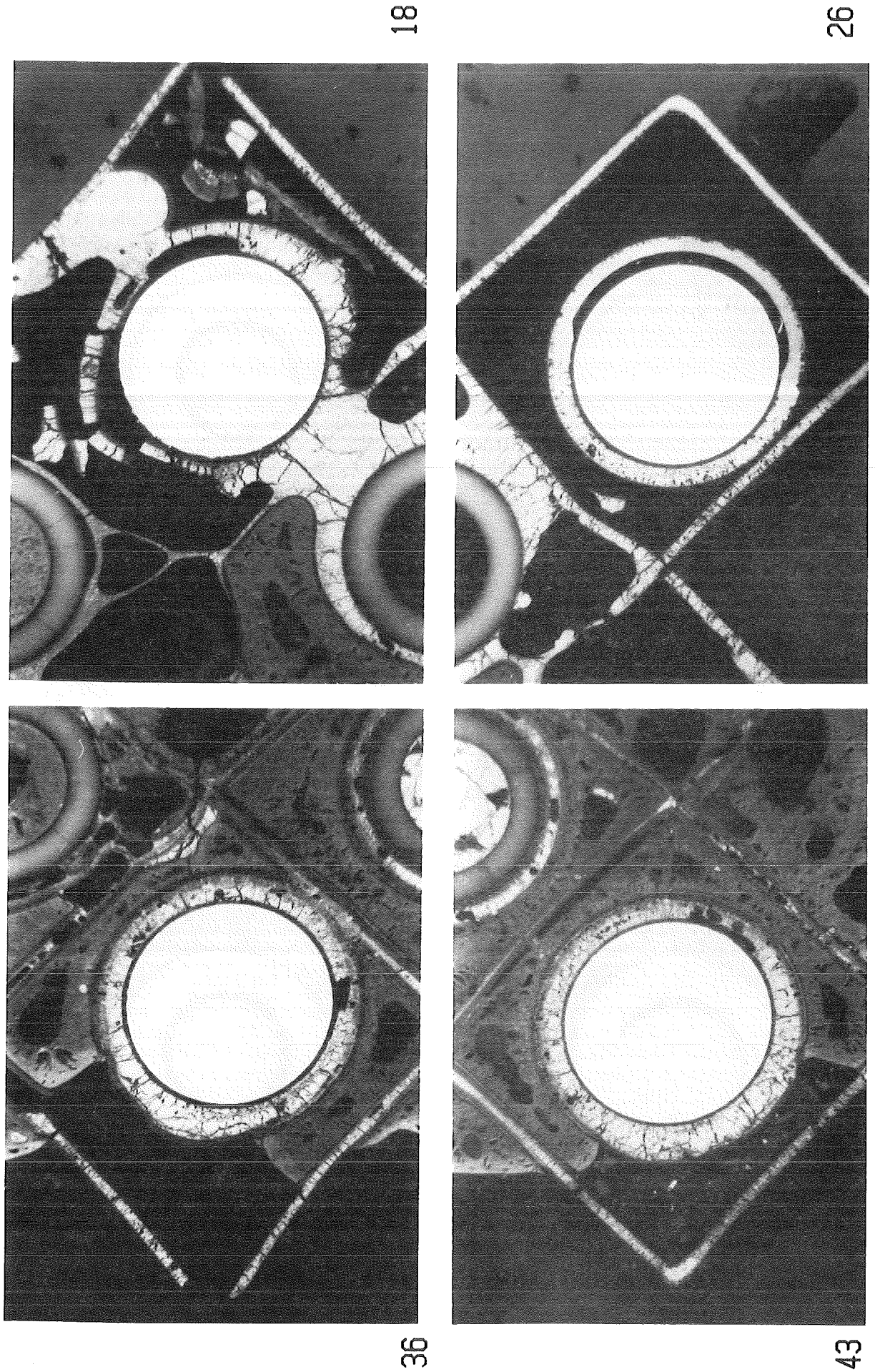

Fig. 133: Enlarged cross sections of heated rods at -55 mm elevation (CORA bundle B)

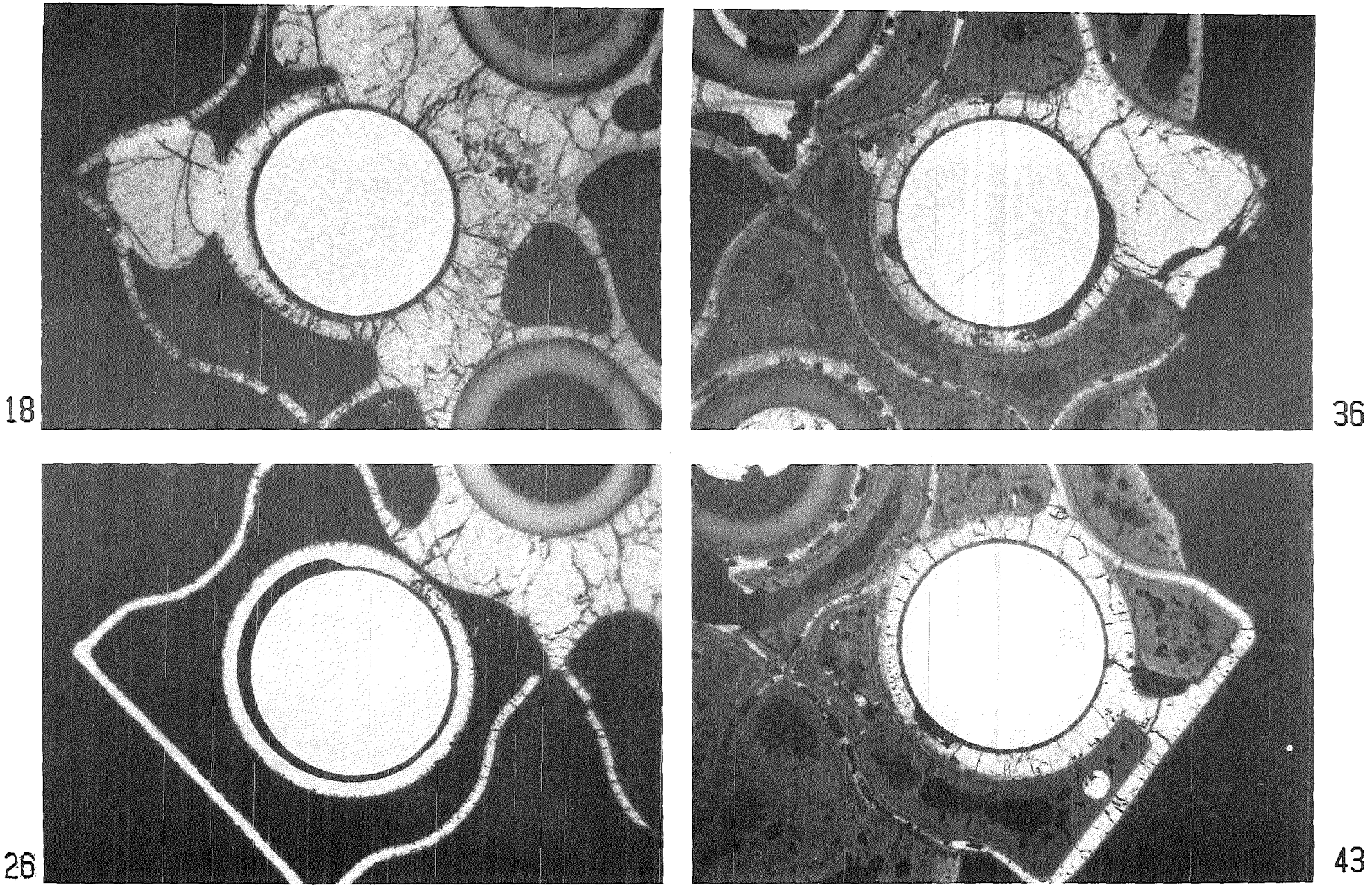

Fig. 134: Enlarged cross sections of heated rods at -71 mm elevation (CORA bundle B)

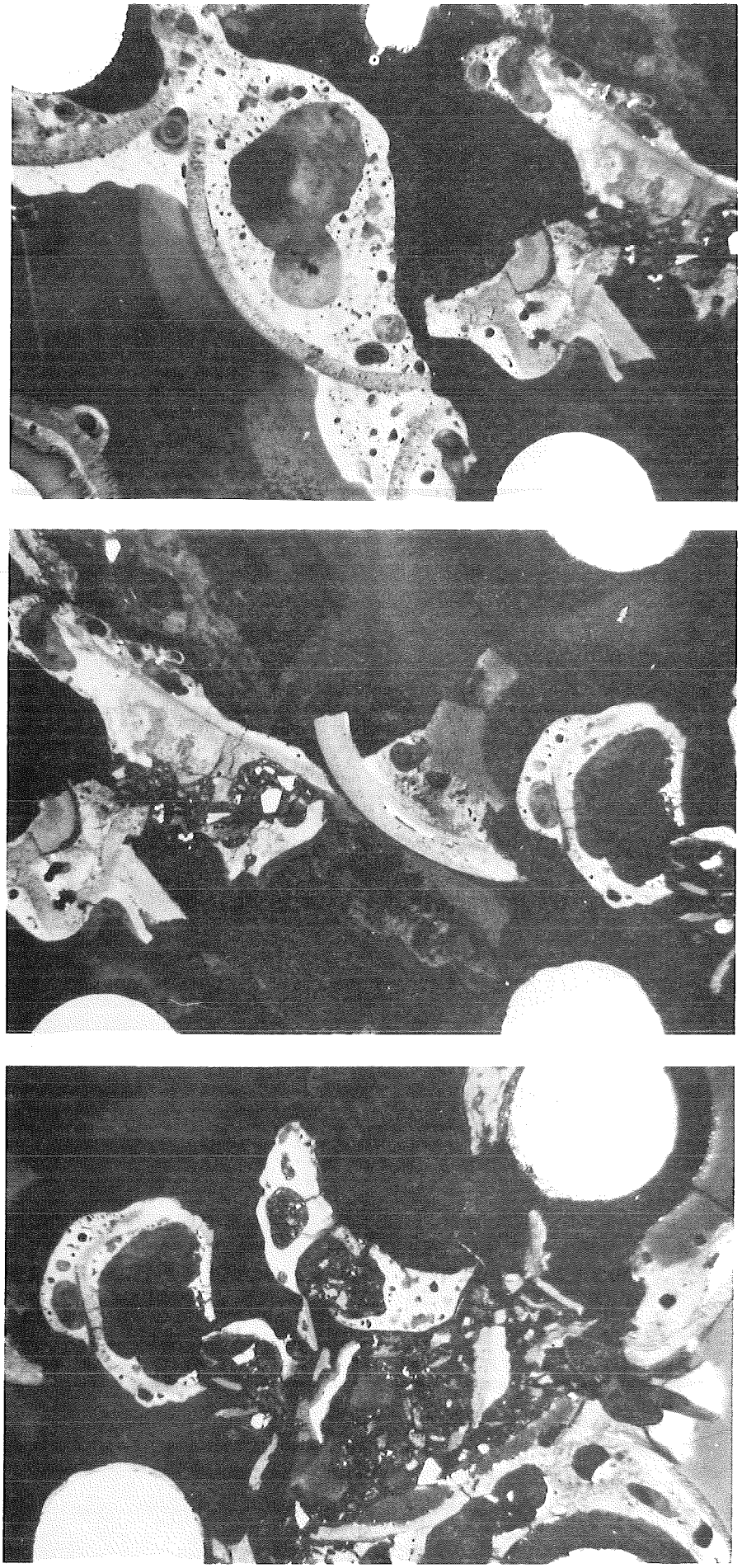

Fig. 135: Enlarged cross sections in region of unheated rods at 269 mm elevation (CORA bundle B)

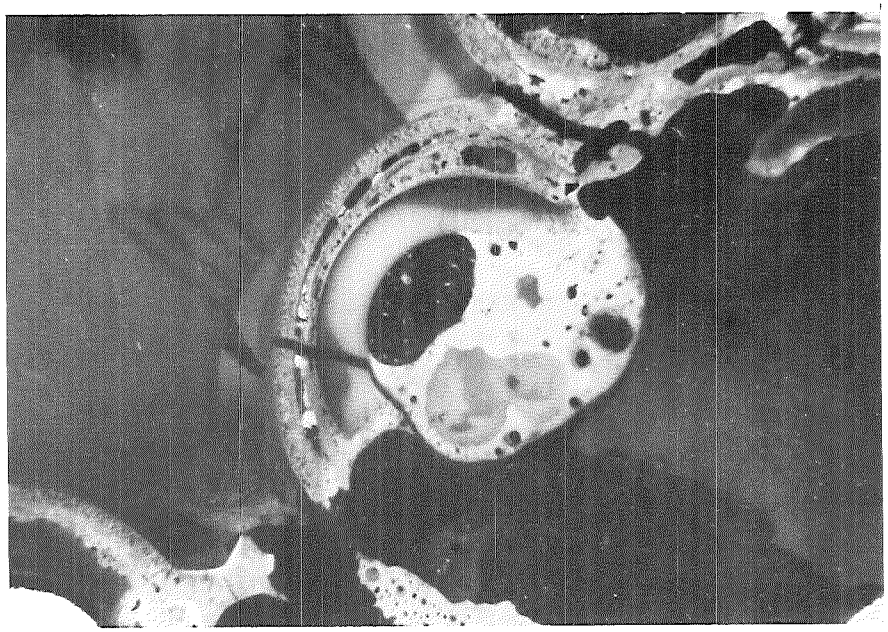

21

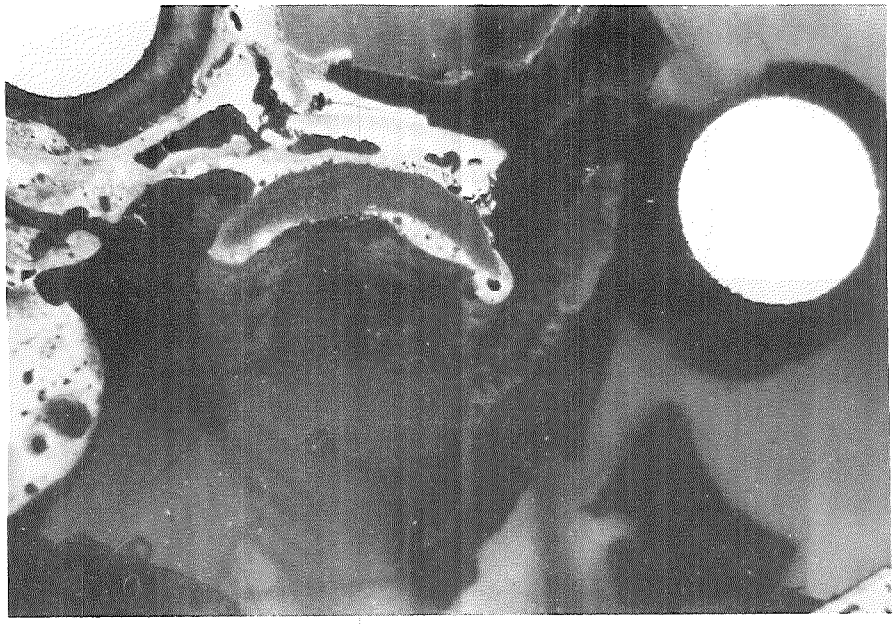

29

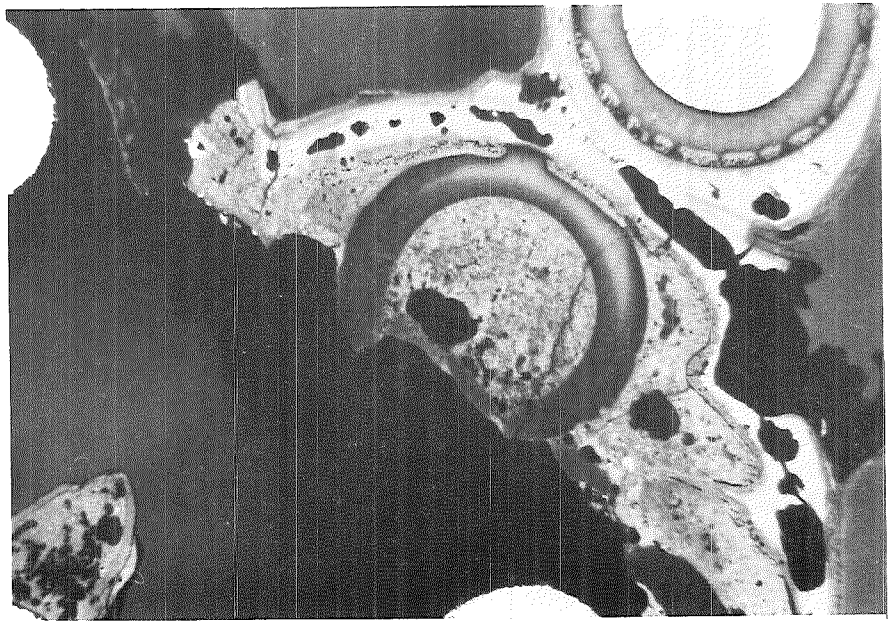

9

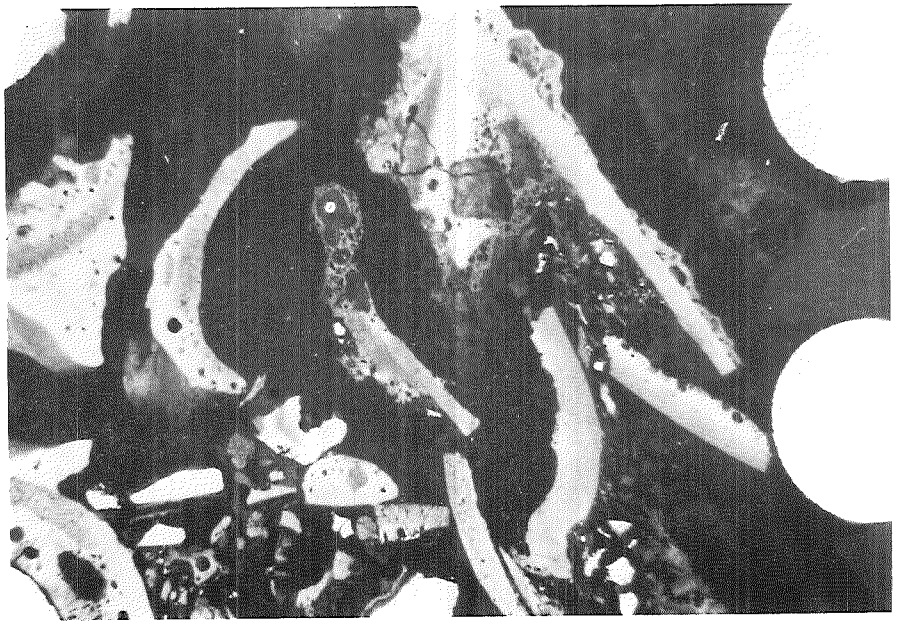

15

Fig. 136: Enlarged cross sections in region of unheated rods at 269 mm elevation (CORA bundle B)

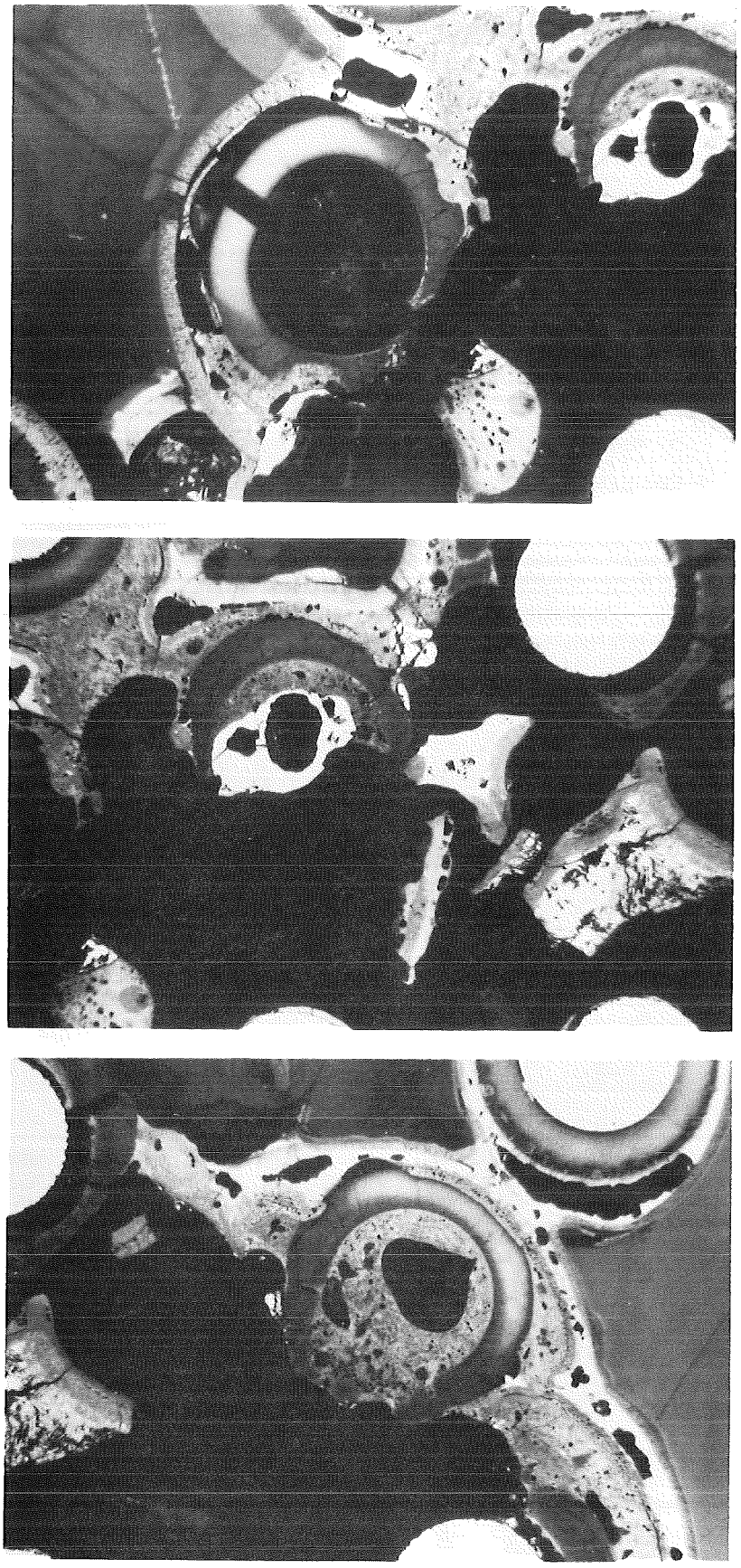

Fig. 137: Enlarged cross sections in region of unheated rods at 251 mm elevation (CORA bundle B)

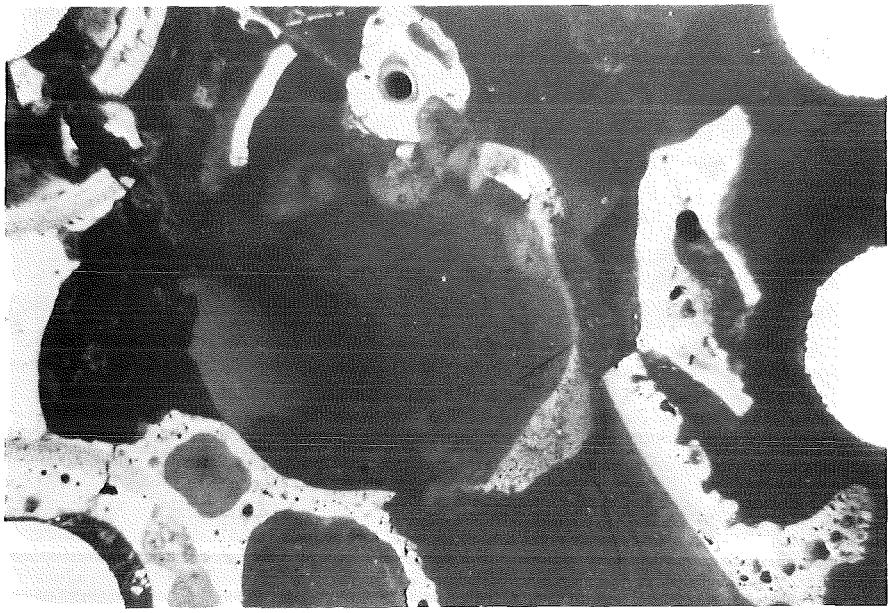

29

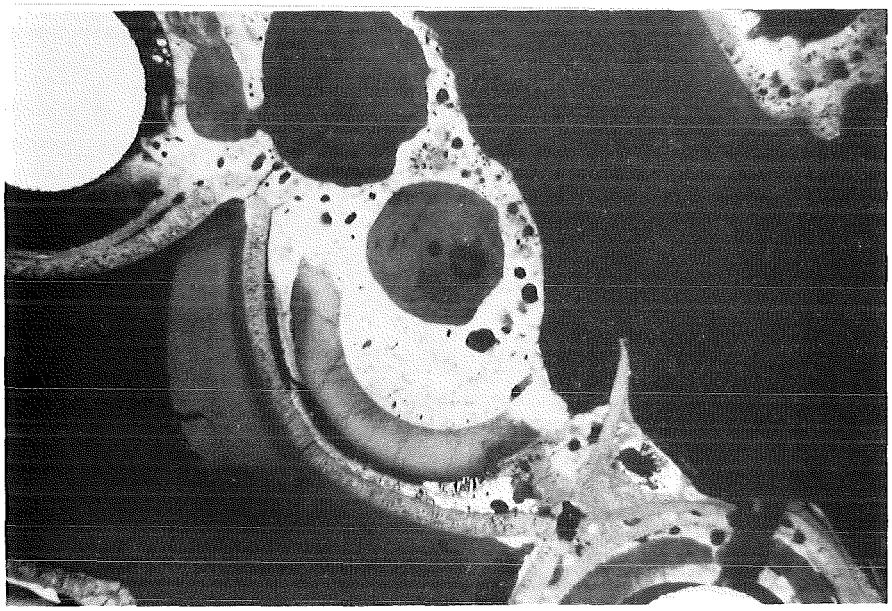

37

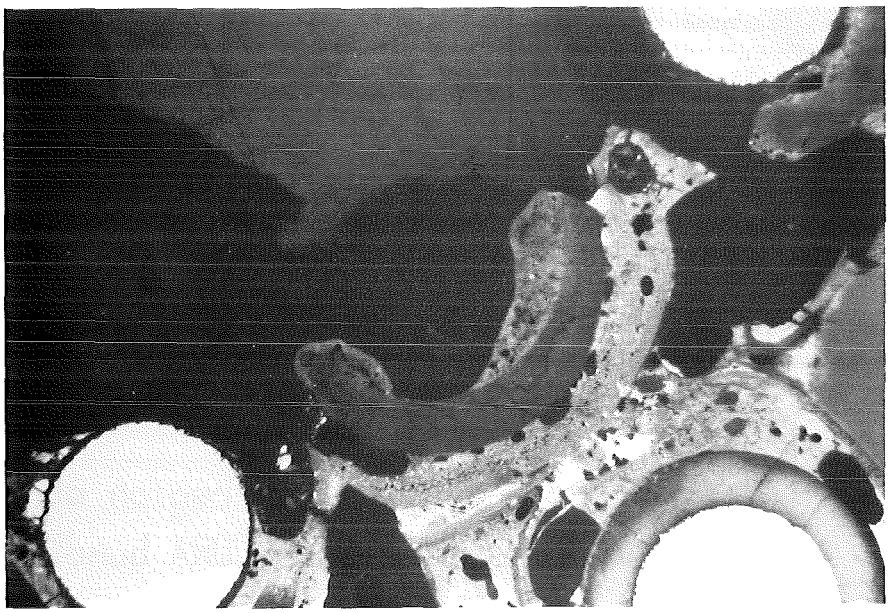

25

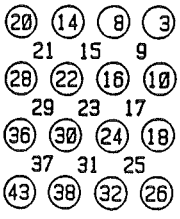

Fig. 138: Enlarged cross sections in region of unheated rods at 251 mm elevation (CORA bundle B)

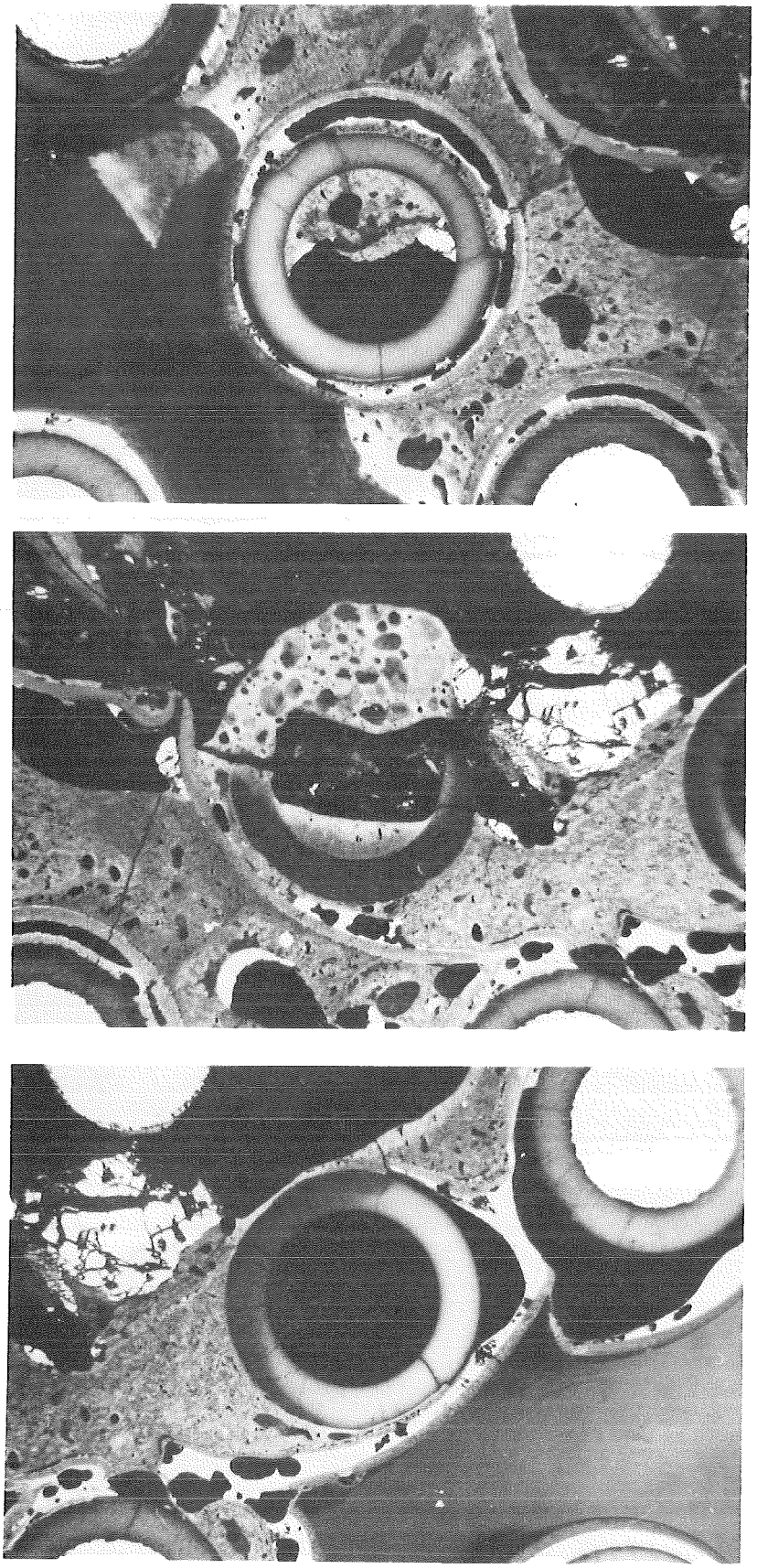

Fig. 139: Enlarged cross sections in region of unheated rods at 109 mm elevation (CORA bundle B)

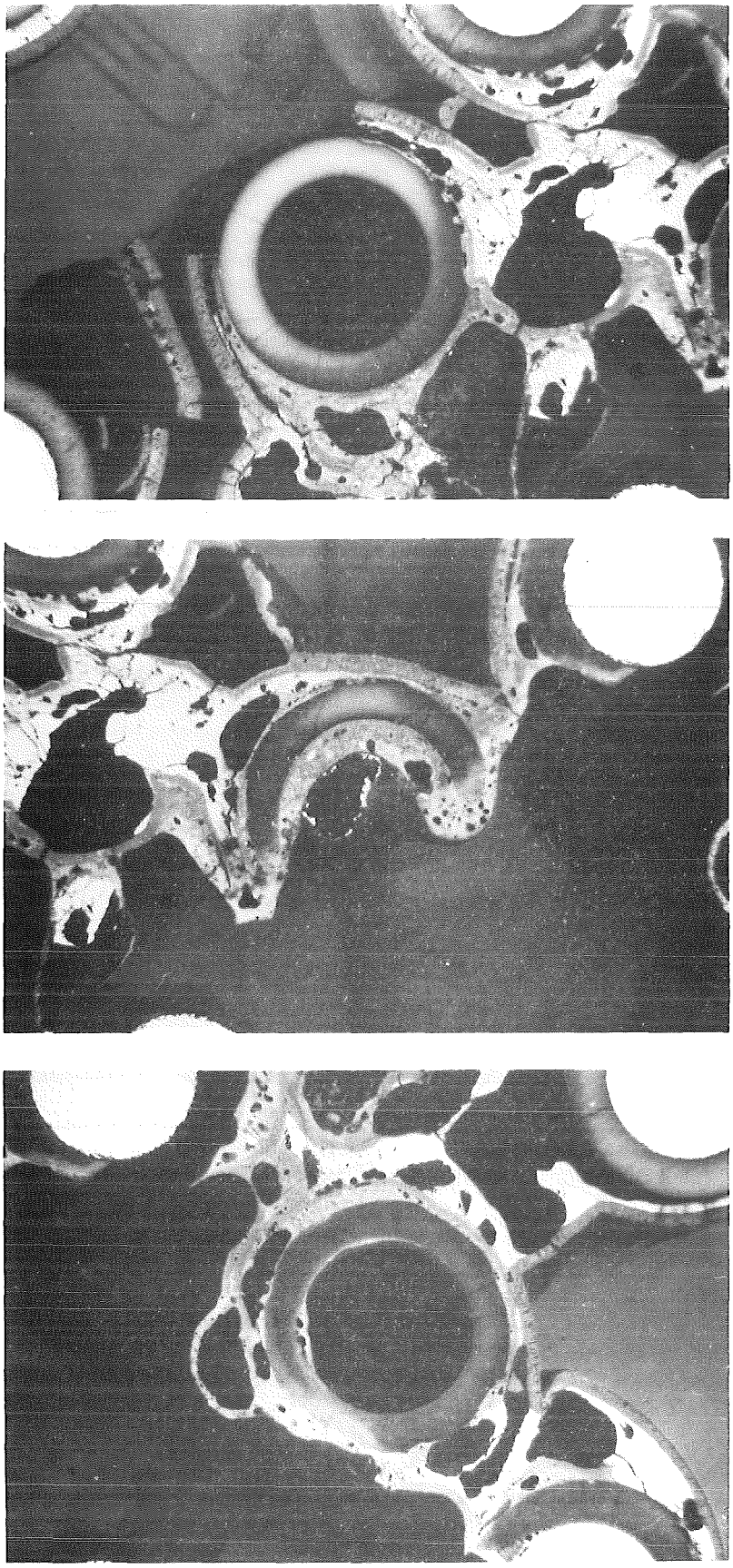

Fig. 140: Enlarged cross sections in region of unheated rods at 109 mm elevation (CORA bundle B)

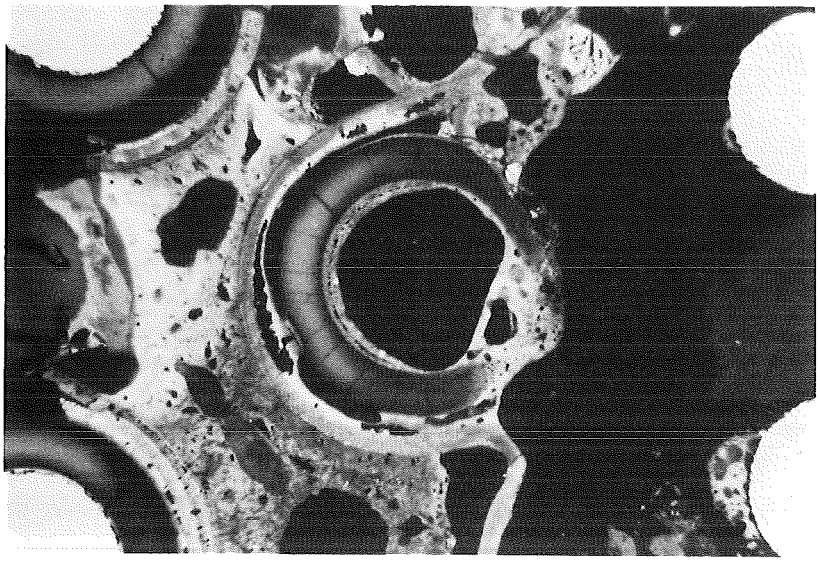

29

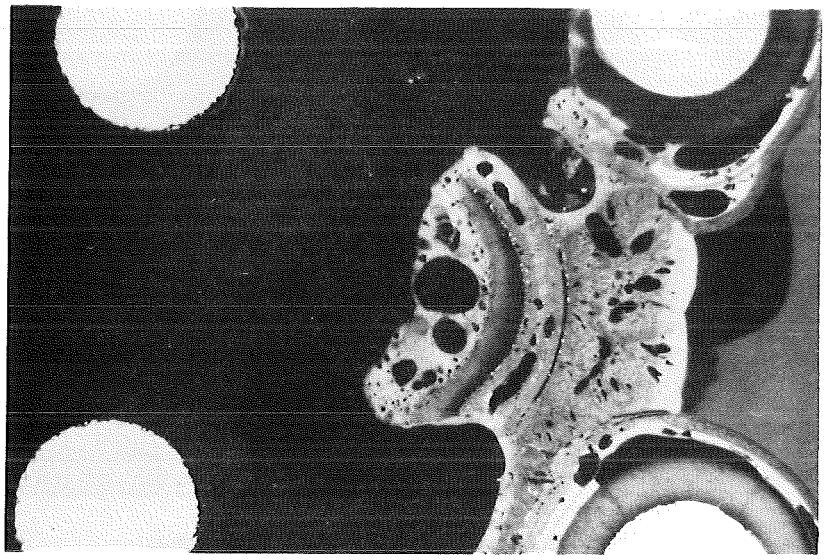

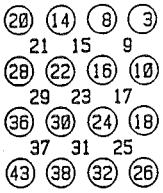

17

Fig. 141: Enlarged cross sections in region of unheated rods at 109 mm elevation (CORA bundle B)

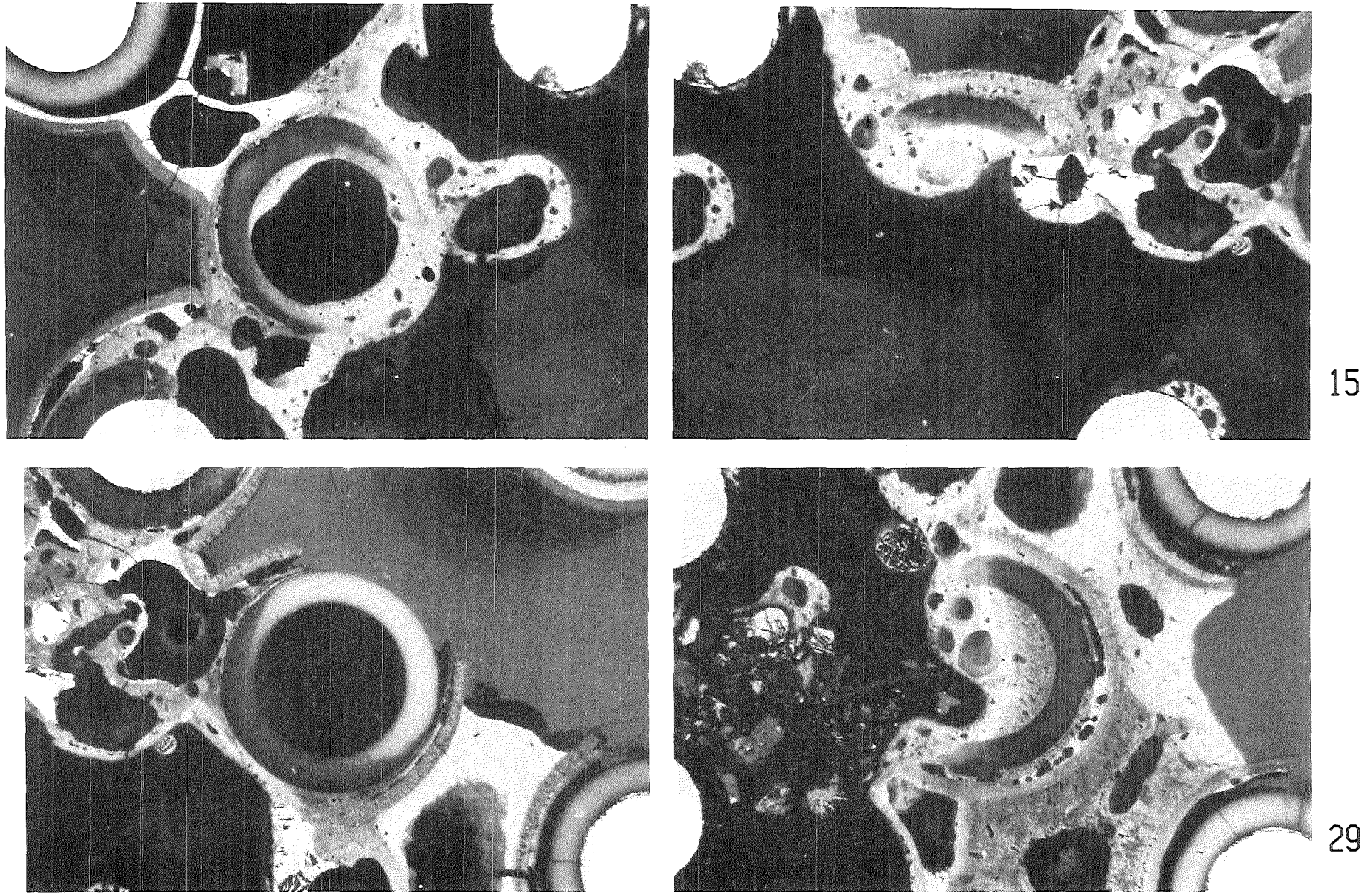

Fig. 142: Enlarged cross sections in region of unheated rods at 93 mm elevation (CORA bundle B)

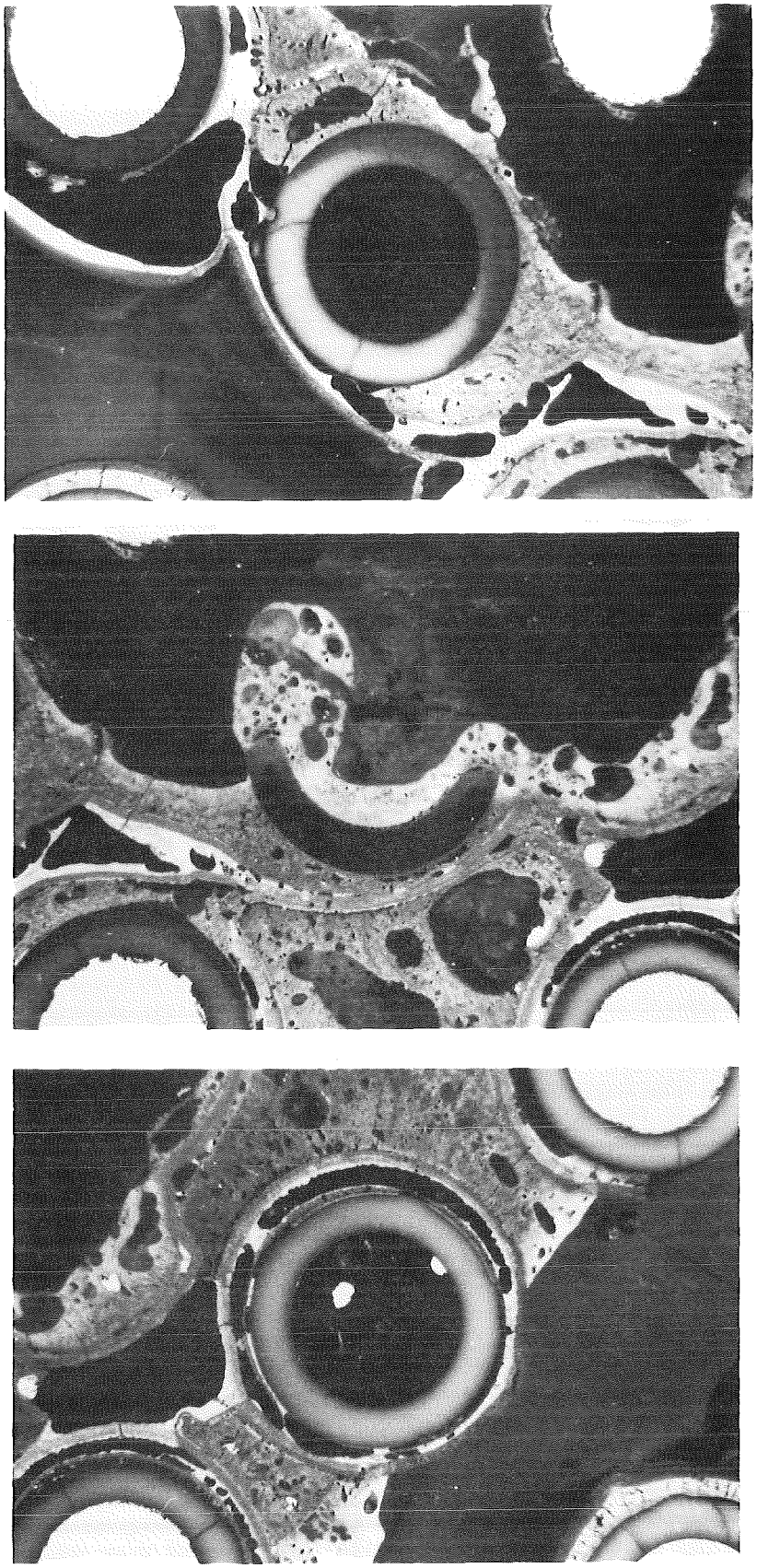

Fig. 143: Enlarged cross sections in region of unheated rods at 93 mm elevation (CORA bundle B)

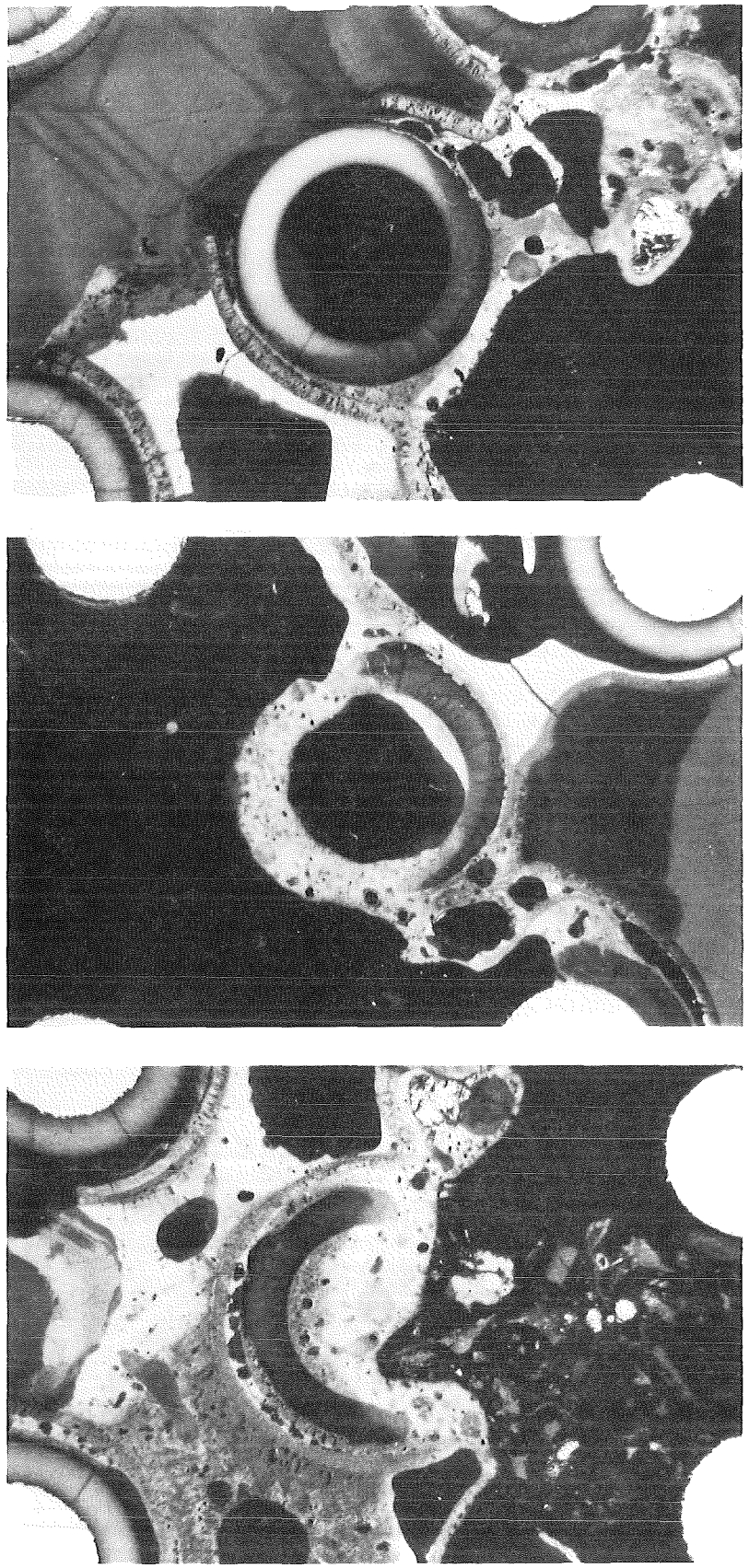

Fig. 144: Enlarged cross sections in region of unheated rods at 91 mm elevation (CORA bundle B)

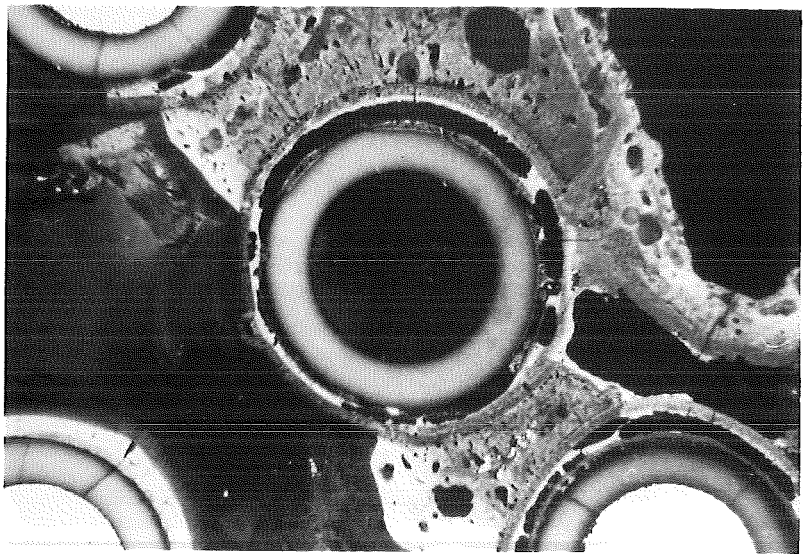

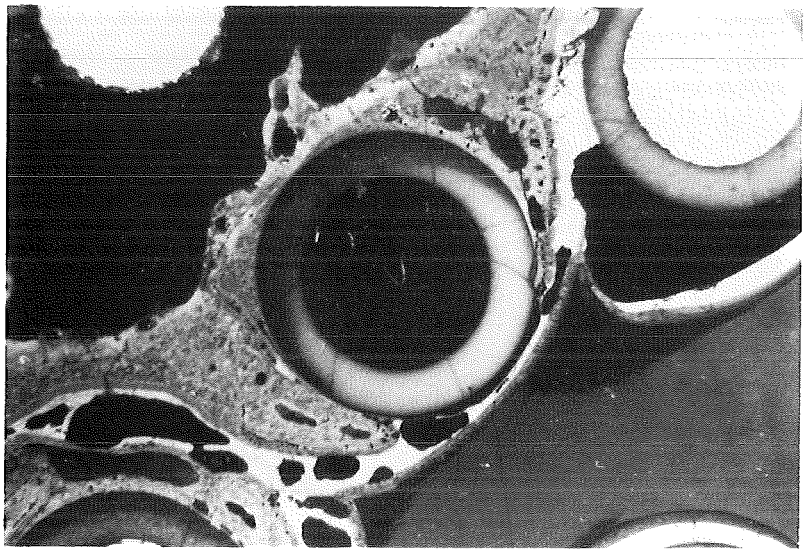

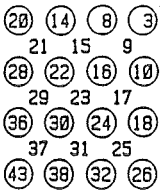

Fig. 145: Enlarged cross sections in region of unheated rods at 91 mm elevation (CORA bundle B)

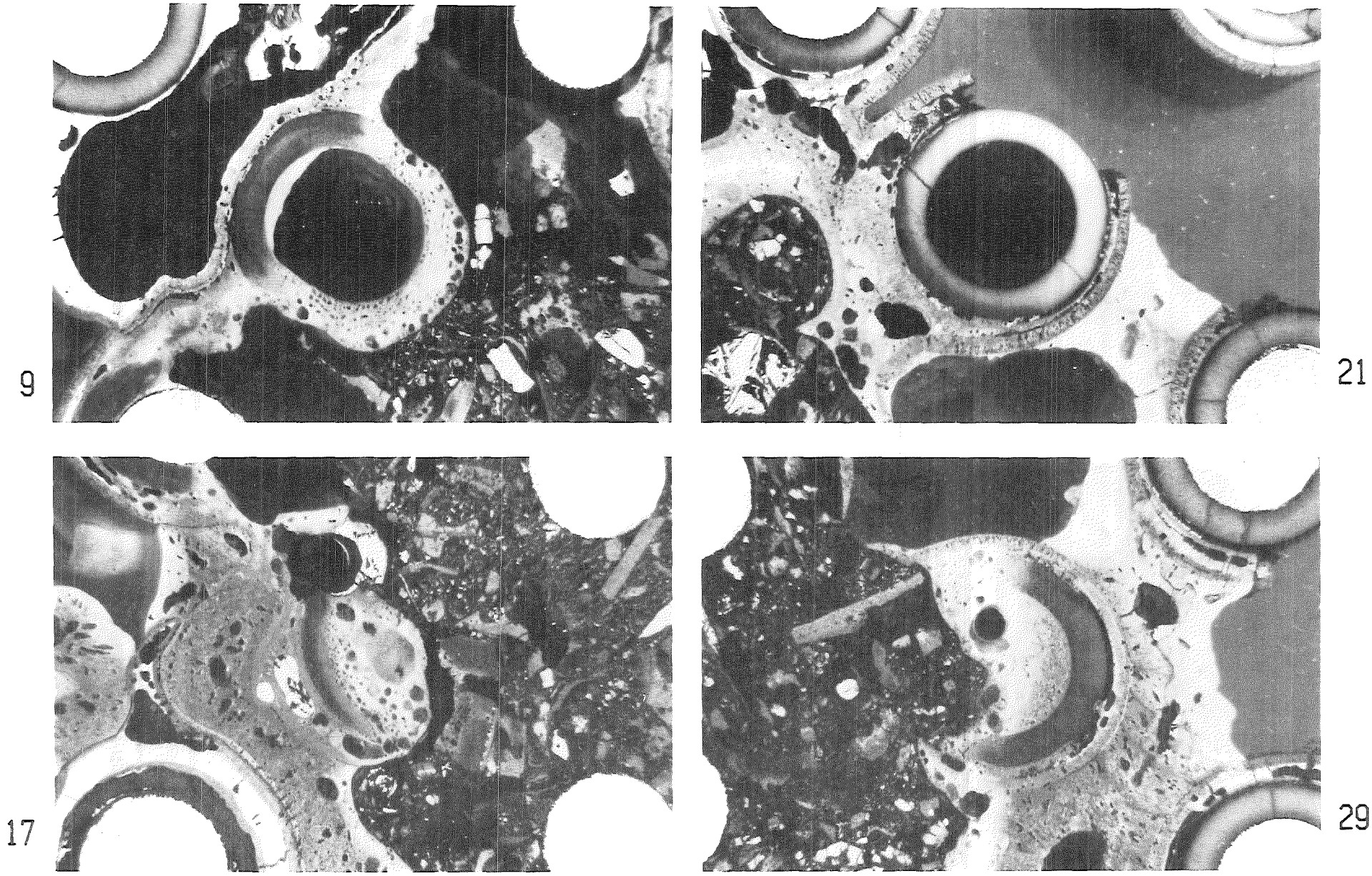

Fig. 146: Enlarged cross sections in region of unheated rods at 75 mm elevation (CORA bundle B)

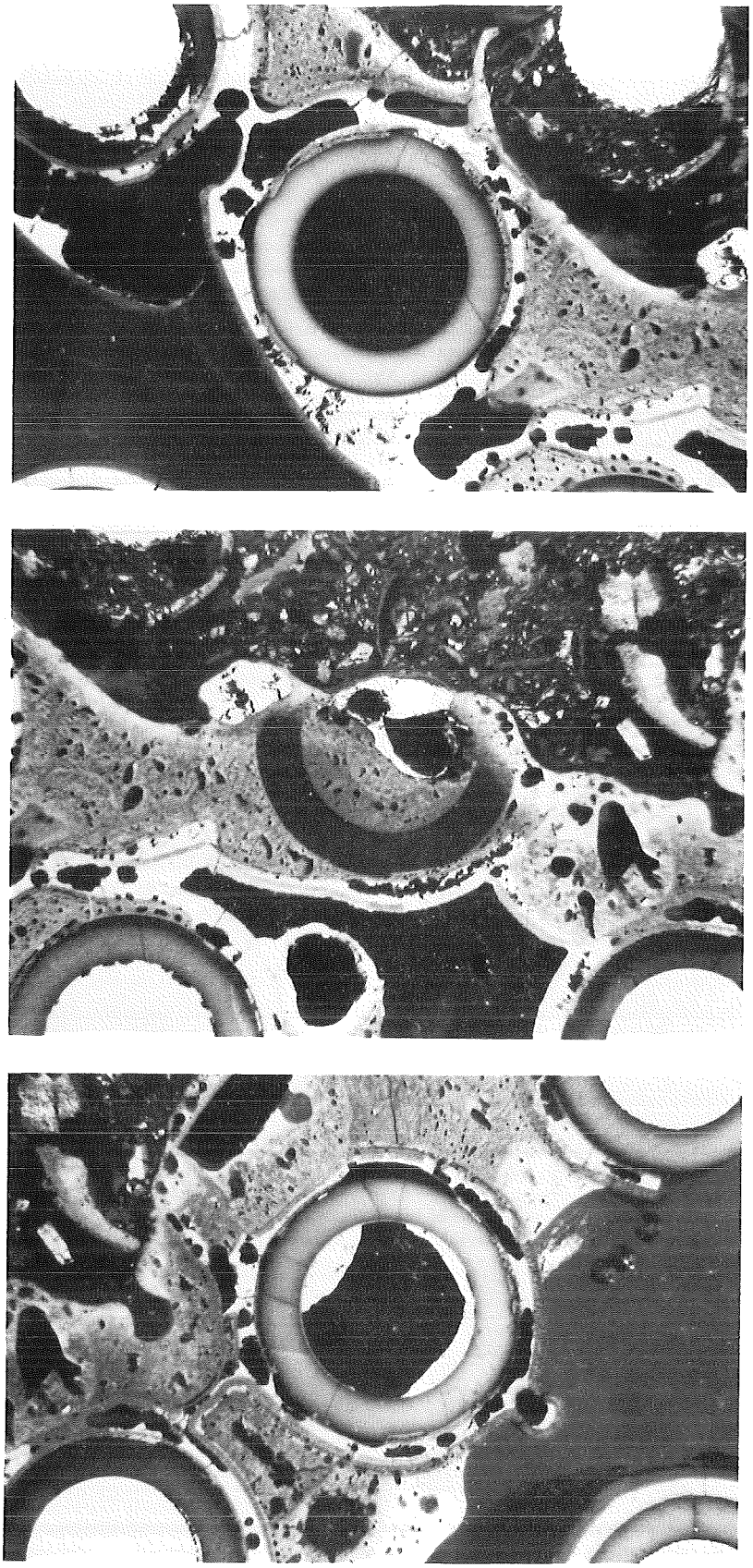

Fig. 147: Enlarged cross sections in region of unheated rods at 75 mm elevation (CORA bundle B)

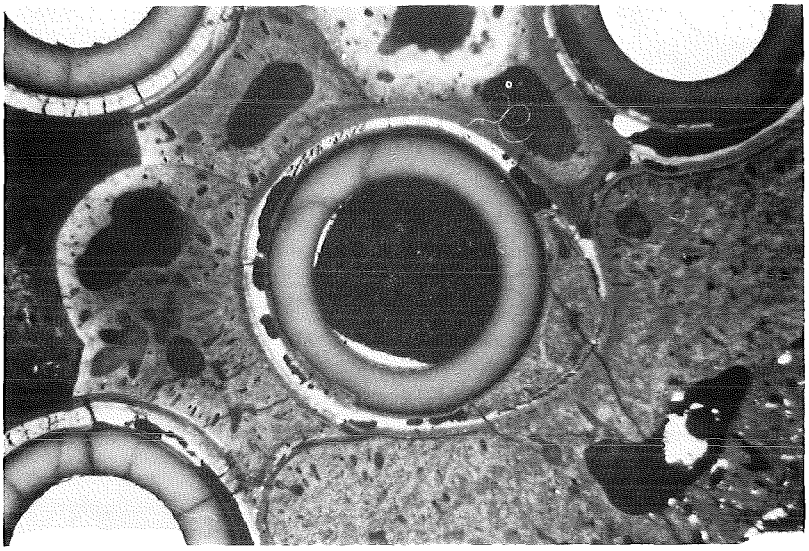

21

15

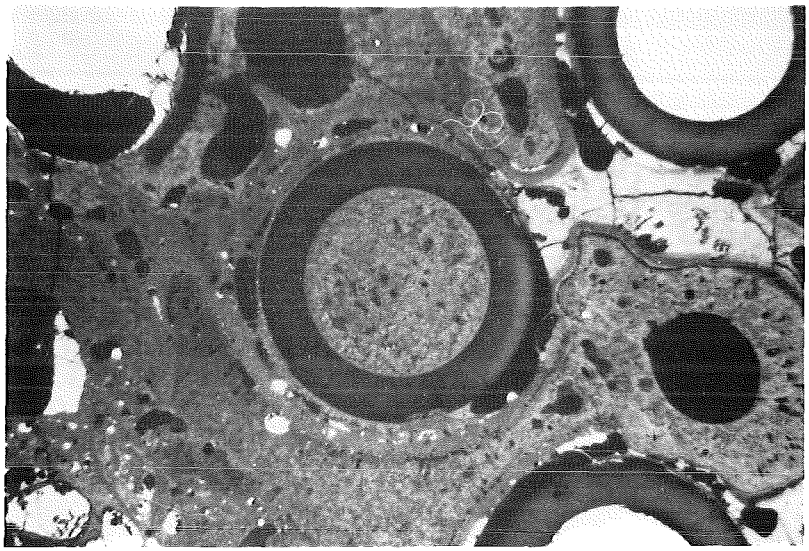

9

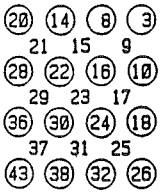

Fig. 148: Enlarged cross sections in region of unheated rods at Ø mm elevation (CORA bundle B)

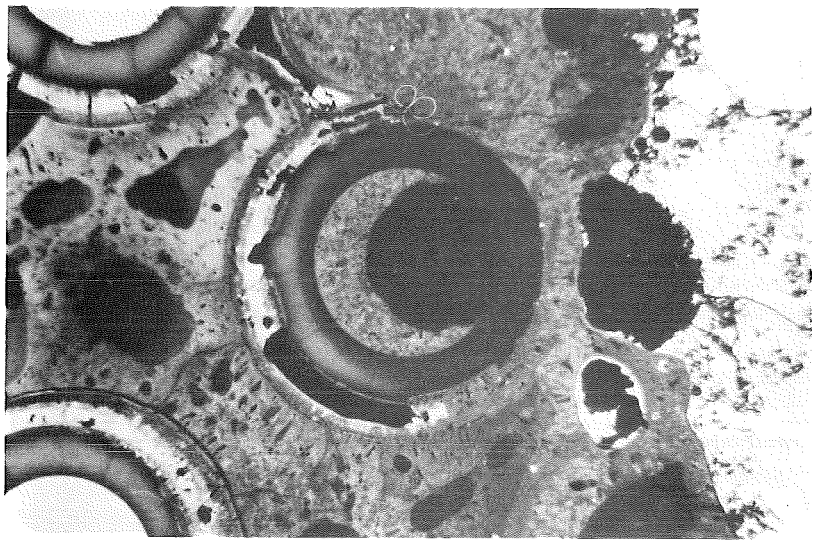

29

23

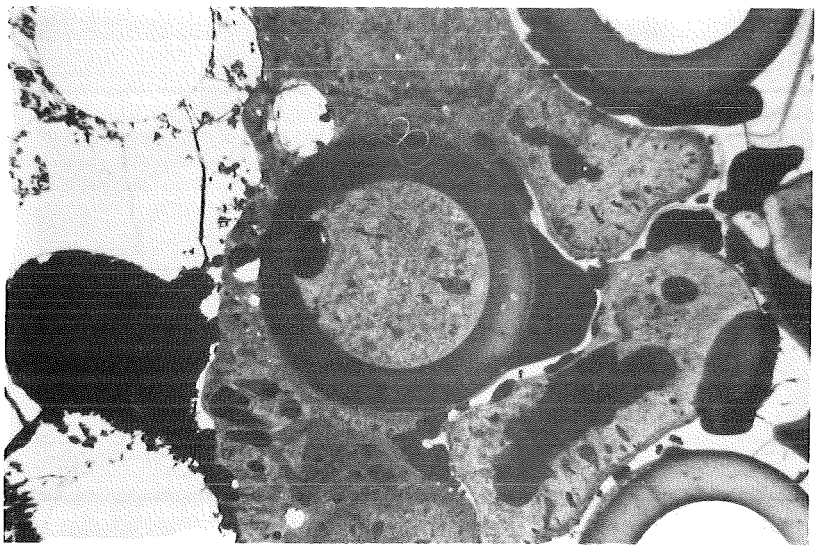

17

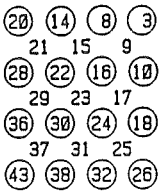

Fig. 149: Enlarged cross sections in region of unheated rods at Ø mm elevation (CORA bundle B)

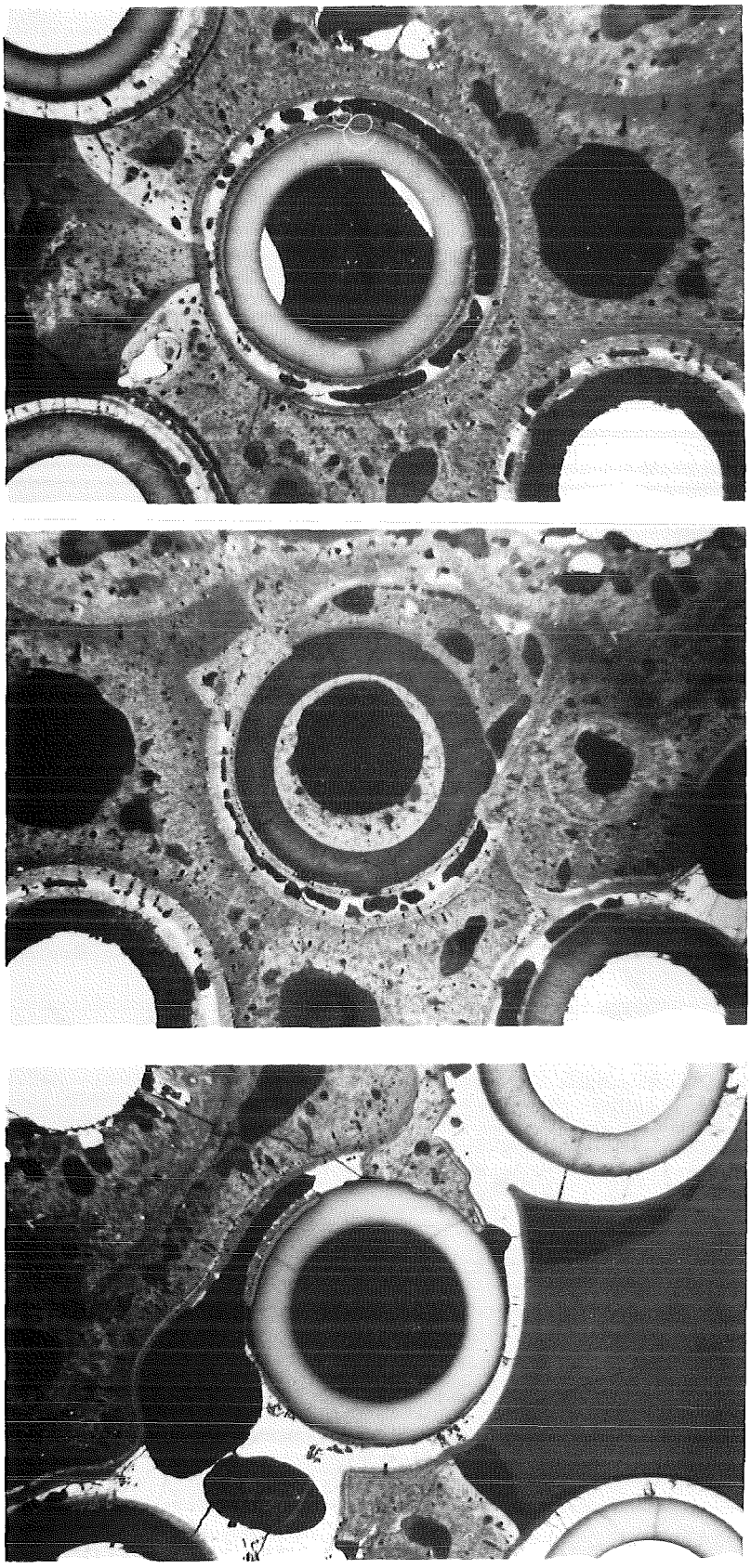

Fig. 150: Enlarged cross sections in region of unheated rods at 0 mm elevation (CORA bundle B)

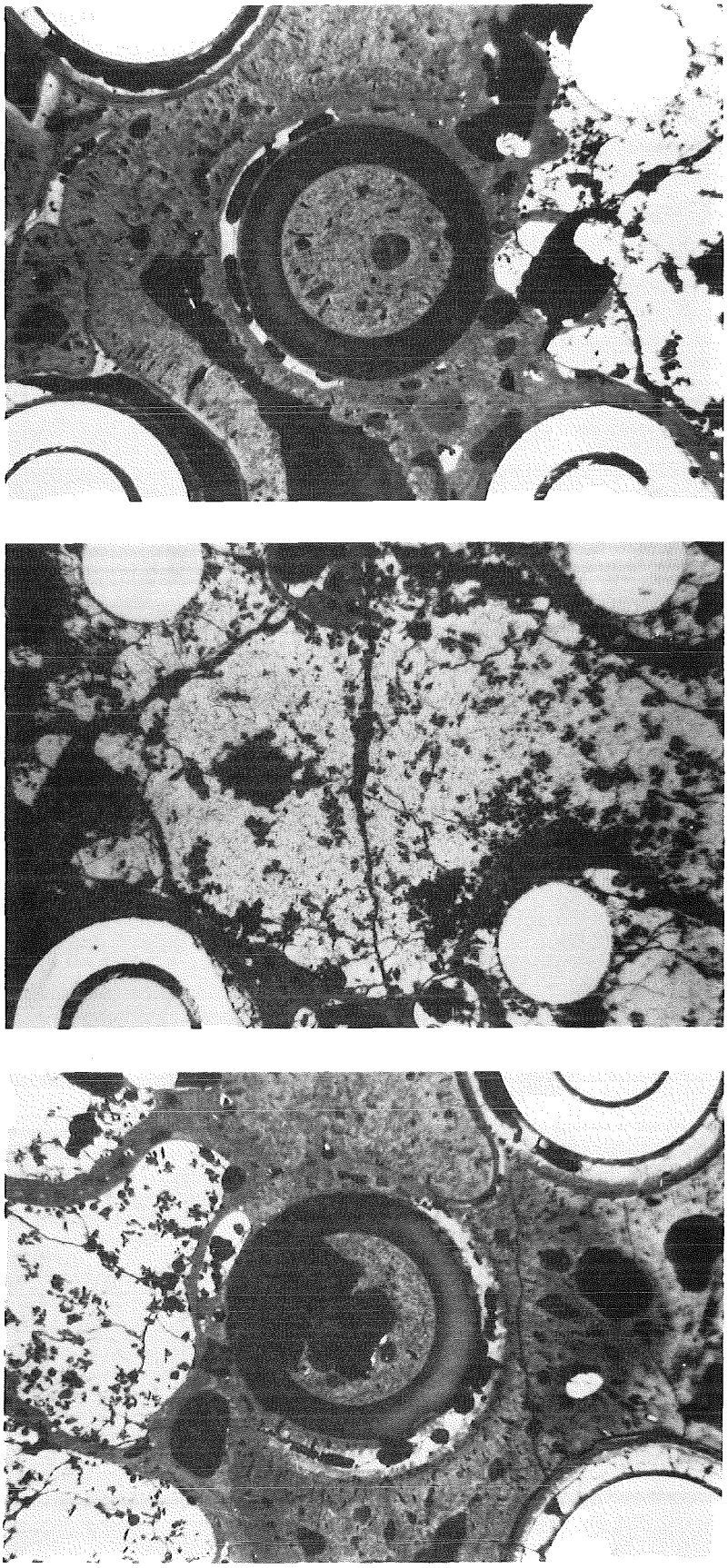

Fig. 151: Enlarged cross sections in region of unheated rods at -16 mm elevation (CORA bundle B)

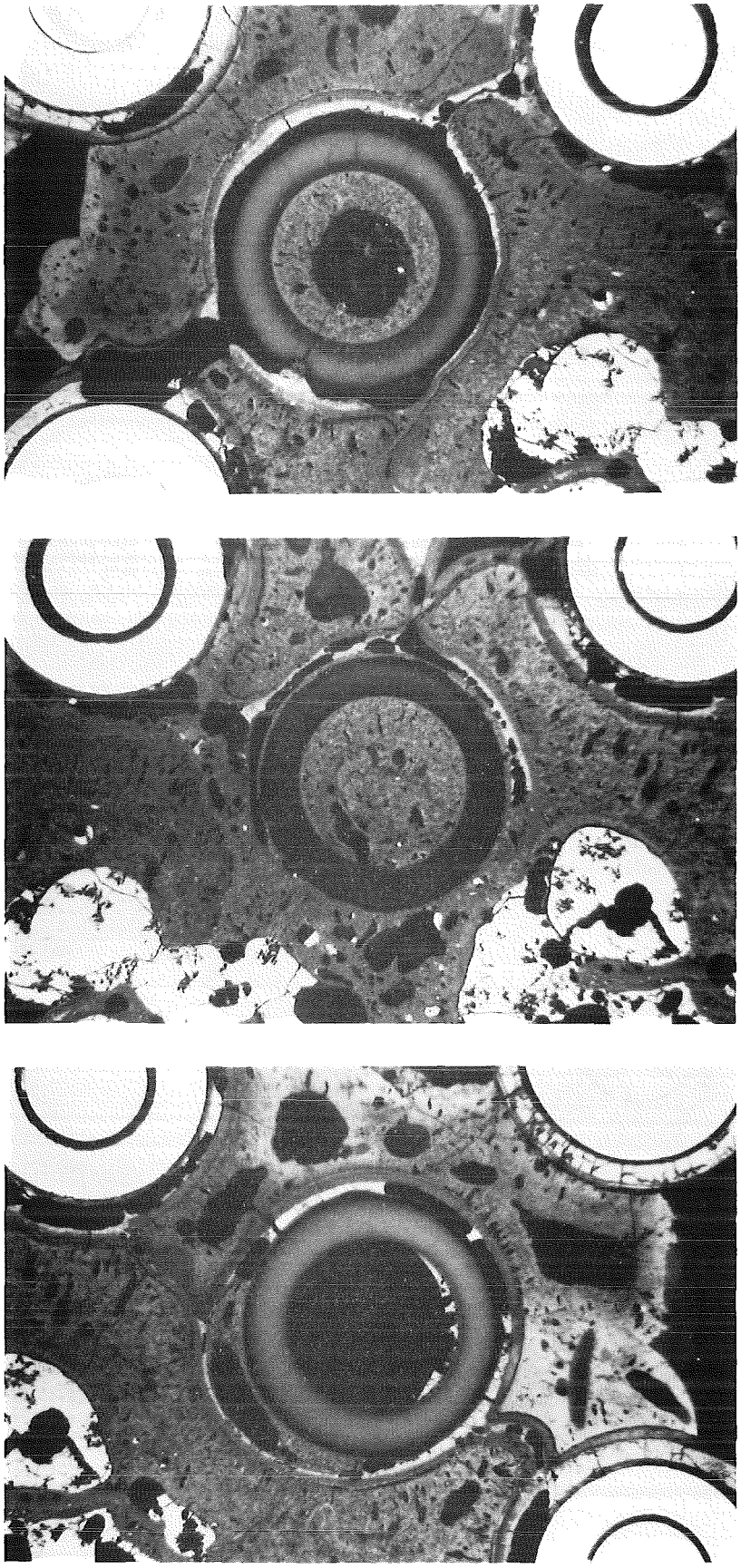

Fig. 152: Enlarged cross sections in region of unheated rods at -16 mm elevation (CORA bundle B)

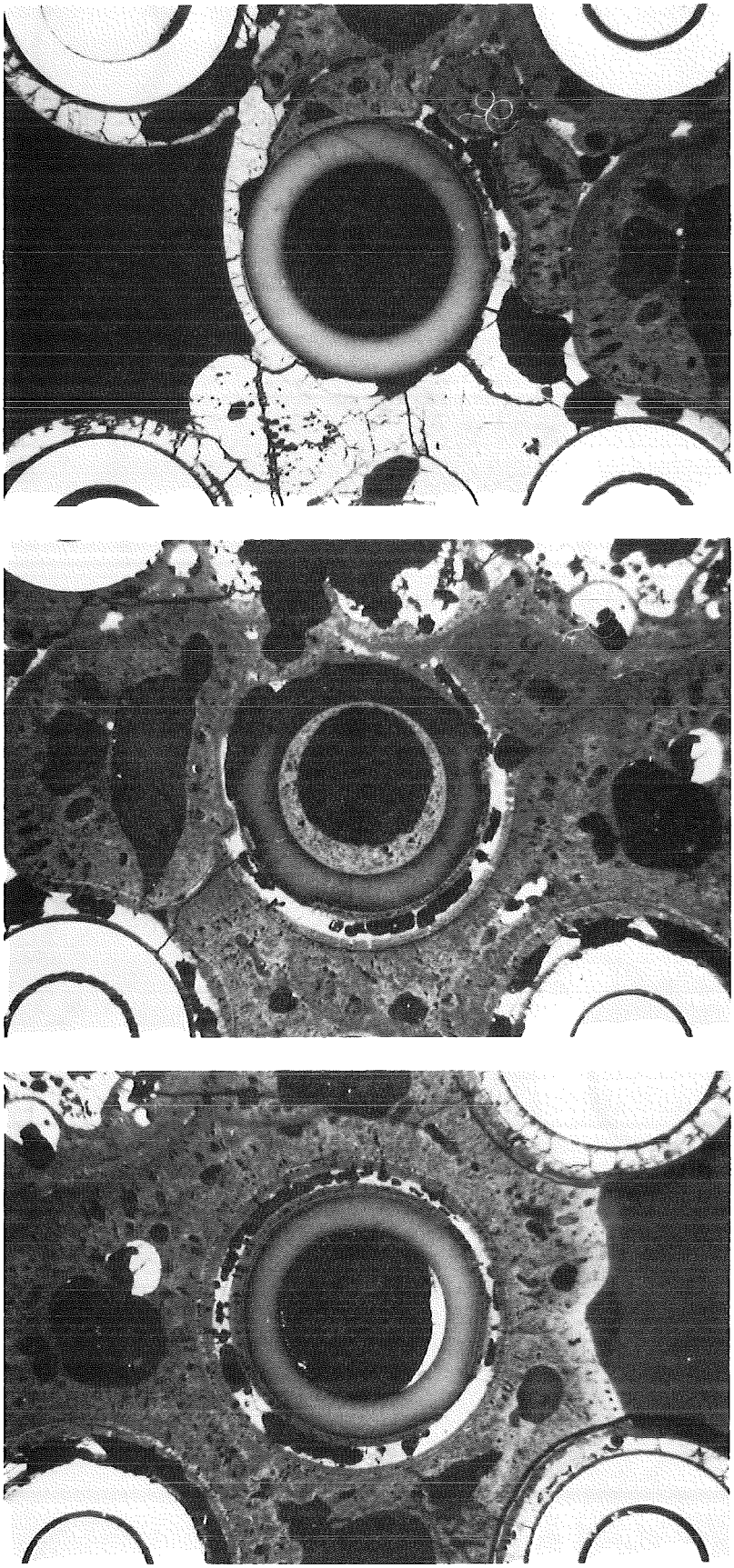

Fig. 153: Enlarged cross sections in region of unheated rods at -16 mm elevation (CORA bundle B)

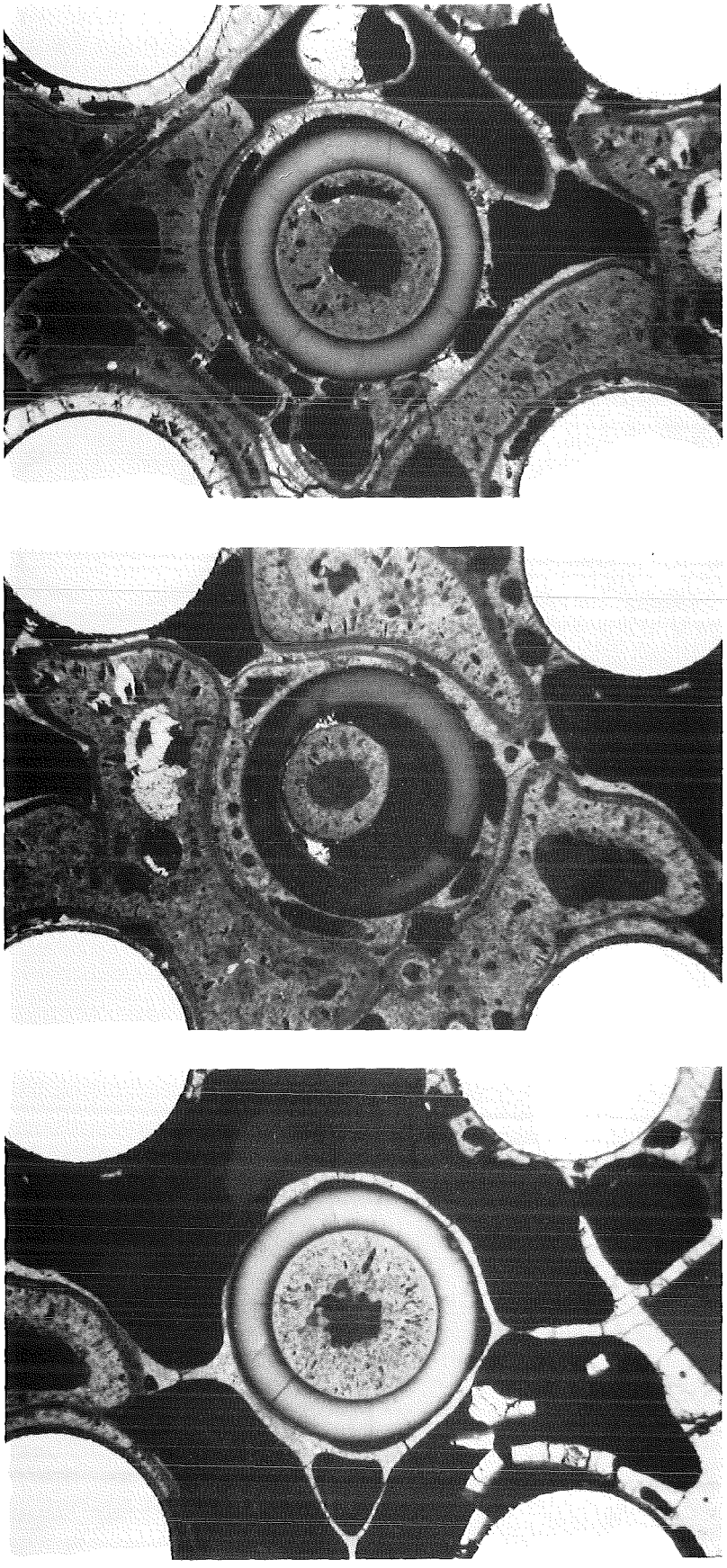

Fig. 154: Enlarged cross sections in region of unheated rods at -55 mm elevation (CORA bundle B)

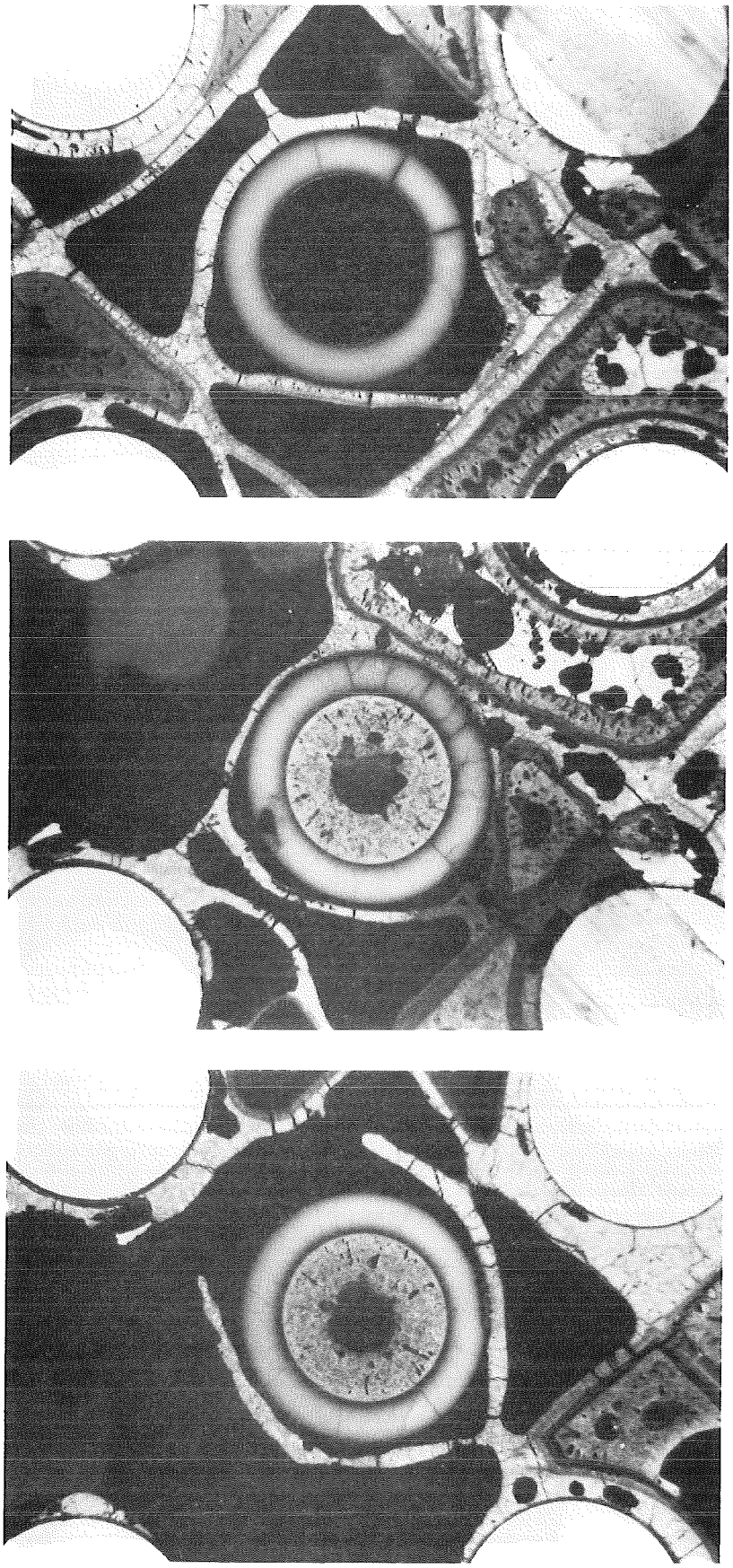

Fig. 155: Enlarged cross sections in region of unheated rods at -55 mm elevation (CORA bundle B)

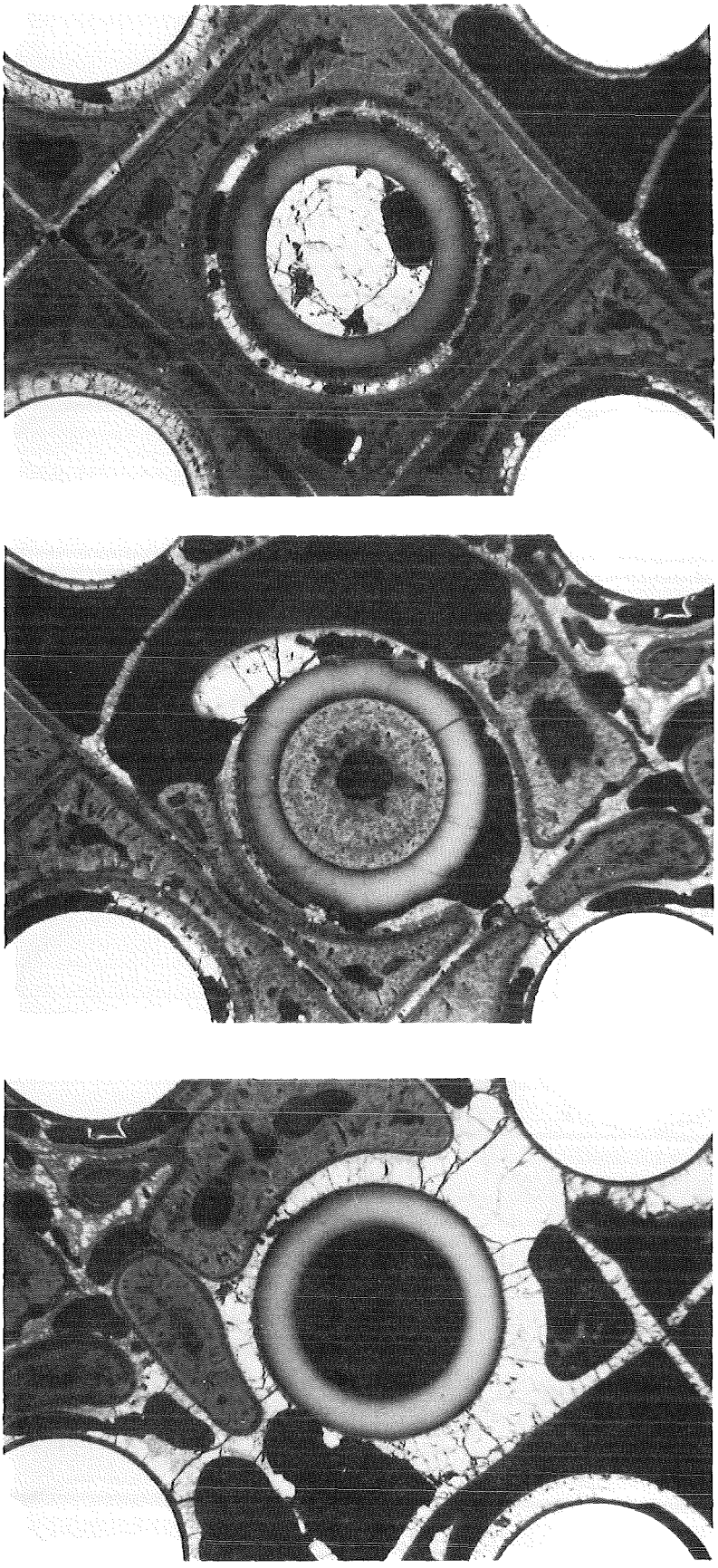

Fig. 156: Enlarged cross sections in region of unheated rods at -55 mm elevation (CORA bundle B)

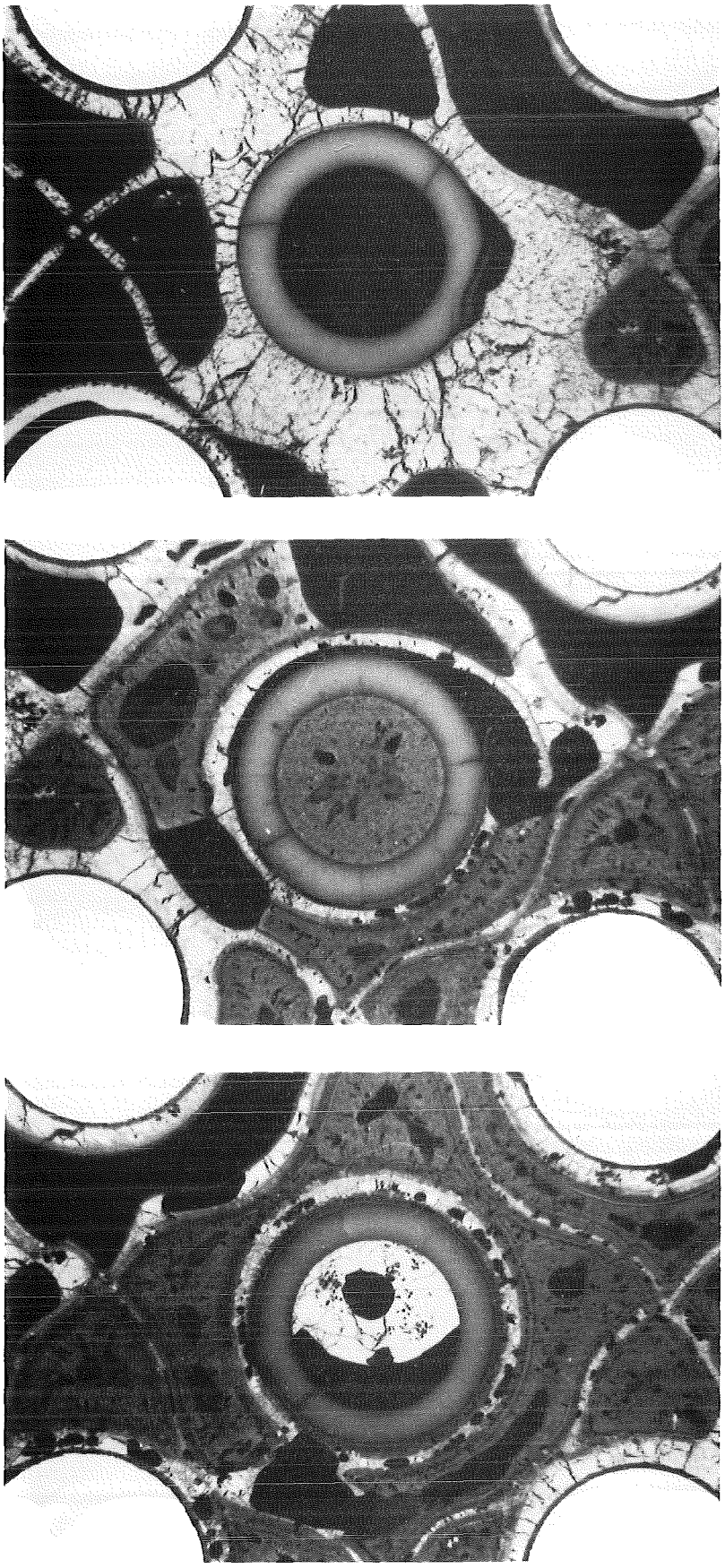

Fig. 157: Enlarged cross sections in region of unheated rods at -71 mm elevation (CORA bundle B)

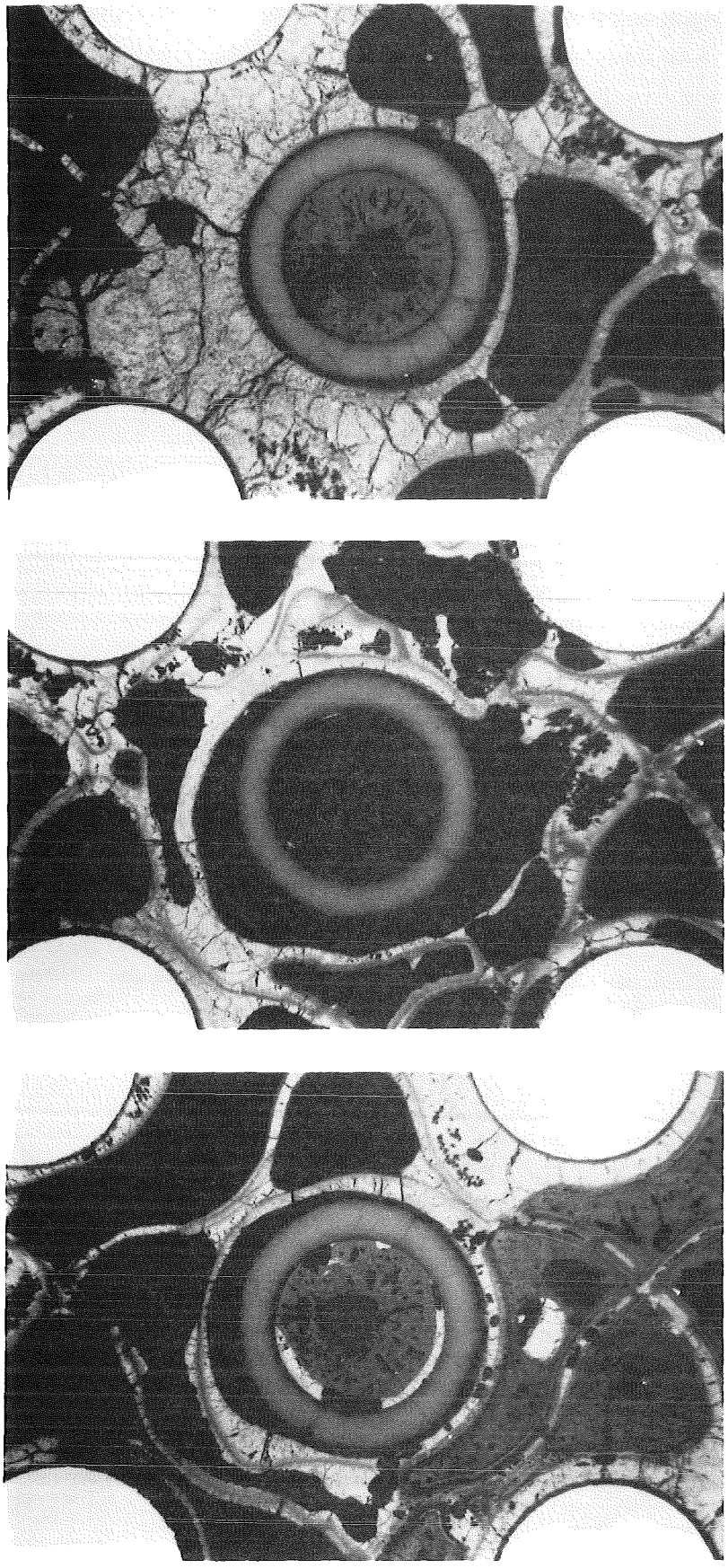

Fig. 158: Enlarged cross sections in region of unheated rods at -71 mm elevation (CORA bundle B)

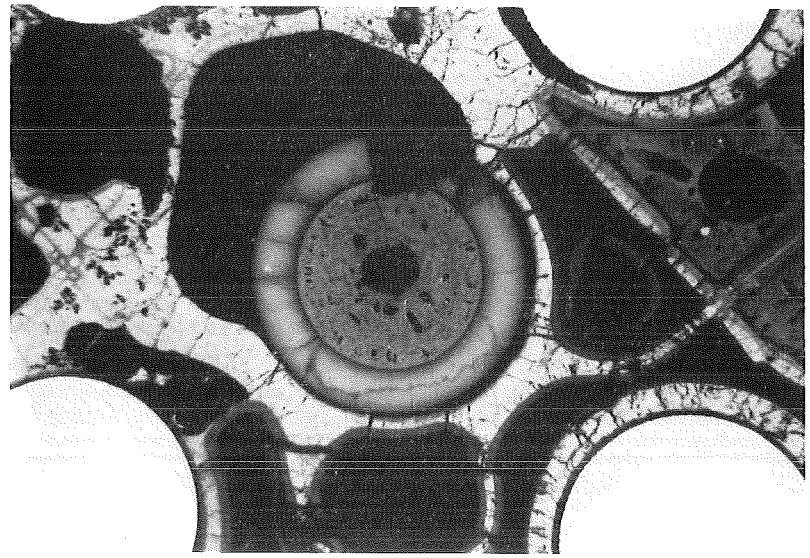

9

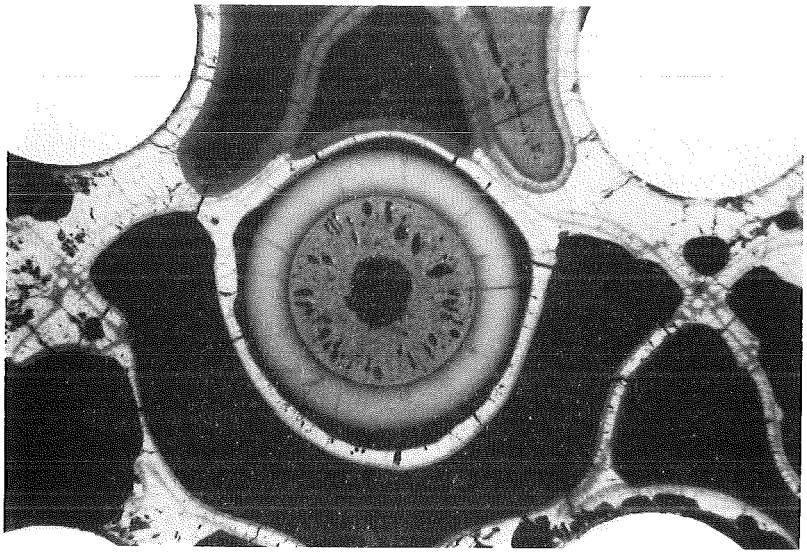

15

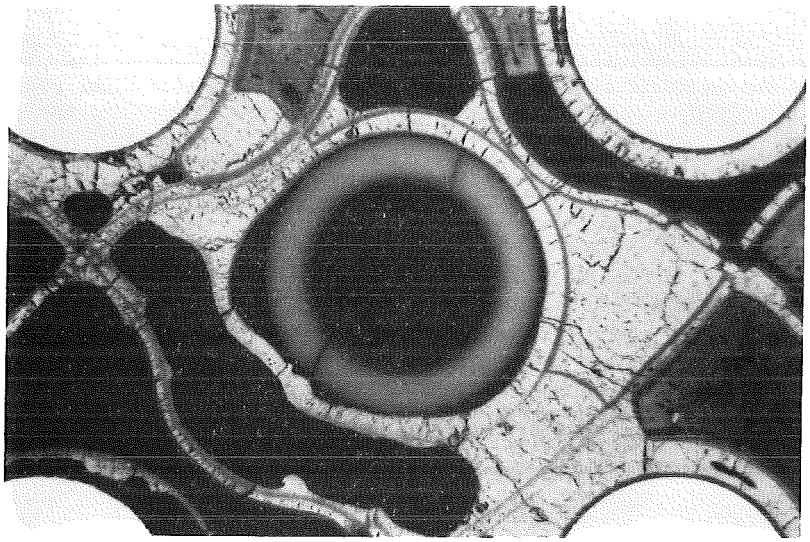

21

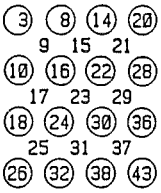

Fig. 159: Enlarged cross sections in region of unheated rods at -71 mm elevation (CORA bundle B)

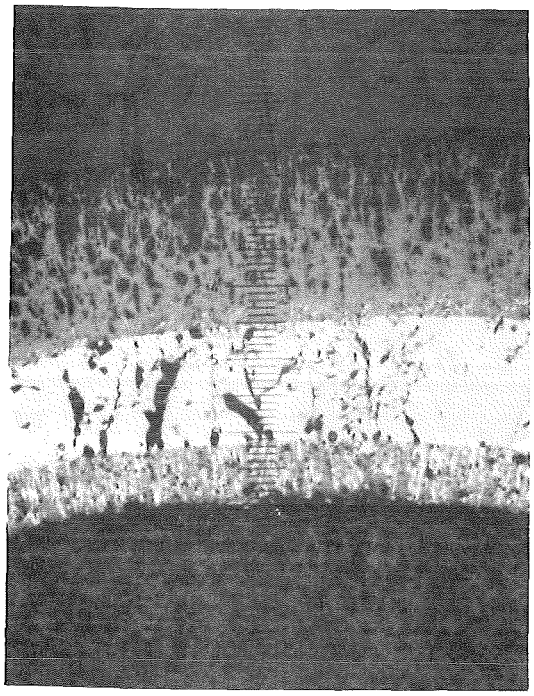

109mm

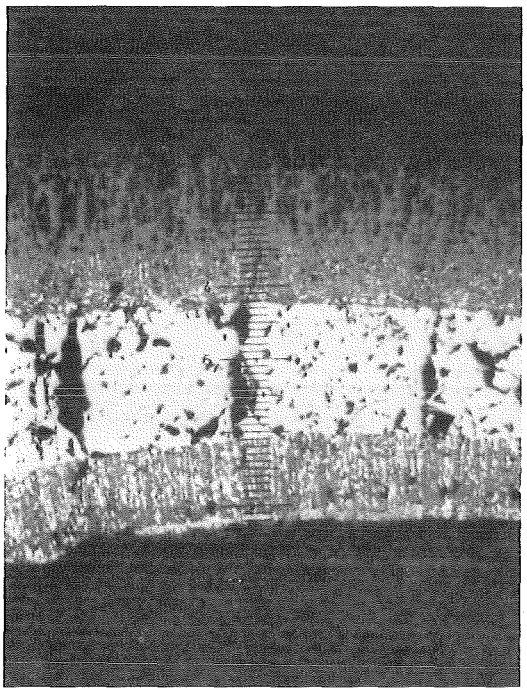

91mm

50×

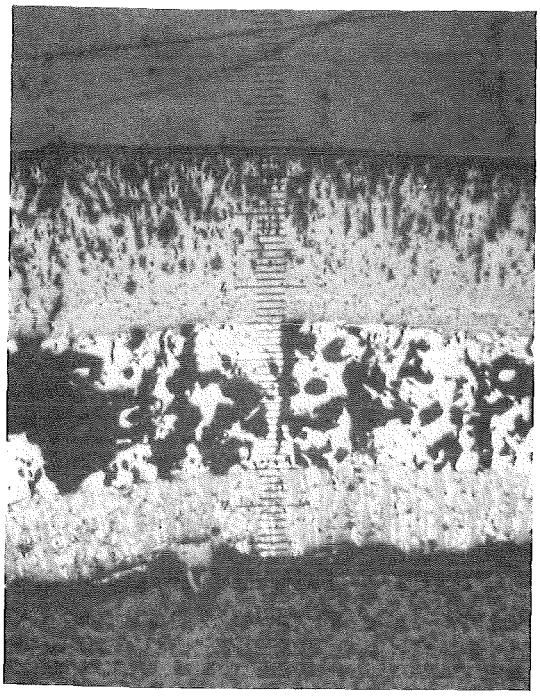

93mm

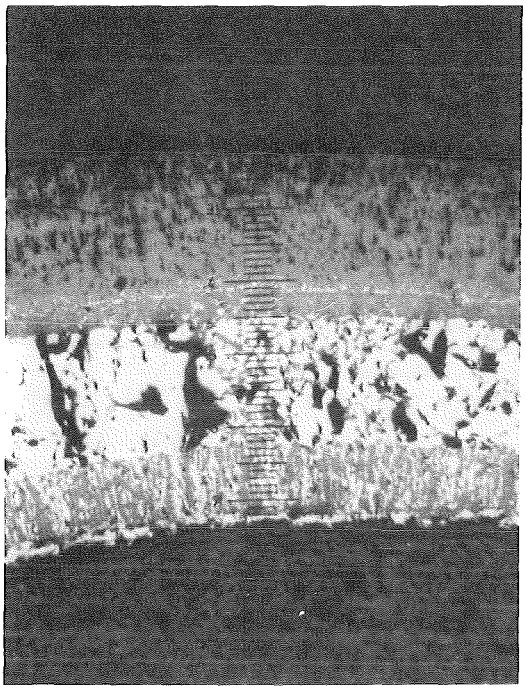

75mm

Fig. 160:
Cladding region of heated fuel rod 43 at elevations given (transient test CORA B)

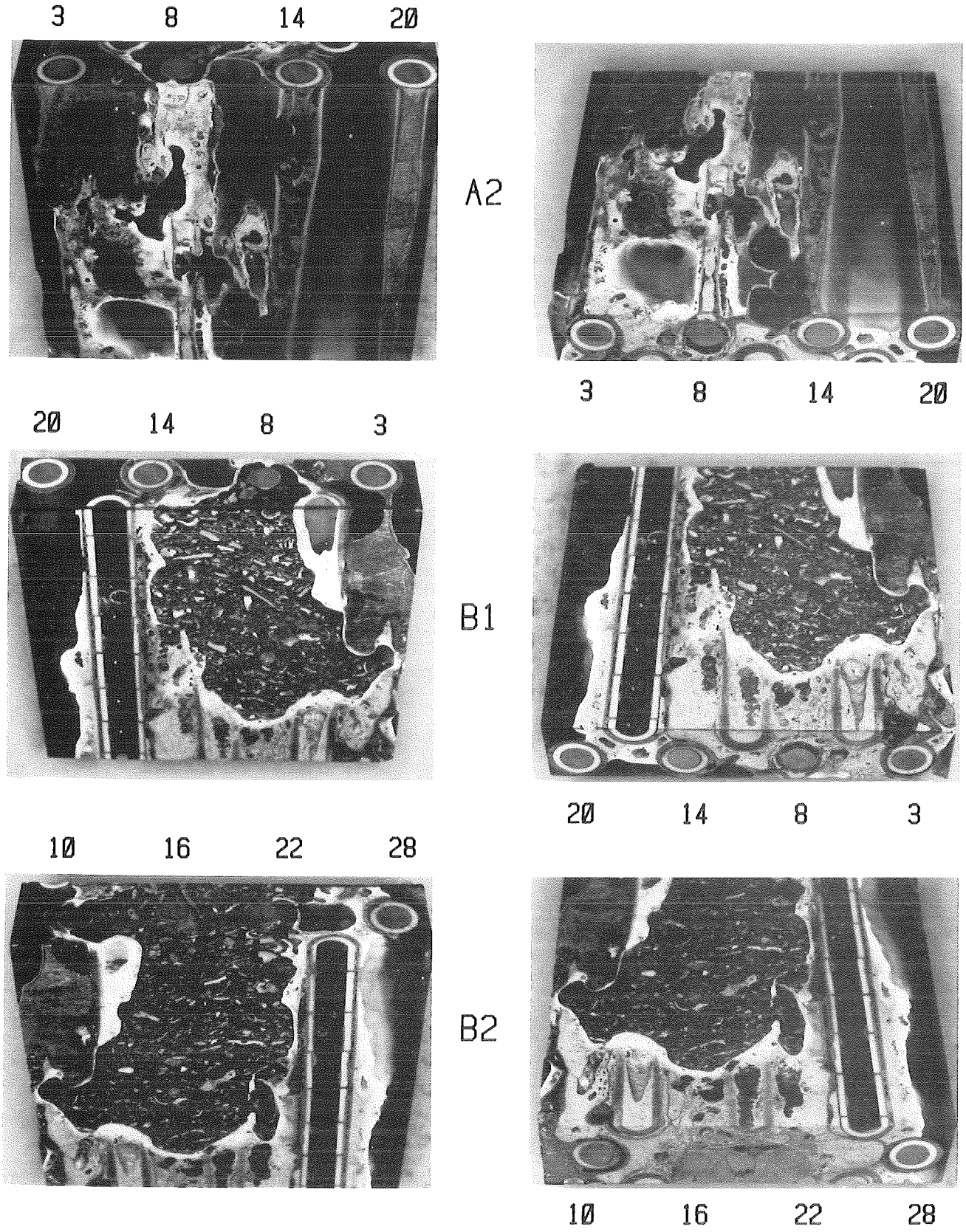

Fig.161 : Vertical cross sections of CORA bundle B between 1 mm and 73 mm elevation.

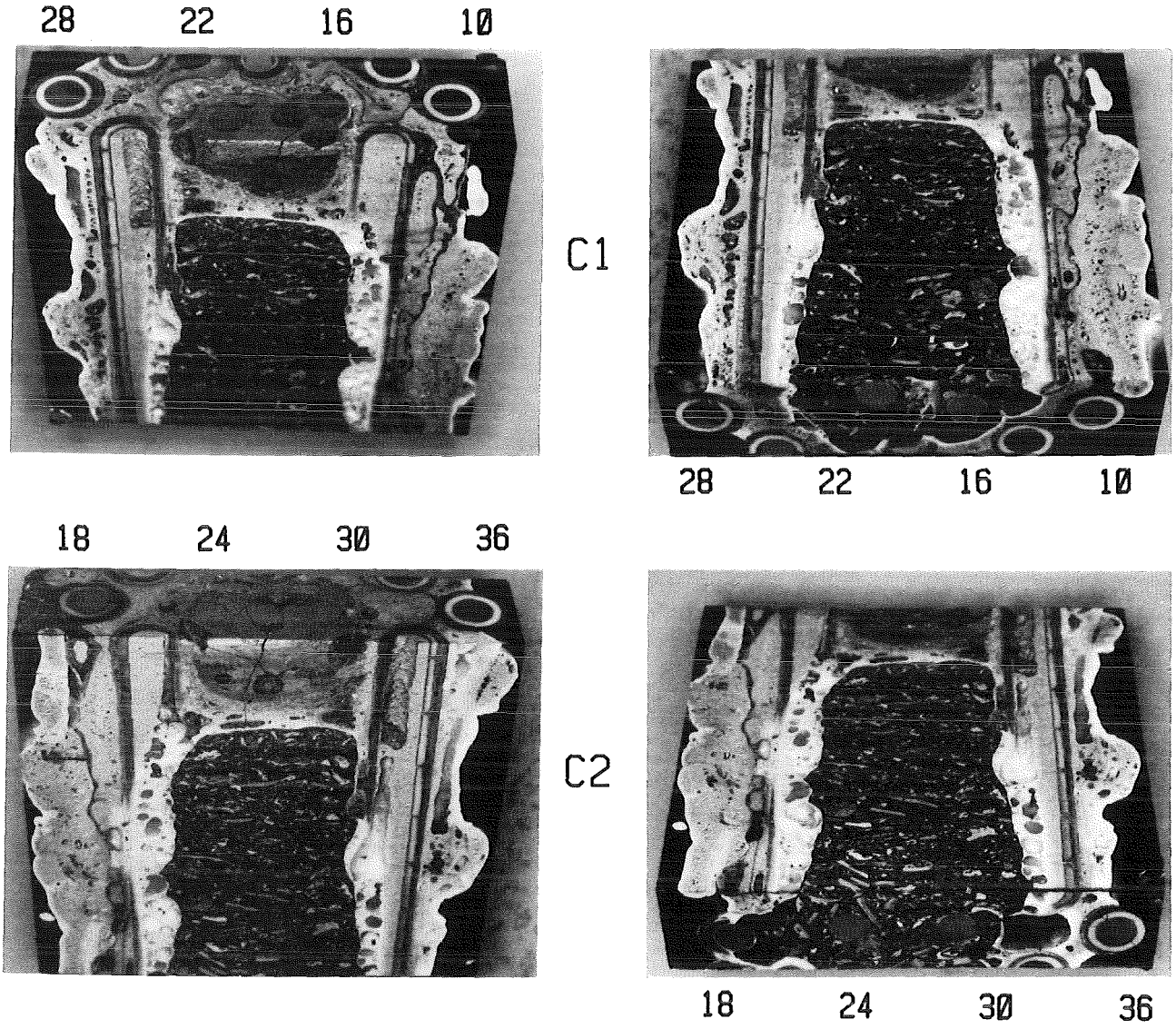

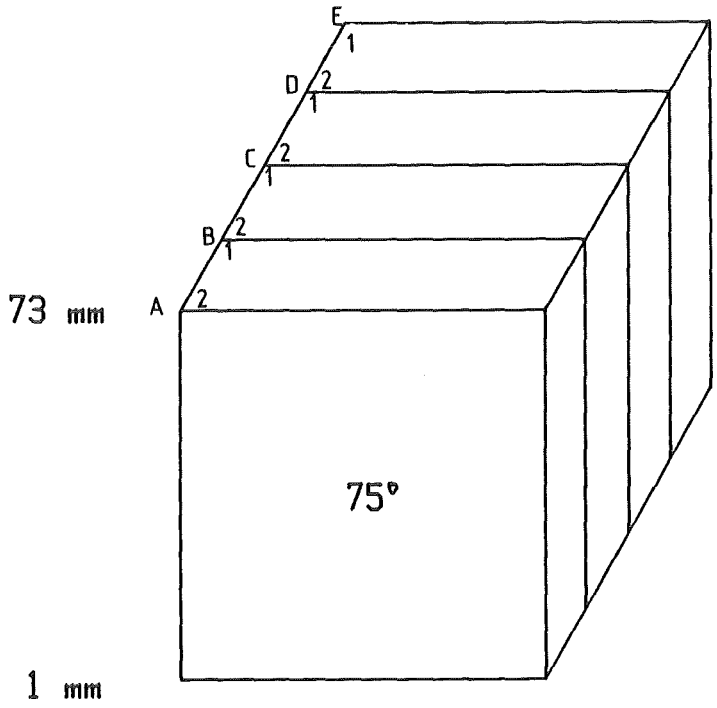

Fig.162: Vertical cross sections of CORA bundle B between 1 mm and 73 mm elevation.

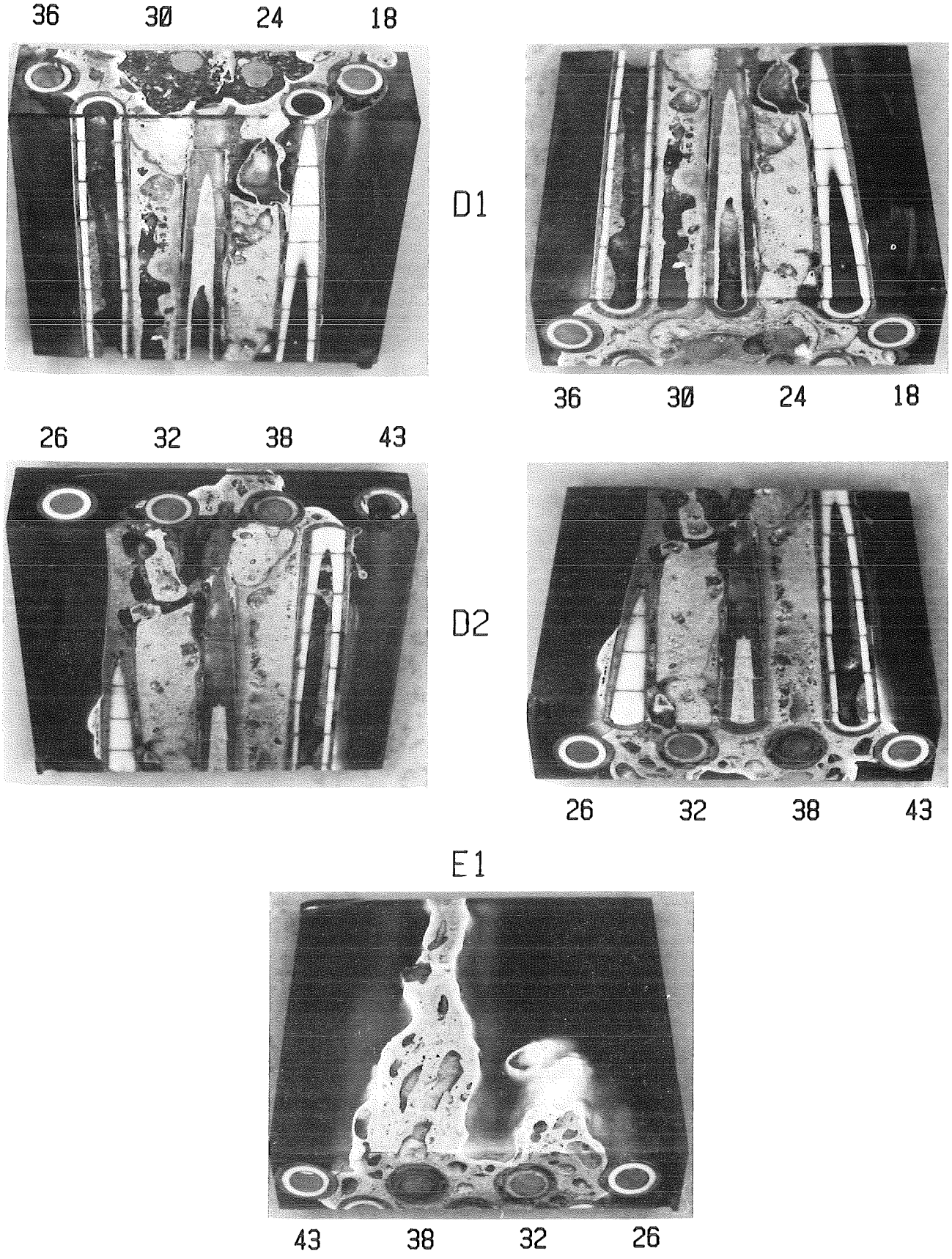

Fig.163: Vertical cross sections of CORA bundle B between 1 mm and 73 mm elevation.

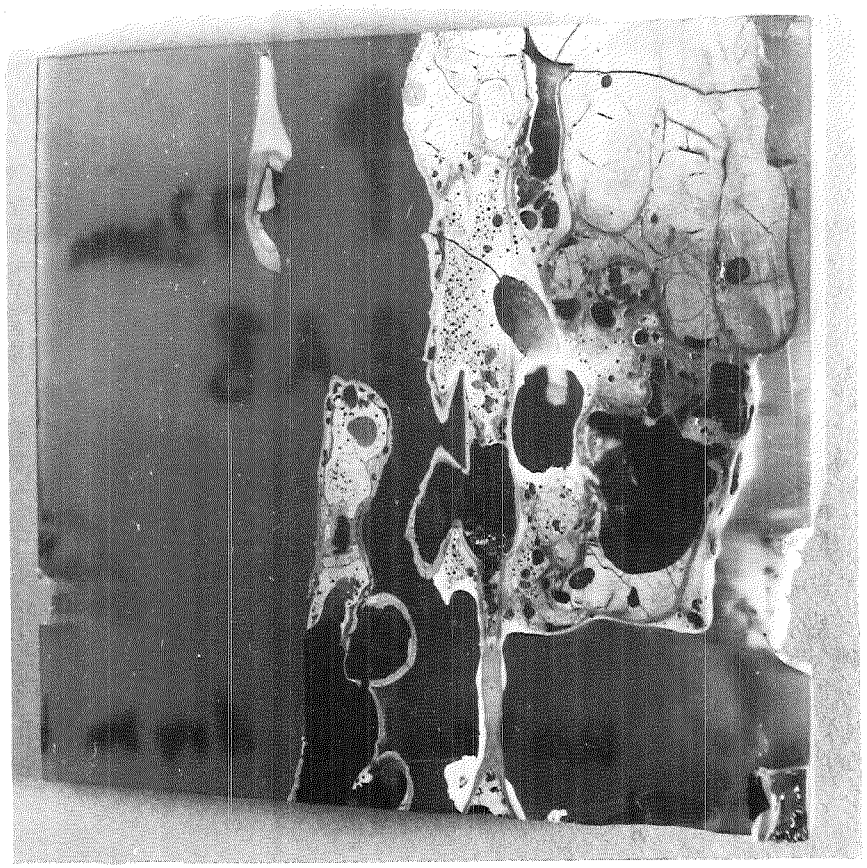

A1

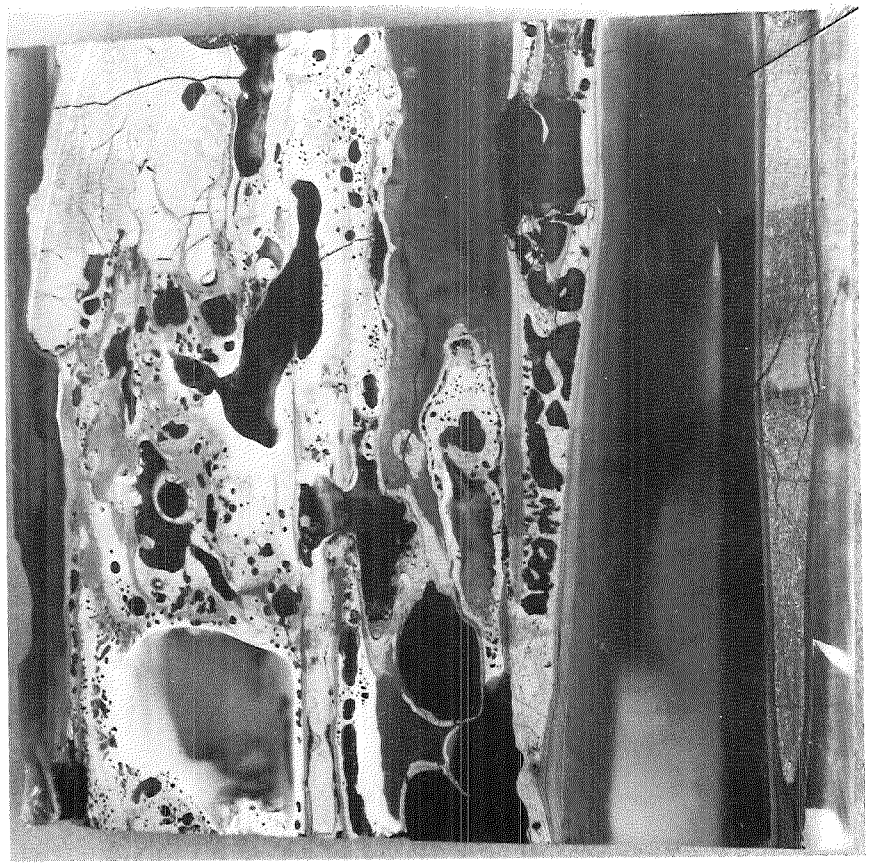

A2

Fig.164: Vertical cross sections of CORA bundle B between 1 mm and 73 mm elevation.

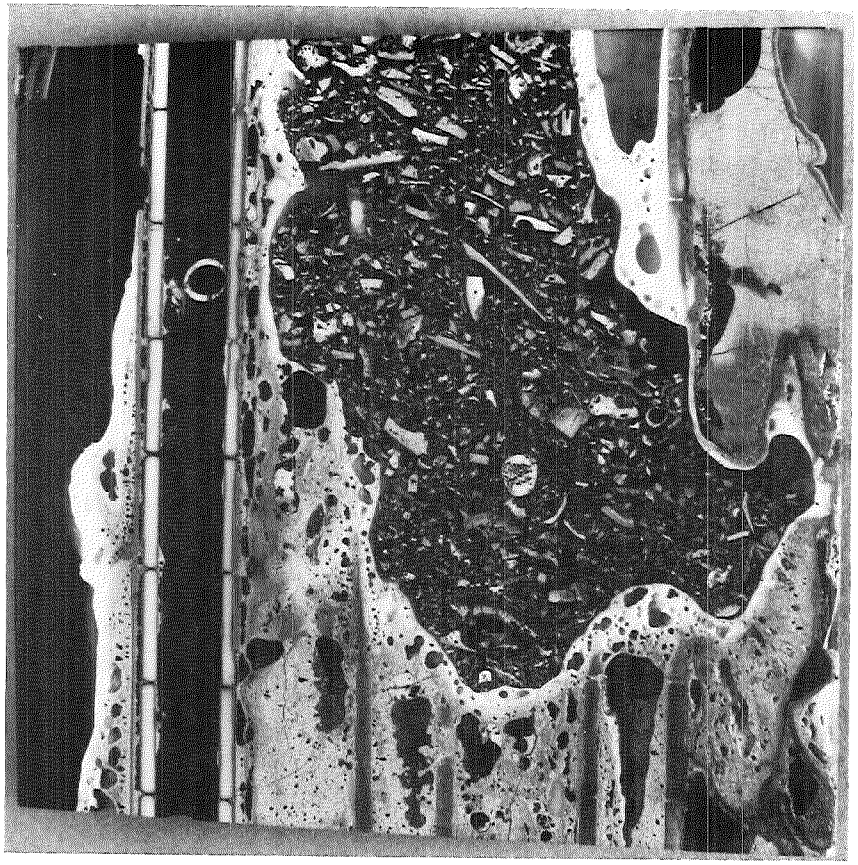

B1

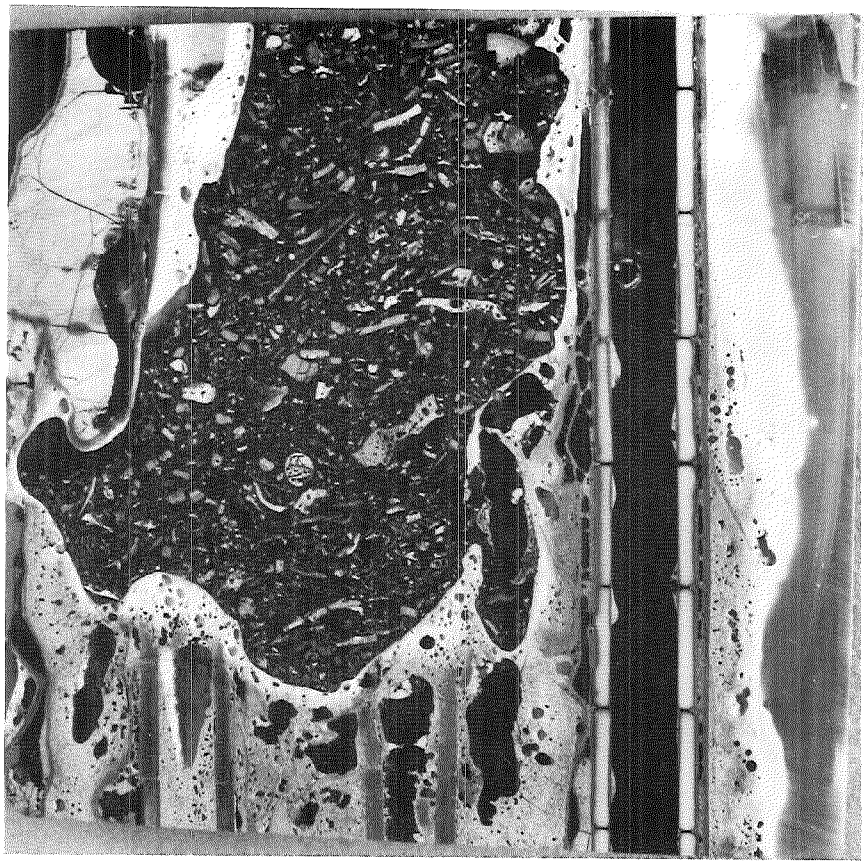

B2

Fig.165: Vertical cross sections of CORA bundle B between 1 mm and 73 mm elevation.

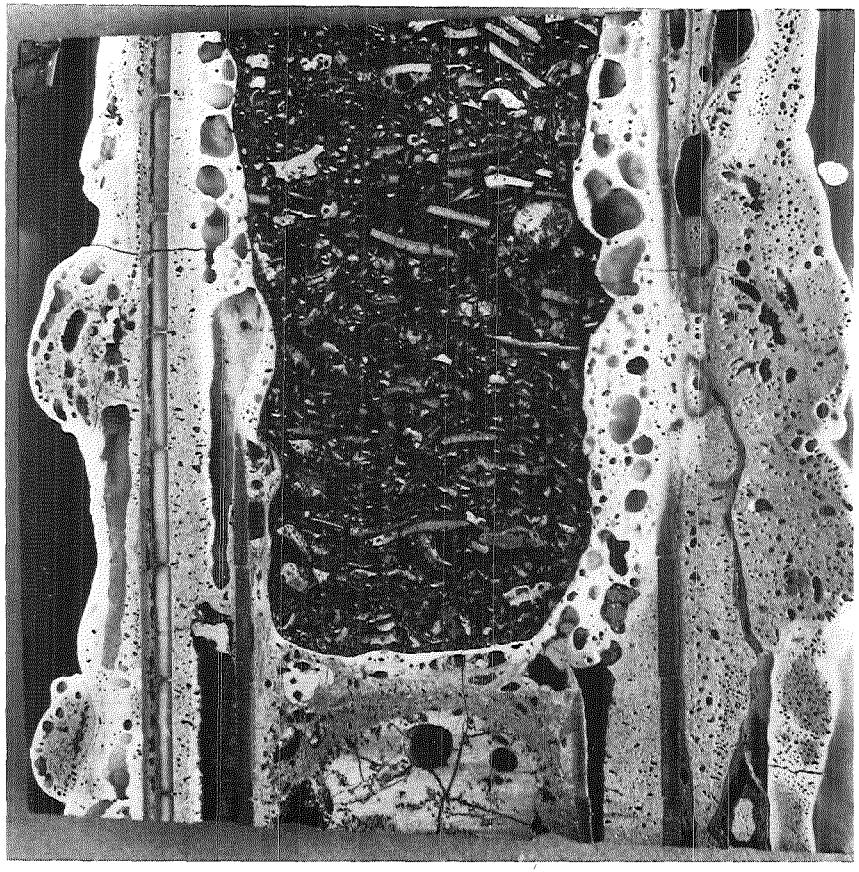

C1

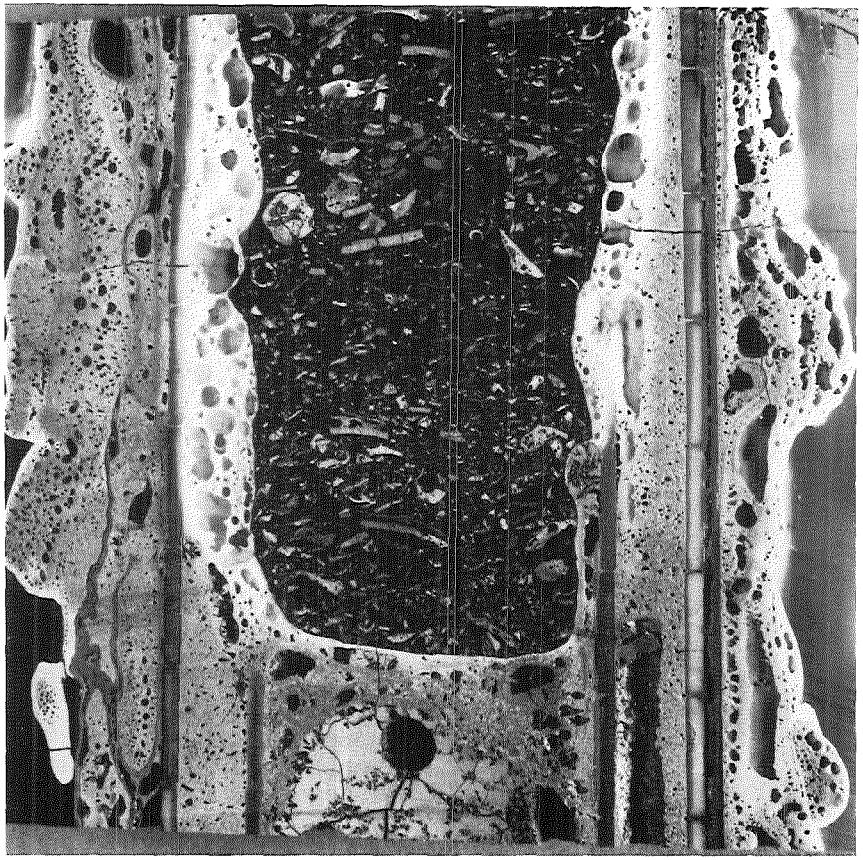

C2

Fig.166: Vertical cross sections of CORA bundle B between 1 mm and 73 mm elevation.

D1

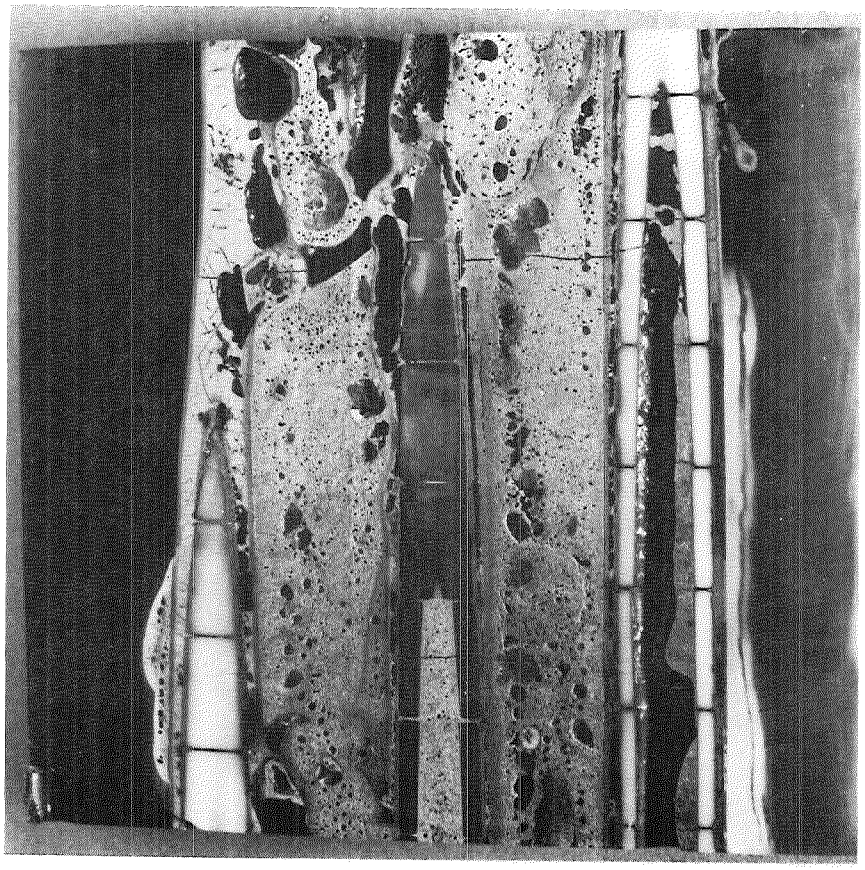

D2

Fig.167: Vertical cross sections of CORA bundle B between 1 mm and 73 mm elevation.

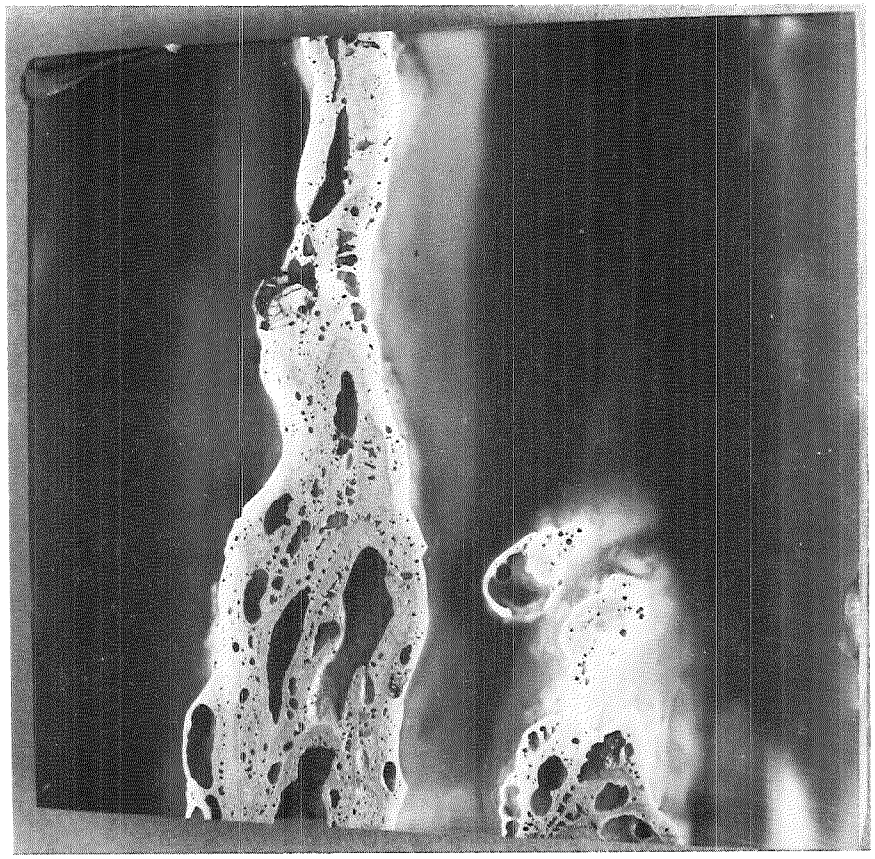

E1

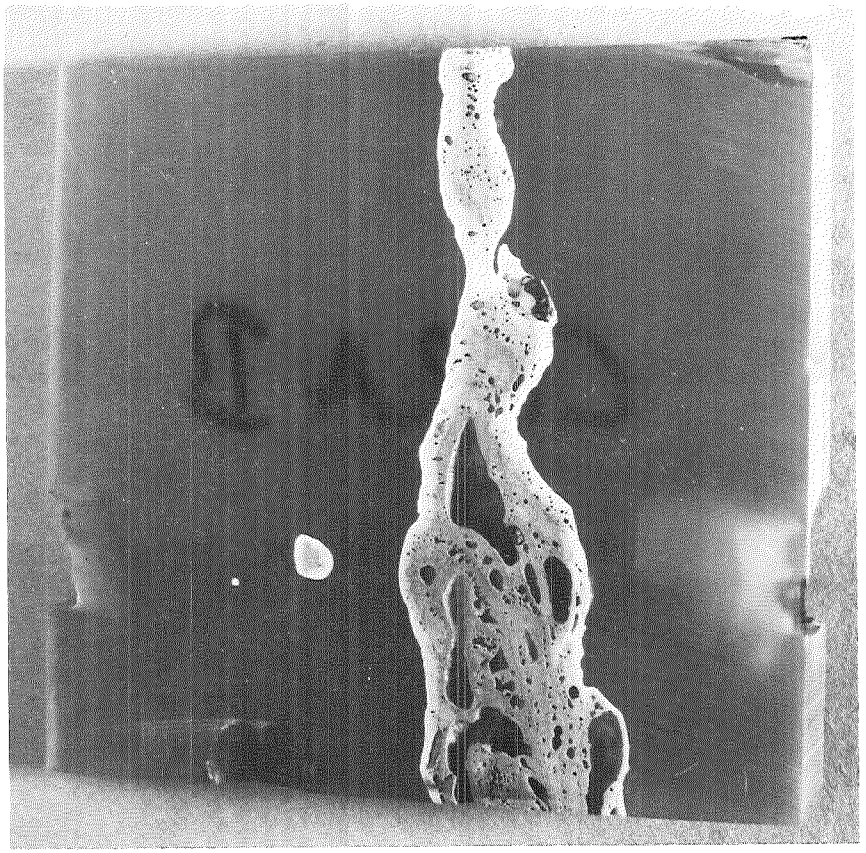

E2

Fig.168: Vertical cross sections of CORA bundle B between 1 mm and 73 mm elevation.

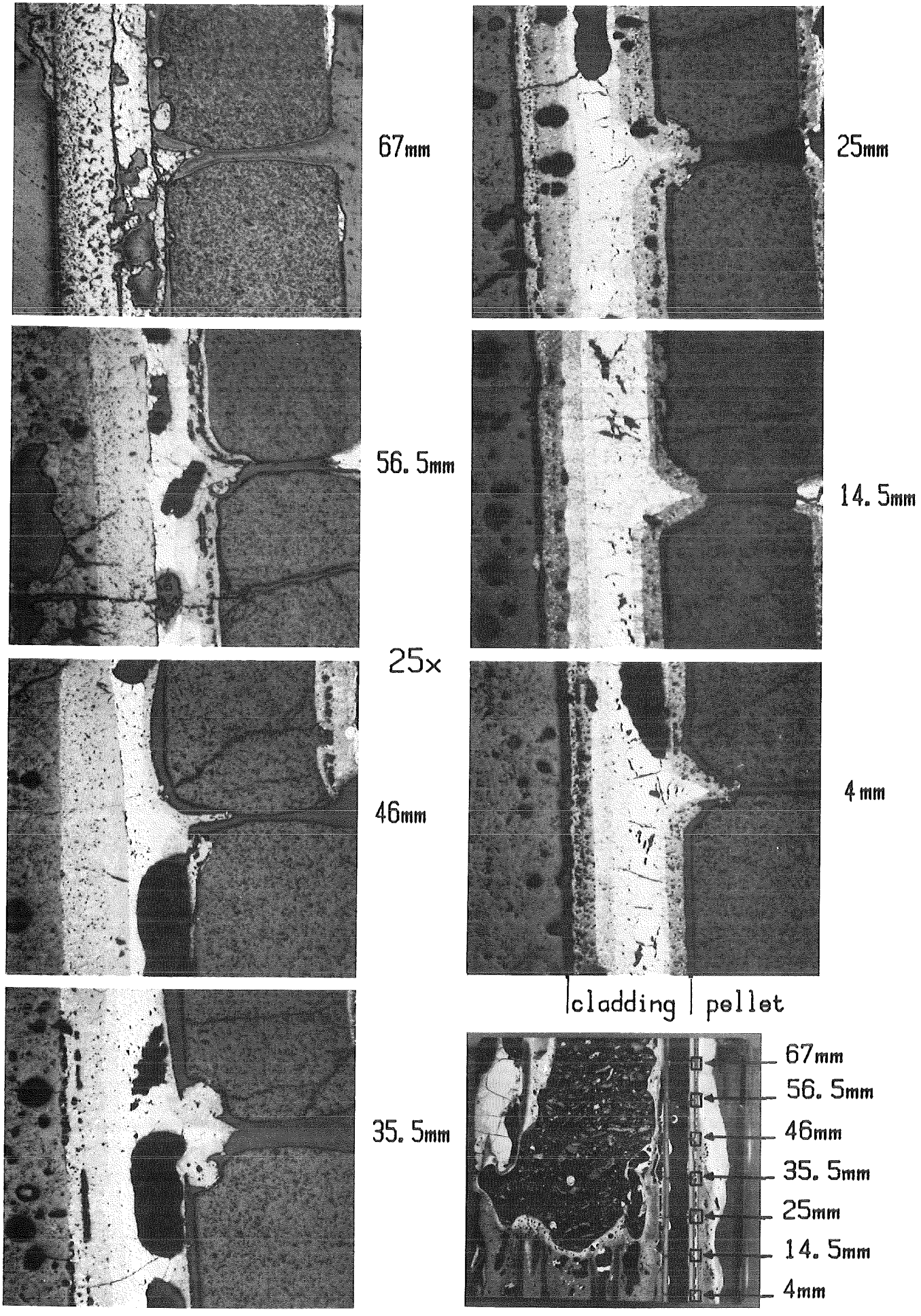

Fig.169: Pellet cladding contact regions of rod 21 (CORA B)

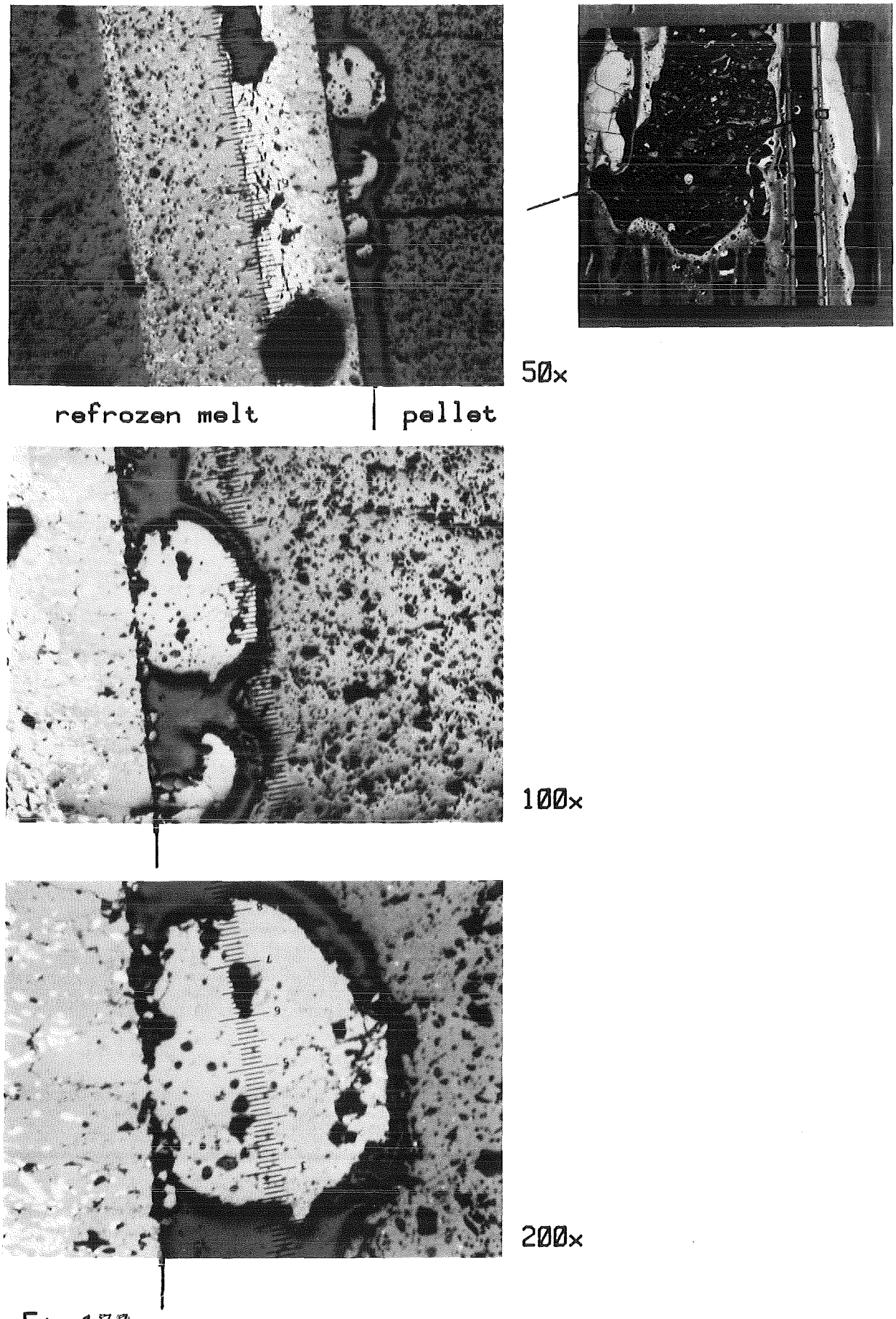

Fig.170:
Pellet cladding contact region (CORA bundle B)

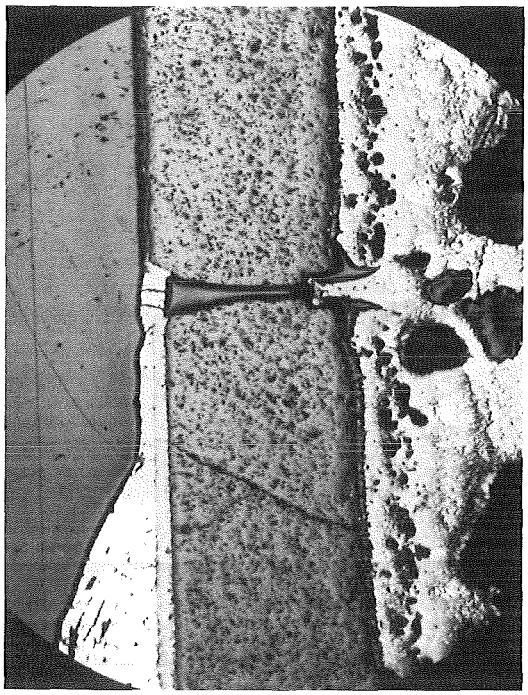

25x

pellet cladding

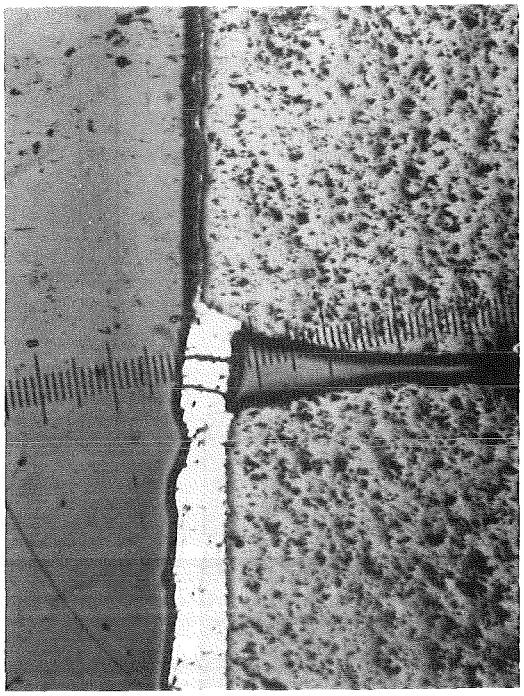

50x

pellet

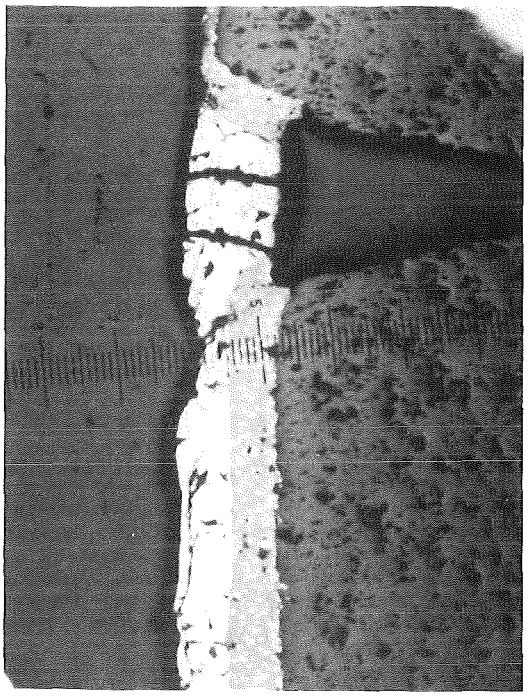

100x

pellet

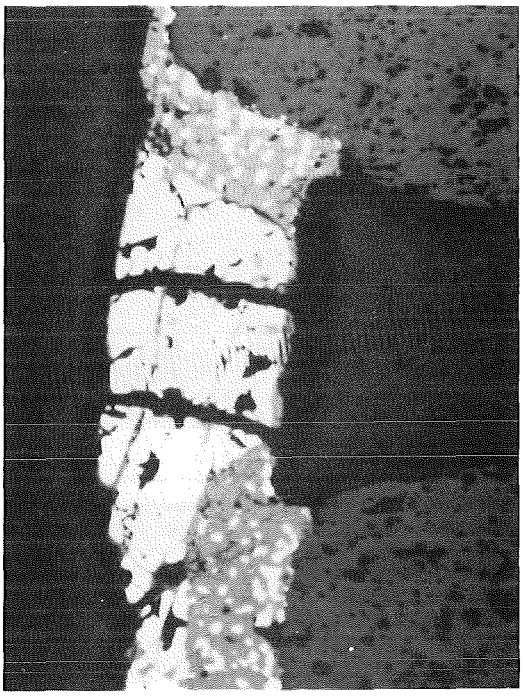

200x

pellet

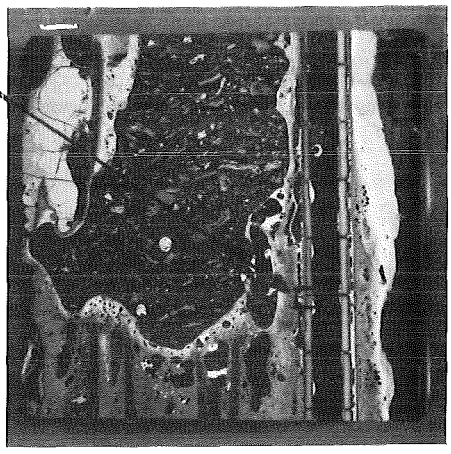

25x

Fig.171 :
Al_2O_3 pellet and Zry cladding interaction (CORA bundle B)

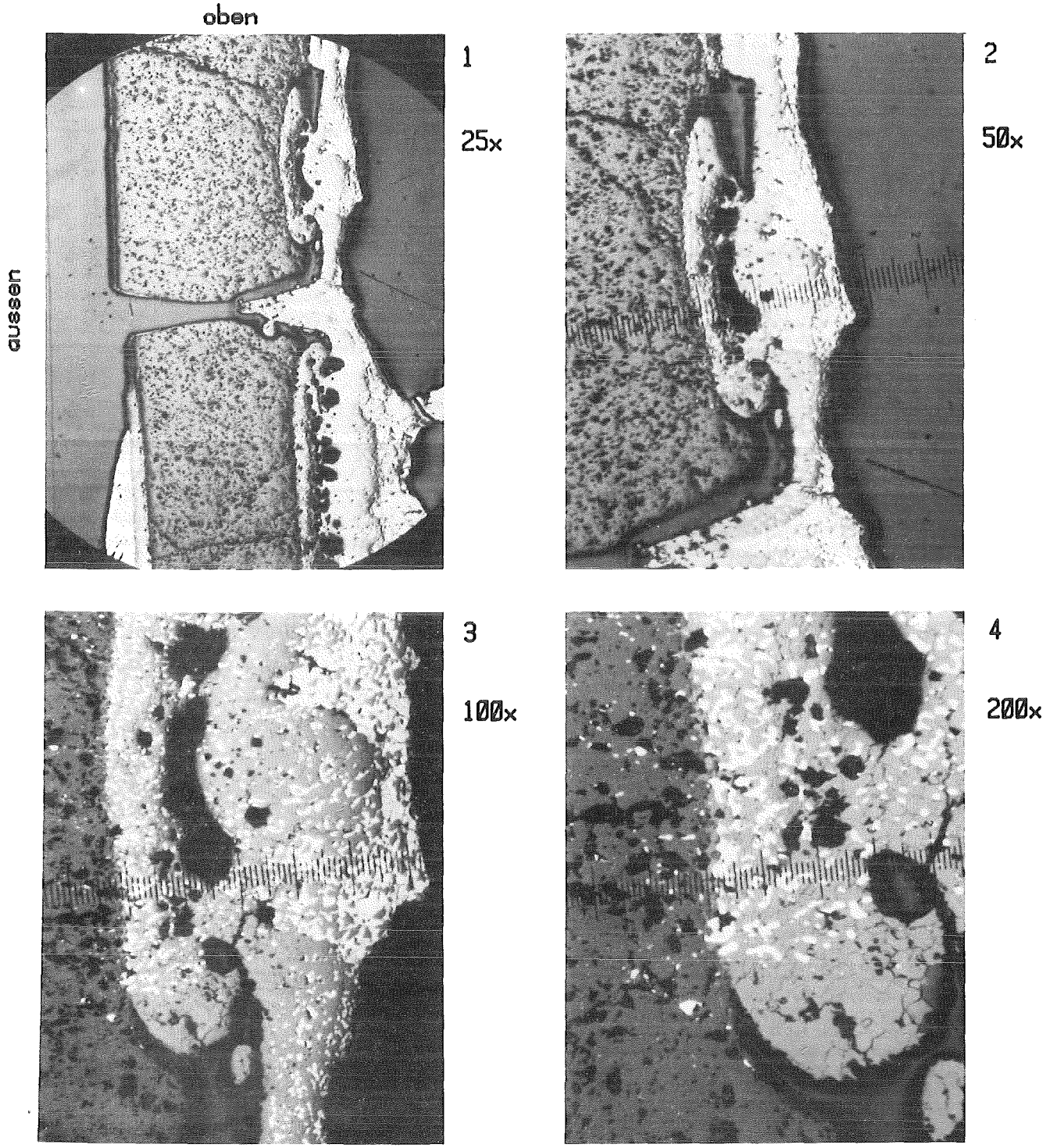

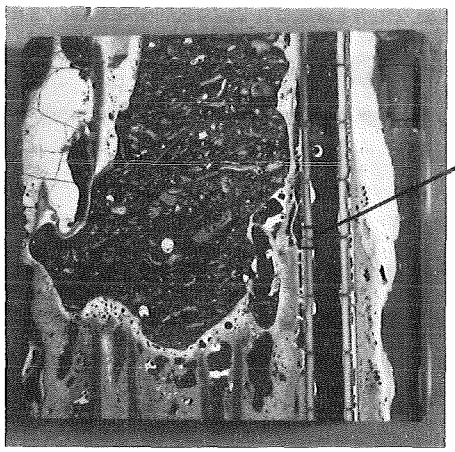

Fig. 172 :
Interaction between AL_2O_3-Pellet and Zry-cladding (CORA bundle B)

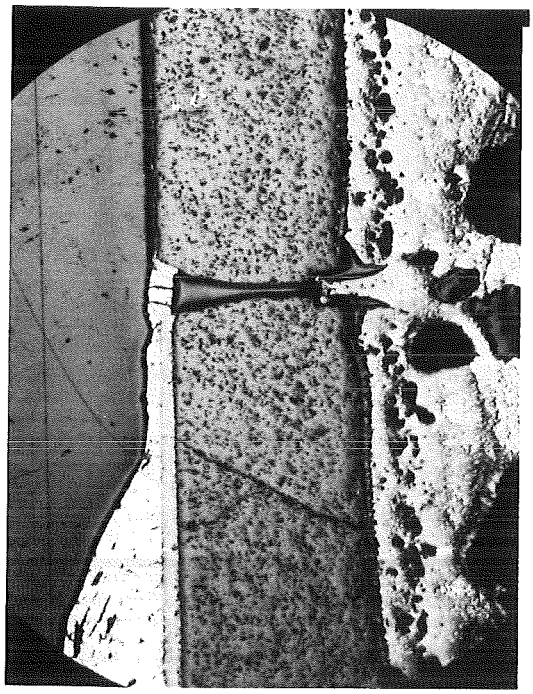

25x

pellet

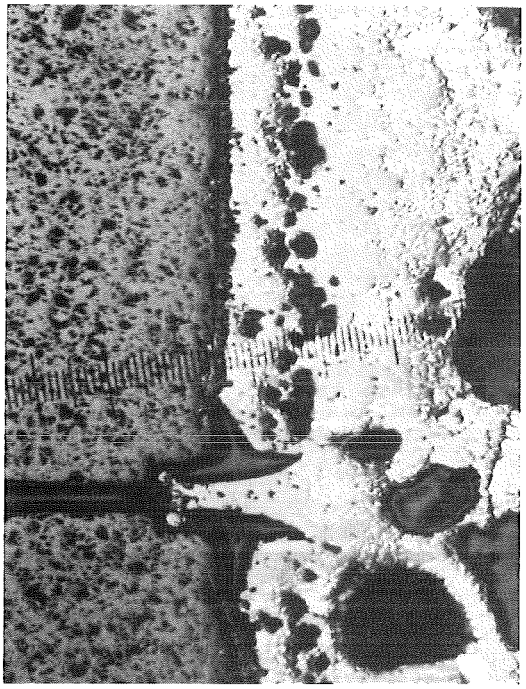

50x

pellet

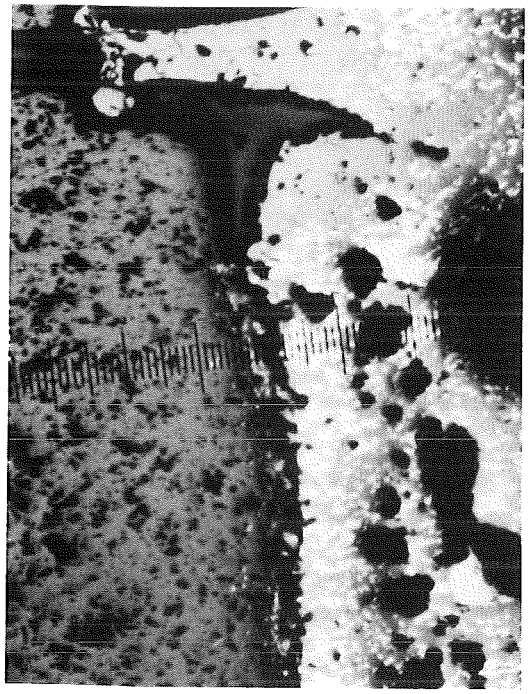

100x

pellet

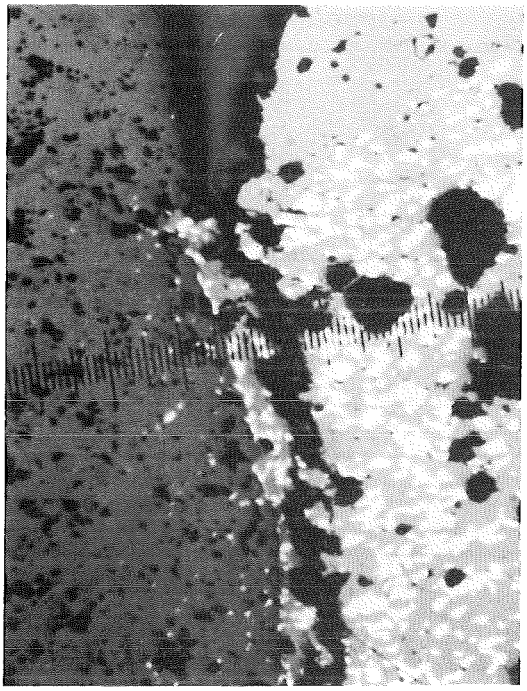

200x

pellet

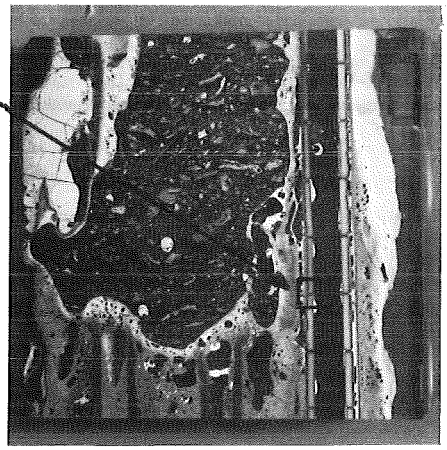

25x

Fig.173 :
Al_2O_3 pellet and Zry cladding interaction (CORA bundle B)

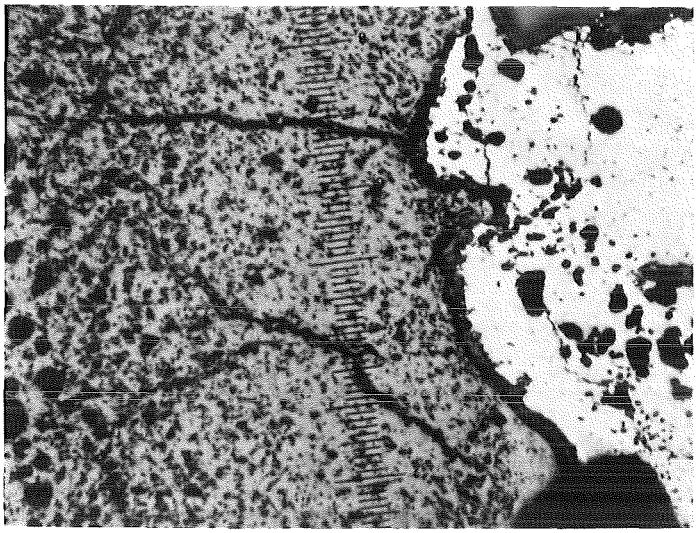

pellet

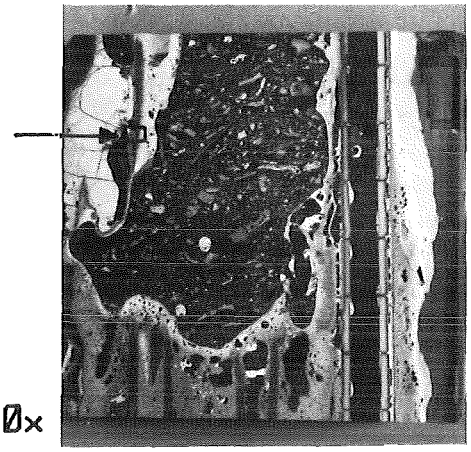

50×

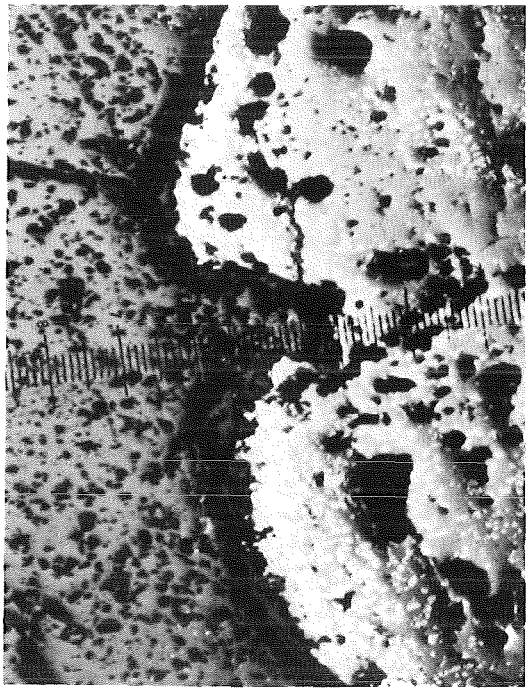

pellet

100×

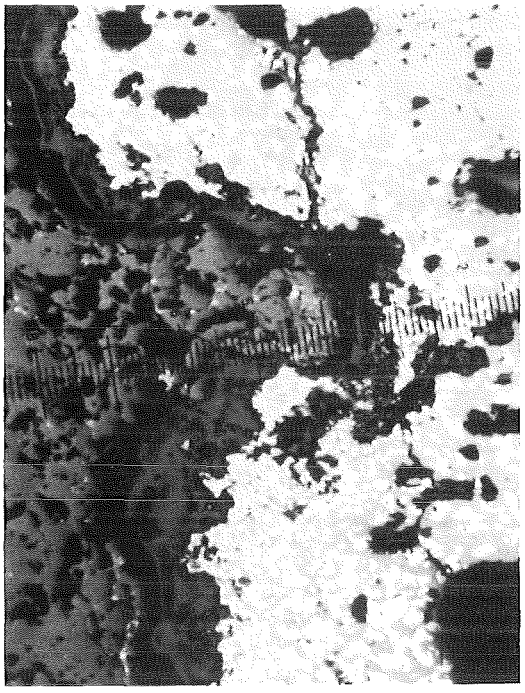

pellet

200×

Fig.174: Al_2O_3 pellet and Zry cladding interaction (CORA bundle B)

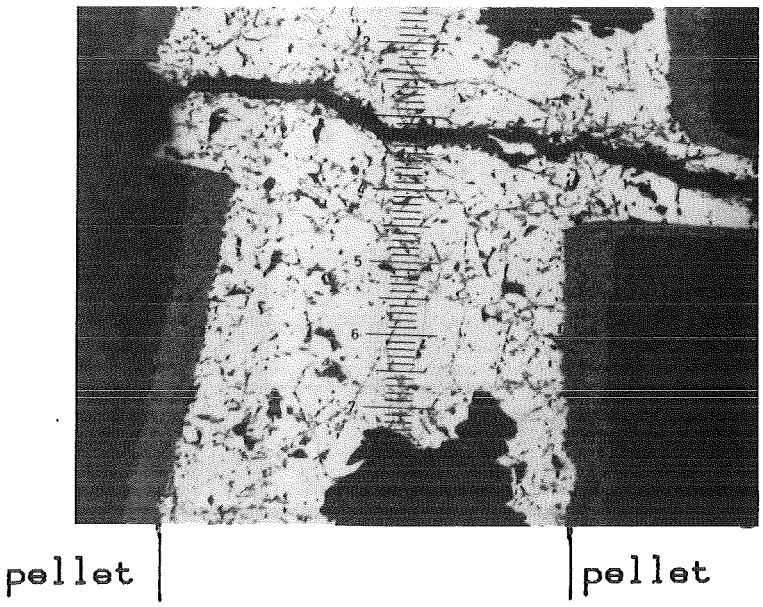

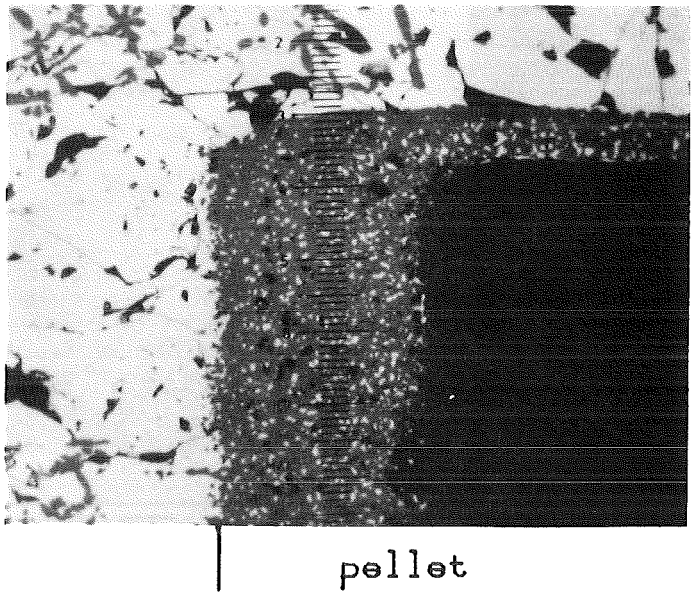

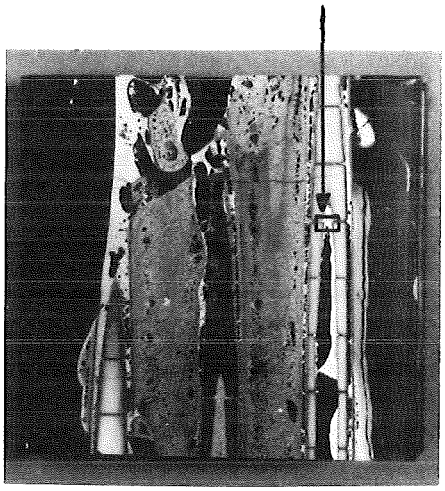

Fig.175: Al_2O_3 pellet and Zry cladding interaction (CORA bundle B)

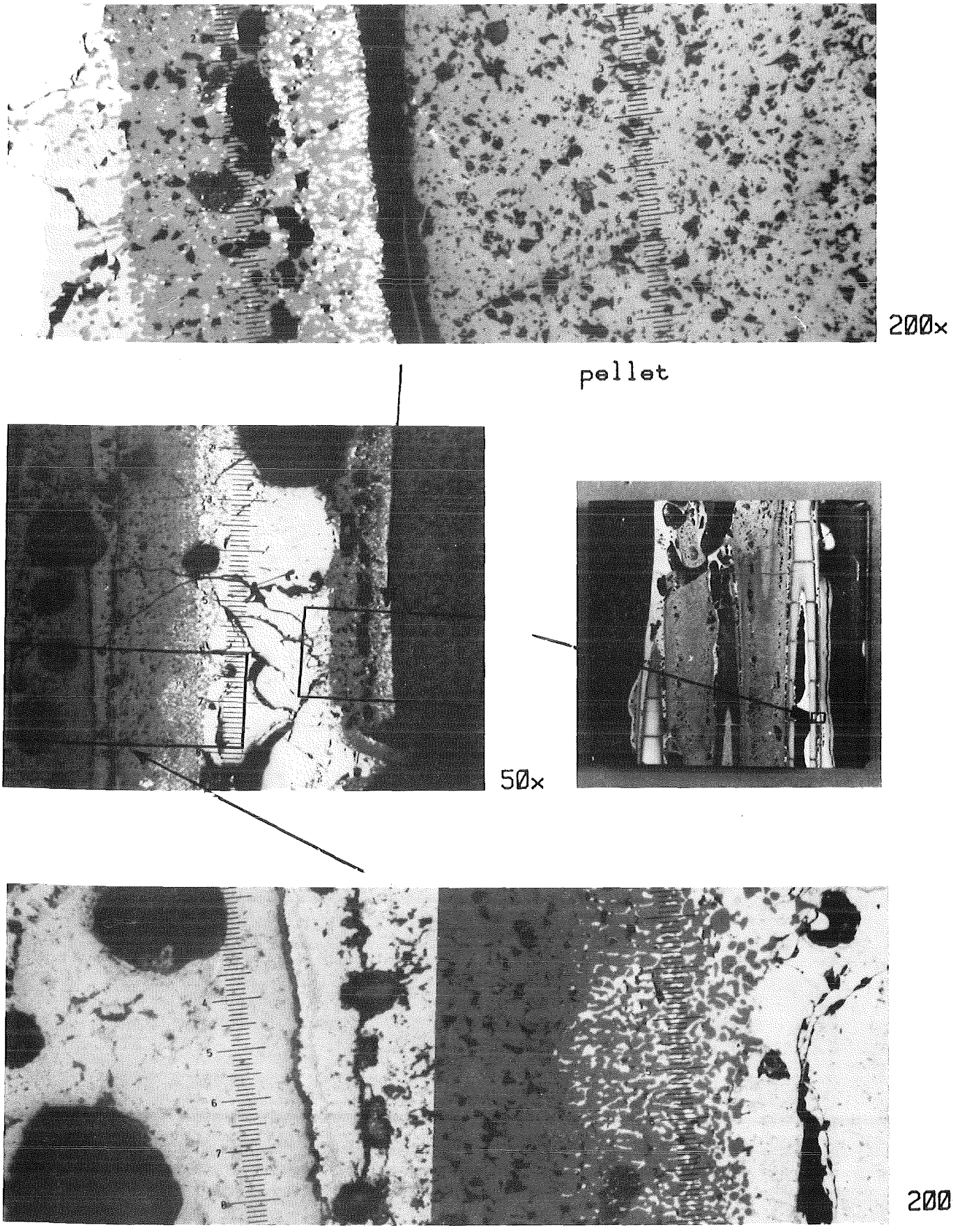

Fig.176 : Al_2O_3 pellet and Zry cladding interaction (CORA bundle B)

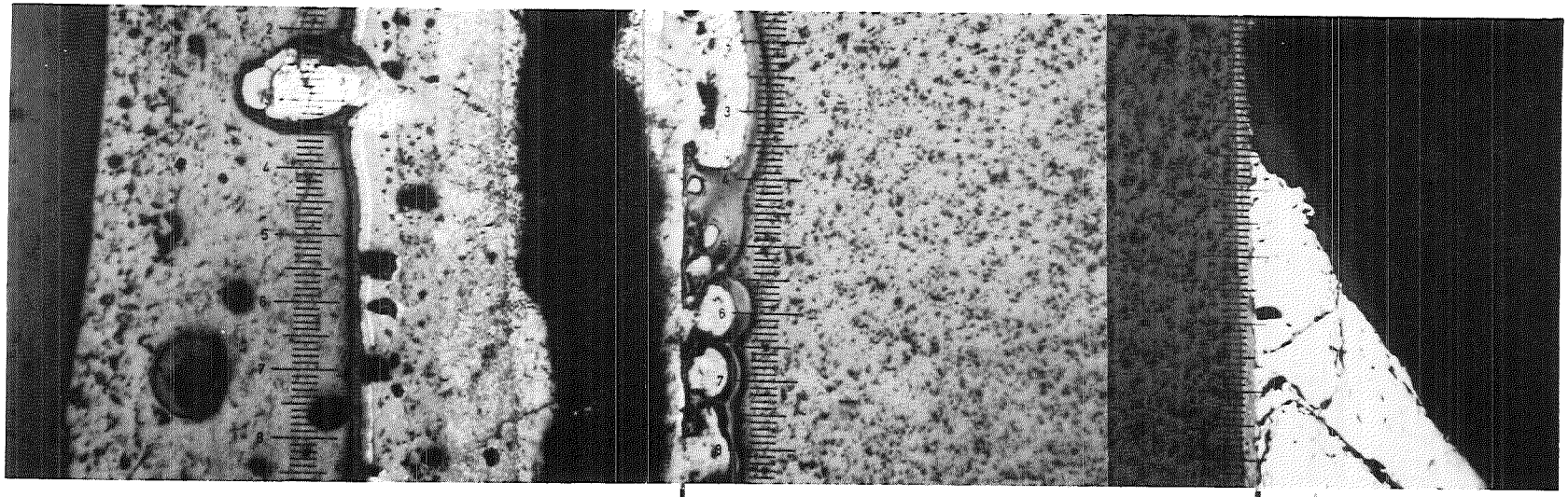

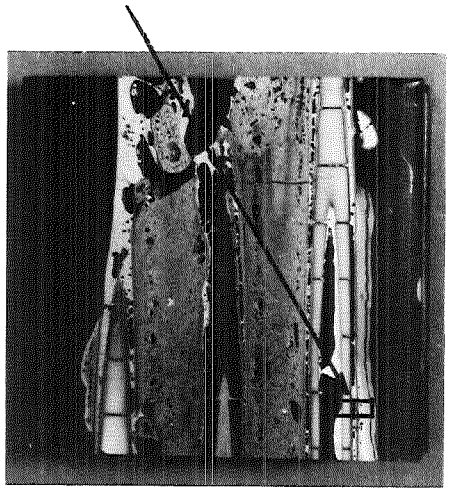

Fig.177 :
Al_2O_3 pellet and Zry cladding interaction (CORA bundle B)

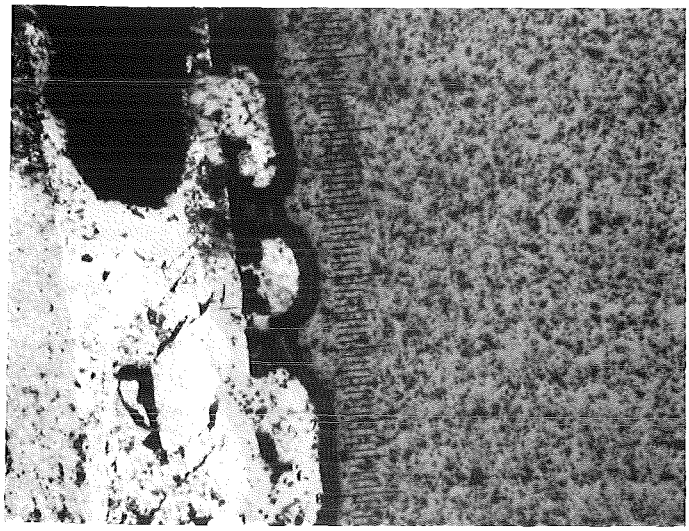

50x

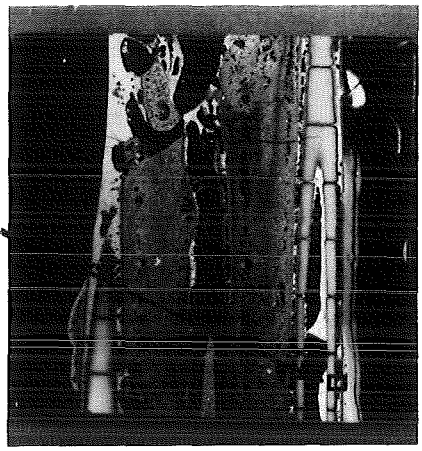

pellet

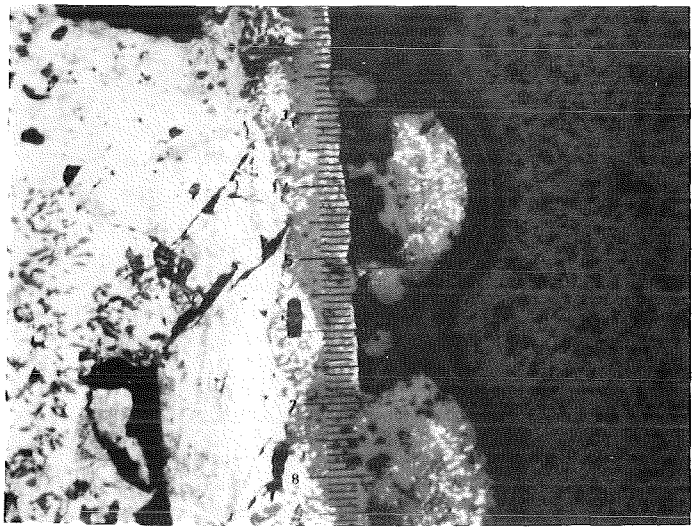

100x

pellet

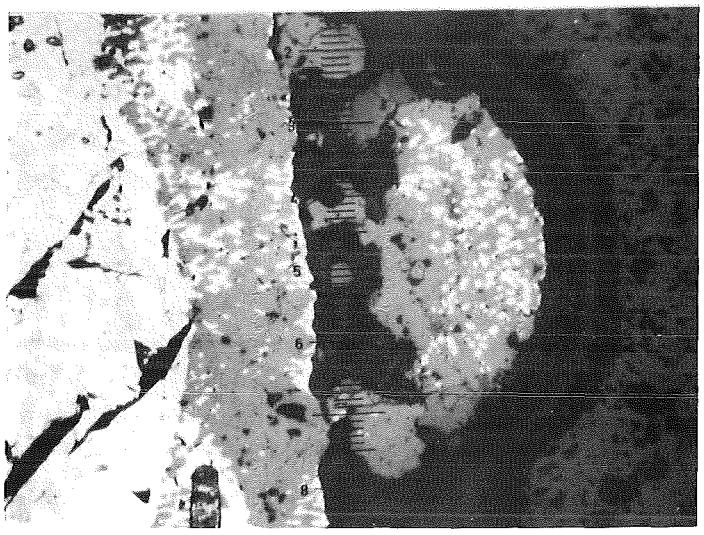

200x

pellet

Fig.178: Al_2O_3 pellet and Zry cladding interaction (CORA bundle B)